

VU Research Portal

Faulty Rivers

Woolderink, Hessel Antonius Gerardus

2021

document version

Publisher's PDF, also known as Version of record

[Link to publication in VU Research Portal](#)

citation for published version (APA)

Woolderink, H. A. G. (2021). *Faulty Rivers: The effect of faulting on river morphodynamics and morphology*. Ipskamp.

General rights

Copyright and moral rights for the publications made accessible in the public portal are retained by the authors and/or other copyright owners and it is a condition of accessing publications that users recognise and abide by the legal requirements associated with these rights.

- Users may download and print one copy of any publication from the public portal for the purpose of private study or research.
- You may not further distribute the material or use it for any profit-making activity or commercial gain
- You may freely distribute the URL identifying the publication in the public portal ?

Take down policy

If you believe that this document breaches copyright please contact us providing details, and we will remove access to the work immediately and investigate your claim.

E-mail address:

vuresearchportal.ub@vu.nl

VRIJE UNIVERSITEIT

Faulty Rivers

The effects of faulting on river morphodynamics and morphology

ACADEMISCH PROEFSCHRIFT

ter verkrijging van de graad Doctor aan
de Vrije Universiteit Amsterdam,
op gezag van de rector magnificus
prof.dr. V. Subramaniam,
in het openbaar te verdedigen
ten overstaan van de promotiecommissie
van de Faculteit der Bètawetenschappen
op donderdag 17 juni 2021 om 13.45 uur
in de aula van de universiteit,
De Boelelaan 1105

door

Hessel Antonius Gerardus Woolderink

geboren te Enschede

promotor: prof.dr. R.T. van Balen

copromotoren: dr. C. Kasse
dr. K.M. Cohen
prof.dr. M.G. Kleinans

Reading committee:

prof.dr. Klaudia Kuiper
prof.dr. Hans Middelkoop
prof.dr. Klaus Reicherter
Dr. Alain Demoulin
Dr. Freek Busschers

Faulty rivers

The effects of faulting on river
morphodynamics and morphology

The background of the cover is an aerial topographic map of a river system. The river is shown in a light green color, winding through a landscape of varying elevations. The terrain is color-coded, with green representing lower elevations and yellow, orange, and red representing higher elevations. The river's path is clearly visible, showing meanders and confluences. At the bottom of the cover, there is a white seismic waveform, which is a jagged line representing ground motion over time. The waveform starts with a sharp peak on the left and then continues with smaller, more frequent oscillations across the bottom of the cover.

H.A.G. Woolderink

The title page shows a Digital Elevation Model of the Meuse and Roer confluence area near Roermond. This area shows multiple indicators of the effects of faulting on river morphodynamics and morphology, and has formed a continuous source of inspiration for me during this PhD project. The digital elevation models were retrieved, and can be freely accessed, from www.ahn.nl and www.geoportal.nrw.

This research is funded by The Netherlands organization for Scientific Research: Reconstruction and Modelling of the Meuse- and Rhine River. Sinuosity Response to Faulting in the Roer Valley Rift System” (NWO; project nr. 821.01.011).

Table of Contents

Chapter 1: Introduction and problem definition

1.1 General Introduction	5
1.2 Aim and objectives	7
1.3 Thesis Outline	7

Chapter 2: *Fluvial, tectonic and sedimentary setting*

2.1 Introducing the Meuse, Roer and Rhine rivers	10
2.2 Tectonic setting of the Lower Rhine Embayment rift system	12
2.3 Late Pliocene and Quaternary	14
2.4 Present-day drainage pattern directions	16
2.5 References	18

Chapter 3: *Spatial and temporal variations in river terrace formation, preservation, and morphology in the Lower Meuse Valley, The Netherlands*

3.1. Introduction	24
3.2. Setting	25
3.2.1 <i>Tectonical and sedimentary setting</i>	26
3.2.2 <i>Climate change and vegetation development</i>	28
3.2.3 <i>Vegetation changes during the Weichselian late glacial and Holocene</i>	29
3.2.4 <i>Existing Lower Meuse Valley terrace stratigraphic schemes</i>	30
3.3. Methods	32
3.3.1 <i>Lithological cross sections and cores</i>	32
3.3.2 <i>Radiocarbon dating</i>	32
3.3.3 <i>Digital Mapping</i>	32
3.4 Results	35
3.4.1 <i>Database of sites with age control</i>	35
3.4.2 <i>Newly dated channel fill sites</i>	36
3.4.3 <i>Terrace map</i>	37
3.5 Discussion	43
3.5.1 <i>Temporal variations in river terrace morphology</i>	43
3.5.2 <i>Spatial variations in river terraces</i>	47
3.6 Conclusions	50
3.7 Acknowledgments	51
3.8 References	51

Chapter 4: *Interplay between climatic, tectonic and anthropogenic forcing in the Lower Rhine Graben, the Roer River*

4.1 Introduction	59
4.2 Setting	61
4.2.1 <i>The Roer and its catchment</i>	61
4.2.2 <i>Geological and sedimentary setting</i>	61
4.2.3 <i>Climate, vegetation and associated changes in river morphology</i>	64
4.3 Methods	66

4.3.1	<i>DEM analysis, lithological cross sections and cores</i>	66
4.3.2	<i>Radiocarbon dating</i>	66
4.3.3	<i>Digital mapping</i>	68
4.3.4	<i>Pollen analysis</i>	69
4.3.5	<i>Gradient lines</i>	69
4.4	Results: terrace characteristics and chronology	71
4.4.1	<i>Level A</i>	73
4.4.2	<i>Level B</i>	75
4.4.3	<i>Level C</i>	77
4.4.4	<i>Level D</i>	79
4.4.5	<i>Level E</i>	80
4.5	Discussion	82
4.5.1	<i>Late Pleniglacial</i>	82
4.5.2	<i>Bølling</i>	83
4.5.3	<i>Bølling-Older Dryas transition</i>	83
4.5.4	<i>Allerød</i>	86
4.5.5	<i>Younger Dryas</i>	86
4.5.6	<i>Early Holocene</i>	87
4.5.7	<i>Middle Holocene</i>	88
4.5.8	<i>Late Holocene</i>	89
4.6	Conclusions	91
4.7	Acknowledgments	92
4.8	References	92

Chapter 5: *Patterns in river channel sinuosity of the Meuse, Roer and Rhine rivers in the Lower Rhine Embayment rift-system, are they tectonically forced?*

5.1	Introduction	103
5.2	Fluvial and tectonic setting	106
5.2.1	<i>Present-day characteristics of the Meuse, Roer and Rhine rivers</i>	106
5.2.2	<i>Tectonic structure and depositional record</i>	107
5.3	Methods	109
5.3.1	<i>Longitudinal profiles</i>	110
5.3.2	<i>Sinuosity</i>	110
5.4	Results and interpretation	111
5.4.1	<i>Longitudinal profiles</i>	111
5.4.2	<i>Sinuosity patterns</i>	111
5.5	Discussion	114
5.5.1	<i>Large-scale sinuosity patterns</i>	116
5.5.2	<i>Local sinuosity anomalies at fault zones</i>	117
5.6	Conclusions	122
5.7	Acknowledgements	123
5.8	References	123

Chapter 6: *Modeling the effects of normal faulting on alluvial river morphodynamics*

6.1	Introduction	130
6.2	Methods	132
6.2.1	<i>Model description</i>	132

6.2.2 <i>Model scenarios</i>	133
6.2.3 <i>Data analysis</i>	135
6.3 Results	134
6.3.1 <i>Subsidence scenarios</i>	134
6.3.2 <i>Uplift scenario's</i>	144
6.3.3 <i>Fault offset</i>	146
6.3.4 <i>Fault location</i>	149
6.4 Discussion	151
6.4.1 <i>Comparison to field studies</i>	151
6.4.2 <i>Tectonic deformation rates</i>	153
6.4.3 <i>Relative time scales</i>	153
6.4.4 <i>Transient response, fault location and preservation potential</i>	155
6.5 Conclusions	156
6.6 References	157
Chapter 7: <i>The effects of faulting on river channel sinuosity; a review, evaluation and application of concepts</i>	
7.1 Introduction	161
7.2 Normal faulting as a factor causing sinuosity changes	162
7.3 Experimental studies	163
7.4 Numerical modelling	165
7.5 Case studies	165
7.6 Combining the evidence	166
7.7 Application to palaeoseismology and river response	168
7.7.1 <i>Feldbiss Fault Zone (Lower Rhine Embayment, the Netherlands)</i>	168
7.7.2 <i>Peel Boundary Fault Zone (Lower Rhine Embayment, the Netherlands)</i>	170
7.8 Conclusions	173
7.9 References	174
Chapter 8: <i>Conclusions and Synthesis</i>	
8.1 Summary of the main conclusions	178
8.1.1 <i>Morphological indicators of faulting from palaeogeographic reconstructions</i>	178
8.1.2 <i>Morphometric indicators</i>	179
8.1.3 <i>Modeling the effects of tectonic deformations on alluvial river morphodynamics.</i>	180
8.2 Synthesis	181
8.3 Future research	184
8.4 References	185
Summary	187
Samenvatting	192
Appendices	197

Chapter 1

Introduction and problem definition

1.1 General Introduction

Fluvial systems are controlled by both internal processes and external forcing factors (Kleinhans and Van den Berg, 2010; Vandenberghe, 1995, 2003; Holbrook and Schumm, 1999; Blum and Tornqvist, 2000; Wang et al., 2014). The different external forcing factors can operate simultaneously. Thus, in order to study the effects of tectonics on alluvial rivers, a disentanglement of the external forcing factors is essential. Faulting in rift systems influences topographic gradients and causes lithological transitions at the earth surface due to vertical (and to some extent horizontal) motions of crustal blocks. Alluvial rivers, on the other hand, tend to level topography as they are able to erode and deposit sediment.

Alluvial rivers can be subjected to faulting on various spatial and temporal scales and show a morphodynamic response to tectonic-induced changes in (valley) gradient (Schumm, 1985). The characteristics of the effects of tectonic deformations on alluvial rivers has been a matter of interest over the past decades (Burnett and Schumm, 1983; Ouchi, 1985; Leeder and Alexander, 1987; Holbrook and Schumm, 1999; Marple and Talwani, 2000; Buratto et al., 2003; Jain and Sinha, 2005; Holbrook et al., 2006; Aswathy et al., 2008; Taha and Anderson, 2008; Petrovski and Timar, 2010; Arcos, 2012; Lahiri and Sinha, 2012; Mack et al., 2012; Whitney and Hengesh, 2015).

However, they remain to a large extent hypothetical due to the small number of physical (Ouchi, 1983, 1985; Jin, 1983, Dykstra, 1988; Peakall, 1996; Germanowski and Schumm, 1993) and numerical modeling studies and the lack of detailed case studies in which the tectonic component is disentangled from other external forcing factors. Furthermore, the conceptual models are primarily based on block-wise tectonic motions (e.g. tilting or uplift of fault-bounded blocks) and rarely focus on local vertical motion at or near a fault zone. Moreover, a planform response of an alluvial river to faulting can be contemporaneous with the vertical response of the river (Schumm et al., 2000). Incision and aggradation rates are largest just after a vertical tectonic movement and will decrease over time as the tectonic altered gradient is restored. Thus, the morphodynamic response of a river to tectonic deformation is transient, which is commonly not taken into account in case studies.

For palaeoseismological studies/inferences, the transient response is important due to the abrupt nature of surface rupturing fault movement. However, the reoccurrence interval of large surface rupturing earthquakes is usually relatively large (e.g. > 1 kyr; Camelbeeck et al., 2007, 2020; Nicol et al., 2010). Slow, gradual fault displacement on the other hand, may cause river morphodynamic changes on a time scale of thousands of years. For these reasons observational data are limited, which hampers development of conceptual models. To further improve the knowledge on the effects of faulting on

alluvial meandering rivers, well-documented case studies combined with quantitative modelling are needed.

The Meuse river system in the Roer Valley Rift System (RVRS) provides a natural laboratory to study the effects of faulting on rivers. The RVRS main fault zones are seismically active (Geluk et al., 1994; Van Balen et al., 2005; Camelbeeck et al., 2007). The Meuse River, and its major tributary the Roer River, cross and parallel multiple fault zones of this active rift system. Moreover, the palaeogeographic, sedimentary, anthropogenic and tectonic setting of this study area are exceptionally well known. The effects of climatic changes on river evolution (morphodynamics, fluvial terrace formation and morphology) of the Rhine-Meuse river system has been studied extensively (Schelling; 1951; Pons and Schelling, 1951; Pons, 1957; Van den Broek and Maarleveld, 1963; Miedema, 1987; Buitenhuis and Wolfert, 1988; Wolfert and De Lange, 1990; Kasse et al., 1995; Berendsen et al., 1995; Van den Berg, 1996; Huisink, 1997; Tebbens et al., 1999; Cohen et al., 2002; Kasse et al., 2005; Erkens et al., 2011; Janssens et al., 2015; Hoek et al., 2017; Kasse et al., 2017). Especially the downstream part of the Meuse Valley (i.e. the Venlo Block) was studied in detail, as this area has the best developed staircase of Lateglacial and Holocene fluvial terraces with different fluvial planforms (Woolderink et al., 2018 and references herein).

The role of tectonics as an external forcing on river dynamics in the study area was recognized in several of these studies, especially in the form of post-depositional faulting of river terraces (Van den Broek and Maarleveld, 1963; Van den Berg, 1996; Huisink, 1997, Tebbens et al., 1999; Cohen et al., 2002). Furthermore, it was shown for the downstream Holocene Rhine-Meuse delta that tectonics had a significant impact on the fluvial terraces of the buried Rhine-Meuse valley and Holocene aggradational systems (Stouthamer and Berendsen, 2000; Berendsen and Stouthamer, 2001; Cohen et al., 2002, 2005). This includes, among others, deformed longitudinal profiles, deflection of river courses, fault-related alignments of terrace scarps, nodal avulsion points at fault zones and differential preservation of river terraces (Stouthamer, 2001; Cohen, 2003; Gouw and Erkens, 2007; Stouthamer et al., 2011). Palaeoseismological trenching at fault zones of the LRE in the last decades has provided evidence that faulting causes slow vertical motions and sudden seismogenic surface ruptures (see Van Balen et al., 2019 for discussion). The latter influences river dynamics and morphology on a short timescale.

However, an integrated overview and study of the effects of both active and passive tectonic forcing (e.g. subsurface lithology differences due to differential subsidence) on river morphodynamics and morphology of the Meuse river system in the Lower Rhine Embayment is still lacking. Therefore, this study focusses on both passive and active tectonic forcing of the Meuse river system. The conceptual models based on the reconstructions will be tested against the results of numerical simulations in the meander

simulation model Nays2D. This combination of approaches helps to improve our knowledge of the effects of faulting on alluvial river morphodynamics and morphology.

1.2 Aim and objectives

The aim of this thesis is to unravel the morphodynamic and morphological response(s) of alluvial rivers to faulting. The objectives are to:

- Reconstruct the palaeogeographic evolution of the downstream part of the Meuse and Roer rivers in order to disentangle the influence of climatic, tectonic and anthropogenic forcings on river morphodynamics and morphology.
- Determine the relation(s) between (transient) morphodynamic river response and tectonic movements at different spatial scales (fault-bounded blocks and faults) and on long and short (earthquake) time-scales, using the Meuse-Roer river system and Roer Valley Rift System (RVRS) data on river morphology and fault activity.
- Use a numerical meander simulation model (Nays2D) to study the effects of various tectonic deformation rates and styles along normal fault zones on alluvial meandering river morphodynamics and morphology and test the conceptual models based on the reconstructions.

1.3 Thesis Outline

This chapter provides a general introduction to the different spatial and temporal scales on which tectonic deformations act on alluvial rivers, for the Meuse River and Roer Valley Rift System in particular. It, furthermore, introduces the problems and gaps in our current knowledge and states the aim and objectives of the thesis. The next chapters cover:

Chapter 2: *Fluvial, tectonic and sedimentary setting*

Chapter 2 provides the essential fluvial, tectonic and sedimentary framework of the study area that is needed for further discussion in the thesis.

Chapter 3: *Spatial and temporal variations in river terrace formation, preservation, and morphology in the Lower Meuse Valley, The Netherlands (Journal paper)*

A detailed palaeogeographic reconstruction of the terrace series over the full length of the Lower Meuse Valley has been performed in this study. This reconstruction provides improved insight into successive morphological responses to combined climatic and tectonic external forcing, as expressed and preserved in different ways along the river.

Chapter 4: *Interplay between climatic, tectonic and anthropogenic forcing in the Lower Rhine Graben, the Roer River (Journal paper)*

In this chapter we perform a detailed and integrated reconstruction of the fluvial morphology and palaeogeography of the Roer River in order to determine responses to combined climatic, tectonic and anthropogenic forcing factors.

Chapter 5: *Patterns in river channel sinuosity of the Meuse, Roer and Rhine rivers in the Lower Rhine Embayment rift-system, are they tectonically forced? (Journal paper)*

This chapter focusses on unravelling tectonically-forced responses of channel sinuosity of rivers that are subjected to various degrees of faulting in the Lower Rhine Embayment, both at the scale of fault-bounded blocks and fault zones.

Chapter 6: *Modeling the effects of normal faulting on alluvial river morphodynamics (Journal paper)*

In this chapter we use a physics-based morphodynamic model (Nays2D), to numerically model the effects of various tectonic deformation rates and styles along normal fault zones on alluvial meandering river morphodynamics and morphology.

Chapter 7: *The effects of faulting on river channel sinuosity; a review, evaluation and application of concepts*

This chapter reviews and evaluates conceptual models of the effects of tectonic deformation, and in particular faulting, on the channel sinuosity of alluvial rivers and the use of sinuosity anomalies as indicators of (active) tectonic deformation.

Chapter 8: *Conclusions and Synthesis*

This chapter summarizes the main conclusions of the thesis and contains a synthesis of the effects of faulting on river morphodynamics and morphology.

Chapter 2

Fluvial, tectonic and sedimentary setting

2.1 Introducing the Meuse, Roer and Rhine rivers

The Meuse River is a circa 900 km long rain fed river that has its headwaters in northeastern France (Fig. 1). The Meuse then flows along the rims of the Paris Basin and crosses the Ardennes Massif before it enters the tectonic system of this study area at Eijsden (Fig. 1). The Meuse River crosses multiple fault zones of the Lower Rhine Embayment (LRE). The Meuse enters its Holocene deltaic reaches where it turns westward in the central Netherlands (Fig. 1). The present-day mean annual discharge is circa 250 m³/s and its bankfull discharge is approximately equal to mean annual flood, which is around 1500 m³/s at Maaseik (Belgium; Table 1). The catchment size of the Meuse river system is 33,000 km². Gradients of the Meuse valley in the study area range between ~60 and 10 cm/km on average. The backwater adaption lengths (e.g. the upstream propagation length of a perturbation to the flow of the river) are between 7.5 to 52.5 kilometers.

The Roer River is the main tributary of the Meuse River in the study area, and has a catchment size of circa 2354 km². The Roer has its source in the Hautes Fagnes (Belgium) and has a length of 165 km. Circa 80 km flows through the RVG (Fig. 1). The Roer enters the RVG at Düren and flows parallel to the direction of the graben and fault zones (Fig. 1). The mean annual discharge of the Roer River is ~21.8 m³/s (at Stah, Germany) and discharge varies between 8 and 124 m³/s (LANUV, n.d.; Table 1). Valley gradient in the study area varies between circa 230 and 90 cm/km. The backwater adaption length increases from 0.8 and 2.9 km in downstream direction.

The Rhine River is the largest river passing through the rift system. It has a length of 1230 km and flows from the Alps in Switzerland, through Germany and the Netherlands to the North Sea (Fig. 1). The Rhine river is a snowmelt and rainfed river and its catchment is circa 185,000 km². The Rhine River enters the Lower Rhine Embayment at Bonn and takes a north easterly course along the margin of the tectonic system (Fig. 1). The river enters its deltaic reach in the Dutch-German border region. The mean annual discharge is around 2200 m³/s at Rees (Germany [Erkens, 2009]) and the mean annual flood discharge is ~6500 m³/s. The adaption length for the backwater effect is around 29 km (Table 1) and valley gradient average in the study area lies between 35-20 cm/km.

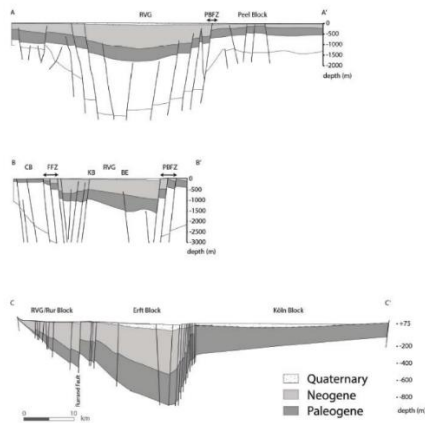
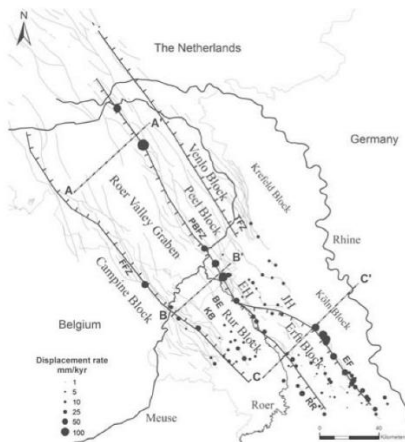
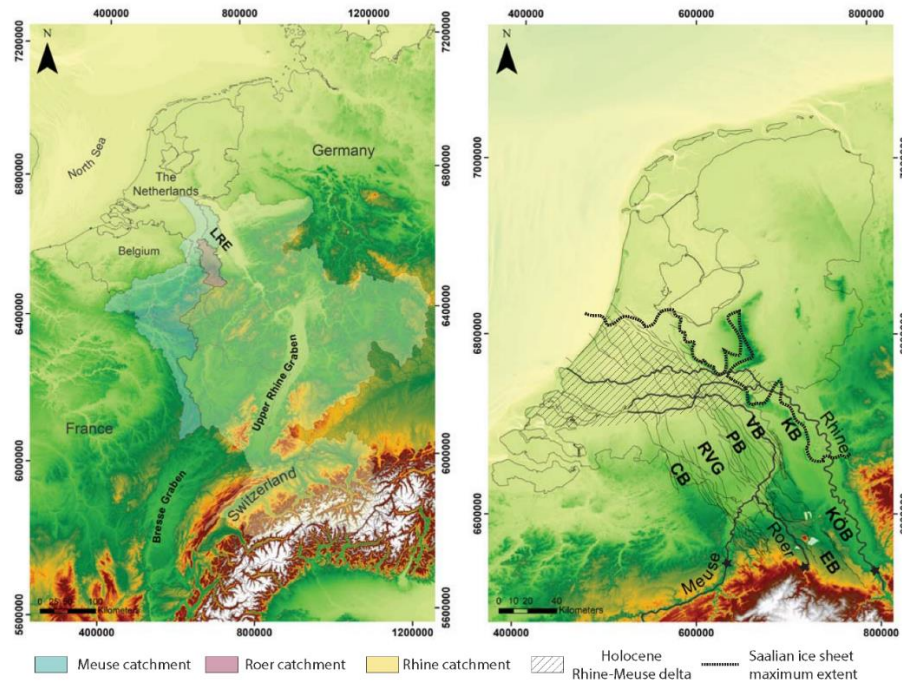


Fig. 1: The Lower Rhine Embayment (LRE) as part of the European Cenozoic rift system. The Meuse, Roer and Rhine rivers flow through the LRE. The Meuse crosses the rift system, the Roer parallels the Roer Valley Graben (RVG) and the Rhine occupies the rift margin. Tectonic displacements are the highest along the north-eastern boundary faults of the Roer Valley Graben (RVG) and Erft Block (EB). Displacement rates are adapted from Gold et al. (2017), Cohen (2003), Van Balen et al. (2019), Michon and Van Balen (2005), Van den Berg et al. (2002), Houtgast et al. (2005) (after Woolderink et al., 2019).

Table 1: Main river characteristics of the gravel and sand reaches of the Meuse, Roer and Rhine rivers.

	Meuse Gravel	Meuse Sand	Roer Gravel	Roer Sand	Rhine Gravel
Qflood (M ³ /S)	1500			85	6500
Width (m)	125	150	40	30	425
Depth (m)	4.5	5.3	1.9	2.6	7.3
Width/depth	27.8	28.6	21.1	11.5	58.2
Gradient Valley (m/km)	0.6	0.1	2.3	0.9	0.35 - 0.20
Grainsize (m)	0.02 - 0.04	0.0005 - 0.001	0.04	0.0005 - 0.001	0.015 - 0.02
Sinuosity range	1.07 - 2.77	1.03 - 3.39	1.05 - 1.42	1.17 - 2.20	1.03 - 1.93
Shields number	0.05	0.40	0.06	1.61	0.06
Adaption length backwater effect (km)	7.5	52.5	0.8	2.9	29.2

2.2 Tectonic setting of the Lower Rhine Embayment rift system

The Lower Rhine Embayment (LRE) forms the northern segment of the European Cenozoic rift system. The Roer Valley Rift System (RVRS) is part of the LRE (Fig. 1). The LRE is situated in the southern Netherlands and adjacent parts of Belgium and Germany (Fig. 1). The tectonic evolution of the LRE has been studied extensively (Fig. 1; Ahorner, 1962; Klostermann, 1983; Zagwijn, 1989; Schirmer, 1990; Ziegler, 1992, 1994; Geluk et al., 1994; Van den Berg, 1996; Houtgast and Van Balen, 2000; Houtgast et al., 2002; Cohen et al., 2002; Schäfer and Siehl, 2002; Michon et al., 2003; Van Balen et al., 2005; Kemna, 2005; Westerhoff et al., 2008).

The horst-graben structure of the LRE consist of asymmetric (half) grabens and symmetric (full) grabens (Fig. 1; Schäfer et al., 2005; Michon and Van Balen, 2005; Westerhoff et al., 2008). The main fault zones of the LRE have a NW-SE orientation (Fig. 1). The most important grabens in the LRE are the Erft Block (EB) and the Roer Valley Graben (RVG)/Rur Block (RB) respectively. The RVG is bounded by the relatively uplifting Campine Block (CB) in the south and the Peel Block (PB) in the north (Van Balen et al., 2005; Westerhoff et al., 2008). The fault systems continue in the subsurface of the Rhine-Meuse delta, where it had a profound influence on river dynamics (Stouthamer and Berendsen, 2001; Cohen et al., 2002, 2005).

The LRE has a general northwest tilting direction, which is a result of subsidence in the North Sea Basin (Kooi et al., 1991; 1998) and the Quaternary uplift of the Rhenish Shield (Van Balen et al., 2000; Demoulin and Hallot, 2009). A secondary tilt direction to the northeast was observed for the tectonic blocks of the RVRS, based on lithostratigraphic mapping of the basin fill (Van Balen et al., 2000). A superimposed regional-scale, glacio-isostatic northward tilting component has been in play in the youngest 20,000 years

(Kiden et al. 2002; Cohen, 2003; Busschers et al., 2007; Hijma et al., 2009), owing to the near-field peripheral position of the region to land ice masses (forebulge collapse).

The NE-SW directed extension led to a maximum of circa 1200-1500 m of subsidence in the RVG since the Late Oligocene (Geluk et al., 1994; Van Balen et al., 2005; Schäfer et al., 2005; Kemna, 2005; Schokker et al., 2005; Westerhoff et al., 2008). An overview of the displacement rates of the (main) fault zones of the LRE is shown in Fig. 1. The highest displacement rate, and maximum sediment accumulation, occurs along the north-eastern boundary faults of the RVG and EB (Ahorner, 1962; Schäfer et al., 1996; Camelbeeck and Meghraoui, 1998; Van den Berg et al., 2002; Houtgast et al., 2002; Michon and Van Balen, 2005; Gold et al., 2017; Woolderink et al., 2019).

The Feldbiss Fault Zone (FFZ) separates the RVG from the CB in the south, while the Peel Boundary Fault Zone (PBFZ) forms the boundary between the RVG and PB in the north (Fig. 1). Both the FFZ and PBFZ reach to the surface and are visible as fault scarps and in seismic and geo-electric profiles (DINOloket, 2019; Paulissen, 1985; Vanneste et al., 2002). The Koningsbosch (KB) and Beegden (BE) faults delineate a small horst within the subsiding RVG (Fig. 1). Present-day and Holocene displacement rates of the KB and BE faults are unknown.

In the southeastern part of the LRE, the PBFZ splits into the Rur (RR) and Erft (EFZ) fault zones. The Rur Fault (RR) separates the RVG/RB from the EB. The Köln Block (KÖB) forms the hanging wall in the eastern part of the LRE, where it is separated from the EB by the Ville horst and Erft Fault Zone (EFZ) (Fig. 1 [Schäfer et al., 2005]). The Ville horst continues to the northwest into the Jackerather (JH) and Erkelenz (EH) horsts respectively (cf. Ahorner, 1962). The continuation of these horst structures form the Peel Block (PB) in the Netherlands (Fig. 1). The PB is bordered by the Venlo Block (VB) that lies to the north (Fig.1).

The VB and PB are separated by the Tegelen Fault Zone (TFZ). The displacement rates of the faults of the TFZ have not been constrained in the study area. (i.e. in the incisive reach of the Meuse River) However, since these faults have no morphologic expression, their average displacement rates should be less than those of the historically seismically active FFZ and the PBFZ.

In the northeast a relatively high block, the Krefeld Block (KB), borders the subsiding VB area (Geluk et al., 1994). The LRE main fault zones are seismically active with the 1756 Düren (Mw 5.7) and 1992 Roermond (Mw 5.4) earthquakes as the most significant examples (Geluk et al., 1994; Camelbeeck et al., 2007). Palaeoseismological data from trench studies over the PBFZ and FFZ shows that fault movement has been episodic (Vanneste and Verbeeck, 2001; Vanneste et al., 2001; Van den Berg et al., 2002; Camelbeeck et al., 2007; Vanneste et al., 2018; Van Balen et al., 2019).

2.3 Late Pliocene and Quaternary

During the Late Pliocene and Early Pleistocene, the LRE was filled in by the Rhine, Meuse and (smaller) Belgian river systems (Fig. 2 A-C; Westerhoff et al., 2008). The northern part of the Netherlands was the realm of the Eridanos river system. Uplift of the Ardennes and Rhenish Massif resulted in a semi-continuous fluvial terrace sequence of the Meuse River (Van den Berg, 1996) and the Rhine River (Zagwijn, 1989; Boenigk, 2002; Boenigk and Frechen, 2006; Kemna, 2008) in the south east of the LRE.

The Rhine River shifted its course several times during the Early Pleistocene, in and out of the RVG (Fig. 2 A-E; Zonneveld, 1974; Zagwijn, 1989; Boenigk, 2002; Kemna, 2008; Westerhoff et al, 2008). At these moments, the Meuse and the smaller Belgian rivers advanced, as transverse rivers, in a north east direction, into the RVG (Fig. 2 A-E). An abrupt change in the direction of the Meuse at the rim of the LRE, from east to north directed, occurred during the Early Pleistocene (Fig. 2 D-E; Van den Berg, 1996; Kemna, 2008, Westerhoff et al., 2008).

During the Middle Pleistocene the Rhine left the RVG permanently, leaving the Meuse River as the main sediment supplier (Fig. 2F). After 500 ka yr the location of the Rhine and Meuse systems was strongly controlled by direct and indirect impacts of glaciation (Fig. 2 F-I; Busschers et al., 2008; Hijma et al., 2012; Cohen et al., 2014; Peeters et al., 2015). During the Saalian glaciation the maximum extent of the ice sheet reached the study area and formed a series of ice-pushed ridges (Fig. 2G). This process forced the Rhine and Meuse to flow in a westward direction (Fig. 2G; Zagwijn, 1974; Cohen, 2003). After deglaciation the Rhine adopted a more northward course for a relatively short period, after which it reoccupied its western course during the Middle Weichselian (Fig. 2H; Zagwijn, 1974; Busschers et al, 2007; Peeters et al., 2015). This westward course was maintained during the Late Weichselian (Busschers et al., 2007; Hijma et al., 2009; Cohen et al., 2012).

During the Lateglacial and Early Holocene climatic changes forced fluvial planform changes of the Rhine and Meuse river systems. These have been studied extensively, also because dating control and palaeogeographic reconstructions are exceptionally developed for both systems (Pons, 1954; Berendsen et al., 1995; Kasse et al., 1995, 2005, 2017; Van den Berg, 1996; Tebbens et al., 1999; Berendsen and Stouthamer, 2000, 2001; Cohen, 2003; Gouw and Erkens, 2007; Erkens et al., 2011; Hijma et al., 2009, Hijma and Cohen, 2011; Janssens et al., 2012; Rensink et al., 2015; Woolderink et al., 2018, 2019). Overall the river pattern of the Meuse and Rhine was braided during the last glacial maximum and had a multi-channel low-sinuosity planform during the Bølling which evolved into a (multi-channel) meandering planform during the Allerød interstadial. Subsequently it was braided (or at least wandering) again during the Younger Dryas cold stage. The Roer and Niers-Rhine rivers did, however, not show a braided phase during

the Younger Dryas (Kasse et al., 2005; Woolderink et al., 2019). Finally, the river planform became meandering again at the onset of the Holocene and evolved in to a single-channel meandering river during the Holocene. Reach-to-reach differences in the geomorphological and sedimentary responses are, however, present along the rivers (Cohen, 2003; Erkens et al., 2011; Woolderink et al., 2018).

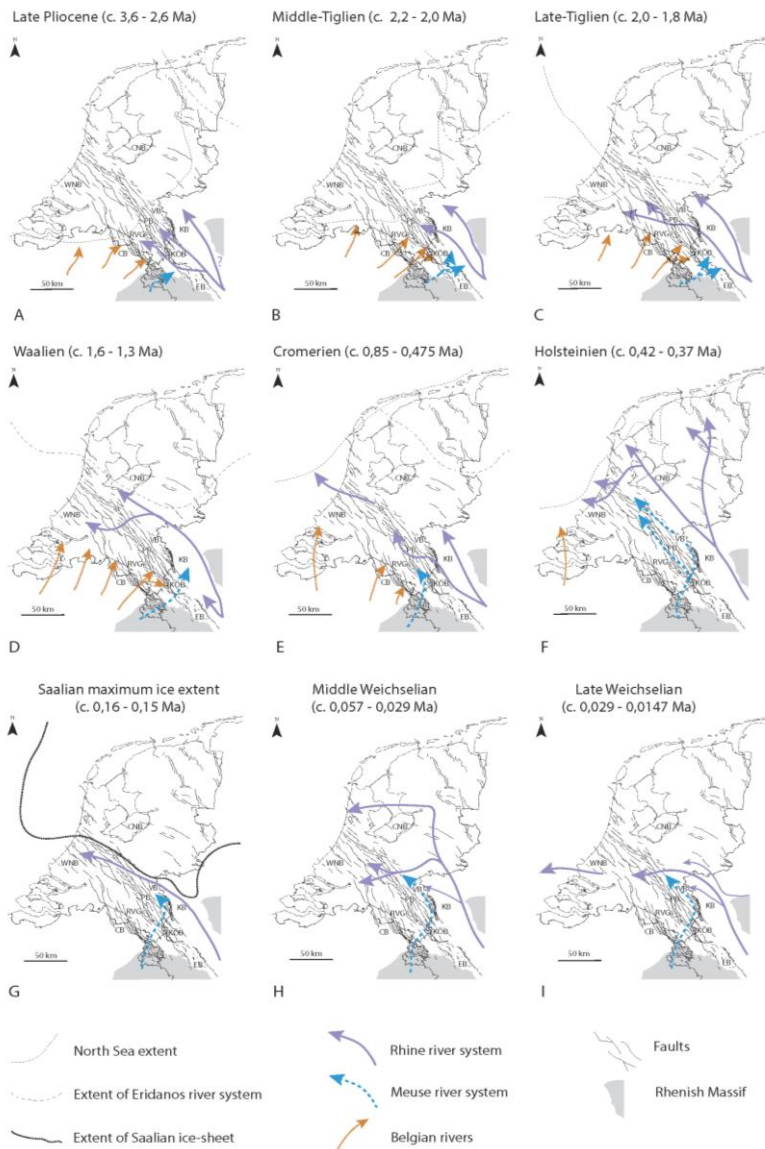


Fig. 2: Late Pliocene and Quaternary evolution of the Rhine-Meuse river system. Panels are modified after Maarleveld, 1956; Zagwijn, 1974, 1986; Van den Berg and Beets, 1987; Kasse, 1988; De Mulder et al. 2003; Busschers et al. 2008; Westerhof et al., 2008; Cohen et al. 2014; Peeters et al., 2015; Southamer et al., 2015.

2.4 Present-day drainage pattern directions

The drainage pattern of the alluvial Meuse catchment in the Lower Rhine Embayment is analyzed for spatial patterns. This analysis is performed because tilting of tectonic blocks can be represented in the drainage pattern, as they determine the surface gradients over which the drainage networks evolves (Fig. 3). The method used for this is normally applied in high-relief study areas, but is now applied to this relatively lowland setting of the alluvial Meuse catchment as well. The linear directional mean, e.g. mean direction of each segment, of the drainage pattern of the Meuse River (including the Roer River as its main tributary) is grouped by stream order (Fig. 3; Strahler, 1957). All stream orders plotted together show a west to northeast orientation. The same holds true for the orientation of the first order streams. The second order, and especially the third order, streams show a main direction to the northwest. The fourth order stream segments represent the Meuse River; they show a northeast flow direction over most of the Lower Meuse Valley (Fig. 3).

The northwest direction of the first order streams is the result of the main tilting direction of the Lower Rhine Embayment (LRE), which is to the northwest. The northeast flow direction of the first-order streams is related to the rotational fault block motions of the relatively uplifting (e.g. the CB and PB) and subsiding blocks (RVG and VB). The northeast direction is perpendicular to the orientation of the main fault zones. Relatively few southwest orientated courses occur from the PB into the RVG, which can also be explained by the northeastern (rotational) tilt of the tectonic blocks.

The mainly northwest flow directions of the second- and third-order streams shows that these streams follow the orientation of the tilting direction of the LRE and its major fault zones (Fig. 3). Most of the first to third order streams (e.g. in the RVG, PB and VB) are relatively young as they formed after the Meuse River left the RVG and PB areas during the Middle Pleistocene (~350 ka BP [Bisschops, 1973; Van den Toorn; 1976; Vandenberghe et al., 1984; Van Balen et al., 2000; Schokker, 2003]). The fact that the first order streams show a more diffuse stream orientation pattern compared to the higher order streams can be explained by their relative size and discharge. The smaller first order streams are more sensitive to local factors in the sedimentary or vegetational setting, controlling stream direction, while the larger 3th or higher order streams are large enough to overcome such local obstructions and follow the larger scale tectonic forced gradients.

The northeast orientation of the fourth order stream (segments) is the result of the two tilting directions of the tectonic blocks of the LRE (i.e. to the northwest and northeast). The northwest direction results from a basin-scale tilting due to subsidence in the North Sea Basin (Kooi et al., 1991; 1998) and the Quaternary uplift of the Rhenish Shield (Van Balen et al., 2000; Demoulin and Hallot, 2009).

The northeast (rotational) tilting direction is caused by the NE-SW directed extension of the rift system. Overfilling of the RVG during the Middle Pleistocene enabled the deflection of the Meuse River towards the northeast (e.g. Van Balen et al., 2000).

From the predominantly northeast orientation of the fourth order stream (segments) it can be derived that the NE tilting direction was dominant over the northwest tilting component. This can be explained by either changing tectonic tilting directions and magnitudes in the LRE over time, as shown by Houtgast and Van Balen (2000), or solely due to a developing gradient advantage as a result of differential sedimentation.

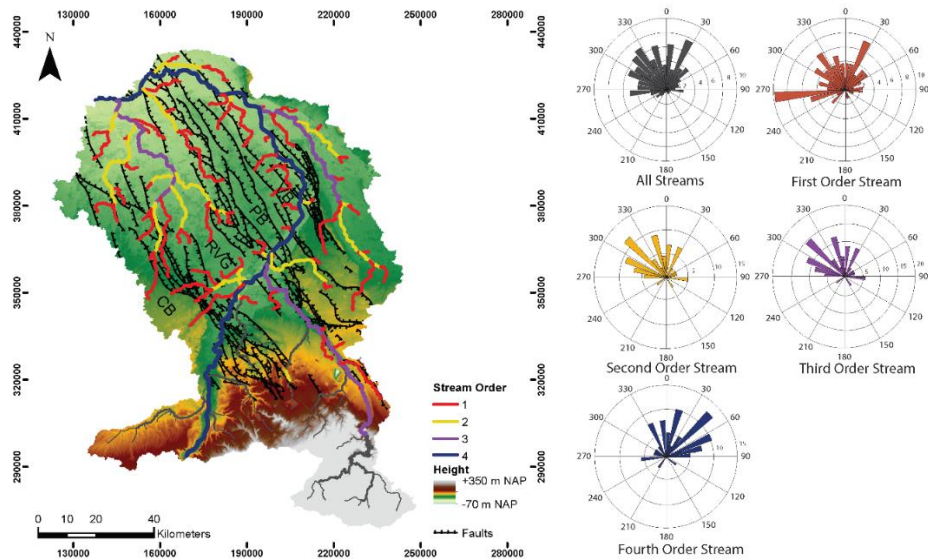


Fig. 3: Drainage network of the alluvial Meuse catchment in the Lower Rhine Embayment rift system. The drainage network is grouped by stream order and the linear directional mean direction of the segments are plotted in the rose-diagrams.

2.5 References

- › Ahorner, L., 1962. Untersuchungen zur quartären Bruchtektonik der Niederrheinischen Bucht. *Quaternary Science Journal*, 13(1), 24-105.
- › Berendsen, H.J.A., Stouthamer, E., 2001. Palaeogeographic Development of the Rhine-Meuse Delta, the Netherlands. Koninklijke van Gorcum, Assen.
- › Berendsen, H.J.A., Hoek, W.Z., Schorn, E., 1995. Late Weichselian and Holocene river channel changes of the rivers Rhine and Meuse in the Netherlands (land van Maas en Waal). In: Frenzel, B., Vandenberghe, J., Kasse, C., Bohncke, S.J.P., Glaser, B. (Eds.), *European River Activity and Climate Change During the Late Glacial and Early Holocene*. Palaoklimaforschung, Vol. 14. ESF Project “European Palaeoclimate and Man,” Special Issue 9. Gustav Fischer Verlag, Stuttgart, pp. 151–171.
- › Bisschops, J.H., 1973. Toelichtingen bij de geologische kaart van Nederland 1: 50.000 blad Eindhoven Oost 51O . Rijks Geologische Dienst, Haarlem
- › Boenigk, W. 2002. The Pleistocene drainage pattern in the Lower Rhine basin. *Netherlands Journal of Geosciences*, 81(2), 201-209.
- › Boenigk, W., Frechen, M. 2006. The Pliocene and Quaternary fluvial archives of the Rhine system. *Quaternary Science Reviews*, 25(5-6), 550-574.
- › Busschers, F.S., Kasse, C., Van Balen, R.T., Vandenberghe, J., Cohen, K.M., Weerts, H.J.T., Wallinga, J., Johns, C., Cleveringa, P., Bunnik, F.P.M., 2007. Late Pleistocene evolution of the Rhine-Meuse system in the southern North Sea basin: imprints of climate change, sea-level oscillation and glacio-isostasy. *Quaternary Science Reviews*, 26(25-28), 3216-3248.
- › Camelbeeck, T., Meghraoui, M., 1998. Geological and geophysical evidence for large palaeo-earthquakes with surface faulting in the Roer Graben (northwest Europe). *Geophysical Journal International*, 132 (2), 347–362. <https://doi.org/10.1046/j.1365-246x.1998.00428.x>.
- › Camelbeeck, T., Vanneste, K., Alexandre, P., Verbeeck, K., Petermans, T., Rosset, P., Mazzotti, S., 2007. Relevance of active faulting and seismicity studies to assessments of long-term earthquake activity and maximum magnitude in intraplate northwest Europe, between the Lower Rhine Embayment and the North Sea. In: Stein, S., Mazzotti, S., (Eds.), *Continental Intraplate Earthquakes: Science, Hazard, and Policy Issues*, Special Paper 425, Geological Society of America, Boulder, Colorado, 193–224.
- › Cohen, K.M., 2003. Differential Subsidence Within a Coastal Prism: Late-Glacial-Holocene Tectonics in the Rhine-Meuse Delta, the Netherlands. (Doctoral dissertation, Utrecht University)
- › Cohen, K. M., Gibbard, P. L., Weerts, H. J. T., 2014. North Sea palaeogeographical reconstructions for the last 1 Ma. *Netherlands Journal of Geosciences*, 93(1-2), 7-29.
- › Cohen, K.M, Stouthamer, E., Berendsen, H.J.A., 2002. Fluvial deposits as a record for late Quaternary neotectonic activity in the Rhine-Meuse delta, the Netherlands. *Netherlands Journal of Geosciences - Geologie en Mijnbouw*, 81, 389–405
- › Cohen, K.M., Stouthamer, E., Pierik, H.J., Geurts, A.H., 2012. Rhine-Meuse delta studies’ digital basemap for delta evolution and palaeogeography. Department of Physical Geography, Universiteit Utrecht, Digital Dataset, DANS (accessed November 10, 2016). <https://doi.org/10.17026/dans-x7g-sjtw>.
- › Data en Informatie van Nederlandse Ondergrond (DINOloket), (2019). DINOloket, <https://www.dinoloket.nl>. (accessed November 11, 2019).

- › Demoulin, A., Hallot, E., 2009. Shape and amount of the Quaternary uplift of the western Rhenish shield and the Ardennes (western Europe). *Tectonophysics*, 474(3-4), 696-708.
- › De Mulder, E.F.J., Geluk, M.C., Ritsema, I., Westerhoff, W.E., Wong, T.E., 2003. De ondergrond van Nederland. *Geologie van Nederland*. Nederlands Instituut voor Toegepaste Geowetenschappen TNO: 379 pp
- › Erkens, G., 2009. *Sediment Dynamics in the Rhine Catchment: Quantification of Fluvial Response to Climate Change and Human Impact*. (Doctoral dissertation, Utrecht University)
- › Erkens, G., Hoffmann, T., Gerlach, R., Klostermann, J., 2011. Complex fluvial response to late glacial and Holocene allogenic forcing in the lower Rhine valley (Germany). *Quaternary Science Reviews* 30, 611–627.
- › Gouw, M. J. P., & Erkens, G., 2007. Architecture of the Holocene Rhine-Meuse delta (the Netherlands)-a result of changing external controls. *Netherlands Journal of Geosciences*, 86(1), 23-54.
- › Geluk, M. C., Duin, E. T., Duser, M., Rijkers, R. H. B., Van den Berg, M. W., Van Rooijen, P., 1994. Stratigraphy and tectonics of the Roer Valley Graben. *Geologie en Mijnbouw*, 73, 129-129.
- › Gold, R. D., Friedrich, A., Kübler, S., Salamon, M. 2017. Apparent Late Quaternary Fault-Slip Rate Increase in the Southern Lower Rhine Graben, Central Europe. *Bulletin of the Seismological Society of America*, 107(2), 563-580.
- › Hijma, M. P., Cohen, K. M., 2011. Holocene transgression of the Rhine river mouth area, The Netherlands/Southern North Sea: palaeogeography and sequence stratigraphy. *Sedimentology*, 58(6), 1453-1485.
- › Hijma, M.P., Cohen, K.M., Hoffmann, G., Van der Spek, A.J.F., Stouthamer, E., 2009. From river valley to estuary: the evolution of the Rhine mouth in the early to middle Holocene (western Netherlands, Rhine-Meuse delta). *Netherlands Journal of Geosciences - Geologie en Mijnbouw*, 88, 13–53.
- › Hijma, M. P., Cohen, K. M., Roebroeks, W., Westerhoff, W. E., & Busschers, F. S., 2012. Pleistocene Rhine–Thames landscapes: geological background for hominin occupation of the southern North Sea region. *Journal of Quaternary Science*, 27(1), 17-39.
- › Houtgast, R. F., Van Balen, R. T., 2000. Neotectonics of the Roer Valley rift system, the Netherlands. *Global and Planetary Change*, 27(1-4), 131-146.
- › Houtgast, R.F., Van Balen, R.T., Bouwer, L.M., Brand, G.B.M., Brijker, J.M., 2002. Late Quaternary activity of the Feldbiss Fault Zone, Roer Valley Rift System, the Netherlands, based on displaced fluvial terrace fragments. *Tectonophysics*, 352, 295–315. [https://doi.org/10.1016/S0040-1951\(02\)00219-6](https://doi.org/10.1016/S0040-1951(02)00219-6).
- › Janssens, M.M., Kasse, C., Bohncke, S.J.P., Greaves, H., Cohen, K.M., Wallinga, J., Hoek, W.Z., 2012. Climate-driven fluvial development and valley abandonment at the last glacial-interglacial transition (Oude IJssel-Rhine, Germany). *Netherlands Journal of Geosciences - Geologie en Mijnbouw* 91, 37–62
- › Kasse, C., 1988. *Early-Pleistocene tidal and fluvial environments in the southern Netherlands and northern Belgium*. (Doctoral Dissertation, Vrije Universiteit Amsterdam)
- › Kasse, C., Van Balen, R. T., Bohncke, S. J. P., Wallinga, J., Vreugdenhil, M., 2017. Climate and base-level controlled fluvial system change and incision during the last glacial–interglacial transition, Roer river, the Netherlands–western Germany. *Netherlands Journal of Geosciences*, 96(2), 71-92.

- › Kasse, C., Hoek, W.Z., Bohncke, S.J.P., Konert, M., Weijers, J., Cassee, M., Van der Zee, R., 2005. Late glacial fluvial response of the Niers-Rhine (western Germany) to climate and vegetation change. *Journal of Quaternary Science* 20, 377–394.
- › Kasse, C., Vandenbergh, J., Bohncke, S.J.P., 1995. Climatic change and fluvial dynamics of the Maas during the Late Weichselian and Early Holocene. In: Frenzel, B., Vandenbergh, J., Kasse, C., Bohncke, S.J.P., Glaser, B. (Eds.), *European River Activity and Climate Change during the Lateglacial and Early Holocene*. *Palaoklimaforschung*, Vol. 14. ESF Project “European Palaeoclimate and Man,” Special Issue 9. Gustav Fischer Verlag, Stuttgart, pp. 123–150
- › Kemna, H. A. 2008. A revised stratigraphy for the Pliocene and Lower Pleistocene deposits of the Lower Rhine Embayment. *Netherlands Journal of Geosciences*, 87(1), 91-105.
- › Kemna, H.A., 2005. Pliocene and Lower Pleistocene Stratigraphy in the Lower Rhine Embayment, Germany. (Doctoral dissertation. Universität Köln).
- › Kiden, P., Denys, L., Johnston, P., 2002. Late Quaternary sea-level change and isostatic and tectonic land movements along the Belgian–Dutch North Sea coast: geological data and model results. *Journal of Quaternary Science*. 17(5-6), 535-546.
- › Klostermann, J., 1983. *Die Geologie der Venloer Scholle (Niederrhein)*. Geologisches Landesamt Nordrhein-Westfalen, Krefeld
- › Kooi, H., Johnston, P., Lambeck, K., Smither, C., Molendijk, R., 1998. Geological causes of recent (~ 100 yr) vertical land movement in the Netherlands. *Tectonophysics*, 299(4), 297-316.
- › Kooi, H., Hettema, M., Cloetingh, S., 1991. Lithospheric dynamics and the rapid Pliocene-Quaternary subsidence phase in the southern North Sea basin. *Tectonophysics*, 192(3-4), 245-259.
- › LANUV (Landesamt für Natur, Umwelt und Verbraucherschutz Nordrhein-Westfalen), (n. d.). Pegel daten Stah in Hydrologische Rohdaten Online (HYGON). <http://luadb.lids.nrw.de/LUA/hygon/pegel.php?stationsinfo=ja&stationsname=Stah&ersterAufruf=aktuelle%2BWerte> (accessed 9 September 2018)
- › Michon, L. Van Balen, R.T., 2005. Characterization and quantification of active faulting in the Roer valley rift system based on high precision digital elevation models. *Quaternary Science Reviews*, 24(3-4), 455-472.
- › Michon, L., Van Balen, R.T., Merle, O., Pagnier, H., 2003. The Cenozoic evolution of the Roer Valley Rift System integrated at a European scale. *Tectonophysics*, 367, 101–126. [https://doi.org/10.1016/S0040-1951\(03\)00132-X](https://doi.org/10.1016/S0040-1951(03)00132-X).
- › Paulissen, E., Vandenbergh, J., Gullentops, F., 1985. The Feldbiss fault in the Maas valley bottom (Limburg, Belgium). *Geologie en Mijnbouw*, 64, 79-87.
- › Peeters, J., Busschers, F. S., & Stouthamer, E., 2015. Fluvial evolution of the Rhine during the last interglacial-glacial cycle in the southern North Sea basin: a review and look forward. *Quaternary International*, 357, 176-188.
- › Pons, L.J., 1954. Het fluviatiele laagterras van Rijn en Maas. [In Dutch] *Boor en Spade* 7, 110.
- › Rensink, E., Isarin, R.F.B., Ellenkamp, G.R., Heunks, E., 2015. Archeologische verwachtingskaart Maasdal tussen Mook en Eijsden. *DANS* (accessed October 20, 2016). <https://doi.org/10.17026/dans-xbe-977w>.
- › Schäfer, A., Siehl, A., 2002. Preface: Rift tectonics and syngenetic sedimentation-the Cenozoic Lower Rhine Basin and related structures. *Netherlands Journal of Geosciences*. 81 (2), 145–147. <https://doi.org/10.1017/S001677460002237X>

- › Schäfer, A., Hilger, D., Gross, G., Von der Hocht, F., 1996. Cyclic sedimentation in Tertiary Lower-Rhine Basin (Germany)—the ‘Liegendrücken’ of the brown-coal open-cast Fortuna mine. *Sedimentary Geology*, 103(3–4), 229–247. [https://doi.org/10.1016/0037-0738\(95\)00091-7](https://doi.org/10.1016/0037-0738(95)00091-7)
- › Schäfer, A., Utescher, T., Klett, M., Valdivia-Manchego, M., 2005. The Cenozoic Lower Rhine Basin—rifting, sedimentation, and cyclic stratigraphy. *International Journal of Earth Sciences*, 94(4), 621–639. <https://doi.org/10.1007/s00531-005-0499-7>
- › Schirmer, W., 1990. Rheingeschichte zwischen Mosel und Maas. *Deuqua-Führer*, 1, 295.
- › Schokker, J., 2003. Patterns and processes in a Pleistocene fluvio-aeolian environment (Doctoral dissertation, Utrecht University).
- › Schokker, J., Cleveringa, P., Murray, A.S., Wallinga, J., Westerhoff, W.E., 2005. An OSL dated middle and Late Quaternary sedimentary record in the Roer Valley Graben (southeastern Netherlands). *Quaternary Science Reviews*, 24(20–21), 2243–2264. <https://doi.org/10.1016/j.quascirev.2005.01.010>
- › Stouthamer, E., Berendsen, H. J. 2001. Avulsion frequency, avulsion duration, and interavulsion period of Holocene channel belts in the Rhine-Meuse delta, the Netherlands. *Journal of Sedimentary Research*, 71(4), 589–598.
- › Strahler, A. N., 1957. Quantitative analysis of watershed geomorphology. *Eos, Transactions American Geophysical Union*, 38(6), 913–920.
- › Tebbens, L.A., Veldkamp, A., Westerhoff, W., Kroonenberg, S.B., 1999. Fluvial incision and channel downcutting as a response to Late-glacial and Early Holocene climate change: the lower reach of the river Meuse (Maas), the Netherlands. *Journal of Quaternary Science* 14, 59–75
- › Vandenberghe, J., Paris, P., Kasse, C., Gouman, M., Beyens, L., 1984. Paleomorphological and Botanical evolution of small lowland valleys: A case study of the mark valley in northern Belgium. *Catena*, 11(1), 229–238.
- › Vanneste, K., Verbeeck, K., 2001. Paleoseismological analysis of the Rurand fault near Julich, Roer Valley graben, Germany: Coseismic or aseismic faulting history? *Geologie en Mijnbouw*, 80(3/4), 155–170.
- › Vanneste, K., Camelbeeck, T., Verbeeck, K., Demoulin, A., 2018. Morphotectonics and past large earthquakes in Eastern Belgium. In: Demoulin, A. (Eds) *Landscapes and Landforms of Belgium and Luxembourg*. *World Geomorphological Landscapes*. (215–236). Springer, Cham. https://doi.org/10.1007/978-3-319-58239-9_13.
- › Vanneste, K., Verbeeck, K., Camelbeeck, T., Paulissen, E., Meghraoui, M., Renardy, F., Jongmans, D., Frechen, M., 2001. Surface-rupturing history of the Bree fault scarp, Roer Valley graben: Evidence for six events since the late Pleistocene. *Journal of Seismology*, 5(3), 329–359.
- › Van Balen, R.T., Bakker, M.A.J., Kasse, C., Wallinga, J., Woolderink, H.A.G., 2019. A Late Glacial surface rupturing earthquake at the Peel Boundary fault zone, Roer Valley Rift System, the Netherlands. *Quaternary Science Reviews*, 218, 254–266.
- › Van Balen, R. T., Houtgast, R. F., Cloetingh, S. A. P. L., 2005. Neotectonics of The Netherlands: a review. *Quaternary Science Reviews*, 24(3–4), 439–454.
- › Van Balen, R.T., Houtgast, R.F., Van der Wateren, F.M., Vandenberghe, J., Bogaart, P.W., 2000. Sediment budget and tectonic evolution of the Meuse catchment in the Ardennes and the Roer Valley Rift System. *Global and Planetary Change*, 27, 113–129.

- › Van den Berg, M.W., 1996. Fluvial Sequences of the Maas: A 10 ma Record of Neotectonics and Climate Change at Various TimeScales. (Doctoral dissertation, Wageningen University)
- › Van den Berg, M. W., & Beets, D. J., 1987. Saalian glacial deposits and morphology in The Netherlands. *Tills and Glaciotectonics*. Balkema, Rotterdam, 235-251.
- › Van den Berg, M., Vanneste, K., Dost, B., Lokhorst, A., Van Eijk, M., Verbeeck, K., 2002. Paleoseismic investigations along the Peel Boundary Fault: geological setting, site selection and trenching results. *Netherlands Journal of Geosciences*, 81(1), 39–60. <https://doi.org/10.1017/S0016774600020552>.
- › Van den Toorn, J.C., 1967. Toelichtingen bij de geologische kaart van Nederland 1: 50.000 blad Venlo West 52W . Rijks Geologische Dienst, Haarlem.
- › Westerhoff, W.E., Kemna, H.A., Boenigk, W., 2008. The confluence area of Rhine, Meuse, and Belgian rivers: Late Pliocene and Early Pleistocene fluvial history of the northern Lower Rhine Embayment. *Netherlands Journal of Geosciences-Geologie en Mijnbouw*, 87(1), 107
- › Woolderink, H.A.G., Kasse, C., Grooteman, L.P.A., Van Balen, R.T., 2019. Interplay between climatic, tectonic and anthropogenic forcing in the Lower Rhine Graben, the Roer River. *Geomorphology*, 344, 25-45.
- › Woolderink, H. A. G., Kasse, C., Cohen, K. M., Hoek, W. Z., Van Balen, R. T., 2019. Spatial and temporal variations in river terrace formation, preservation, and morphology in the Lower Meuse Valley, The Netherlands. *Quaternary Research*, 91(2), 548-569.
- › Zagwijn, W.H., 1974. The palaeogeographic evolution of the Netherlands during the Quaternary. *Geologie en Mijnbouw* 5: 369-385
- › Zagwijn, W.H., 1989. The Netherlands during the Tertiary and the Quaternary: a case history of coastal lowland evolution. *Geologie en Mijnbouw*, 68, 107-120.
- › Zagwijn, W.H., 1986. Plio-Pleistocene climatic change: evidence from pollen assemblages. *Mem. Sot. Geol. It.* 31: 145-152.
- › Ziegler, P.A., 1994. Cenozoic rift system of western and central-Europe, an overview. *Geologie en Mijnbouw*, 73(2–4), 99–127.
- › Ziegler, P. A., 1992. European Cenozoic rift system. *Geodynamics of rifting*, 1, 91-111.
- › Zonneveld, JI, 1974. The terraces of the Maas (and the Rhine) downstream of Maastricht. *Annals of the Geological Society of Belgium*.

Chapter 3

Spatial and temporal variations in river terrace formation, preservation, and morphology in the Lower Meuse Valley, The Netherlands

Abstract

The Lower Meuse Valley crosses the Roer Valley Rift System and provides an outstanding example of well-preserved late glacial and Holocene river terraces. The formation, preservation, and morphology of these terraces vary due to reach-specific conditions, a phenomenon that has been underappreciated in past studies. A detailed palaeogeographic reconstruction of the terrace series over the full length of the Lower Meuse Valley has been performed. This reconstruction provides improved insight into successive morphological responses to combined climatic and tectonic external forcing, as expressed and preserved in different ways along the river. New field data and data obtained from past studies were integrated using a digital mapping method in GIS. Results show that late glacial river terraces with diverse fluvial styles are best preserved in the Lower Meuse Valley downstream sub-reaches (traversing the Venlo Block and Peel Block), while Holocene terrace remnants are well-developed and preserved in the upstream sub-reaches (traversing the Campine Block and Roer Valley Graben). This reach-to-reach spatial variance in river terrace preservation and morphology can be ascribed to tectonically driven variations in river gradient and subsurface lithology, and to river-driven throughput of sediment supply.

Published as: Woolderink. H. A. G., Kasse. C., Cohen. K. M., Hoek. W. Z., Van Balen, R. T., 2019. Spatial and temporal variations in river terrace formation, preservation, and morphology in the Lower Meuse Valley, The Netherlands. Quaternary Research, 91(2), 548-569.

3.1. Introduction

The behaviour of fluvial systems is in part controlled by internal processes determining hydraulic gradient, sediment mobility, channel dimensions, and rates of migration (Kleinmans and Van den Berg, 2010) and for the other part by response to external forcing such as climate change, base level fluctuations and tectonic conditions (Vandenberghe, 1995, 2003; Holbrook and Schumm, 1999; Blum and Tornqvist, 2000; Wang et al., 2014). For example, erosion by a river occurs whenever the sediment in transport is less than the transport capacity and the remaining stream power exceeds the erosion resistance of the subsurface (e.g., Van Balen et al., 2010). A river terrace can be defined as a patch of higher elevated former floodplain that was abandoned due to incision of the river (Leopold et al., 1964). In tectonically uplifting areas (or areas with another form of base-level lowering) fragments of such produced terraces, with a range of ages, tend to preserve along the sides of valleys. Climate-driven changes (either abrupt or gradual) in precipitation, vegetation cover, sediment supply, or the presence of permafrost can accentuate terrace formation, preservation, and style of dissection (e.g., Antoine et al., 2000; Blum and Tornqvist, 2000; Vandenberghe 2002, 2003; Bridgland and Westaway, 2008; Kleinmans and Van den Berg, 2010). The Meuse river provides an outstanding example of preservation of different fluvial styles in late glacial and Holocene river terraces in an active rift structure (Roer Valley Rift System, RVRS; Van Balen et al., 2000) and will, therefore, serve as a case study on variations in river terrace formation, preservation, and morphology due to tectonics.

Over the last decades, several studies have been performed on the Weichselian and Holocene terraces of the Lower Meuse Valley (LMV) between Maastricht and Nijmegen (Fig. 1; Pons and Schelling, 1951; Pons, 1954; Van Den Broek and Maarleveld, 1963; Van den Berg, 1989, 1996; Berendsen et al., 1995; Kasse et al., 1995, 2005; Huisink, 1997, 1999; Tebbens et al., 1999; Rensink et al., 2015; Isarin et al., 2017). These studies show a general consensus that the youngest terraces in the study area are climate-controlled and hold remnants of cold-stage braided river types, dating from the Weichselian Late Pleniglacial and Younger Dryas, and warm-stage meandering river types of Bølling-Allerød and Holocene age. Most of these existing studies, however, only cover restricted parts of the Meuse valley and/or are restricted to certain time periods (Fig. 2, see section LMV terrace stratigraphic schemes). An integrated temporal and spatial reconstruction of the geomorphic activity is however, lacking. Such a reconstruction is needed, as a river's response to an external forcing may vary along the river system, owing to both catchment and reach-specific characteristics (Schumm, 1981; Starkel et al., 2007; Erkens et al., 2009). It is likely that these regional and temporal variations in fluvial response are, in turn, represented in the formation, preservation, and morphology of river terraces, which has been insufficiently considered in the reconstructions produced so far. In this paper we, therefore, compile and synthesize existing information on dated features such as meander-scar fills, point bars, and aeolian dunes acquired from published and unpublished data, into a GIS database. In addition,

the database is extended with the wealth of new data, mainly from archaeological exploration, which has become available in the past years. Furthermore, new palynological interpretations and absolute dating of abandoned channel fills are provided for an area of specific interest. The results are presented as a terrace map as well as a series of palaeogeographic maps for the whole of the LMV. This detailed palaeogeographic reconstruction of the Lower Meuse Valley will then provide the basis for improved insight into regional and temporal variations in river terrace formation, preservation, and morphology.

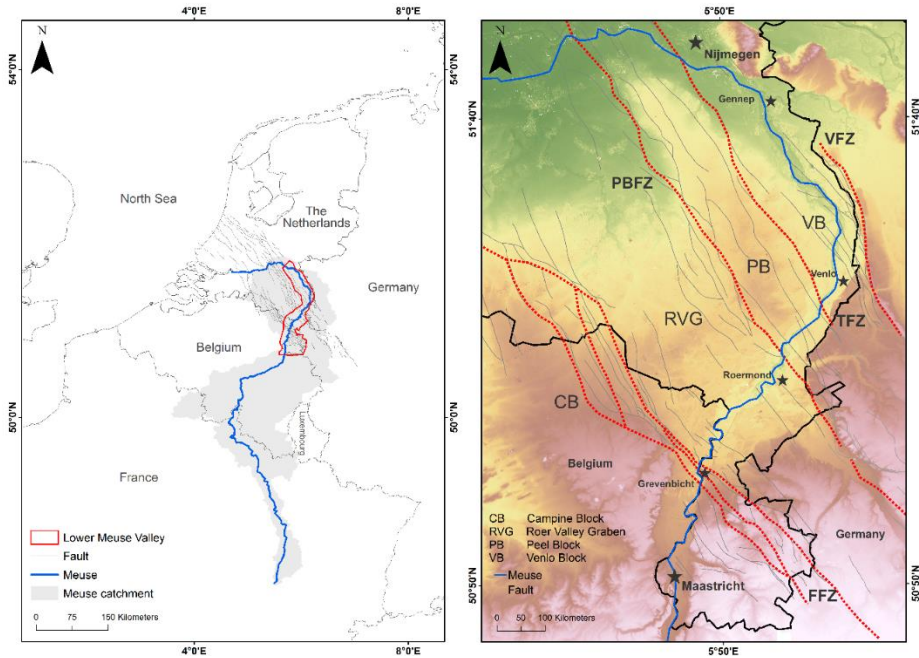


Fig. 1: The Meuse river (Figure 1A) and the position of the Lower Meuse Valley (LMV) within the Roer Valley Rift System (RVRS). Red dotted lines in Figure 1B indicate major fault zones of the RVRS that are crossed by the Meuse. FFZ, Feldbiss Fault Zone; PBFZ, Peel Boundary Fault Zone; TFZ, Tegelen Fault Zone; VFZ, Viersen Fault Zone. Coordinate system: WGS 1984/ UTM zone 31N.

3.2. Setting

The ~900-km-long rainfed river Meuse has a catchment size of 33,000 km². The Meuse has its headwaters in north-eastern France. From here it passes through the north-eastern part of the Paris Basin and the Ardennes Massif, where it is incised into bedrock, before entering the alluvial reach through the RVRS in the border region of Belgium and The Netherlands (Fig. 1). This active rift system is located in the southern Netherlands, north-eastern Belgium and adjacent parts of Germany (Houtgast and Van Balen, 2000). In the LMV, the annual mean discharge of the Meuse is approximately 250 m³ / s.

The bankfull discharge is $\sim 1500 \text{ m}^3/\text{s}$ at Maaseik (Belgium; Paulissen, 1973; Bogaart et al., 2003; Ward et al., 2009).

This study focuses on the segment of the Meuse (the LMV) between Maastricht and Nijmegen. This area provides the opportunity to study a well-preserved terrace morphology with light detection and ranging (LIDAR) data. In addition, the Meuse crosses several fault-bounded blocks of the RVRS within the LMV (Fig. 1), of which the tectonic activity is well-known (Geluk et al., 1994; Van den Berg, 1996; Houtgast and Van Balen, 2000; Cohen et al., 2002; Houtgast et al., 2002; Michon et al., 2003; Michon and Van Balen, 2005; Van Balen et al., 2005), making it a suitable area for studying the interaction between neotectonics and fluvial morphology. Several modest tributaries (Jeker, Geul, Geleenbeek, Rur, and Swalm) join the Meuse in the LMV, of which the Rur is the largest. A confluence between the Meuse and the Niers-Rhine course was present in the north of the study area (near Gennep, Fig. 1) during the last glacial maximum (LGM) and into the Weichselian late glacial (Van de Meene and Zagwijn, 1978; Huisink, 1999), which was presumably abandoned during the Younger Dryas/Early Holocene transition (Kasse et al., 2005; Janssens et al., 2012). The study area extends a little further north to enter regions where continuations of the Meuse terraces lay buried below younger deposits of the Rhine-Meuse delta (Berendsen and Stouthamer, 2001; Cohen et al., 2002, 2009, 2012; Hijma et al., 2009).

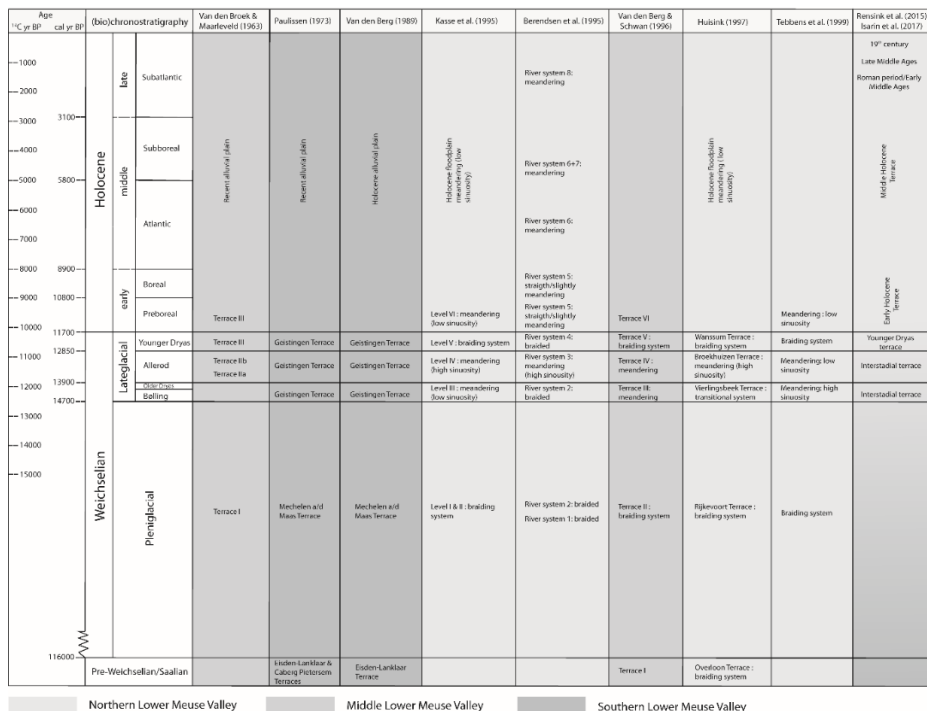


Fig. 2: Overview of the existing terrace stratigraphic schemes for the Weichselian and Holocene terraces of the Lower Meuse Valley. Subdivision of the Holocene after Zagwijn (1986).

3.2.1 Tectonical and sedimentary setting

The horst-graben structure of the RVRS comprises the Campine Block (CB), Roer Valley Graben (RVG), Peel Block (PB), and Venlo Block (VB), respectively (Fig. 3). The CB and PB are expressed as topographic highs while the RVG and VB are lows within the topography of the region (Fig. 1 and 3). The Feldbiss Fault Zone (FFZ), consisting of the Heerlerheide (HH), Geleen (GF), and Feldbiss (FF) faults, separates the subsiding RVG from the CB in the south, whereas the Peelboundary Fault Zone (PBFZ) forms the boundary between the RVG and PB in the north. The Koningsbosch (KB) and Beegden (BE) faults delineate a small horst within the subsiding RVG. The boundary between the PB and the relative subsiding VB is situated along the Tegelen Fault Zone (TFZ; Fig. 3). The present-day extension phase of the RVRS started during the Late Oligocene and experienced a change of the extension direction from a WNW-ESE to a NE-SW direction since the Early Miocene (Geluk et al., 1994; Van Balen et al., 2002a, 2002b, 2005; Michon et al., 2003). Geluk et al. (1994) indicate that the central RVG subsided ~1000–1200 m while the PB experienced no more than 200 m of subsidence. The Quaternary subsidence history of the RVRS was studied in detail by Houtgast and Van Balen (2000), who concluded that the average subsidence rate of the RVG was ~60–90 mm/ka during the Quaternary, whereas the PB and CB subsided with a rate of 46 mm/ka and 27 mm/ka, respectively.

The displacement rate along the FFZ showed to be around 41–71 mm/ka since the middle and late Pleistocene, while the displacement along the PBFZ ranged between 50–78 mm/ka since the Late Pleniglacial (Houtgast and Van Balen, 2000; Cohen et al., 2002; Michon and Van Balen, 2005). The uplift of the Ardennes, upstream of the RVRS, has resulted in a relatively complete fluvial terrace sequence of the last 5–10 glacial cycles. Moreover, within the RVRS, active differential subsidence has caused terraces and buried terraces to be preserved over the same time span (Van den Berg, 1996; Van Balen et al., 2000). In the LMV study area, this resulted in marked differences in the lithology of the subsurface where the river crosses different terrace bodies preserved at different tectonic blocks (Fig. 3). The longitudinal profile of the (Holocene) LMV, which is characterized by an upstream part with a relatively high valley gradient (~0.5 m/km) and a flatter downstream part with a gradient of ~0.15 m/km, shows a knick in slope that roughly coincides with a change in the subsurface lithology. Fine marine and coastal deposits of Miocene age are present in the shallow subsurface of the PB and northern part of the CB (Fig. 3). Within the RVG these deposits are found at a depth of over 200 m. The shallow subsurface of the RVG consist primarily of coarse fluvial deposits of Rhine and Meuse. The shallow subsurface of the VB, and to a lesser extent the northern most part of the CB, is composed of fine fluvial sediments. These fine-grained fluvial sediments are, however, absent on the PB (Fig. 3). Finally, a thin cover (~0–15 m) of coarse fluvial sediments of the Meuse is found over the whole course of the LMV, which partly corresponds to the active layer of the river bed (~1 m).

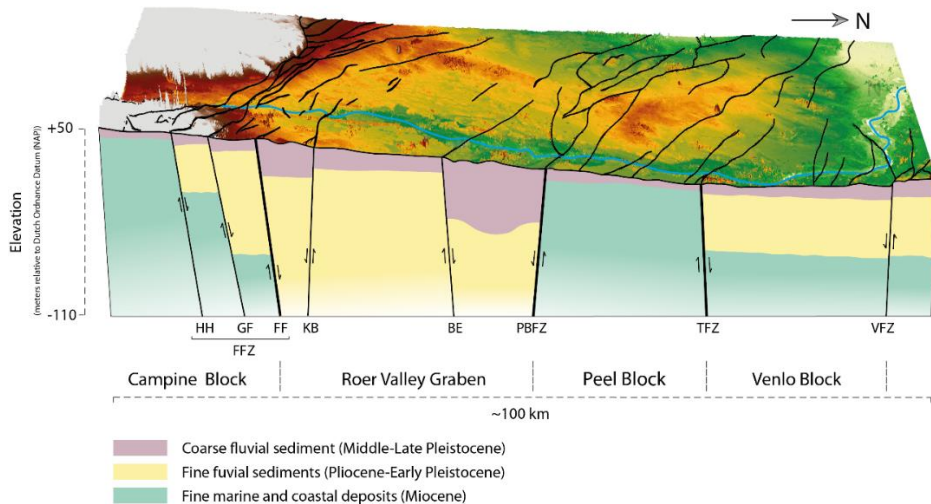


Fig. 3: Schematic lithological cross section of the Lower Meuse Valley. Cross section is based on lithological borehole data of the Geological Survey of The Netherlands (DINOloket, 2017).

3.2.2 Climate change and vegetation development

Vegetation is a major controlling factor in river activity and morphology, as it influences bank/bar stability, sediment load, and discharge (Kasse et al., 1995; Hoek, 1997; Vandenberghe, 2003). Furthermore, vegetation cover changes influence the availability of aeolian sediments on a local scale. Additionally, biostratigraphy can be used as a relative dating tool when the possibility for absolute dating is lacking. For this study, the regional late glacial-Early Holocene vegetation history for the northern LMV (Hoek et al., 2017), together with the biostratigraphy of a representative Holocene site (i.e., Well-Aijen; Bos and Zuidhoff, 2015), were used as a reference for (re)interpretation of palynological data. Figure 4 shows an overview of the late glacial and Holocene vegetation development in the LMV. Since vegetation development is linked to climate change, estimations of the mean annual temperature ($^{\circ}\text{C}$) and total annual precipitation (mm/yr) are given in Figure 4 for each “time-slice” of the late glacial and the Holocene based on Bogaart and Van Balen (2000). Figure 4 also gives an indication of the mean annual peak flood discharge (Q_{at}), as such bankfull discharges are assumed to be responsible for most of the morphodynamic changes in a river system. Modelled discharges based on GCM output and data on land cover change showed a 6.6% increase in mean annual discharge and a decrease in recurrence time of high flow events ($Q > 3000 \text{ m}^3 \text{ s}^{-1}$) for the Late Holocene (compared to the Middle Holocene; Ward et al., 2008). Deforestation and the start of large-scale agriculture are indicated to be responsible for the modelled change in discharge regime and a threefold increase in suspended sediment yield (Ward et al., 2008, 2009).

3.2.3 Vegetation changes during the Weichselian late glacial and Holocene

Pollen analyses show that a sparse vegetation cover was present during the Late Pleniglacial (~19.0–14.7 ka), although many places were barren due to the low mean annual temperatures and total precipitation. This period is characterized by deposition of aeolian cover sands interbedded with deflation horizons (Kasse et al., 2007). Due to a rise in temperature, a dwarf shrub and herbaceous plant cover could develop during the earliest phase of the late glacial, which can be considered as the transition from tundra towards shrub-tundra (Hoek and Bohncke, 2002). As a result of continued warming and increased precipitation during the Bølling (~14.7–14.0 ka), a predominantly open landscape with birch shrubs and birch trees developed (Hoek and Bohncke, 2002). The subsequent short Older Dryas period (~14.0–13.9 ka) is characterized by a relative open landscape with sparse vegetation, which locally led to renewed aeolian deflation and deposition. Although temperatures and precipitation were supposedly not as high as during the Bølling, a rather open *Betula* forest developed during the *Betula* phase of the Allerød (~13.9–12.85 ka) after which *Pinus* started to dominate and the landscape changed into a pine forest during the second phase of the Allerød. As temperature decreased at the start of the Younger Dryas (~12.85–11.7 ka) the vegetation cover opened, leading to a steppe-like landscape (Hoek et al., 2017). During this period, the characteristic aeolian river dunes were formed along the eastern bank of the Meuse. Due to the colder climate and decreased vegetation cover, peak discharges increased substantially during the Younger Dryas. The transition from the late glacial into the Holocene is characterized by a strong increase in temperature and precipitation. This climatic “improvement” resulted in the gradual development of a dense birch forest during the first part of the Preboreal after which it was replaced by a pine forest during the last phase of the Preboreal (~11.7–10.8 ka).

The succeeding Boreal (~10.8–8.9 ka) is characterized by the immigration of thermophilous deciduous trees and shrubs (Fig. 4). During the course of the Boreal, the pine forest developed into a relatively open mixed deciduous forest (Bos and Zuidhoff, 2015). The expansion of this mixed deciduous forest continued during the Atlantic (~8.9–5.8 ka). During the latter part of the Atlantic, the landscape gradually opened due to the first occurrence of farmers in the Meuse valley (Bos and Zuidhoff, 2015). The occurrence of *Fagus* is characteristic for the Subboreal (~5.8–3.1 ka). The start of the Subatlantic (~3.1–0 ka) still experienced a relatively closed vegetation cover, although expanding agriculture led to a more open landscape with an increase of grasses, heathers, and cereals later on during the Subatlantic (Bos and Zuidhoff, 2015).

Age 14C yr BP	cal yr BP	(bio)chronostratigraphy		Characteristic pollen assemblage	T (°C)	P (mm/year)	E (mm/year)	Qaf (m3/s)
1000		Holocene	late	Subatlantic	9.6	734	466	1300
2000								
3000	3100							
4000			middle	Subboreal				
5000	5800							
6000			Atlantic					
7000								
8000	8900	Weichselian	early	Boreal	2.6	648	322	2700
9000	10800			Preboreal				
10000	11700		Lateglacial	Younger Dryas				
11000	12850			Allerød				
12000	13900	Older Dryas						
13000	14000		Bolling	8.1	698	429	1600	
14000	14700							
14000			Pleniglacial		-2.1	478	222	2000
15000								

Fig. 4: Overview of the regional late glacial (after Hoek et al., 2017) and Holocene (after Bos and Zuidhoff, 2015) vegetation history of Lower Meuse Valley together with the reconstructed mean annual temperature, T (°C); total annual precipitation, P (mm/yr); total annual evapotranspiration, E (mm/yr); and mean annual flood discharge, Qaf (m³/s) (after Bogaart and Van Balen, 2000). Late glacial biochronostratigraphy after Hoek (1997) and Holocene after Zagwijn (1986).

3.2.4 Existing Lower Meuse Valley terrace stratigraphic schemes

Several terrace stratigraphic schemes have been proposed during the last decades for the Weichselian and Holocene terraces of the LMV (Fig. 2). The northern LMV (between Venlo and Nijmegen) is the most intensively studied reach due to the well-preserved terrace fragments, with clearly recognizable fluvial styles. Terrace maps based on soil development were made by Schelling (1951), Pons and Schelling (1951), Pons (1957), and Miedema (1987). Detailed geomorphological maps were produced by Buitenhuis and Wolfert (1988) and Wolfert and De Lange (1990). Kasse et al. (1995) and Huisink (1997) discriminated terrace levels using a combination of elevation, morphology, sedimentology, and palynological data. Tebbens et al. (1999) based their subdivision on morphology and a large number of radiocarbon dates (40) of basal residual channel infillings. Additionally, Berendsen et al. (1995) introduced a division of the buried terrace surfaces in the most northern part of the study area, based on a set of 14,000 hand

borings and dated basal organic channel fills, which was expanded upon by Cohen et al. (2002) and Cohen (2003). These studies discriminated late glacial and Early Holocene terraces and channel belts based on elevation, buried-surface morphology and pedogenesis, architecture, lithology, pollen, and ^{14}C -dating.

The middle LMV (between Grevenbicht and Venlo), which comprises the RVG and PB, was studied by Van den Broek and Maarleveld (1963) and Van den Berg and Schwan (1996). They based their terrace scheme on differences in elevation, fluvial style, and soil development.

The Dutch part of the southern LMV (between Maastricht and Grevenbicht) has been studied by Van den Berg (1989). He established his results on relief, morphology, and terrace correlation based on gradient lines. Later on, Houtgast et al. (2002) partly updated the terrace stratigraphy for the Meuse terraces around the FFZ. The terraces in the Belgian part of the southern LMV were investigated by Paulissen (1973). In this work, the terraces are discriminated based on a combination of morphological and geological mapping, radiocarbon dating, and sediment analysis. Thus, although several studies are available for the LMV, an integrated temporal and spatial reconstruction of the Lower Meuse geomorphological activity since the Weichselian last glacial maximum is lacking. Recently, Rensink et al. (2015) and Isarin et al. (2017) produced a map of terraces with ages starting from the Younger Dryas. Their map covers the entire LMV and is based on geoarcheological investigations, morphology (digital elevation model), and absolute and relative dating. However, due to the archaeological focus, their map is partly inconsistent with fluvial morphologic principles. Moreover, Late Pleniglacial and early late glacial terraces are missing from their palaeogeographic reconstructions. This study presents an internally consistent and detailed palaeogeographic reconstruction of the whole LMV, based on stratigraphic principles and genetic points of view. Our terrace map starts at the Weichselian last glacial maximum and thus includes several important climatic transitions. Thus, in comparison to Rensink et al. (2015), our terrace map focuses on dynamic fluvial evolution and covers a longer time span. In addition, it is also based on more and partly new data. We use the reconstructions in order to address regional differences in responses to external forcings within a river system, which has been insufficiently considered up to now despite the well-known tectonic activity.

3.3 Methods

3.3.1 Lithological cross sections and cores

Transects were hand cored over abandoned channels at selected locations, identified in LIDAR imagery (AHN2, 2017). The transects served to find the most suitable sampling locations for radiocarbon dating and/or pollen analysis on abandoned-channel fills. Reconnaissance coring used a soil auger, a 20-mm diameter gouge, and occasionally a suction corer to retrieve water logged sandy sediments from below the groundwater table. Sediments were described in the field for lithology, carbonate content, colour, grainsize (NEN 5104), and presence of plant remains. At sites of thickest infill, sediment cores were taken in meter-long sections with a modified Livingstone piston sampler and, in case of sandy or compacted peat, with a 60-mm diameter gouge. Cores were wrapped in plastic foil, transported, and stored in a cool room. Sediment cores Maaseik and Oude Hoeve Meeswijk were subsampled in the field because of the fragile state of the cores.

3.3.2 Radiocarbon dating

Materials for radiocarbon dating were picked from split core halves on inspection of the sediments in the laboratory, targeting botanic macrofossils. Selected subsamples (slices of core material, 1–2 cm thick) were treated with diluted potassium hydroxide (peat samples) or disodium pyrophosphate (clayey samples), to disperse organic compounds or clay bonds, respectively. Subsequently the samples were wet sieved over a 200 μm mesh. Terrestrial macro remains were extracted from the remaining sample material by use of a binocular microscope and identified to species level. Table 1 shows the sample depth, sampled material, and the macro remains selected for radiocarbon dating. The macro remains were (AMS) radiocarbon dated at the Beta Analytic laboratory (Miami, Florida).

3.3.3 Digital Mapping

Digital mapping was performed making use of a GIS system originally developed for the Rhine-Meuse delta. The system splits mapping of geomorphological elements (individual meander scars, terrace fragments) from cataloguing naming, dating, and literature referencing results for individual elements (Berendsen et al., 2001, 2007; Cohen et al., 2012). The coverage of the GIS database was extended to include the full study area. Existing information on dated geomorphological features, such as fine-grained meander-scar fills, point bars, and aeolian dunes, was acquired from published sources and institutional databases (i.e., from journal papers, archaeological reports, and geological survey mapping activities) and made browsable in GIS (Fig. 5A). Furthermore, geomorphological datasets of continuous cover (e.g., AHN2 [2017])

LIDAR data, Fig. 5B), lithological databases (cores and outcrop descriptions; from new fieldwork in this study, but also abundant pre-existing data from institutional databases), and earlier mappings (geological, geomorphological, pedological, archaeological, and historical) were collected. Using GIS visualization and geological analysis, this dataset was manually (re)interpreted to the geomorphological and geological maps featured in this paper. These maps honor the dating information as well as the geomorphic crosscutting relations (Fig. 5C). The embedded geological reconstruction is described in the further sections of this paper. The morphostratigraphic correlation decisions at the level of individual meander/terrace fragment elements (polygons in the GIS layer, newly digitized), are described in the catalogue part of the database (Fig. 5D). Linkage of GIS polygons and dating information stored in the catalogue (using channel belt and terrace fragment identification numbers [#IDs]), allows quick generation of a terrace or age map (Fig. 5E) as well as time-slice map series of the palaeogeographic evolution (Fig. 5F). In this way, the GIS becomes a tool for iterative partial improving of the reconstruction (Berendsen et al., 2007; Cohen et al., 2012; Pierik et al., 2016) and not just a storage and visualization system.

In order to produce internally consistent geological-geomorphological maps and palaeogeographic reconstructions, it is essential to assign an age to each terrace remnant in an architecturally correct manner. In this study, we map and date terrace morphology from successive stages of river abandonment. The final stage of river bed sedimentary activity is therefore considered as the moment that produces the “end date” of a channel. In other words, the last stage in which flow through the channel is capable of bedload transport, is considered to be the last moment at which a channel was morphologically active and featured in the terrace age maps. Ages obtained from organics at the base of a finegrained channel infill, for our study, provide a minimum age of channel activity (a terminus ante quem date for this activity) and are therefore, in most cases, assumed to be the end of river bed activity. In the same philosophy (dated) overbank deposits provide a minimum age for the underlying riverbed sediments. Terrace remnants that are not directly dated are nevertheless attributed with an “end date” based on correlation (i.e., height, morphology, lithology, and historical maps) to locations where dates are obtained. Due to incision of the Meuse since the Late Pleniglacial, relative elevation at local scale provides a means for such correlation. It should, however, be emphasized that correlation of intra-Holocene terraces is, in some cases, difficult based on height differentiation alone. In these cases, other correlation methods (e.g., lithology, spatial continuity of geomorphological features, and historical maps) become more important in the correlation of individual terrace fragments.

The mapping uses a customized color legend consisting of 12 age classes for the staircase of Meuse terraces. One unit covers pre-LGM time, eight units LGM to Early Holocene, and three units the rest of the Holocene period. The legend uses age boundaries that for the late glacial follow Hoek et al. (2017) and for the Holocene subdivision follow

Zagwijn (1986; IntCal13 recalibrated). In parts of the mapping the dating resolution is still suboptimal and we therefore used broader Holocene age-classes, grouping them into an early- (Preboreal and Boreal; ca. 11.7–8.9 ka), middle- (Atlantic and Subboreal, ca. 8.9–3.1 ka), and Late Holocene (Subatlantic, youngest 3.1 ka) age class. It should be stressed that whenever the adjectives “early,” “middle,” and “late” are used for the Holocene in this paper they refer to the subdivisions indicated above. The capitalized form “Early,” “Middle,” and “Late” Holocene is used whenever we refer to the formal subdivision of the Holocene Series/Epoch as defined by Walker et al. (2012). The map time series (Fig. 5F) distinguishes active channel belts and abandoned terrace fragments, and uses shading to indicate “later reworked” from “preserved up to present” (as in Berendsen and Stouthamer [2001] and Cohen et al. [2012]). This palaeogeographical reconstruction output allows us to calculate (and conceptually optimize through iterative editing) the spatial extent of the active channel belt as it varied through space and time. It is emphasized here that the map series displays the eventually reached width at the end of activity as catalogued for each discriminated unit (the above #IDs). Owing to lateral migration activity in phases prior to abandonment, this displays a somewhat larger width than the river channel would have had at any instantaneous moment (i.e., channel belt width > active channel width). Both the map of the LMV Weichselian and Holocene terraces, as well as the map time series are projected in the Dutch national grid (Amersfoort/RD New). The GIS database and associated age and palaeogeographic maps are freely available for download at: <https://doi.org/10.17026/dans-xkk-f29b>.

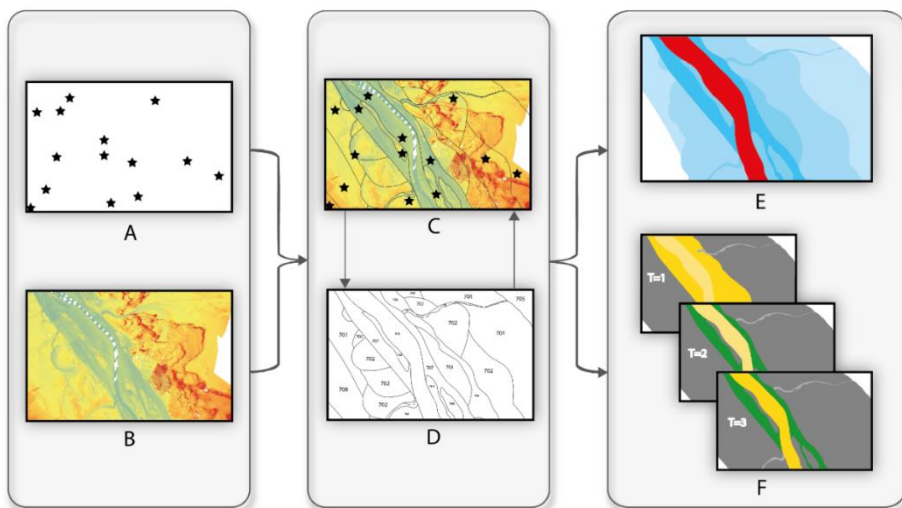


Fig. 5: Flowchart of the digital mapping method: (A) dated geomorphic features; (B) LIDAR data; (C) dating information as well as the geomorphic cross-cutting relations; (D) digitized terrace fragments (polygons) with attached catalogue part of the database; (E) terrace or age map output; and (F) time-slice map series of the palaeogeographic evolution. For more information, see main text.

3.4 Results

3.4.1 Database of sites with age control

A first aim of this study is to synthesize previous studies and create an overview of the status of data availability regarding the fluvial geomorphology along the Lower Meuse. At present, our database consists of 381 dates from 255 unique site locations, which include the four new sites presented in this study. The distribution of dating methods, as well as the dated time periods, are given in Figure 6. The majority of these dates (71%) are derived from channel fills and had direct dating of channel abandonment and accumulation of infill as their original purpose. Other dates were performed on, amongst others, aeolian dunes, point-bar deposits, bedload deposits, levees, and floodplain deposits. Of all the channel-fill dating's, 44% targeted the basal channel infill, whereas the rest was taken from higher up in the fill sequence (often in addition to sampling the very base). The reason for this, in some cases, has been the difficulty to pick suitable datable (organic) materials from channel fills that trapped clastic deposits in their initial filling phases. Figure 6 shows that only a small percentage of the dates is of (Late) Pleniglacial age. This might be due to a lack of datable organic material, or due to the fact that a large part of the (Late) Pleniglacial channels was reworked later on. The relatively high amount of Atlantic dates can be ascribed to the extensive peat formation, and therefore available climate archives, in many of the (upper) residual channel fills in the study area during this time (Cohen, 2003; Zuidhoff and Huizer, 2015). As over one-third of the dates were performed in an archaeological context, a peak in Subatlantic dates is to be expected as well. Although already a large amount of data is available within the current database, it is designed so that new data/sites can be easily added and is, therefore, a starting point rather than a finished product.

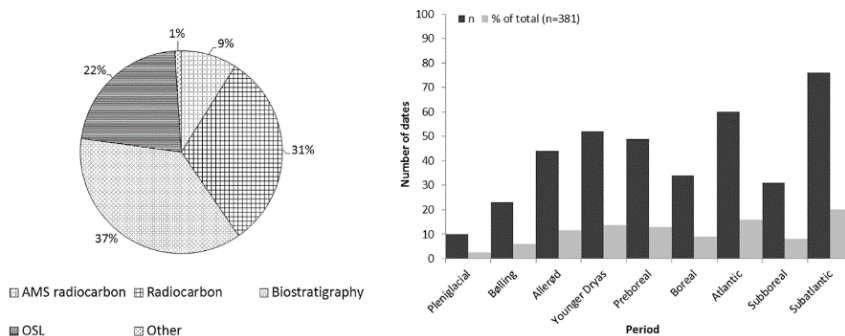


Fig. 6: Distribution of dating methods and dated time periods of Lower Meuse Valley sites with age control in the database.

Table 1: Location and dating results of the selected paleochannels.

Site name	x	y	Sample depth	Extracted Macro remains	Sample name	d ¹³ C	Conventional radiocarbon age
<i>Maaseik</i>	183306	346648	209- 207 cm	Leaf fragments / <i>Betula</i> seeds	Beta-454391: Meik212	-28	9160 +- 30 yr BP
<i>Vijverbroek</i>	185286	352934	390- 387 cm	Leaf fragments <i>Carex</i> seeds	Beta-454393: Vijv388.5	-27.1	2240 +- 30 yr BP
<i>Wurfeld</i>	181995	344665	290- 288 cm	Leaf fragments <i>Betula</i> seeds	Beta-454392: Wur2A289	-28.5	9720 +- 40 yr BP
<i>O.H. Meeswijk</i>	180522	334165	386- 376 cm	Leaf fragments	Beta-454394: BSI-381	-26.9	780 +- 30 yr BP

3.4.2 Newly dated channel fill sites

Cross sections were made over four newly investigated paleochannels and their (basal) infill was AMS ¹⁴C dated (Fig. 7A; Table 1 and Supplementary Information), as these channels are positioned in an area of specific interest, i.e., around the Feldbiss Fault zone, which is suspected to have a pronounced effect on the fluvial dynamics of the Meuse. Moreover, only few absolute dates were available for this region. The Vijverbroek meander was selected because it is a very distinct meander at the outer rim of the Holocene plain. It has laterally eroded the Pleniglacial terrace and could therefore provide an indication of the start of lateral erosion by Holocene channels in this region. Two of the four channels, the Wurfeld and Maaseik meanders (Fig. 7B), provided radiocarbon ages of 9720± 40 ¹⁴C yr BP (Beta-454392) and 9160 ±30 ¹⁴C yr BP (Beta-454391), indicating that these channels were abandoned during the Preboreal. The dates for the Wurfeld and Maaseik meanders also indicate the moment of the abandonment by avulsion of the meander belt of which they are part. The avulsive abandonment of the channels is supported by the lithology of the infillings. The lithological cross sections show that the Wurfeld meander, which is located upstream (Fig. 7), has a stage of clastic infill prior to the peat formation in the abandoned channel. This clastic infill indicates narrowing of the channel before a full cutoff, most likely representing the transitional stage of active abandonment as described by Toonen et al. (2012) for avulsion-abandoned channels. The fact that the Maaseik residual channel does not show such a distinct clastic channel infill may be ascribed to the more downstream position of this meander to the avulsion location.

The radiocarbon age of Oude Hoeve Meeswijk (780 ± 30 ^{14}C yr BP (Beta-454394); Fig. 7C) shows that this channel was abandoned during the Subatlantic. The infill of the Vijverbroek meander (Fig. 7D), dated to 2240 ± 30 ^{14}C yr BP (Beta-454393), indicates that the channel was abandoned at the beginning of the late Holocene.

3.4.3 Terrace map

The map of the LMV Weichselian and Holocene terraces (Fig. 8) shows the preservation of terrace remnants by age of abandonment in ^{14}C yr BP. The boundaries of the age classes were also calibrated to cal yr BP (IntCal13) to enhance correlation with e.g., archaeological periods. Four AHN2 (2017) LIDAR-based topographic profiles were drawn over the course of the LMV. These are situated on the four different tectonic blocks to illustrate height differences between the successive terraces (Fig. 9). To illustrate the contrasts in fluvial style of the terrace fragments over different tectonic blocks along the course of the LMV, we highlight representative subareas in Figure 10. The classification of channel planform is based on Leopold and Wolman (1957), Nanson and Knighton (1996), and Kleinhans and Van den Berg (2010).

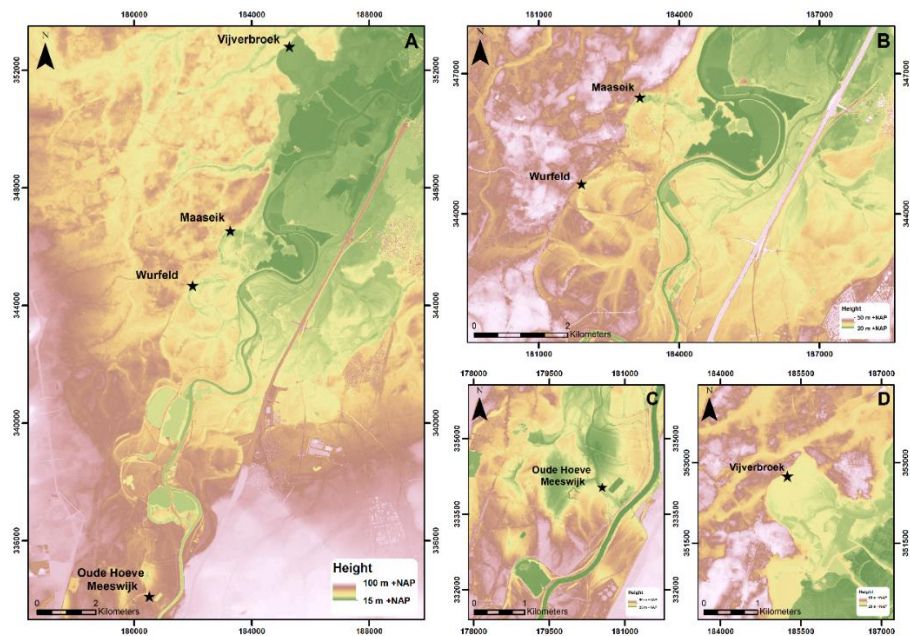


Fig. 7: (A) Location of the four new AMS ^{14}C -dated paleochannels in the southern Lower Meuse Valley, (B) Wurfeld and Maaseik core locations, (C) Oude Hoeve Meeswijk core location, and (D) Vijverbroek core location. Cross sections can be found in the supplementary material.

3.4.3.1 Topographic profiles

Overall, the topographic profiles (Fig. 9) indicate that the height differentiation between the Weichselian Pleniglacial and late glacial terraces ($\Delta \sim 2\text{--}4$ m) is greater than that between the different Holocene paleofloodplains ($\Delta \sim 1\text{--}1.5$ m). The profiles also show that the height differentiation between the successive terrace remnants is more pronounced on the VB (profile A-A') and especially the PB (profile B-B') compared to the RVG (profile C-C') and CB (profile D-D'), where differentiation between successive terrace remnants in the latter two may be as small as ~ 0.5 m.

3.4.3.2 General overview

The terrace map shows that late glacial terrace remnants are well-preserved on the VB and PB. Holocene terrace remnants are, on the other hand, best preserved in the south, on the CB and in the RVG. The overall trend on the VB and PB is that of an incising and narrowing river plain, preserving a set of successive river terraces (Fig. 8 and 9). An exception to this is the ca. 1000-yr-long Allerød period, during which individual meanders seem to have widened (by lateral migration) compared to Bølling precursors (Fig. 8). The CB and RVG show a less complete preservation of successive river plains and late glacial terrace remnants are scarce. A broad amalgamation of middle and late Holocene meanders is present (Fig. 8), especially where the river enters the RVG from the CB. The average width of the complete Holocene river plain is approximately 1400 m on the VB (Fig. 9; profile A-A') and 550 m on the PB (profile B-B') compared to ~ 3000 m in the RVG (profile C-C') and ~ 2000 m on the CB (profile D-D').

3.4.3.3 Description of terrace remnants

Terrace remnants of LGM and Late Pleniglacial age are preserved throughout the LMV (Fig. 8). The LGM and Late Pleniglacial terrace fragments show a morphology of many low-sinuuous and shallow channels separated by multiple bars, indicating a braided river system. The maximum width of the LGM and Late Pleniglacial braidplain varies over the course of the LMV, from ~ 6000 m across the CB to 18,000, 8000 and 12,500 m in the RVG and on the PB and VB, respectively (Fig. 11A). Thus, starting at the CB, the braidplain first widens in the RVG, then narrows over the PB, before diverging again on the VB (Fig. 8). This suggests that the uplifted PB block acted as a bottleneck and choked the LGM braidplain width. Preservation of the LGM and Late Pleniglacial system is the same for the different tectonic blocks, except for the CB in the south. This is likely because here the LGM and Late Pleniglacial braidplain is bound by bedrock and by relatively coarse-grained Pre-Weichselian fluvial deposits. This limited valley width caused efficient reworking by the Meuse in the subsequent late glacial and Holocene (Fig. 8).

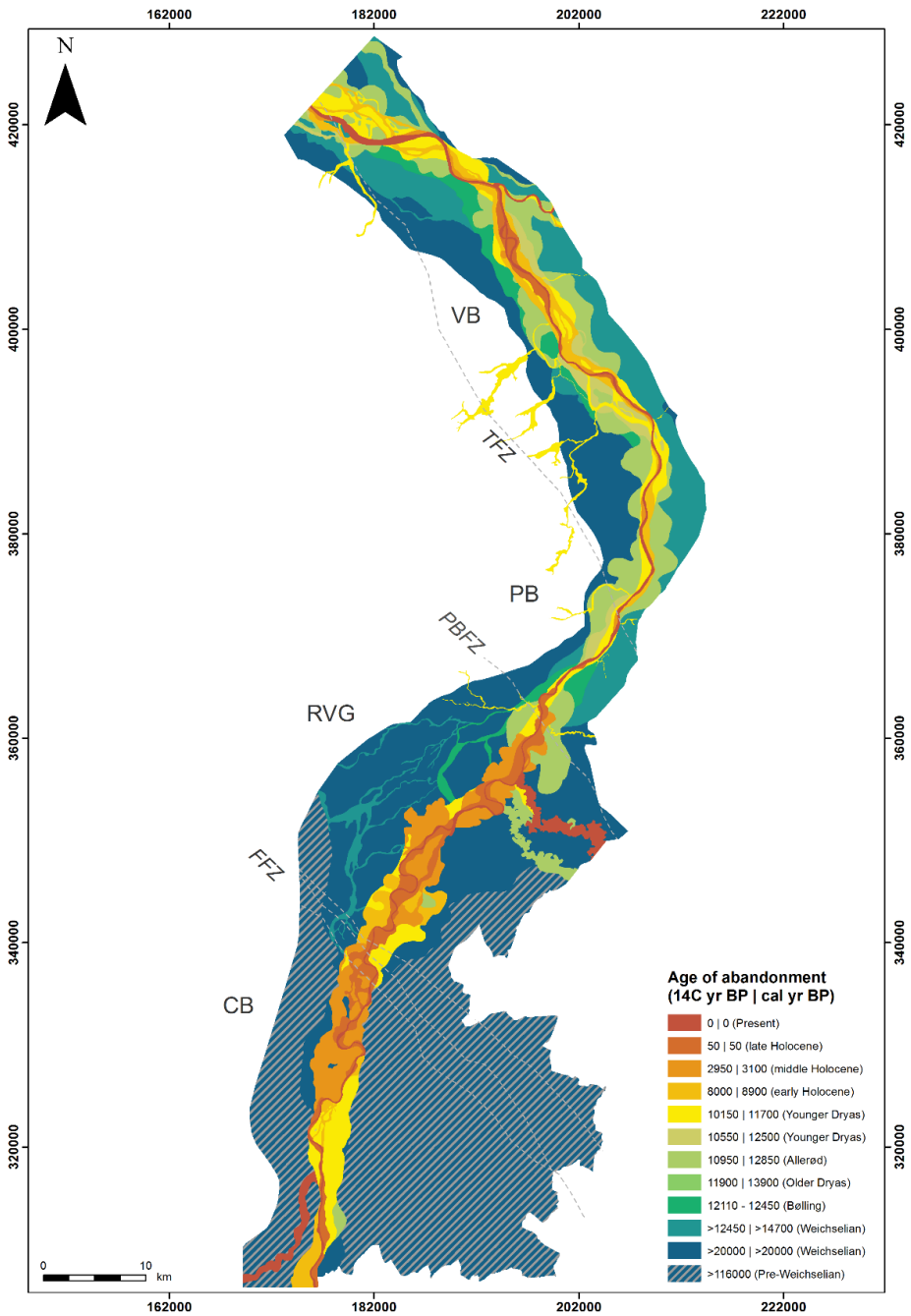


Fig. 8: Map of the Lower Meuse Valley Weichselian and Holocene terraces. The present-day channel of the Meuse is represented by 0 yr BP.

Preservation of the Bølling system is variable over the LMV. Bølling terrace remnants are present on the VB, PB, and in the RVG (Fig. 8). The terrace remnants show a low sinuosity, multi-channel planform (Fig. 10O–Q). The maximum width of the Bølling plain varies from ~7000 m in the RVG to ~3750 and ~5000 m on the PB and VB, again showing the bottleneck of the uplifting PB. Furthermore, the river system is narrower compared to the LGM and Late Pleniglacial braided plain (Fig. 11B). It is striking that no terrace remnants of Bølling age could be distinguished at the CB.

Allerød terrace remnants are primarily located on the VB and PB (Fig. 8) and contain a high-sinuosity meandering planform with point-bar ridges and swales (Fig. 10L and M). The lateral extent of the Allerød plain varies between ~3000 m and ~5000 m on the PB and VB, respectively. Lateral displacement of the Allerød meanders resulted in reworking of parts of the LGM, Late Pleniglacial, and Bølling terrace remnants (Fig. 11C). The CB holds only one Allerød terrace fragment of a large, low-sinuosity meander, preserved in the very south (Fig. 10N). In the RVG Allerød age meanders are only present in the north, bordering the PBFZ (Fig. 12A). This hampers reconstruction of the width of the Allerød meander belt (as presumed for this time) in a critical part of the study area that is the CB-RVG transition (Fig. 12C). The Allerød meander complex bordering the PBFZ (in part overbuild by the city of Roermond) has an anomalous (extremely high) sinuosity and scroll morphology. It, furthermore, shows upstream migration while all other Allerød meander forms show downstream migration.

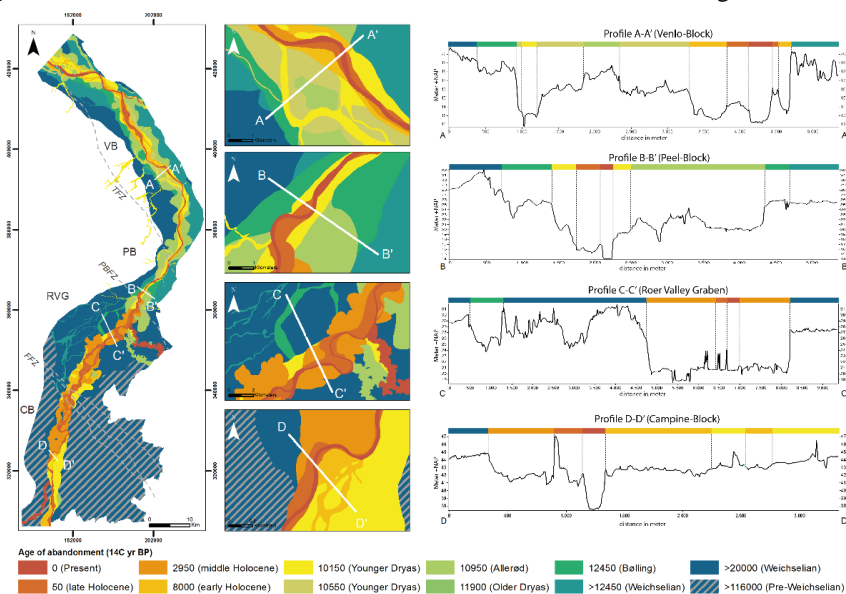


Fig. 9: LIDAR-based topographic profiles of the Lower Meuse Valley terrace sequence on the four different tectonic blocks. Profile A-A' on the Venlo Block; profile B-B' on the Peel Block; profile C-C' in the Roer Valley Graben; profile D-D' on the Campine Block. Topographic profiles include man-made structures (i.e. dikes, roads, and excavations) that were ignored for the interpretation of the terrace levels. Elevation is in meters relative to Dutch Ordnance Datum (NAP).

Remnants of the Meuse river system in the Younger Dryas are present throughout the LMV. However, preservation of the Younger Dryas system is marginal in the northern part of the CB and in the central RVG compared to the rest of the LMV. Terrace fragments of the Younger Dryas (Fig. 10H–K) show a morphology with multiple channels and bars, indicating a multi-channel to a braided river plain. At the transition between the CB and the RVG (i.e., around the FFZ), however, the palynologically dated Younger Dryas terrace fragments of Kingbeekdal, Dukkelaar, and Korbusch exhibit a meandering rather than a braided planform (Fig. 12; CD). The Younger Dryas braid belt width maximizes to ~5000 m on the CB, widens a bit to ~5700 m in the RVG, then narrows down to ~2000 m on the PB, after which it modestly widens again to ~3400 m on the VB. The Younger Dryas braidplain thus was significantly wider on the CB and in the RVG than across the PB and VB. On the PB and VB, the Younger Dryas river incised and narrowed its river plain compared to Allerød meandering and earlier braided stages (Fig. 9 and 11D).

Early Holocene terrace remnants are primarily observed on the VB. Their preservation is minimal on the CB and in the RVG. Remnants of this age are absent on the PB. Planform fluvial style of the early Holocene terrace patches differs between the VB and the CB-RVG transition zone (Fig. 10E–G). While in the RVG high-sinuosity meandering channels are present on the terrace fragments (Fig. 10F and 12C), the terrace remnants in the VB and CB show a multi-channel low-sinuosity planform (Fig. 10E, 10G, 11E). It should be noted that in the RVG Early Holocene channels of true meandering style have only been found just downstream of the FFZ. The width of the Early Holocene channel belts is at least ~1500 m on the CB (based on preserved remnants). A maximum for the estimated width is ~5000 m (similar to the Younger Dryas) if channel belt width of the Middle Holocene meander belt is assumed to be representative for the Early Holocene. The width of the Early Holocene river plain increases up to ~6000 m in the RVG. Further downstream it reduces to a maximum width of ~500 m on the PB (i.e., the space in-between preserved Younger Dryas fragments). The width of the Early Holocene plain increases to a maximum of ~2200 m on the VB. As in previous time periods, this indicates that the PB is a bottleneck in the width of the channel belt in the Early Holocene.

Middle Holocene terrace remnants have primarily been preserved on the CB and in the RVG (Fig. 8). On the PB and VB, they are present as part of a point-bar series. Middle Holocene terrace remnants have a low-sinuosity single channel planform at the VB and PB (Fig. 11F), while the terrace fragments in the RVG contain remnants of a highly sinuous meandering channel with lateral channel migration and crosscut channels (Fig. 10A–D). At the CB, the Middle (and Late) Holocene terraces comprise remnants indicating both a low-sinuosity planform (southern CB), with a narrow plain of ~700 m, as well as a high-sinuosity planform (northern CB) that has a maximum lateral extent of ~4500 m. Several small Pleniglacial and Younger Dryas terrace fragments are present within the Middle (and Late) Holocene river system of the CB. The maximum lateral

extent of the Middle Holocene system is ~4000 m in the RVG. On the PB it is ~600 m and on the VB ~700 m.

Late Holocene terrace remnants are well-preserved over the entire LMV. On the VB, PB, and southern CB, a low sinuosity to straight river pattern is observed for the late Holocene Meuse. The RVG and northern CB, on the other hand, show a high-sinuosity river pattern during the late Holocene. The maximum width of the Late Holocene river plain varies from ~1800 m on the CB and ~2200 m in the RVG, to ~600 m on the PB and ~1100 m on the VB. So, while the maximum lateral extent of the river plain is decreasing on the CB and in the RVG (compared to the preceding Middle Holocene), the width on the PB remains almost the same and is somewhat increasing on the VB.

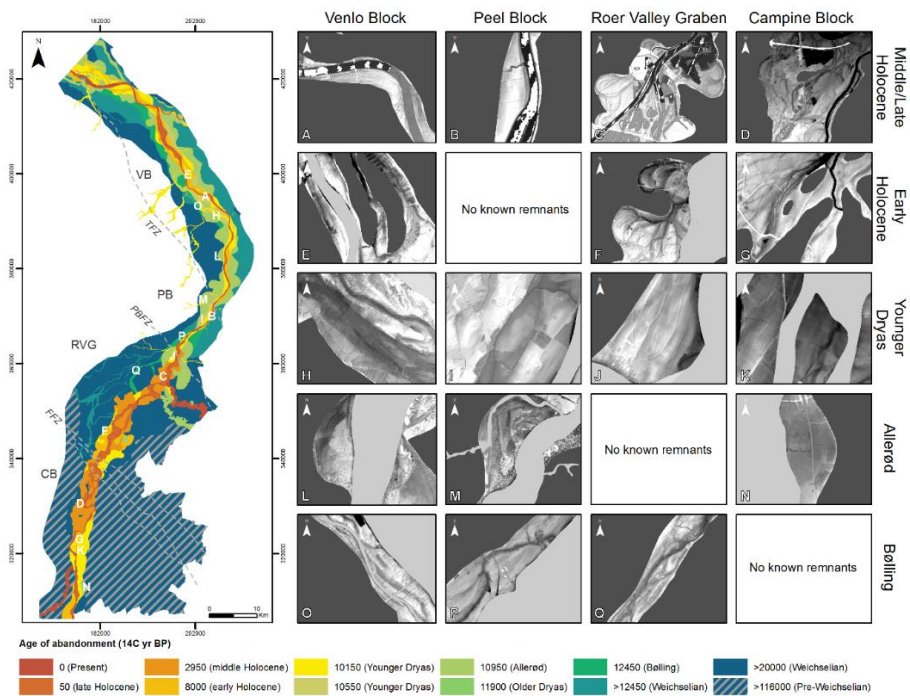


Fig. 10: Contrasts in fluvial style of the late glacial and Holocene terrace remnants on the different tectonic blocks along the course of the Lower Meuse Valley. Dark grey overlay in the morphology panels indicate older terraces, light grey overlay indicates younger terraces.

3.5 Discussion

The general consensus on the LMV (Kasse et al., 1995; Huisink, 1997; Tebbens et al., 1999) is that the (abrupt) climate and associated vegetation changes in northwestern Europe since the LGM were the steering forces behind the differentiation in fluvial style of successive fluvial terraces (reconfirmed and further specified in the current study). This was also identified in studies on the rivers Warta and Vistula in Poland and the Seine in France (Vandenberghe et al., 1994; RoblinJouve, 1995; Starkel, 1995). As noted earlier in such studies, however, the river morphology may vary for each valley reach (Vistula [Starkel et al., 2007] and the Upper and Lower Rhine [Erkens et al., 2009, 2011]), which is also the case in the LMV. Although climatic forcing was uniform for the entire LMV, spatial variation exists in the morphological planform and preservation of the various stages of late glacial and Holocene valley development. Figure 13 summarizes how various reaches of the Meuse river adjusted their morphological planform to the same climate forcing, depending on their tectonic setting (i.e., relative uplift or subsidence), subsurface composition, and upstream-downstream propagation of morphological change. Below, we first review the observed climate-driven changes in fluvial morphology through time. Hereafter, we will discuss the spatial variations observed within the LMV terrace remnants.

3.5.1 Temporal variations in river terrace morphology

The wide braided river system of the LGM and Late Pleniglacial (Fig. 13) can be explained by a scarce vegetation cover combined with a high sediment load and peak (spring) discharges (due to a nival discharge regime originating from a hinterland with permafrost-affected subsoil). Peak discharges flooded the braided river plain, depositing sediment as channel bars. During falling and low stages, water concentrated in numerous small and shallow, low-sinuosity erosive channels separated by bars/islands (Kasse et al., 1995). The main channel(s) of this kind of fluvial system are not preserved because they were used as the starting channel for the next lower terrace. Their positions, however, can be reconstructed by the morphology and confluence of the smaller abandoned channels. Warming and increased precipitation during the Bølling period (Vandenberghe and Bohncke, 1985; Renssen and Isarin, 2001) led to increasing vegetation cover and a more mixed discharge regime that includes rain (storm) discharge peaks. The developing vegetation cover (e.g., *Betula*, *Juniperus*, and dwarf scrubs) on the LGM and Late Pleniglacial braidplain stabilized the LMV river banks, while upstream in the Ardennes, establishing vegetation along the valley edges increasingly trapped hillslope delivered sediments. In the LMV, the regime and sediment-supply changes resulted in a concentration of discharge into a decreasing number of channels. At times of peak discharge, these channels inundated the floodplains. Along the edge of the channels, modestly elevated natural levees were formed (with sandy loamy textures), presumably due to the trapping of sediment by establishing vegetation on the banks.

Away from the channels, flood sediments were trapped, blanketing abandoned braidplain terraces with floodplain loam. Contraction of discharge in a fewer number of channels raised the stream power in these channels, causing them to incise. The loam cover stabilized the floodplain and river banks, helping to deepen the thalweg of the remaining channels. Over time, the more regular discharge regime, increasing vegetation cover, and soil development drove further fluvial change, causing the abandonment of the low-sinuosity multichannel system during the Bølling, in favor of a lesser number of larger and higher sinuosity meandering system in the Allerød (Fig. 13; Kasse et al., 1995; Hoek et al., 2017). This transition is probably a gradual development.

Over time, the beginning meandering channels from the Bølling period became increasingly more sinuous. As a result, meanders that became abandoned in the Allerød have a higher sinuosity than those already abandoned in the Bølling period. In this way, the LMV river system developed from a braided to a multi-channel low-sinuosity planform, to a relatively high sinuosity single-channel planform over the Late Pleniglacial to Bølling to Allerød periods (Fig. 13), as concluded previously by Kasse et al. (1995), Makaske and Nap (1995), Huisink (1997), and from sites to the north of the study area by Cohen (2003). The system transition from Late Pleniglacial braided to highly-sinuosity meandering planform during the Allerød is observed in lowland rivers throughout Europe (Antoine, 1993; Vandenberghe et al., 1994; Brown, 1995; Gabris, 1995; Kalicki, 1995; Roblin-Jouve, 1995; Rose, 1995; Starkel, 1995; Vandenberghe, 2002; Erkens et al., 2009, 2011; Janssens et al., 2012). As concluded in general terms by Schumm (1973, 1981), such gradual morphological transitions in lowland alluvial valleys might well have occurred faster in some reaches than in others, i.e., the main climatic change at the onset of the Bølling can be considered as the external forcing trigger, and the resulting geomorphological changes as a complex response.

Climatic cooling at the onset of the Younger Dryas resulted in a decreased vegetation cover as well as the reestablishment of discontinuous permafrost, both in the study area (Bohncke et al., 1993; Kasse et al., 1995, 2005; Hoek et al., 2017) and in the hinterland (Vandenberghe and Pissart, 1993). As a consequence, spring discharges and sediment transport capacity increased, leading to the observed shift into a braided fluvial system during the Younger Dryas (Fig. 13). However, it is known from the Warta (Poland) and Tisza (Hungary) rivers, for example, that such a shift into a braided planform is not self-evident, as these rivers retained their meandering planform during the Younger Dryas stade (Vandenberghe et al., 1994; Kasse et al., 2010). The observed width of the braidplain during the ~1200-yr-long Younger Dryas period is considerably less (~3 times) than that of the LGM and (Late) Pleniglacial (Fig. 8). This might be due to increased floodplain/bank strength by deposition of overbank loams during the Bølling/Allerød or by the incised position of the river during the start of the Younger Dryas, increasing the volume of sediment that needs to be eroded for the river to extent its plain laterally.

In general, only the outer edges of the Younger Dryas river plain, which predominantly contain the smaller secondary channels, are preserved over the course of the LMV (Fig. 8). As no remnants of the main Younger Dryas channel are likely to be preserved (because of reworking), it might be proposed that this main channel had a less braiding planform, in which case the Younger Dryas river within the LMV might be better characterized as a wandering river (i.e., transitional between braided and meandering) rather than a fully braided one. The morphology of the Younger Dryas terrace fragments on the VB, containing multiple parallel low-sinuosity braided channels, show that this was most likely the case in the LMV.

The rapid rise in temperature at the start of the Holocene caused the discharge regime to change (again) from nival to rainstorm-dominated. Furthermore, the local permafrost within the LMV degraded quickly and the depth of seasonal frost decreased, both contributing to an enhanced soil infiltration capacity. Together with an increasing vegetation cover, this resulted in the concentration of discharge into a decreasing number of channels until only one channel remained. In parallel, renewed trapping of overbank loams occurred and bank stability increased. In other words, very similar “stepwise channel abandonment” occurred in the LMV during the Early Holocene, as reconstructed, over much greater valley width in the Bølling period.

The avulsion of the Wurfeld and Maaseik meander belt during the Preboreal indicates that multiple (meandering) channels were active during the Early Holocene in the RVG and, most likely, also during the late glacial (Fig. 13). Multi-channel meandering systems, simultaneously active during the Early Holocene, were also recognized by Erkens et al. (2009) for the Rhine river in the Upper Rhine Graben and for the Meuse in the downstream Rhine-Meuse delta (Cohen et al., 2002, 2009, 2012; Hijma et al., 2009). After climatic amelioration in the Preboreal, the Holocene climate stabilized and gave way to continued vegetation succession. This led to the development of a mixed deciduous forest by the end of the Boreal and further stabilization of river banks and (floodplain) soils. Consequently, concentration of discharge continued, leading to a single-channel meandering system during the Middle Holocene in the LMV (Fig. 13).

The final phase of terrace formation within the LMV, during the Late Holocene, can be ascribed to human impact. Deforestation and wide-spread agricultural practices in the study area and the hinterland in the last 4000 yr, have led to increased discharges (6.6%), higher sediment load (~300% increase), and increased bank stability by overbank deposits (Dambeck and Thiemeyer, 2002; Bos et al., 2008; Ward, 2009; Erkens, 2009; Erkens et al., 2009). At some locations, lateral channel activity could increase by, for instance, deforestation of levees and floodplain in combination with an increased discharge (e.g., the Stokkem site on the CB [Paulissen, 1973]).

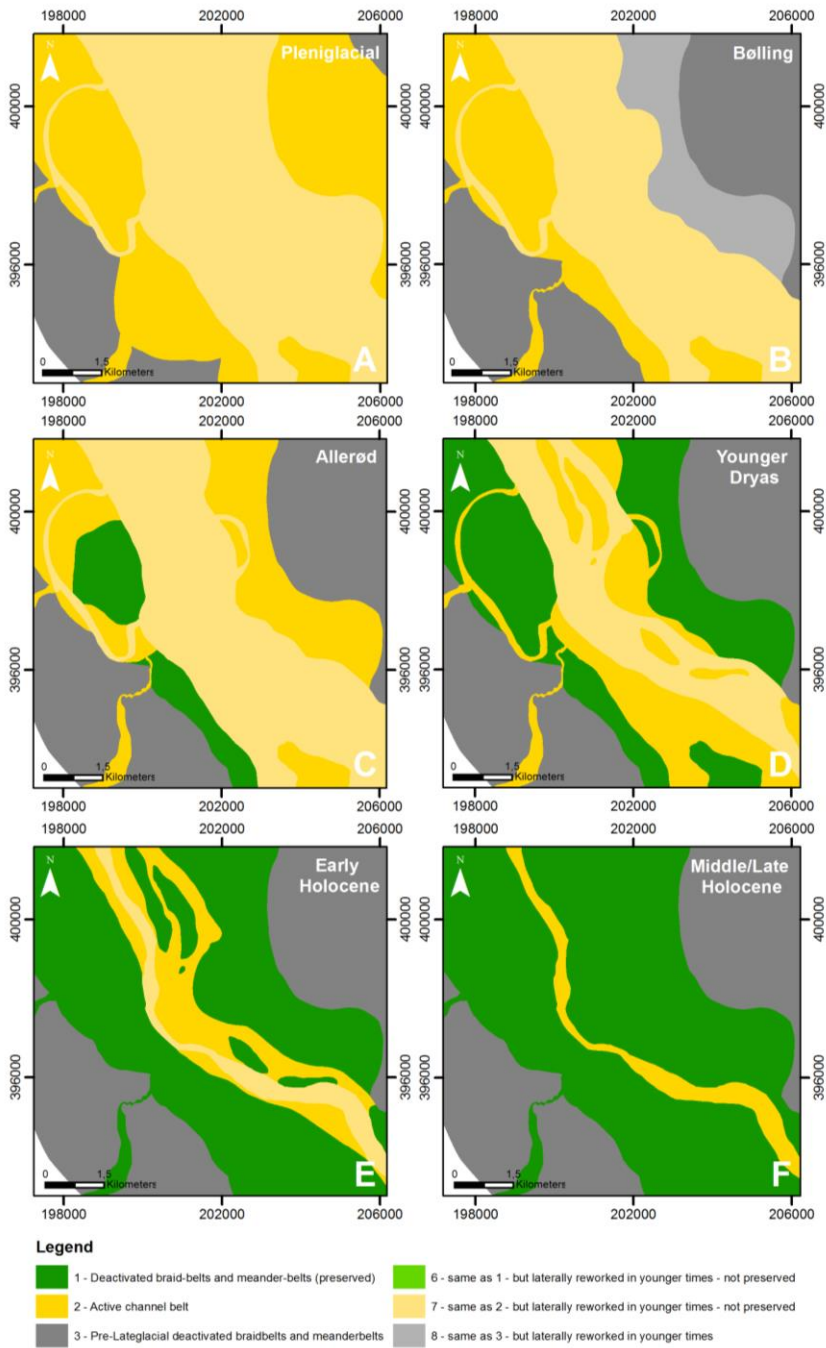


Fig. 11: Palaeogeographic reconstruction of a part of the Lower Meuse Valley on the Venlo Block, letters are referred to in the main text. Legend after Berendsen and Stouthamer (2001) and Cohen et al. (2012).

3.5.2 Spatial variations in river terraces

The fact that most preceding studies on LMV terraces have focused on the record in the northern half of the study area ascribes this region to hold a well-preserved terrace record of distinct fluvial styles. Sufficient lateral movement was possible at the VB for the river to adjust its planform to changing climatic conditions, while, at the same time, the river was able to incise and thereby preserve its former plain (Fig. 8, 9, and 13). Additionally, the relatively low gradient (~ 0.15 m/km) and subsidence, together with the downstream position, i.e., in the Niers-Rhine confluence as it was functioning in Late Pleniglacial, Bølling-Allerød, and Younger Dryas times (Kasse et al., 2005), provided favourable conditions for terrace formation and preservation.

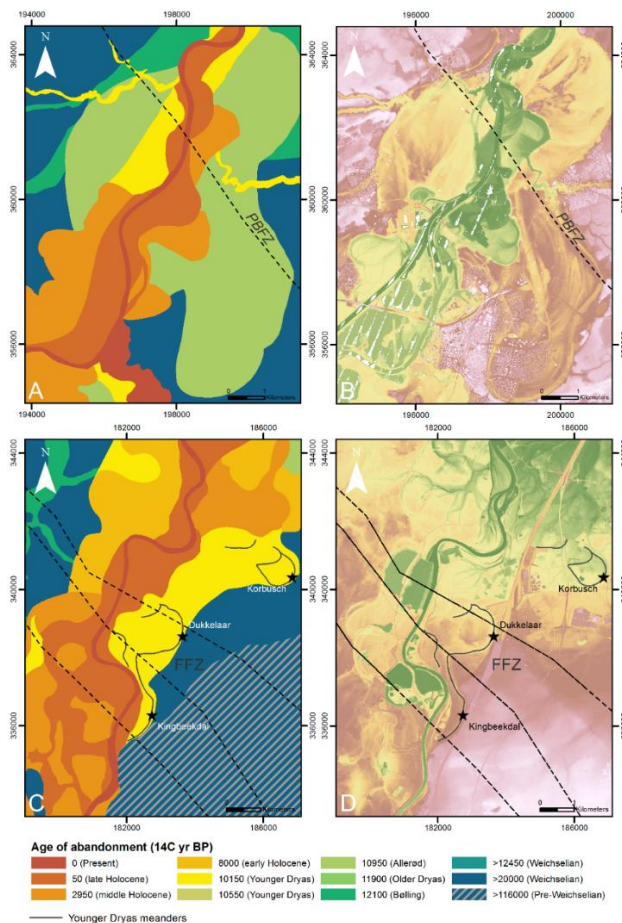


Fig. 12: Locations of anomalous river morphology along fault zones of the Roer Valley Rift System in the Lower Meuse Valley. Terrace map and digital elevation model images of the late glacial and Holocene river terraces around the Peel Boundary Fault Zone (A and B) and the Feldbiss Fault Zone (C and D). Black dotted lines represent the faults.

The PB forms a bottleneck in the course of the LMV where the width of the river plain has reduced significantly over the PB compared to the upstream RVG, especially since the Younger Dryas (Fig. 13). This narrowing can be explained by a combination of relative uplift of the PB with respect to the adjacent VB and RVG, and to restricted lateral mobility of the incised river channel, due to the cohesive subsurface of the PB. The intensified narrowing since the Younger Dryas is probably caused by continued lowering of the thalweg in the resistive subsurface, limiting the available energy for lateral displacement (i.e., vertical incision exceeds lateral movement; Fig. 13).

Lateral movement dominates over vertical incision in the subsiding RVG, where the lithology of the subsurface consists of coarse fluvial deposits, which is represented by a Holocene high-sinuosity meandering river with a relatively wide plain (Fig. 13). The amount of lateral displacement during the Holocene is higher in the RVG compared to the other tectonic blocks and is most likely caused by a combination of a relatively high gradient (~0.5 m/km) and subsidence rate together with a high sediment load in this sub-reach. This relatively high sediment load is probably the result of the narrow river plain and erosional character of the Meuse river on the upstream CB and in the hinterland (Ardennes). This combination of factors makes avulsion of river channels a likely process in this area.

On the southern CB, where the Meuse has to cut through Cretaceous and Paleogene limestone, vertical incision clearly prevailed over lateral movement (Fig. 13). The domination of vertical incision over lateral displacement reduces in the northern CB, where the subsurface consist of similar cohesive sediments as at the PB. Here, several Pleniglacial and late glacial terrace fragments lie within the Holocene river plain, indicating that a multi-channel/avulsive system was present during the Middle Holocene and most likely already during the Younger Dryas or Early Holocene. This resulted in the relatively poor preservation of older terraces due to reworking by the laterally active younger channels. The fact that the planform of the Holocene Meuse on the northern CB is sinuous rather than straight, i.e., like on the PB, is probably caused by the more upstream position of the CB along the course of the LMV. This upstream position resulted in a higher gradient, and therefore higher stream power, and greater sediment load, making the river more likely to move laterally by either meandering or avulsion. The meandering Younger Dryas channels at the Feldbiss Fault Zone (FFZ; Fig. 12C and D) indicate that the Meuse, at this location, either remained in a meandering mode since the Allerød, or that the river started to meander within the Younger Dryas. Meandering Younger Dryas river planforms were also observed in the Warta and Tisza (Vandenberghé et al., 1994; Kasse et al., 2010). In case of the Meuse river, possible causes which may be responsible for this anomalous meandering planform are a (sudden) change in gradient as the river crosses the active FFZ into the RVG or a change in lithology or grain size of the subsurface over the fault zone (passive tectonic control; Fig. 3). The same holds true for the anomalous planform of the Allerød meander at

Roermond, where vertical displacement along the active PBFZ (~66 mm/ ka; Michon and Van Balen, 2005) hampered downstream migration of the meander, forcing it to move laterally and in upstream direction. The different morphological development around the FFZ during the Younger Dryas and PBFZ during the Allerød suggests that the normal faults of the FFZ and PBFZ influenced the river dynamics of the Meuse. It strongly suggests that fault zones within the RVRS executed direct controls on local fluvial morphology in the Weichselian late glacial and Holocene, which will be the subject of a separate paper.

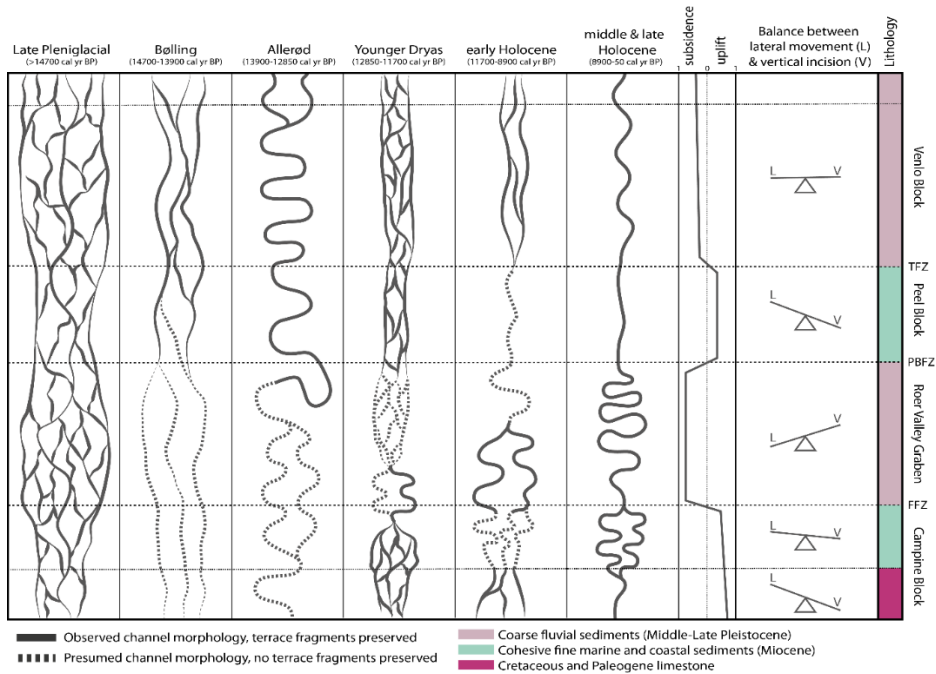


Fig. 13: Reach-to-reach variations of fluvial planform in the Lower Meuse Valley during the late glacial and Holocene, depending on tectonic movement, subsurface composition and upstream-downstream propagation of morphological change.

3.6 Conclusions

The palaeogeographic evolution and associated changes in fluvial style in the Lower Meuse Valley at the transition of the Weichselian to the Holocene are controlled by changes in climate and associated hydrological, vegetational, and sedimentary responses. The Lower Meuse Valley was braided during the last glacial maximum and had a multi-channel low-sinuosity planform during the Bølling that evolved into a meandering planform during the Allerød interstade. Subsequently, it was braided again during the Younger Dryas cold stage. Finally, it became meandering again at the onset of the Holocene. However, reach-to-reach differences in the geomorphological and sedimentary responses are clear:

- (1) Late glacial terrace fragments are best preserved on the relative uplifting PB and VB downstream in the study area, owing to a combination of low gradients and channel-belt width choking effects of the incisional reach traversing the PB. Late glacial morphology is, on the other hand, poorly preserved in the RVG and on the CB, owing to a relatively high gradient and greater sediment supply, driving Holocene channels to erode them by lateral migration and avulsions.
- (2) Holocene channel belts are narrow with low-sinuosity to straight channel patterns on the uplifting PB and VB, while channel-belt activity occurred in a broader zone by channels of greater sinuosity in the RVG and the north of the CB.
- (3) At locations where the river crosses fault zones, separating the tectonic blocks, local terrace preservation and fluvial style exhibit anomalies to the overall trends. These anomalies are (1) an Allerød meander at the PBFZ that is highly sinuous and locally scrolls in upstream direction; and (2) a Younger Dryas meandering pattern preserved just downstream of the FFZ.

From the aforementioned, it can be inferred that, although changes in climate may be uniform, reach-to-reach specific conditions are able to modulate the effects of such a largescale climatic forcing on a river system in the form of spatial variations in river terrace formation, preservation, and morphology. This implies that extrapolation of sub-reach specific morphological expression of large-scale allogenic forcing factors may lead to erroneous interpretations for other subreaches of the same river system. As it turns out, the regional variance in tectonic setting within the LMV had a pronounced effect on the formation, preservation and morphology of fluvial terraces, as it is responsible for spatial and temporal variations in river (valley) gradient, available accommodation space, sediment supply, and subsurface lithology.

3.7 Acknowledgments

This research is part of a PhD project “Reconstruction and Modelling of the Meuse- and Rhine River. Sinuosity Response to Faulting in the Roer Valley Rift System” funded by The Netherlands organization for Scientific Research (NWO; project nr. 821.01.011). We would like to thank Dr. Bas van Geel for his indispensable help with the selection and preparation of the botanical macrofossils, which were sent in for radiocarbon dating. Furthermore, we would like to thank Professor Dr. M.G. Kleinhans for the discussions and helpful remarks on earlier drafts of this paper. Marlies Janssens is thanked for her valuable contribution to the database and we would like to thank Armin Menkovic for providing the data concerning the faults in the study area. Patrick Kiden and an anonymous reviewer are thanked for their constructive reviews that helped improve this paper.

3.8 References

- › AHN 2, n.d.. Retrieved May 1, 2017, from <http://www.ahn.nl/index.html>
- › Antoine, P., 1993. Le système de terrasses du bassin de la Somme: Modèle d'évolution morpho-sédimentaire cyclique et cadre paléoenvironnemental pour le paléolithique. *Quaternaire* 4, 3-16. <http://dx.doi.org/10.3406/quate.1993.1986>
- › Antoine, P., Lautridou, J.P., Laurent, M., 2000. Long-term fluvial archives in NW France: response of the Seine and Somme rivers to tectonic movements, climatic variations and sea-level changes. *Geomorphology* 33, 183-207. [https://doi.org/10.1016/S0169-555X\(99\)00122-1](https://doi.org/10.1016/S0169-555X(99)00122-1)
- › Berendsen, H.J.A., Stouthamer, E., 2001. Palaeogeographic development of the Rhine-Meuse delta, the Netherlands. Koninklijke van Gorcum, Assen. http://dx.doi.org/10.1046/j.1365-3091.2002.00469_1.x
- › Berendsen, H.J.A., Cohen, K.M., Stouthamer, E., 2001. Maps and cross-sections. In: Berendsen, H.J.A., Stouthamer, E., 2001: Palaeogeographic development of the Rhine-Meuse delta, the Netherlands. Koninklijke van Gorcum, Assen. http://dx.doi.org/10.1046/j.1365-3091.2002.00469_1.x
- › Berendsen, H.J.A., Cohen, K.M., Stouthamer, E., 2007. The use of GIS in reconstructing the Holocene palaeogeography of the Rhine–Meuse delta, the Netherlands. *International Journal of Geographical Information Science* 21, 589-602. <https://doi.org/10.1080/13658810601064918>
- › Berendsen, H.J.A., Hoek, W.Z., Schorn, E., 1995. Late Weichselian and Holocene river channel changes of the rivers Rhine and Meuse in the Netherlands (land van Maas en Waal). In: Frenzel, B., Vandenberghe, J., Kasse, C., Bohncke, S.J.P., Glaser, B. (Eds.), *European river activity and climate change during the Lateglacial and early Holocene*, 'European Palaeoclimate and Man 9, Palaoklimaforschung 14, Gustav Fischer Verlag, Stuttgart, pp. 151-171.
- › Blum, M.D., Törnqvist, T.E., 2000. Fluvial responses to climate and sea level change: A review and look forward. *Sedimentology* 47, 2-48. <http://dx.doi.org/10.1046/j.1365-3091.2000.00008.x>

- › Bogaart, P.W., Van Balen, R.T., 2000. Numerical modeling of the response of alluvial rivers to Quaternary climate change. *Global and Planetary Change* 27, 147-163. [https://doi.org/10.1016/S0921-8181\(01\)00064-9](https://doi.org/10.1016/S0921-8181(01)00064-9)
- › Bogaart, P.W., Van Balen, R.T., Kasse, C., Vandenberghe, J., 2003. Process-based modelling of fluvial system response to rapid climate change II. Application to the river Maas (the Netherlands) during the last Glacial–Interglacial transition. *Quaternary Science Reviews* 22, 2097-2110. [https://doi.org/10.1016/S0277-3791\(03\)00144-6](https://doi.org/10.1016/S0277-3791(03)00144-6)
- › Bohncke, S.J.P., Vandenberghe, J., Huijzer, A., 1993. Periglacial environments during the Weichselian Late Glacial in the Maas valley, the Netherlands. *Geologie En Mijnbouw* 72, 193.
- › Bos, J.A.A., Zuidhoff, F.S., 2015. De restgeul van well-aijen, een reconstructie van de vegetatieontwikkeling van het noord-limburgse Maasdal gedurende het Holoceen (mesolithicum-vroeg-romeinse tijd). ADC-Rapport 3599/BAAC Rapport A-12.0274, 92 pp.
- › Bos, J.A.A., Dambeck, R., Kalis, A.J., Schweizer, A., Thiemeyer, H., 2008. Palaeoenvironmental changes and vegetation history of the northern upper Rhine graben (southwestern Germany) since the Lateglacial. *Netherlands Journal of Geosciences/Geologie En Mijnbouw* 87, 67-90.
- › Bridgland, D., Westaway, R., 2008. Climatically controlled river terrace staircases: A worldwide Quaternary phenomenon. *Geomorphology* 98, 285-315. <https://doi.org/10.1016/j.geomorph.2006.12.032>
- › Brown, A.G., 1995. Lateglacial–Holocene sedimentation in lowland temperate environments: Floodplain metamorphosis and multiple channel systems. In: Frenzel, B., Vandenberghe, J., Kasse, C., Bohncke, S.J.P., Glaser, B. (Eds.), *European river activity and climate change during the Lateglacial and early Holocene*, 'European Palaeoclimate and Man 9, Palaoklimaforschung 14, Gustav Fischer Verlag, Stuttgart, pp. 21-35.
- › Buitenhuis, A., Wolfert, H.P., 1988. Geomorfologische kaart van nederland 1: 50.000: Toelichting op kaartblad 46 Gennep. Stichting voor bodemkartering.
- › Cohen, K.M., 2003. Differential subsidence within a coastal prism: Late-Glacial-Holocene tectonics in the Rhine-Meuse delta, the Netherlands. Published doctoral dissertation, Universiteit Utrecht.
- › Cohen, K.M., Stouthamer, E., Berendsen, H.J.A., 2002. Fluvial deposits as a record for late Quaternary neotectonic activity in the Rhine-Meuse delta, the Netherlands. *Netherlands Journal of Geosciences/Geologie En Mijnbouw* 81, 389–405.
- › Cohen, K.M., Stouthamer, E., Hoek, W.Z., Berendsen, H.J.A., Kempen, H., 2009. Zand in banen: zanddieptekaarten van het rivierengebied en het IJsseldal in de provincies Gelderland en Overijssel. Provincie Gelderland. Derde, geheel herziene druk, 130 pp.
- › Cohen, K.M., Stouthamer, E., Pierik, H.J., Geurts, A.H., 2012. Rhine-Meuse delta studies' digital basemap for delta evolution and palaeogeography. Dept. Physical Geography. Utrecht University. Digital Dataset. DANS. <https://doi.org/10.17026/dans-x7g-sjtw>
- › Dambeck, R., Thiemeyer, H., 2002. Fluvial history of the northern upper Rhine river (southwestern Germany) during the Lateglacial and Holocene times. *Quaternary International* 93, 53-63. [https://doi.org/10.1016/S1040-6182\(02\)00006-X](https://doi.org/10.1016/S1040-6182(02)00006-X)
- › DINoloket, n.d.. Retrieved July 11, 2017, from <https://www.dinoloket.nl>.
- › Erkens, G., 2009. Sediment dynamics in the Rhine catchment: Quantification of fluvial response to climate change and human impact. Published doctoral dissertation, Universiteit Utrecht.

- › Erkens, G., Dambeck, R., Volleberg, K.P., Bouman, M.T.I.J., Bos, J.A.A., Cohen, K.M., Wallinga, J., Hoek, W.Z., 2009. Fluvial terrace formation in the northern upper Rhine graben during the last 20000 years as a result of allogenic controls and autogenic evolution. *Geomorphology* 103, 476-495. <https://doi.org/10.1016/j.geomorph.2008.07.021>
- › Erkens, G., Hoffmann, T., Gerlach, R., Klostermann, J., 2011. Complex fluvial response to Lateglacial and Holocene allogenic forcing in the lower Rhine valley (Germany). *Quaternary Science Reviews* 30, 611-627. <https://doi.org/10.1016/j.quascirev.2010.11.019>
- › Gábris, G., 1995. River activity as a function of changing palaeoenvironmental conditions during the Lateglacial–Holocene period in Hungary. In: Frenzel, B., Vandenberghe, J., Kasse, C., Bohncke, S.J.P., Glaser, B. (Eds.), *European river activity and climate change during the Lateglacial and early Holocene*, 'European Palaeoclimate and Man 9, Palaoklimaforschung 14, Gustar Fischer Verlag, Stuttgart, pp. 205-212.
- › Geluk, M.C., Duin, E.J.T., Duser, M., Rijkers, R.H.B., Van den Berg, M.W., Van Rooijen, P., 1994. Stratigraphy and tectonics of the roer valley graben. *Geologie En Mijnbouw* 73, 129-129.
- › Hijma, M.P., Cohen, K.M, Hoffmann, G., Van der Spek, A.J.F., Stouthamer, E., 2009. From river valley to estuary: The evolution of the Rhine mouth in the early to middle Holocene (western Netherlands, Rhine-Meuse delta). *Netherlands Journal of Geosciences* 88, 13-53. <https://doi.org/10.1017/S0016774600000986>
- › Hoek, W.Z., 1997. Palaeogeography of Lateglacial vegetations. Aspects of Lateglacial and early Holocene vegetation, abiotic landscape and climate in the Netherlands. Published doctoral dissertation, Vrije Universiteit Amsterdam.
- › Hoek, W.Z., 1997. Atlas to Palaeogeography of Lateglacial vegetations. Maps of Lateglacial and early Holocene landscape and vegetation in The Netherlands, with an extensive review of available palynological data. Published doctoral dissertation, Vrije Universiteit Amsterdam.
- › Hoek, W.Z., Bohncke, S.J.P., 2002. Climatic and environmental events over the last termination, as recorded in the Netherlands: A review. *Netherlands Journal of Geosciences* 81, 123-137. <https://doi.org/10.1017/S001677460002062X>
- › Hoek, W.Z., Lammertsma, E.I., Bohncke, S.J.P., Bos, J.A.A., Bunnik, F., Kasse, C., Schokker, J., Westerhoff, W., 2017. Lateglacial and Early Holocene vegetation development and fluvial system changes in the northern Meuse valley, the Netherlands: A review of palynological data. *Netherlands Journal of Geosciences* 96, 93-114. <https://doi.org/10.1017/njg.2017.4>
- › Holbrook, J., Schumm, S.A., 1999. Geomorphic and sedimentary response of rivers to tectonic deformation: A brief review and critique of a tool for recognizing subtle epeirogenic deformation in modern and ancient settings. *Tectonophysics* 305, 287-306. [https://doi.org/10.1016/S0040-1951\(99\)00011-6](https://doi.org/10.1016/S0040-1951(99)00011-6)
- › Houtgast, R.F., Van Balen, R.T., 2000. Neotectonics of the roer valley rift system, the Netherlands. *Global and Planetary Change* 27, 131-146. [https://doi.org/10.1016/S0921-8181\(01\)00063-7](https://doi.org/10.1016/S0921-8181(01)00063-7)
- › Houtgast, R.F., Van Balen, R.T., Bouwer, L.M., Brand, G.B.M., Brijker, J.M., 2002. Late Quaternary activity of the feldbiss fault zone, roer valley rift system, the Netherlands, based on displaced fluvial terrace fragments. *Tectonophysics* 352, 295-315. [https://doi.org/10.1016/S0040-1951\(02\)00219-6](https://doi.org/10.1016/S0040-1951(02)00219-6)
- › Huisink, M., 1997. Lateglacial sedimentological and morphological changes in a lowland river in response to climatic change: The Maas, southern Netherlands. *Journal of Quaternary*

Science 12, 209-223. [http://dx.doi.org/10.1002/\(SICI\)1099-1417\(199705/06\)12:3<209::AID-JQS306>3.0.CO;2-P](http://dx.doi.org/10.1002/(SICI)1099-1417(199705/06)12:3<209::AID-JQS306>3.0.CO;2-P)

- › Huisink, M., 1999. Changing river styles in response to climate change: Examples from the Maas and Vecht during the Weichselian Pleni- and Lateglacial. Published doctoral dissertation, Vrije Universiteit Amsterdam.
- › Isarin, R.F.B., Rensink, E., Ellenkamp, G.R., Heunks, E., 2017. Of Meuse and man: The geomorphogenetic and archaeological predictive maps of the dutch Meuse valley. *Netherlands Journal of Geosciences* 96, 183-196. <https://doi.org/10.1017/njg.2017.5>
- › Janssens, M.M., Kasse, C., Bohncke, S.J.P., Greaves, H., Cohen, K.M., Wallinga, J., Hoek, W.Z., 2012. Climate-driven fluvial development and valley abandonment at the last glacial-interglacial transition (oude IJssel-Rhine, Germany). *Netherlands Journal of Geosciences* 91, 37-62. <https://doi.org/10.1017/S001677460000055X>
- › Kalicki, T., 1995. Lateglacial and Holocene evolution of some river valleys in Byelorussia. In: Frenzel, B., Vandenberghe, J., Kasse, C., Bohncke, S.J.P., Glaser, B. (Eds.), *European river activity and climate change during the Lateglacial and early Holocene*, 'European Palaeoclimate and Man 9, Palaoklimaforschung 14, Gustar Fischer Verlag, Stuttgart, pp. 89-100.
- › Kasse, C., Bohncke, S.J.P., Vandenberghe, J., and Gábris, G., 2010. Fluvial style changes during the last glacial–interglacial transition in the middle Tisza valley (Hungary). *Proceedings of the Geologists' Association* 121, 180-194. <https://doi.org/10.1016/j.pgeola.2010.02.005>
- › Kasse, C., Hoek, W.Z., Bohncke, S.J.P., Konert, M., Weijers, J., Cassee, M., Van der Zee, R., 2005. Late glacial fluvial response of the Niers-Rhine (western Germany) to climate and vegetation change. *Journal of Quaternary Science* 20, 377-394. <http://dx.doi.org/10.1002/jqs.923>
- › Kasse, C., Vandenberghe, J., Bohncke, S.J.P., 1995. Climatic change and fluvial dynamics of the Maas during the Late Weichselian and Early Holocene. In: Frenzel, B., Vandenberghe, J., Kasse, C., Bohncke, S.J.P., Glaser, B. (Eds.), *European river activity and climate change during the Lateglacial and early Holocene*, 'European Palaeoclimate and Man 9, Palaoklimaforschung 14, Gustar Fischer Verlag, Stuttgart, pp. 123-150.
- › Kasse, C., Vandenberghe, D., De Corte, F., Van den Haute, P., 2007. Late Weichselian fluvio-aolian sands and coversands of the type locality grubbenvorst (southern Netherlands): Sedimentary environments, climate record and age. *Journal of Quaternary Science* 22, 695-708. <http://dx.doi.org/10.1002/jqs.1087>
- › Kleinhans, M.G., van den Berg, J.H., 2010. River channel and bar patterns explained and predicted by an empirical and a physics based method. *Earth Surface Processes and Landforms* 36, 721-738. <http://dx.doi.org/10.1002/esp.2090>
- › Leopold, L.B., Wolman, M.G., 1957. River channel patterns: braided, meandering, and straight. *Geological Survey professional paper 282-B*. US Government Printing Office, Washington, DC.
- › Leopold, L.B., Wolman, M.G., Miller, J.P., 1964. *Fluvial Processes in Geomorphology*. W.H. Freeman and Company, San Fransico.
- › Makaske, B., Nap, R., 1995. A transition from a braided to a meandering channel facies, showing inclined heterolithic stratification (Late Weichselian, central Netherlands). *Geologie En Mijnbouw* 74, 13-20.

- › Michon, L., Van Balen, R.T., 2005. Characterization and quantification of active faulting in the roer valley rift system based on high precision digital elevation models. *Quaternary Science Reviews* 24, 455-472. <https://doi.org/10.1016/j.quascirev.2003.11.009>
- › Michon, L., Van Balen, R.T., Merle, O., Pagnier, H., 2003. The Cenozoic evolution of the roer valley rift system integrated at a European scale. *Tectonophysics* 367, 101-126. [https://doi.org/10.1016/S0040-1951\(03\)00132-X](https://doi.org/10.1016/S0040-1951(03)00132-X)
- › Miedema, R., 1987. Soil formation, microstructure and physical behaviour of late Weichselian and Holocene Rhine deposits in the Netherlands. Published doctoral dissertation, Landbouwwuniversiteit Wageningen.
- › Nanson G.C., Knighton A.D., 1996. Anabranching rivers: their cause, character and classification. *Earth Surface Processes and Landforms* 21: 217-239. [http://dx.doi.org/10.1002/\(SICI\)1096-9837\(199603\)21:3<217::AID-ESP611>3.0.CO;2-U](http://dx.doi.org/10.1002/(SICI)1096-9837(199603)21:3<217::AID-ESP611>3.0.CO;2-U)
- › Paulissen, E., 1973. De morfologie en de kwartairstratigrafie van de maasvallei in Belgisch Limburg. Published doctoral dissertation, Verhandelingen van de Koninklijke Vlaamse academie voor wetenschappen, letteren en schone kunsten van België.
- › Pierik, H.J., Cohen, K.M., Stouthamer, E., 2016. A new GIS approach for reconstructing and mapping dynamic Late Holocene coastal plain palaeogeography. *Geomorphology* 270, 55-70. <https://doi.org/10.1016/j.geomorph.2016.05.037>
- › Pons, L.J., 1954. Het fluviaatle laagterras van Rijn en Maas. *Boor En Spade* 7, 110.
- › Pons, L.J., 1957. De Geologie, de bodenvorming en de waterstaatkundige ontwikkeling van het land van Maas en Waal en een gedeelte van het rijk van Nijmegen. Published doctoral dissertation, Landbouwwuniversiteit Wageningen.
- › Pons, L.J., Schelling, J., 1951. De Laatglaciale afzettingen van de Rijn en de Maas. *Geologie En Mijnbouw* 13, 293-297.
- › Rensink, E., Isarin, R.F.B., Ellenkamp, G.R., Heunks, E., 2015. Archeologische verwachtingskaart maasdal tussen Mook en Eijsden. *DANS*. <https://doi.org/10.17026/dans-xbe-977w>
- › Renssen, H., Isarin, R.F., 2001. The two major warming phases of the last deglaciation at 14.7 and 11.5 ka cal BP in Europe: Climate reconstructions and AGCM experiments. *Global and Planetary Change* 30, 117-153. [https://doi.org/10.1016/S0921-8181\(01\)00082-0](https://doi.org/10.1016/S0921-8181(01)00082-0)
- › Roblin-Jouve, A., 1995. Lateglacial and Early Holocene geomorphology of the upper Seine river valley. In: Frenzel, B., Vandenberghe, J., Kasse, C., Bohncke, S.J.P., Glaser, B. (Eds.), *European river activity and climate change during the Lateglacial and early Holocene*, 'European Palaeoclimate and Man 9, Palaoklimaforschung 14, Gustar Fischer Verlag, Stuttgart, pp. 191-203.
- › Rose, J., 1995. Lateglacial and Early Holocene river activity in lowland Britain. In: Frenzel, B., Vandenberghe, J., Kasse, C., Bohncke, S.J.P., Glaser, B. (Eds.), *European river activity and climate change during the Lateglacial and early Holocene*, 'European Palaeoclimate and Man 9, Palaoklimaforschung 14, Gustar Fischer Verlag, Stuttgart, pp. 51-74.
- › Schelling, J., 1951. Een bodemkartering van noord-Limburg (gemeenten Ottersum, Gennep en Bergen). Published doctoral dissertation, Landbouwwuniversiteit Wageningen.
- › Schumm, S.A., 1973. Geomorphic thresholds and complex response of drainage systems. *Fluvial Geomorphology* 6, 69-85.
- › Schumm, S.A., 1981. Evolution and response of the fluvial system, sedimentologic implications. *Society of Economic Paleontologists and Mineralogists, Special Publication* 31, 19-29.

- › Starkel, L., 1995. The place of the Vistula river valley in the Late Vistulian-Early Holocene. In: Frenzel, B., Vandenberghe, J., Kasse, C., Bohncke, S.J.P., Glaser, B. (Eds.), *European river activity and climate change during the Lateglacial and early Holocene*, 'European Palaeoclimate and Man 9, Palaoklimaforschung 14, Gustar Fischer Verlag, Stuttgart, pp. 75-88.
- › Starkel, L., Ge, P., Superson, J., 2007. Last Glacial-Interglacial cycle in the evolution of river valleys in southern and central Poland. *Quaternary Science Reviews* 26, 2924-2936. <https://doi.org/10.1016/j.quascirev.2006.01.038>
- › Tebbens, L.A., Veldkamp, A., Westerhoff, W., Kroonenberg, S.B., 1999. Fluvial incision and channel downcutting as a response to Late-glacial and Early Holocene climate change: The lower reach of the river Meuse (Maas), the Netherlands. *Journal of Quaternary Science* 14, 59-75.
- › Toonen, W.H., Kleinhans, M.G., Cohen, K.M., 2012. Sedimentary architecture of abandoned channel fills. *Earth Surface Processes and Landforms* 37, 459-472. <http://dx.doi.org/10.1002/esp.3189>
- › Van Balen, R.T., Busschers, F.S., Tucker, G.E., 2010. Modeling the response of the Rhine-Meuse fluvial system to Late Pleistocene climate change. *Geomorphology* 114, 440-452. <https://doi.org/10.1016/j.geomorph.2009.08.007>
- › Van Balen, R.T., Houtgast, R.F., Cloetingh, S.A.P.L., 2005. Neotectonics of the Netherlands: A review. *Quaternary Science Reviews* 24, 439-454. <https://doi.org/10.1016/j.quascirev.2004.01.011>
- › Van Balen, R.T., Houtgast, R.F., Van der Wateren, F.M., Vandenberghe, J., 2002. Neotectonic evolution and sediment budget of the Meuse catchment in the ardennes and the roer valley rift system. *Netherlands Journal of Geosciences* 81, 211-215. <https://doi.org/10.1017/S0016774600022459>
- › Van Balen, R.T., Houtgast, R.F., Van der Wateren, F.M., Vandenberghe, J., Bogaart, P.W., 2000. Sediment budget and tectonic evolution of the Meuse catchment in the ardennes and the roer valley rift system. *Global and Planetary Change* 27, 113-129. [https://doi.org/10.1016/S0921-8181\(01\)00062-5](https://doi.org/10.1016/S0921-8181(01)00062-5)
- › Van Balen, R.T., Verweij, J.M., Van Wees, J.D., Simmelink, H., Van Bergen, F., Pagnier, H., 2002. Deep subsurface temperatures in the roer valley graben and the peellblock, the Netherlands-new results. *Netherlands Journal of Geosciences* 81(01), 19-26. <https://doi.org/10.1017/S0016774600020539>
- › Van de Meene, E., Zagwijn, W., 1978. Die Rheinläufe im deutsch-niederländischen grenzgebiet seit der Saale-Kaltzeit. *Fortschr. Geol. Rheinl. u. Westf.* 28, 345-359.
- › Van den Berg, M.W., 1989. Toelichting op kaartblad 59-62, geomorfologische kaart Nederland, 1:50.000. Staring Centrum, Rijks Geologische Dienst, Wageningen.
- › Van den Berg, M.W., 1996. Fluvial sequences of the Maas: A 10 ma record of neotectonics and climate change at various time-scales. Published doctoral dissertation, Landbouwniversiteit Wageningen.
- › Van den Berg, M.W., Schwan, J.C.G., 1996. Millennial climatic cyclicity in Weichselian Late Pleniglacial to Early Holocene fluvial deposits of the river Maas in the southern Netherlands. pp. 99-121. In: Van den Berg, M.W., 1996. *Fluvial sequences of the Maas: A 10 ma record of neotectonics and climate change at various time-scales*. Published doctoral dissertation, Landbouwniversiteit Wageningen.

- › Van den Broek, J.M.M., Maarleveld, G.C., 1963. The Late Pleistocene terrace deposits of the Meuse. Mededelingen Geologische Stichting NS 16, 13-24.
- › Vandenberghé, J., 1995. Timescales, climate and river development. *Quaternary Science Reviews* 14, 631-638. [https://doi.org/10.1016/0277-3791\(95\)00043-0](https://doi.org/10.1016/0277-3791(95)00043-0)
- › Vandenberghé, J., 2002. The relation between climate and river processes, landforms and deposits during the Quaternary. *Quaternary International* 91, 17-23. [https://doi.org/10.1016/S1040-6182\(01\)00098-2](https://doi.org/10.1016/S1040-6182(01)00098-2)
- › Vandenberghé, J., 2003. Climate forcing of fluvial system development: An evolution of ideas. *Quaternary Science Reviews* 22, 2053-2060. [https://doi.org/10.1016/S0277-3791\(03\)00213-0](https://doi.org/10.1016/S0277-3791(03)00213-0)
- › Vandenberghé, J., Bohncke, S.J.P., 1985. The Weichselian Late Glacial in a small lowland valley (mark river, Belgium and the Netherlands). *Bulletin De l'Association Française Pour l'Étude Du Quaternaire* 22, 167-175.
- › Vandenberghé, J., Pissart, A., 1993. Permafrost changes in Europe during the Last Glacial. *Permafrost and Periglacial Processes* 4, 121-135.
- › Vandenberghé, J., Kasse, C., Bohncke, S.J.P., Kozarski, S., 1994. Climate related river activity at the Weichselian Holocene transition: A comparative study of the Warta and Maas rivers. *Terra Nova* 6, 476-485. <http://dx.doi.org/10.1111/j.1365-3121.1994.tb00891.x>
- › Walker, M.J.C., Berkelhammer, M., Björck, S., Cwynar, L.C., Fisher, D.A., Long, A.J., Lowe, J.J., Newnham, R.M., Rasmussen, S.O., Weiss, H., 2012. Formal subdivision of the Holocene Series/Epoch: a discussion paper by a working group of INTIMATE (Integration of ice-core, marine and terrestrial records) and the subcommission on Quaternary stratigraphy (International Commission on Stratigraphy). *Journal of Quaternary Science* 27 (7), 649-659. <http://dx.doi.org.vu-nl.idm.oclc.org/10.1002/jqs.2565>
- › Wang, X., Van Balen, R., Yi, S., Vandenberghé, J., Lu, H., 2014. Differential tectonic movements in the confluence area of the Huang Shui and Huang He rivers (Yellow River), NE Tibetan Plateau, inferred from fluvial terraces. *Boreas* 43, 469-484. <http://dx.doi.org/10.1111/bor.12054>
- › Ward, P.J., 2009. Simulating discharge and sediment yield characteristics in the Meuse basin during the Late Holocene and 21st century. Published doctoral dissertation, Vrije Universiteit Amsterdam.
- › Ward, P.J., Renssen, H., Aerts, J.C.J.H., Van Balen, R.T., Vandenberghé, J., 2008. Strong increases in flood frequency and discharge of the river Meuse over the Late Holocene: Impacts of long-term anthropogenic land use change and climate variability. *Hydrology and Earth System Sciences Discussions* 12, 159-175.
- › Ward, P.J., Van Balen, R.T., Verstraeten, G., Renssen, H., Vandenberghé, J., 2009. The impact of land use and climate change on Late Holocene and future suspended sediment yield of the Meuse catchment. *Geomorphology* 103, 389-400.
- › Wolfert, H.P., de Lange, G.W., 1990. Geomorfologische kaart van Nederland, 1:50.000 en toelichting, kaartblad 52 Venlo. Stichting voor Bodemkartering.
- › Zagwijn, W.H., 1986. Nederland in het Holoceen. *Geologie van Nederland, Deel, Rijks Geologische Dienst, Haarlem.*
- › Zuidhoff, F.S., Huizer, J., 2015. De noordelijke Maasvallei door de eeuwen heen. Vijftienduizend jaar landschapsdynamiek tussen Roermond en Mook. Inventariserend archeologisch onderzoek 'Verkenning Plus' project Maasvallei voor vijftien deelgebieden. ADC- Monografie 19/ADC-rapport 3750. ADC Archeoprojecten, Amersfoort.

Chapter 4

Interplay between climatic, tectonic and anthropogenic forcing in the Lower Rhine Graben, the Roer River

Abstract

The Roer is a small river which drains the Rhenish shield and conflues with the Meuse River. Up to now the geological, climatological, biostratigraphical, and pedological setting of the Roer Valley were not sufficiently integrated to disentangle the effects of external forcing factors on the Roer River. In this study we perform a detailed and integrated reconstruction of the fluvial morphology and palaeogeography of the Roer River in order to determine responses to combined climatic, tectonic and anthropogenic forcing factors. The Roer River has formed five terrace levels since the Weichselian Late Pleniglacial. Fluvial planform of the Roer River was predominantly climate-controlled during the Lateglacial and Early Holocene. Reach-to-reach variations in river terrace formation and fluvial planform change occur due to variations in tectonic setting, subsurface geology, base-level fluctuations and the confluence with tributary systems. Differential subsidence by active faulting in the Roer Valley Graben during the early Lateglacial caused a preferential usage of the down-tilt channels of the, up to then, double channel belt systems in the Roer Valley. This preferred channel avulsion towards a fault zone, leaving an underfit system on the up-tilted side, and the clustering of Holocene Roer channels along that fault zone, meet the criteria for a lateral response of the Roer River to a tectonic forcing. Anthropogenic influences in the form of deforestation and land-use changes during the Late Holocene are responsible for the formation of a final terrace level and overbank sediments.

Published as: Woolderink, H. A. G., Kasse, C., Grooteman, L. P. A., Van Balen, R. T., 2019. Interplay between climatic, tectonic and anthropogenic forcing in the Lower Rhine Graben, the Roer River. Geomorphology, 344, 25-45.

4.1 Introduction

Fluvial systems are controlled by climate, tectonics, base-level fluctuations and anthropogenic factors (Schumm, 1973, Schumm, 1981; Vandenberghe, 1995, Vandenberghe, 2003; Holbrook and Schumm, 1999; De Moor, 2007; Verstraeten et al., 2009; Notebaert and Verstraeten, 2010; Erkens et al., 2011; Wang et al., 2014). These different external forcing factors often operate simultaneously, making it difficult to extract the effects of the individual forcings from the fluvial record. However, with detailed geological, climatological, biostratigraphical, and pedological reconstructions a main forcing factor can, most often, be recognized. Such a disentanglement of the external forcing factors is essential for distinguishing the effects of each individual forcing on river dynamics and planform change.

In northwestern Europe, the planform response of fluvial systems to climate-related changes in precipitation, permafrost occurrence, vegetation cover and sediment supply have been studied extensively for the Weichselian Late Pleniglacial to Holocene time period. Generally, the cold stadials and glacial periods are associated with braided planforms. The warm interstadials and interglacial periods are, on the other hand, characterized by meandering river systems (Berendsen et al., 1995; Kasse et al., 1995, Kasse et al., 2005, Kasse et al., 2010, Kasse et al., 2017; Rose, 1995; Vandenberghe, 1995, Vandenberghe, 2002, Vandenberghe, 2003; Huisink, 1997; Tebbens et al., 1999; Antoine et al., 2000; Blum and Törnqvist, 2000; Cohen, 2003; Busschers et al., 2007; Bridgland and Westaway, 2008; Hijma et al., 2009; Erkens et al., 2011; Janssens et al., 2012; Starkel et al., 2015; Woolderink et al., 2018). However, the effects of climate change on fluvial planform will vary over the course of a river system due to reach-specific characteristics such as river (valley) gradient, available accommodation space, sediment supply, and subsurface lithology (Schumm, 1981; Houben, 2003; Starkel et al., 2007; Erkens et al., 2009; Woolderink et al., 2018). Many of these reach-specific characteristics are the result of variations in tectonic setting and active faulting (Holbrook and Schumm, 1999; Woolderink et al., 2018).

Diagnostic characteristics for recognizing the (lateral) response of a river to a tectonic forcing were established over the past decades by both experimental studies and research on natural systems. Such characteristics include, amongst others, (i) a preferred channel avulsion towards a fault zone, (ii) an asymmetric position of channel belts in the river valley, (iii) the presence of a “underfit” river system in the up-tilted side of the valley, (iv) distinct differences in soil type between the up-tilted and down-tilted sides of the river valley, and (v) the gradual infill of a zone of subsidence (Dury, 1970; Mike, 1975; Bridge and Leeder, 1979; Nanson, 1980; Schumm, 1986; Alexander and Leeder, 1987; Leeder and Alexander, 1987; Dumont et al., 1996; Peakall, 1998; Holbrook and Schumm, 1999; Peakall et al., 2000; Burrato et al., 2003; Stouthamer and Berendsen, 2007). Anthropogenic forcing factors such as agriculture, mining, deforestation and river

regulation have a pronounced influence on river discharges and sediment yield which, in turn, drive fluvial dynamics and planform change (De Moor, 2007; De Moor et al., 2008; Ward et al., 2008, Ward et al., 2009; Verstraeten et al., 2009; Notebaert and Verstraeten, 2010).

The ~165 km long Roer River, which is a tributary of the Meuse River, is positioned in the tectonically active Lower Rhine Graben and provides an excellent case to evaluate the effects of the interplay between climatic, tectonic and anthropogenic forcings on river morphology and dynamics. Furthermore, due to the well-known settings of the Roer, it is possible to differentiate between the external forcings and appoint a main forcing factor for different periods.

The aims of this study are to (1) reconstruct the palaeogeographic evolution and fluvial morphology of the Roer River since the Weichselian Late Pleniglacial; (2) explore reach-to-reach variations within the Roer Valley; and (3) identify the effects of climatic, tectonic and anthropogenic forcing on the Roer.

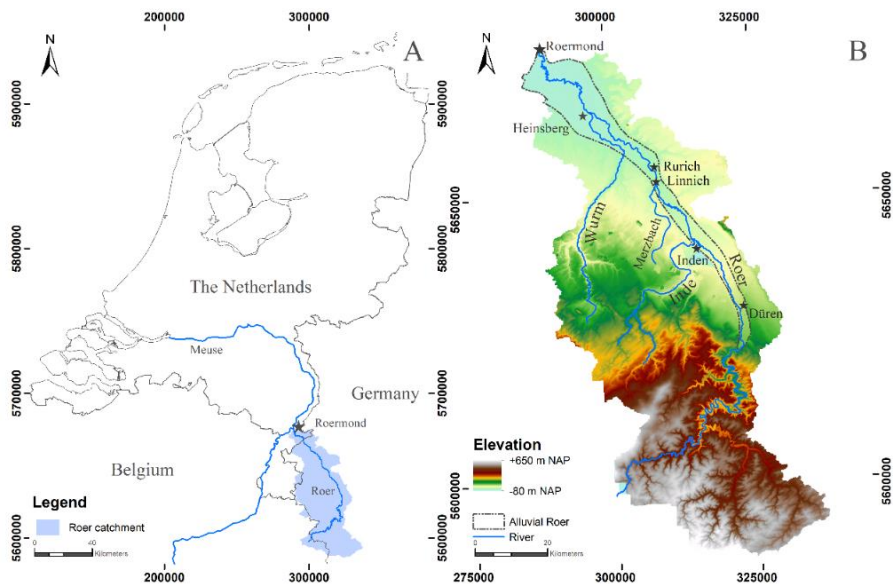


Fig. 1: (A) Overview of the Roer River, which flows from eastern Belgium via Germany to the Netherlands. The Roer River debouches in the Meuse at Roermond. (B) LIDAR elevation model (AHN2, n.d.; Land NRW, n.d.) of the Roer catchment with its main tributaries the Inde, Merzbach and Wurm. The study area (the alluvial part of the Roer Valley) is outlined by the dashed line. Coordinates in ETRS 1989 UTM Zone 32 N.

4.2 Setting

4.2.1 The Roer and its catchment

The Roer River (or Rur in German) has its source in the Hautes Fagnes (Belgium, ~660 m above sea level; Fig. 1). It flows through the northern part of the Eifel region (Germany) to debouche in the Meuse at Roermond (the Netherlands, ~18 m above sea level; Fig. 1). The catchment size of the Roer river is ~2354 km². The mean annual discharge is ~21.8 m³ s⁻¹ (at Stah, Germany). Discharge varies between 8 and 124 m³ s⁻¹ (LANUV, n.d.). The total length of the Roer is ~165 km. The upstream, bedrock dominated, part of the Roer River has a length of ~80 km. The downstream, alluvial part in the Roer Valley Graben is ~85 km. The study area comprises the alluvial part of the Roer (Fig. 1B) because it is susceptible to pattern change and shifts in channel position due to erosion and sedimentation of the river bed and banks (Schumm, 1985).

The Roer has several tributaries within the study area which drain higher elevated, loess covered Pre-Weichselian river terraces of the Rhine and Meuse (Fig. 1; Schirmer, 1990). The Roer has incised into these Rhine-Meuse terraces, during which it formed a series of terraces (Kasse et al., 2017). The terraces that formed since the Weichselian Late Pleniglacial are the subject of this study.

4.2.2 Geological and sedimentary setting

The alluvial part of the Roer River is situated in the active Roer Valley Rift System (RVRS), which is part of the Lower Rhine Embayment (LRE). The RVRS is situated in the southern Netherlands and adjacent parts of Belgium and Germany and forms the northern segment of the European Cenozoic rift system (Fig. 2; Schirmer, 1990; Ziegler, 1992; Michon et al., 2003; Kemna, 2005; Van Balen et al., 2005; Westerhoff et al., 2008). The main fault zones of the LRE and RVRS have a NW-SE orientation (Fig. 2A). The tectonic evolution of the LRE and RVRS have been studied extensively (Ahorner, 1962; Klostermann, 1983; Zagwijn, 1989; Geluk et al., 1994; Ziegler, 1994; Van den Berg, 1996; Houtgast and Van Balen, 2000; Cohen et al., 2002; Houtgast et al., 2002; Schäfer and Siehl, 2002; Michon et al., 2003; Michon and Van Balen, 2005; Schäfer et al., 2005; Westerhoff et al., 2008).

The RVRS experienced continuous subsidence since the Late Oligocene due to NE-SW directed extension, which led to a maximum of ~1200 m of subsidence in the Roer Valley Graben (RVG) (Geluk et al., 1994; Kemna, 2005; Schäfer et al., 2005; Schokker et al., 2005; Van Balen et al., 2005; Westerhoff et al., 2008). The RVRS is composed of full- and half-grabens (Fig. 2B; [Michon and Van Balen, 2005; Schäfer et al., 2005; Westerhoff et al., 2008]). The most important graben, for this study, is the RVG. The northern part of the RVG is asymmetric (half-graben) while its southern part is

symmetric (full-graben) (Fig. 2, transects A-A' and B-B'; [Michon and Van Balen, 2005]). Farther towards the southeast, in Germany, the symmetric graben transitions into two half-grabens (Fig. 2, transect C-C'; [Schäfer et al., 2005; Westerhoff et al., 2008]).

The RVG is bounded by the Campine Block (CB) in the south and the Peel Block (PB) and Erft Block (EB) in the north (Fig. 2). The Feldbiss Fault Zone (FFZ) separates the RVG from the CB. The Peel Boundary Fault Zone (PBFZ) forms the boundary between the RVG and the PB/EB. In Germany the PBFZ splits into the Rurrand (RR) and Erft (EF) fault zones (Fig. 2; Vanneste and Verbeeck, 2001; Michon et al., 2003; Van Balen et al., 2005; Westerhoff et al., 2008). A small horst within the subsiding RVG is delineated by the Koningsbosch (KB) and Beegden (BE) faults (Fig. 2).

Fault displacement rates of the (main) fault zones in the LRE and RVG have been studied in great detail by means of trenching, offset measurements of (terrace) surfaces with digital elevation models, lithological/geological offsets based on corings and wells, and outcrops in open-cast mines (Ahorner, 1962; Schäfer et al., 1996; Camelbeeck and Meghraoui, 1998; Houtgast et al., 2002; Van den Berg et al., 2002; Michon and Van Balen, 2005; Gold et al., 2017).

The primarily fault-controlled subsidence of the RVG has been shown to decrease from the northwestern (~184 mm/ky) to the southeastern (~120 mm/ky) part of the graben (Houtgast and Van Balen, 2000; Michon et al., 2003; Michon and Van Balen, 2005; Van Balen et al., 2005; Westerhoff et al., 2008). Fig. 2 shows an overview of the displacement rates of the (main) bounding faults of the RVG. It can be derived from Fig. 2 that the highest displacement rates occur along the northeastern boundary faults (i.e., the PBFZ and RR), leading to the observed maximum sediment accumulation of Neogene and Quaternary sediments along these fault zones (Boenigk, 1978; Michon and Van Balen, 2005; Schäfer et al., 2005; Boenigk and Frechen, 2006; Westerhoff et al., 2008).

The fault zones within the LRE and RVG are presently seismically active with the 1756 Düren and 1992 Roermond earthquakes (Mw 5.7 and Mw 5.4, respectively) as the most important examples (Geluk et al., 1994; Camelbeeck et al., 2007). Several trench studies have been performed to study past earthquake activity in the geological record. Van den Berg et al. (2002) conclude that two faulting events, with a maximum magnitude of Mw 6.0–6.5, occurred along the PBFZ between 15.8 and 13.0 ka cal BP.

Moreover, results from a recent trench study along the same PBFZ show that a faulting event occurred around 14.0 ka cal BP, which had an estimated magnitude of Mw 6.8 (Van Balen et al., 2019). These faulting events caused a vertical displacement along the PBFZ of approximately 1 m (Van den Berg et al., 2002; Michon and Van Balen, 2005; Van Balen et al., 2018, Van Balen et al., 2019).

A trench study over the Rurrand fault zone in Germany showed that fault movement was episodic, but the stratigraphic control was not sufficient to constrain the timing of the displacement events at this location (Vanneste and Verbeeck, 2001). Similar results were obtained by trench studies on faults of the FFZ (Camelbeeck et al., 2000; Houtgast et al., 2003; Vanneste et al., 2008). Houtgast et al. (2005) showed, by a compilation of results, that an increase in fault activity along the bounding fault zones of the RVG/LRE occurred between 15.0 and 10.0 ka cal BP.

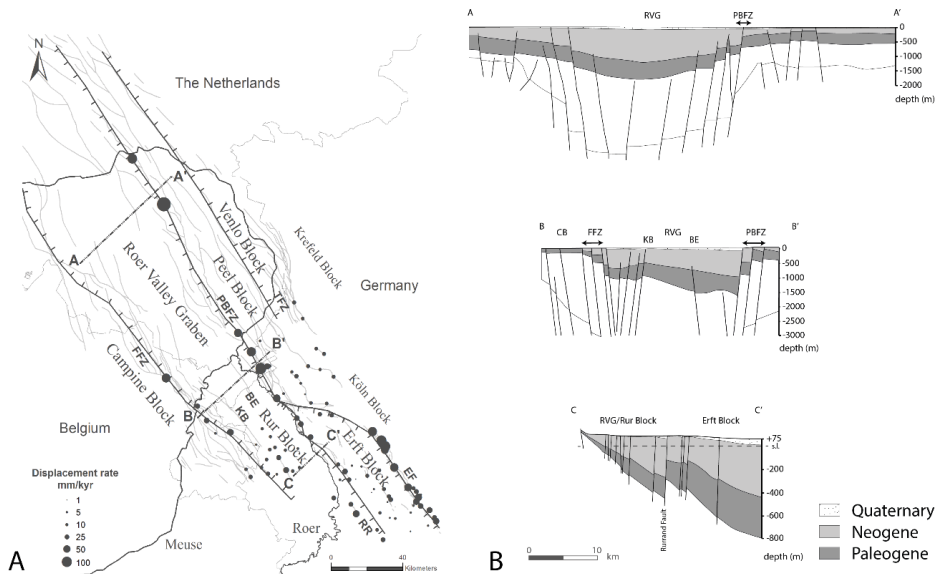


Fig. 2: (A) Tectonic setting of the Roer River in the Roer Valley Rift System (RVRS) and Lower Rhine Embayment (LRE) in the Netherlands and Germany. Transects A-A', B-B' and C-C' are shown in panel B. Displacement rates are adapted from Gold et al. (2017), Cohen (2003), Van Balen et al. (2018), Michon and Van Balen (2005), Van den Berg et al. (2002), Houtgast et al. (2005) and coring transects (Appendix C). Abbreviations of the fault zones are described in the main text. (B) Cross sections A-A', B-B' and C-C' as indicated in panel A that show the geometry of the Roer Valley Graben and the accumulation of its Neogene and Quaternary sediment fill. Cross sections are modified after Michon and Van Balen (2005) and Schäfer et al. (2005).

4 2.3 Climate, vegetation and associated changes in river morphology

Climate change and vegetational development since the Weichselian Late Pleniglacial have been studied extensively for the study area (Kalis and Bunnik, 1990; Hoek, 1997a, Hoek, 1997b [site Gulickshof]; Bunnik, 1999; Bogaart and Van Balen, 2000; Bos and Zuidhoff, 2015; Bakels, 2017; Hoek et al., 2017; Woolderink et al., 2018). Fig. 3 shows the (bio)chronostratigraphy for the (southeastern) Netherlands together with the characteristic pollen assemblages and associated Pollen Assemblage Zones (PAZ). The PAZ subdivision follows Hoek, 1997a, Hoek, 1997b for the Lateglacial, and Zagwijn (1986) and Bos and Zuidhoff (2015) for the Holocene. Moreover, reconstructed mean July temperatures are shown in Fig. 3.

A general, climate-forced, fluvial morphological trend was established for the Rhine and Meuse rivers (Fig. 3; Vandenberghe et al., 1994; Berendsen et al., 1995; Kasse et al., 1995; Huisink, 1997; Vandenberghe, 2002; Erkens et al., 2009, Erkens et al., 2011; Janssens et al., 2012; Woolderink et al., 2018). In the Last Glacial Maximum (LGM; ~19.0–14.7 ka cal BP) these rivers had a braided planform due to a scarce vegetation cover, high sediment load and a nival discharge regime. During the Bølling (~14.7–14.0 ka cal BP) temperatures and precipitation increased (Renssen and Isarin, 2001), which led to an increased vegetation cover, a more mixed discharge regime and reduced sediment load.

This, in turn, forced fluvial planform change from a braided to a multi-channel low-sinuosity planform. Continued vegetation development and a more regular discharge regime during the Allerød (~13.9–12.85 ka cal BP) resulted in a meandering river system. The successive Younger Dryas (~12.85–11.7 ka cal BP) is characterized by climatic cooling, a decreased vegetation cover and re-establishment of discontinuous permafrost (Kasse et al., 1995, Kasse et al., 2005; Woolderink et al., 2018). This led to an increased sediment supply to the river that, together with a more nival discharge regime, resulted in a braided or wandering fluvial planform.

Climatic warming and a more regular discharge regime during the onset of the Holocene resulted in a rapid degradation of permafrost, increasing vegetation cover and reduced sediment supply. These changes resulted in the change from a braided/wandering system during the Younger Dryas to a multi-channel low-sinuosity planform during the Preboreal (~11.7–10.8 ka cal BP). From the Boreal onwards (10.8–0.0 ka cal BP), climate stabilized and continued vegetation succession prevailed, which resulted in a meandering (or anastomosing) river pattern.

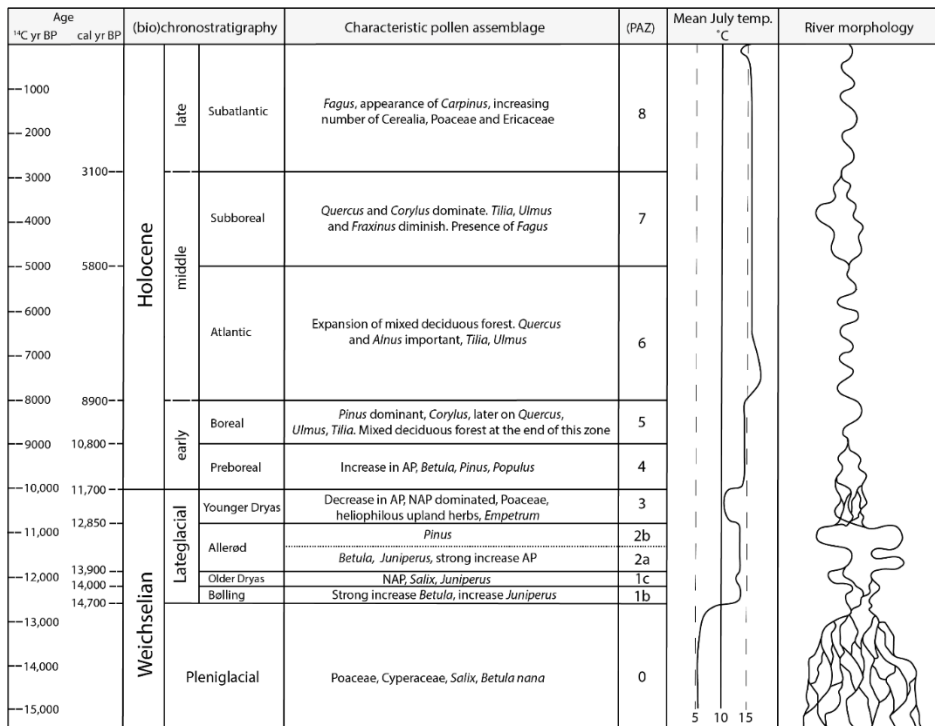


Fig. 3: (Bio)chronostratigraphy for the (southeastern) Netherlands together with the characteristic pollen assemblages and associated Pollen Assemblage Zones (PAZ). The PAZ subdivision follows Hoek, 1997a, Hoek, 1997b for the Lateglacial and Zagwijn (1986) plus Bos and Zuidhoff (2015) for the Holocene. Mean July temperatures are modified after Berendsen et al. (1995). River morphology is based on the development of the Rhine-Meuse river system.

Large-scale deforestation in the Rhine, Meuse and Roer catchments since the Younger Neolithic (~6.4–5.4 ka cal BP) and especially the Bronze Age (~3.95–2.75 ka BP) resulted in a significant increase in sediment supply to the river valleys in the Late Holocene (~3.1–0 ka cal BP) (Kalis and Bunnik, 1990; Schirmer, 1995; Bunnik, 1999; Dambeck and Thiemeyer, 2002; Houben, 2003; De Moor, 2007; Bos et al., 2008; Erkens et al., 2009; Gerlach et al., 2012). For example, landscape evolution modelling predicted a threefold increase in suspended sediment yield in the Meuse catchment for the Late Holocene compared to the preceding Middle Holocene (Ward et al., 2009).

Although this general trend in fluvial planform change could be established, it was recognized that fluvial style changes in the Rhine and Meuse tributaries differ from the main rivers (Kasse et al., 2005, Kasse et al., 2017; De Moor et al., 2008; Janssens et al., 2012). For example, the shift from a meandering system during the Allerød to a braided/wandering planform during the Younger Dryas was not observed for the Niers Rhine, Lippe and Oude IJssel, or for the lower most part of the Roer River (Kasse et al., 2005, Kasse et al., 2017; Janssens et al., 2012). Furthermore, it is known from other (lowland) rivers in Europe, such as the Scheldt (Belgium), Tisza (Hungary) and Warta

(Poland) that a shift from meandering to braided during the Allerød/Younger Dryas transition did not always occur (Kozarski et al., 1988; Kiden, 1991; Vandenberghe et al., 1994; Gábris and Nádor, 2007; Kasse et al., 2010). Moreover, even within the same river, reach-to-reach variations in morphological expression to the same climatic forcing may occur, as was observed for the Rhine and Meuse rivers (Erkens et al., 2009; Woolderink et al., 2018).

4.3 Methods

4.3.1 DEM analysis, lithological cross sections and cores

Terrace levels and abandoned channels were identified and selected in LIDAR imagery (1 m resolution [AHN2, n.d.; Land NRW, n.d.]). Hereafter, transects were hand cored over the channels in order to find the most suitable locations for sampling the abandoned channel fills to perform radiocarbon dating and/or pollen analysis. A soil auger, gouge and suction corer (in case of water-logged sandy sediments) were used in the field and sediments were described for lithology, carbonate content, colour, grain size (NEN 5104) and presence of plant remains. Sediment cores (~1 m long) were taken with either a modified Livingstone piston sampler or an \varnothing 60 mm gouge. The cores were subsampled in the field and put into plastic bags before transport and storage in a cool room until further analysis in the laboratory.

4.3.2 Radiocarbon dating

Selected subsamples of the cores were treated with diluted potassium hydroxide (peat samples) or disodium pyrophosphate (clayey samples), to disperse organic compounds or clay bonds. After this the samples were sieved over a 200 μ m mesh and terrestrial macro remains were picked from the samples subsequently. The targeted macrofossils were then treated following the Acid-Alkali-Acid (AAA) method and dried overnight at 90 °C, after which the samples were (AMS) radiocarbon dated at the Centrum voor Isotopen Onderzoek (CIO) in Groningen, the Netherlands. The location, sample depth, and sample material are given in Table 1.

Table 1: Location, sample depth, sample material and age of the AMS radiocarbon dates. Coordinates in Dutch (RD NEW) coordinate system.

Sample	x	y	depth (cm below surface)	material	% C	$\delta^{13}\text{C}$ (‰)	age ^{14}C	age cal yr BP
Erzelbach Core	219636	331339	118	<i>Corylus</i> seed fragment	52.4	-29.41	3373±17	3684-3644
Erzelbach III	219630	331331	220	Rounded wood fragment	48.9	-25.16	5136±19	5933-5890
Schafhausen	206179	340331	80-75	Undeterminable organic fraction	49.9	-27.44	10475±30	12,559-12,378
Kapbusch	212634	337724	88-84	<i>Carex</i> seeds	50.5	-26.23	10695±30	12,718-12,589
Kapbusch	212634	337724	153-150	<i>Carex</i> seeds, <i>Betula</i> seeds	46.9	-25.92	11915±20	13,796-13,704
Ivenhain	218406	333149	180-175	Mosses, <i>Betula</i> seeds, <i>Carex</i> seeds	46.2	-32.23	13495±40	16,444-16,060
Haaserdriesch	201867	345194	224-220	<i>Betula</i> seeds	52.4	-28.22	12235±35	14,270-14,005
Geraerds	201146	347022	117-114	<i>Carex</i> seeds	52.7	-26.16	11720±30	13,598-13,451
Karken	202476	345852	110-107	<i>Betula</i> seeds, <i>Carex</i> seeds, <i>Alnus</i> seeds	48.0	-26.68	11525±20	13,436-13,296
Bolberg	203888	351371	157-155	Wood	47.3	-27.95	3200±10	3450-3388
Turfkoelen	204183	351563	236-234	Fragment of Pine cone	61.2	-25.72	9420±30	10,726-10,576

4.3.3 Digital mapping

Digital mapping of the Roer Valley was performed using a system that splits mapping of geomorphological elements from cataloguing naming, literature referencing and dating results for individual elements (Berendsen et al., 2001, Berendsen et al., 2007; Cohen et al., 2012; Pierik et al., 2016; Woolderink et al., 2018). Fig. 4 shows the steps involved in the digital mapping method (Woolderink et al., 2018). As a first step, dated geomorphological elements were collected from existing publications, (institutional) databases or new fieldwork and stored in a GIS database (Fig. 4A). Furthermore, LIDAR height data and data from previous geological, pedological, geomorphological and historical mappings were used to identify geomorphological elements (Fig. 4B). These datasets were combined and manually (re)interpreted, using cross-cutting relations, to a geomorphological/geological map (Fig. 4C). The correlation decisions of the geomorphological elements (represented by GIS polygons) are described in the catalogue of the database (Fig. 4D). As a final step, an age map (Fig. 4E) and a time-slice map series (Fig. 4F) of the palaeogeographic evolution were generated based on linking of GIS polygons and dating information from the catalogue. For further, more detailed information on the digital mapping method we refer to Berendsen et al. (2007), Cohen et al. (2012), Pierik et al. (2016) and Woolderink et al. (2018).

The age map shows the final stage of river-bed sedimentary activity that is, in this study, considered to be the last moment at which bedload transport occurred in a channel. A (basal) channel infill, therefore, provides a minimum age of channel activity (a *Terminus Ante Quem* date for this activity). Geomorphological elements that are not dated directly are attributed with an end-date based on correlation on height, morphological continuity, lithology, pedology and historical maps, to a dated element. The time series map separates active channel belts from abandoned ‘terrace’ fragments. Shading of the assigned colours indicates ‘later reworked’ and ‘preserved up to present’ parts of the (abandoned) geomorphological elements and/or terrace fragments (Berendsen and Stouthamer, 2001; Cohen et al., 2012). The time slice map series shows the maximum spatial extent of the successive active channel belts and is, therefore, larger than the active channel belt at any instantaneous point in time. The map outputs are presented at full scale in Appendix A. Moreover, the GIS database and associated maps will be available for download as part of the “Digital Basemap for the Lower Meuse Valley Palaeogeography” (Woolderink and Cohen, 2018) at: [doi:10.17026/dans-xkk-f29b](https://doi.org/10.17026/dans-xkk-f29b).

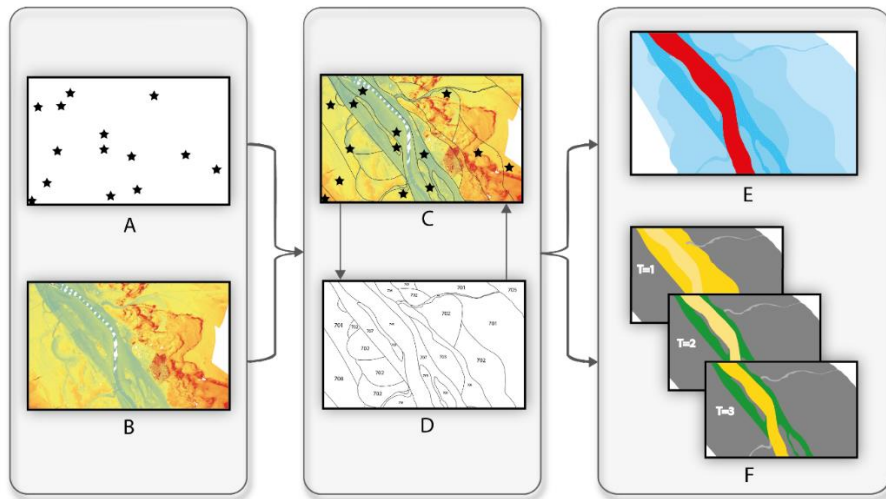


Fig. 4: Flowchart of the digital mapping method. (A) Dated geomorphological features; (B) LIDAR elevation data; (C) dating information as well as the geomorphic cross-cutting relations; (D) digitized terrace fragments (polygons) with attached catalogue part of the database; (E) terrace or age map output; (F) time-slice map series of the palaeogeographic evolution (adapted from Woolderink et al., 2018).

4.3.4 Pollen analysis

Sub-samples were taken for pollen analysis from the most basal part of the channel fills to investigate the start of infill and, therefore, time of abandonment of the channels. The pollen samples were treated following the standard method by Faegri and Iversen (1989), after which they were mounted in glycerine jelly. Pollen types were subsequently identified using Faegri and Iversen (1989) and Moore et al. (1991). The pollen-sum includes trees, shrubs, upland herbs, heathers and Poaceae. Pollen diagrams were digitized and visualized using the Tilia software package (Grimm, 1992). Local Pollen Assemblage Zones (LPAZ) were differentiated based on changes in the main pollen taxa. Successively, the LPAZ were correlated to the Pollen Assemblage Zones (PAZ) of the biostratigraphic framework for the Lower Meuse Valley, the Netherlands (Fig. 3; Zagwijn, 1986; Hoek, 1997a, Hoek, 1997b; Bos and Zuidhoff, 2015; Hoek et al., 2017; Woolderink et al., 2018). The full pollen diagrams of the studied sites, together with a description of the Local Pollen Assemblage Zones (LPAZ) and biostratigraphic correlation to the regional Pollen Assemblage Zones (PAZ), can be found in Appendix B. Moreover, the lithological transects over the abandoned channels are provided in Appendix C.

4.3.5 Gradient lines

Longitudinal gradients were constructed for each of the terrace levels. As a first step the geomorphological boundaries of the terrace fragments were digitized to polygons. Then, ~300 random points were placed within the polygon boundaries via a GIS computing

step (e.g., “create random points” ArcGIS), excluding man-made structures and mining locations to the best of our abilities. Surface elevation points were then extracted from a LIDAR digital elevation model (AHN2, n.d.; Land NRW, n.d.) for each point and subsequently plotted against a valley reference line. This reference line was drawn through the middle of the alluvial Roer Valley. Finally, trend-lines were plotted through the data points to obtain the gradients of the terrace levels.

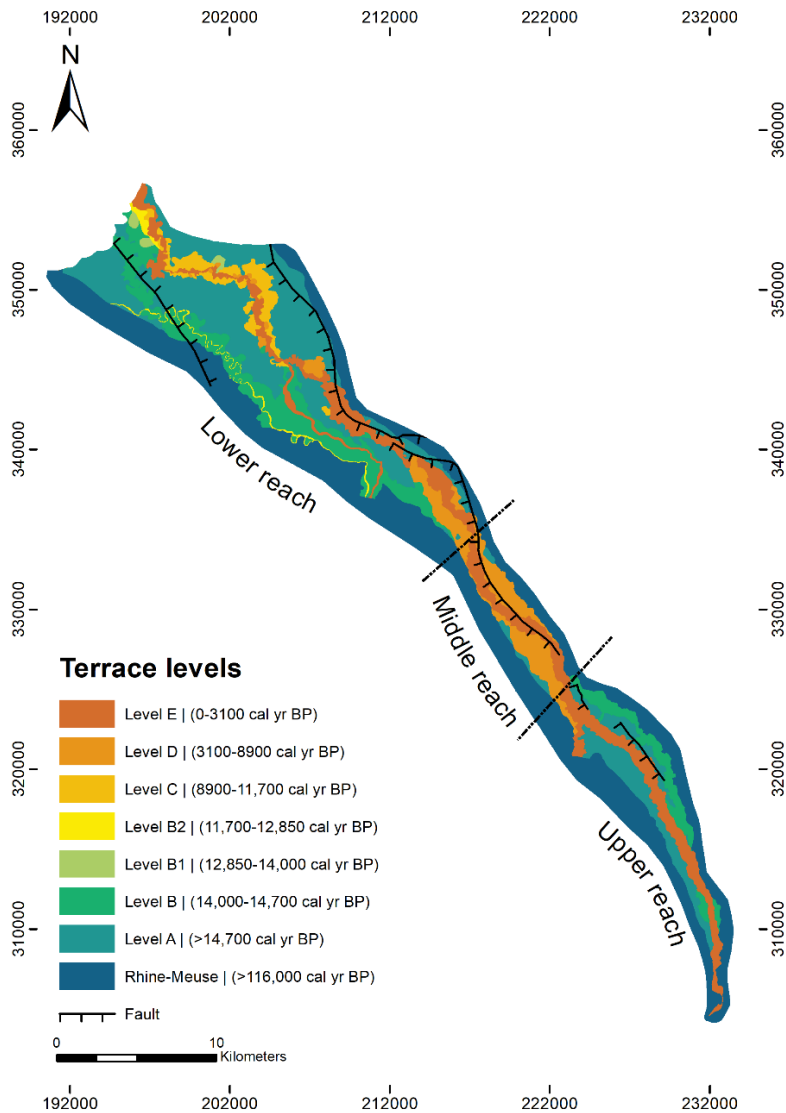


Fig. 5: Terrace levels of the Roer River within the Roer Valley Graben since the Weichselian Late Pleniglacial. The fault zones at the northern boundary are the Peel Boundary Fault Zone (PBFZ) and Rurrand Faultzone (RR) as shown in Fig. 2. Coordinates are in the Dutch (RD NEW) coordinate system.

4.4 Results: terrace characteristics and chronology

Five terraces were discriminated for the alluvial Roer within our study (Fig. 5). The alluvial Roer Valley was subdivided into an upper, middle and lower reach based on the terrace mapping (Fig. 5). The distinction of the terraces builds on the work of Kasse et al. (2017) and Janssens (2011), who introduced a subdivision of terraces for the lowermost part of the Roer Valley, close to the Meuse confluence. Kasse et al. (2017) and Janssens (2011) determined several large-scale lithological trends in (overbank) sedimentation within the different terrace levels, of which a summary is incorporated below. Additionally, Schalich (1968) distinguished multiple overbank sediment sequences for the middle Roer Valley in Germany. Our study maps the final stage of river-bed sedimentary activity, and overbank deposits will, therefore, provide a minimum age for the underlying river-bed sediments. To determine the time of abandonment of the different terraces/morphological levels, several abandoned channels were identified in LIDAR imagery and subsequently hand cored to retrieve the thickest infill. The locations of the abandoned channels are depicted in Fig. 6. The infills were dated biostratigraphically and, in some cases, by AMS radiocarbon dating. Fig. 7 shows the “main” pollen diagrams of the investigated sites. The diagrams show the ratio between the groups that make up the pollen-sum, e.g., ‘trees and shrubs’, ‘upland herbs’, ‘Poaceae’ and ‘Heathers’, as well as the percentage of pine (*Pinus*) and birch (*Betula*).

The sites Haaserdriesch, Karken, Geraerds, Bolberg and Turfkoelen were studied by Janssens (2011) and Kasse et al. (2017). In this study they were sampled for AMS radiocarbon dating to improve age control. The newly investigated sites Erzelbach, Schafhausen, Kapbusch and Ivenhain were sampled for pollen analysis and radiocarbon dating. Palaeochannel sites Kitscherholz, Rurich, Gutt Grittern and Bennebroek did not contain sufficient organic material for radiocarbon dating and were, therefore, only sampled for pollen analysis. The results of all AMS ^{14}C dates are in Table 1. Fig. 8 shows the start of the basal infill of the abandoned channels.

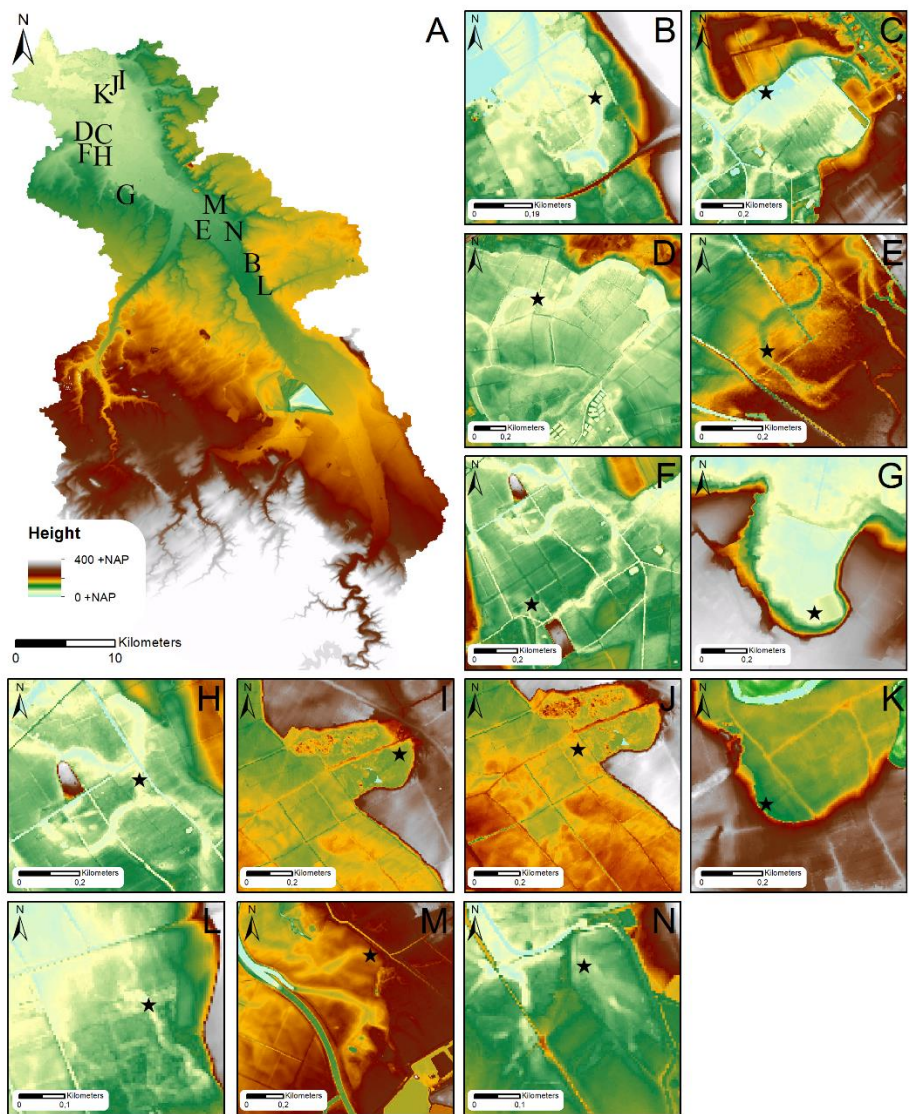


Fig. 6: (A) Overview of the locations of the investigated abandoned channels in the Roer Valley. (B) Site Ivenhain, (C) site Karken, (D) site Geraerds, (E) site Kapbusch, (F) site Haaserdriesch, (G) site Schafhausen, (H) site Kitscherholz, (I) site Turfkoelen, (J) site Bolberg, (K) site Bennebroek, (L) site Erzelbach, (M) site Gutt Grittern, and (N) site Rurich.

4.4.1 Level A

4.4.1.1 Morphology and preservation

Level A is characterized by an undulating relief with, in the lower reach, a cover of aeolian sediments (Fig. 9B). Fluvial morphology is almost absent on level A, except for some abandoned (meander) channels at the valley sides (Fig. 6B). Level A is predominantly present in the lower and upper reach of the alluvial Roer Valley (Fig. 5). The presence of level A in the middle reach of the Roer is limited to the valley sides (Fig. 5, Fig. 10).

For this study, level A is the highest level in the Roer Valley (Fig. 10; profiles A-A', B-B', G-G' and H-H'). The height of the terrace scarp between level A and the most recent terrace level E decreases from ~10 m to ~2 m in the upstream direction (Fig. 10; profiles A-A' and B-B'). In the upper reach of the Roer Valley the maximum height of the terrace scarp between level A and level E is ~3 m (Fig. 10; profile G-G' and H-H'). The elevation of level A declines from 137 m a.s.l. in the upper part of the Roer Valley to 28 m a.s.l. downstream, near the confluence point with the Meuse River. Level A has a gradient of ~3.0 m/km in the upper reach of the Roer Valley. The gradient decreases to ~2.2 m/km and ~0.6 m/km in the middle and lower reach the Roer Valley, respectively (Fig. 11).

4.4.1.2 Sedimentology

Near the confluence with the Meuse, the basal part of level A is characterized by fine to medium and locally gravelly coarse sands that are covered by 1–2 m of loamy sand and sandy loam. This sequence is overlain by ~5 m of slightly loamy, fine to medium sand with fining-upward sequences of up to 2 m thick (Kasse et al., 2017). In the more upstream part of the lower reach of the Roer Valley (near the Dutch-German border), the same sequence is characterized by medium to coarse gravelly sands, which are overlain by 2 to 3 m of loamy fine to medium sand (Vreugdenhil, 2011). In the middle and upper Roer Valley the base of the sequences consists mainly of sandy gravels with clasts up to 5 cm in diameter (Grooteman, 2018; BGR, n.d.). The thickness of the overlying fine-grained (mainly silt) deposits decreases to ~1 to 1.5 m in the upper Roer Valley (BGR, n.d.).

4.4.1.3 Chronology

Pollen data and radiocarbon dating show that the channel at site Ivenhain starts filling in during the Late Pleniglacial (~19.0–14.7 ka cal BP), indicating that this channel was abandoned during, or just before that time (Figs. 6B, Fig. 7, Fig. 8). A Late Pleniglacial age for level A is supported by an OSL date of 15.5 ± 1.1 ka (Stella Maris 3, Kasse et al. 2017)

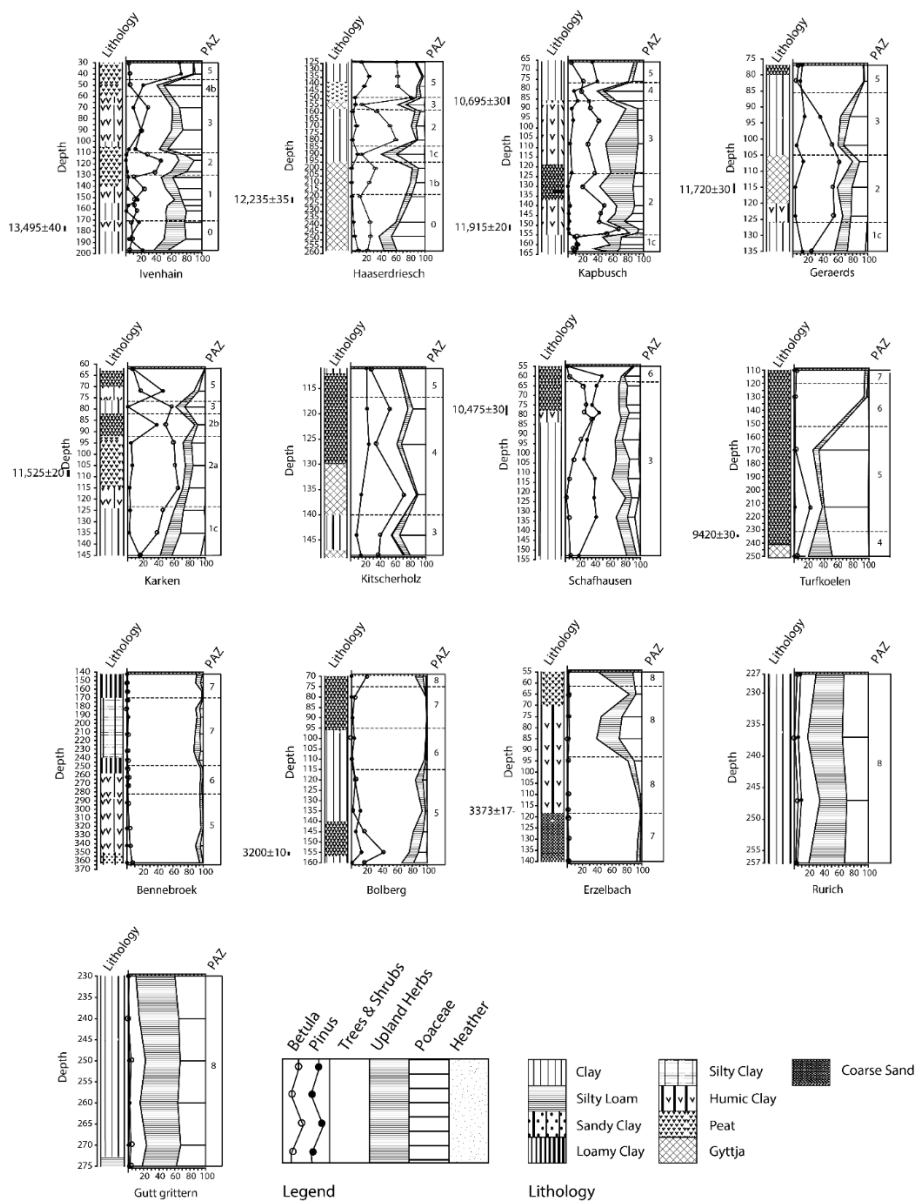


Fig. 7: Main pollen diagrams of the investigated channel fills together with the lithology and performed radiocarbon dates. Depths of diagrams are in centimeters below surface level.

4.4.2 Level B

4.4.2.1 Morphology and preservation

In the lower reach of the Roer Valley, level B can be distinguished from other terrace levels as an incised meander belt with well-developed and clearly recognizable high-sinuosity meanders and local neck-cut-offs (Figs. 6C, D, E and 9C). This incised meander belt can be traced in the upstream direction to ~27 km upstream of the Meuse confluence point (Fig. 5, Fig. 11). In the upstream Roer Valley, the fluvial morphology on level B is less well preserved compared to the lower Roer Valley. This is probably due to younger overbank deposits on top of level B. In the upper Roer Valley, level B is, therefore, primarily distinguished based on the maturity of soils (i.e., mature “gley soils” versus younger and less well-developed “gley-vega” soils [NRW, n.d.]) and historical mapping. The Tranchot-maps (~1801–1810) were used for the discrimination of relatively dry arable lands and wetter pasture lands, where the latter were interpreted as younger floodplain levels that inundate regularly.

The height of level B decreases from ~130 m to ~25 m a.s.l. in the downstream direction (Fig. 10). Incision of level B into level A decreases from ~3 m to ~1 m in the upstream direction in the lower reach of the Roer Valley (Fig. 10; profiles A-A' and B-B'). In the northwestern part of the lower Roer Valley, a small SE-NW terrace scarp separates a local, intermediate, sublevel (B2) between level B and the next level C (Kasse et al., 2017). Just upstream of the confluence with the Wurm, level B is situated at a similar height, or ~1 m lower than the youngest terrace level E (Fig. 10; profiles C-C' and D-D'). In the upper reach of the Roer Valley, level B is separated from level A by a small (~0.5–1.0 m) terrace scarp (Fig. 10; profiles G-G' and H-H'). Some NW-SE orientated linear scarps are present on level B in the upstream Roer Valley (Fig. 5). These lineaments can be ascribed to faults. Level B has a gradient of ~2.9 m/km in the upper reach of the Roer Valley, which decreases to ~0.7 m/km in the lower reach of the Roer Valley (Fig. 11).

4.4.2.2 Sedimentology

In the lower Roer Valley, near the confluence with the Meuse, the lithological successions of level B are characterized by a channel lag deposit of fine gravel and medium to coarse sand (300–850 μm). This channel lag is overlain by a fining-upward sequence of ~3 m that consists of coarse and medium to fine sands. This fining-upward sequence is finally overlain by a loamy sand and sandy loam unit of ~1–2 m, which can be interpreted as overbank or floodplain sediments. In the lower Roer Valley, the total thickness of the level B sequence is between 5 and 6 m (Kasse et al., 2017). The thickness decreases to ~3 m in the upstream direction, near the Dutch-German border (Vreugdenhil, 2011). Although lithological trends are similar as in the downstream area, the gravel content of the channel lag deposits increases in this more upstream position.

Thickness of the sediment sequence decreases to ~2 m near the transition to the middle Roer Valley (Appendix C, site Kapbusch).

4.4.2.3 Chronology

Based on pollen data, the palaeochannels Karken (Fig. 6C), Geraerds (Fig. 6D), and Kapbusch (Fig. 6E) started infilling during the Older Dryas period (~14.0–13.9 ka cal BP). This is supported by ¹⁴C dates higher up in the channel fills (Table 1, Fig. 7, Fig. 8). This implies that these channels have a minimum age of Older Dryas and that their final channel activity can, most probably, be placed in the Bølling (~14.7–14.0 ka cal BP). The channel at site Haaserdriesch (Fig. 6F), however, started infilling during the Late Pleniglacial (~19.0–14.7 ka cal BP), indicating that this channel was abandoned earlier than the other sites on level B. The pollen diagram of Haaserdriesch was re-interpreted in this study based on new insights due to AMS ¹⁴C dating of terrestrial seeds (*Betula*: Table 1) in the fill. For this re-interpretation we refer to Appendix B. The infills of palaeochannels at Schafhausen (Fig. 6G) and Kitscherholz (Fig. 6H) were biostratigraphically dated as Younger Dryas (~12.85–11.7 ka cal BP; Fig. 7), indicating a final stage of activity during the Younger Dryas for these channels.

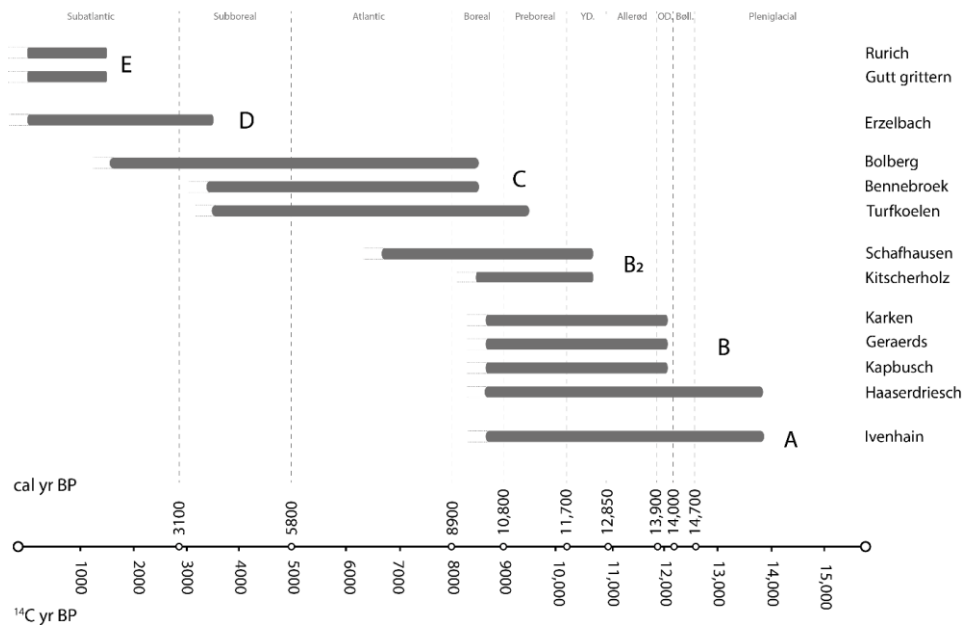


Fig. 8: Start and duration of the infill of the abandoned channels on the different terrace levels. Letters refer to the associated terrace levels as discussed in Section 4.

4.4.3 Level C

4.4.3.1 Morphology and preservation

Level C is characterized by a meandering morphology (Fig. 9D). Residual channels of level C are, however, subdued due to channel infill and a cover of overbank deposits. Level C is only present in the lower Roer Valley, approximately between the confluence with the Meuse (at Roermond) and the Dutch-German border (Fig. 5). The height of level C decreases from ~33 m a.s.l. upstream to ~20 m a.s.l. near the confluence with the Meuse River at Roermond. Level C is incised in level A and has a terrace scarp of up to 5 m in the lower reach of the Roer Valley (Fig. 10; profile A-A'). The gradient of level C is ~1.1 m/km (Fig. 11).

4.4.3.2 Sedimentology

The basal lithology of level C consists of a poorly-sorted, gravelly sand and gravel channel lag that contains clay pebbles and plant remains. This basal gravel is overlain by a moderately-sorted, medium to coarse grained, fining-upward sand unit that can be interpreted as a pointbar sequence (Janssens, 2011; Kasse et al., 2017). These sands are generally covered with a unit (~1.5–2 m) of (slightly) silty clay that is strongly oxidized and compacted. The clay unit is likely formed by overbank and floodplain sedimentation. It may represent the same unit as the “old overbank sediment sequence” described by Schalich (1968) for the middle Roer Valley. According to Schalich (1968), this overbank sequence consists mainly of reworked Pleistocene solifluction material and a minor fraction of loess and younger erosion materials. The top of the level C sequence is characterized by a coarser-grained layer of ~1.5 m, which consist of sandy, silty or clayey loam. This unit is also interpreted as a (younger) overbank deposit. The thickness of the sediment sequences of level C decreases from ~5 m near the Roer-Meuse confluence, to ~3 m at the most upstream occurrence of level C (Janssens, 2011).

4.4.3.3 Chronology

Based on pollen analysis, the abandoned channel of Turfkoelen (Figs. 6I and 7) has a basal infill of (Late) Preboreal age (~11.7–10.8 ka cal BP [Janssens, 2011]). This is supported by a radiocarbon date of a pine cone that gave an age of 9420 ± 30 yr BP (~10.7 ka cal BP [IntCal13 calibrated]). An age of deposition between 10.0 ka cal BP and 8.5 ka cal BP was derived for the “old overbank sequence” by Schalich (1968), supporting the conclusion that the underlying channel deposits are 10.0 ka cal BP or older.

The basal infills of Bolberg (Figs. 6J and 7) and Bennebroek (Figs. 6K and 7) show that infilling started during the Boreal (~10.8–8.9 ka cal BP), which means that final activity of the channels occurred during either the Boreal or the end of the preceding Preboreal.

At site Bolberg, a ^{14}C date of 3200 ± 10 yr BP, at 157–155 cm depth, is considered too young based on the palynological results (see discussion in Appendix B). We assume that the material that was sent in for dating probably was a piece of root of a younger vegetation cover.

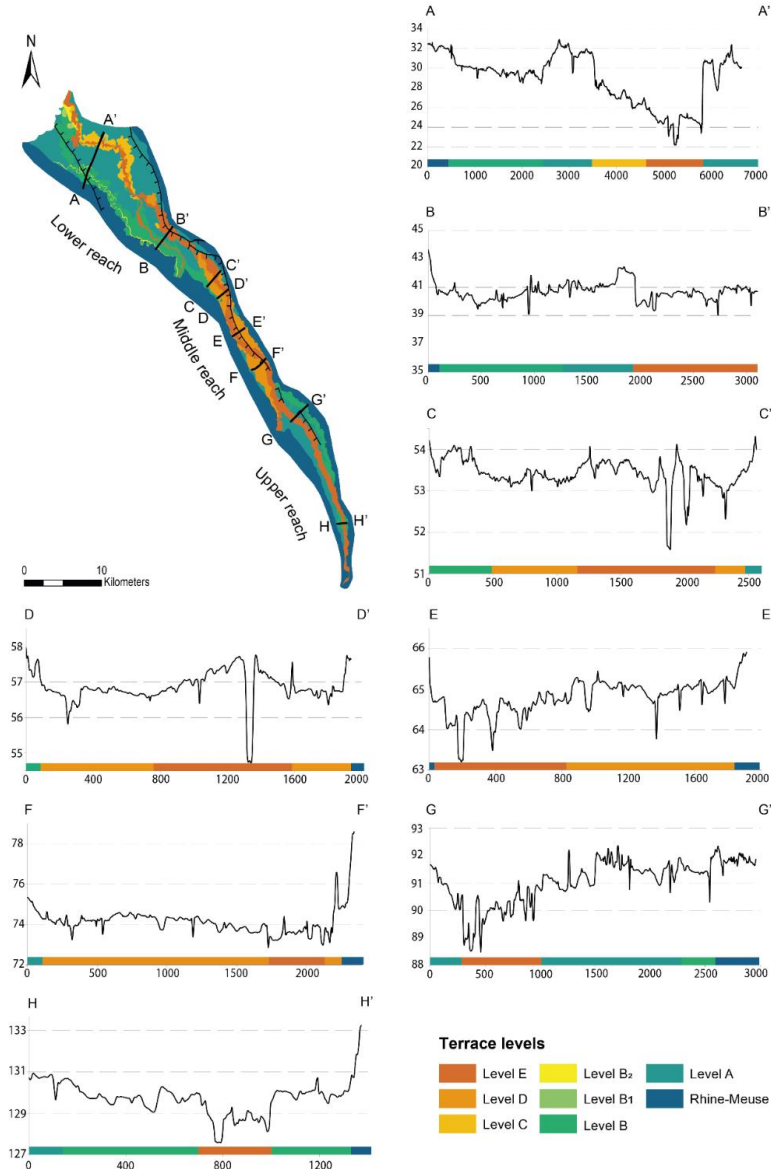


Fig. 10: Topographic cross sections of the terrace levels over the course of the Roer River. Terrace levels are best differentiated in the lower Roer Valley (A-A', B-B'). The zone around transects C-C' and D-D' is characterized by minimal terrace differentiation and by levee formation. Topographic differences between the most recent terrace level E and older Late Pleniglacial and Lateglacial terraces are present in the upper reach of the Roer Valley (G-G' and H-H'). Elevation of the profiles is in meters above sea-level. Distance along profiles is in kilometers.

4.4.4 Level D

4.4.4.1 Morphology and preservation

Channel remnants of level D show multiple fluvial planforms. In the lower Roer Valley, level D is present in the form of individual meanders (Fig. 9E). In the middle Roer Valley, the morphology of level D is dominated by multiple channels that converge and diverge regularly, indicating an anastomosing river planform (Fig. 9F). Level D could not be distinguished in the upstream reach of the Roer Valley (Fig. 5). The elevation of level D declines from 87 m a.s.l. in the middle part of the Roer Valley to 23 m a.s.l. downstream in the lower Roer Valley. The terrace scarp between level D and the current terrace level E is ~1 m in the lower reach of the Roer Valley. At the transition between the lower and middle reach, level D is positioned at a similar height as adjacent levels A and B (Fig. 10; profiles C-C' and D-D'). In this area the levels are separated based on morphology, pedology and historical maps. The height difference between level D and the lowest terrace level E is ~0.5 m in the middle Roer Valley (Fig. 10; profile E-E' and F-F'). The gradient of level D decreases from ~2.1 m/km in the middle reach to ~1.5 m/km in the lower reach of the Roer Valley (Fig. 11).

4.4.4.2 Sedimentology

The lithological succession of deposits of level D consists of a poorly-sorted, gravelly sand and gravel channel lag at the base. The channel lag is overlain by a fining-upward sequence of ~2 m, which consists of coarse to very fine sand with increasing silt content and loamy layers (Janssens, 2011). This unit is covered by a fine-grained layer of loam and sandy loam with a thickness of up to ~1 m (Janssens, 2011; BGR, n.d.). These deposits likely represent the “young” overbank sediments as defined by Schalich (1968), which consist mainly of reworked loess.

4.4.4.3 Chronology

The Erzelbach channel (Fig. 6L) has a biochronostratigraphically dated start of infill of Subatlantic age (~3.1–0 ka cal BP). Pollen samples from the bedload material of Erzelbach, however, show an assemblage that is representative for the Subboreal (Fig. 7). A ¹⁴C date on a hazelnut fragment found at the bedload to channel fill contact gave an age of 3373 ± 17 yr BP (~3.7 ka cal BP [IntCal13 calibrated]). An additional ¹⁴C date on a piece of rounded wood from a channel lag under the levee/overbank sediments of the Erzelbach channel (Appendix C) was dated to 5136 ± 19 yr BP (~5.9 ka cal BP [IntCal13 calibrated]). Therefore, the activity of the Erzelbach channel is bracketed between circa 5.9–3.7 ka cal BP. The activity of level D is further confined by the age of the overlying “younger overbank sequence” as defined by Schalich (1968). These overbank deposits are dated by the presence of brick fragments and artefacts in the associated bedload material. Deposition of this “younger overbank sequence” probably started during the early Subatlantic, although most of the overbank sediments

accumulated between 1.4 and 0.7 ka cal BP (Schalich, 1968). It should, therefore, be noted that the start of overbank accumulation could be diachronous over the study area. Nevertheless, the end of activity of level D is, for this study, dated to the Subboreal-Subatlantic transition (~3.1 ka cal BP).

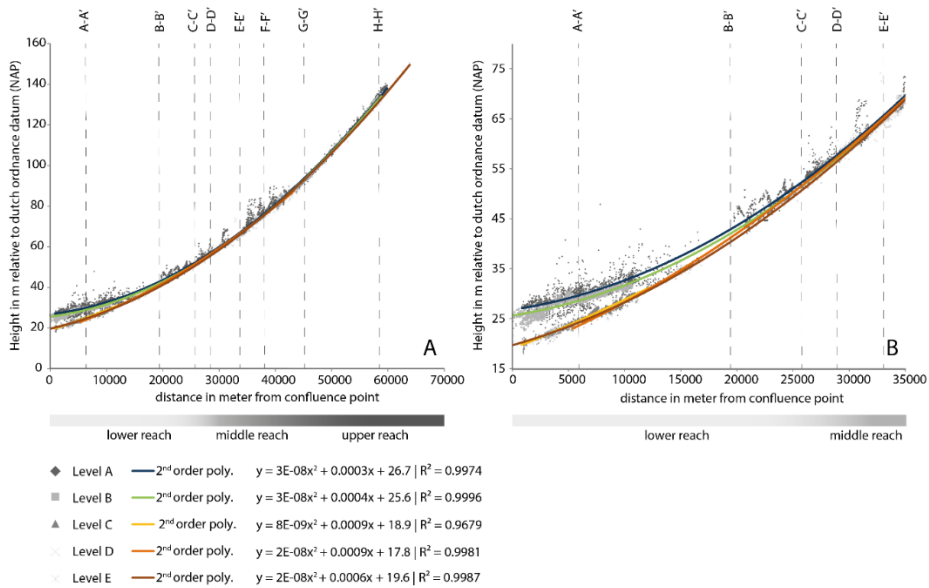


Fig. 11: (A) Longitudinal gradient lines of the terrace levels of the Roer River. Dashed lines indicate the locations of the topographic profiles in Fig. 10. (B) Zoom-in on the lower and middle Roer Valley longitudinal gradient lines that clearly show the incision of the Roer from the Late Pleniglacial (level A) to the Lateglacial (level B) and Holocene (levels C, D and E).

4.4.5 Level E

4.4.5.1 Morphology and preservation

Level E is characterized by a meandering fluvial planform (Figs. 6M, N and 9G). The morphology on level E is well preserved and residual channels have not been filled completely, even though level E is partially covered with levee and floodplain deposits (Janssens, 2011). Level E is present over the full length of the Roer Valley and is incised in levels C and D (Fig. 5, Fig. 10). The elevation of level E decreases from ~150 m a.s.l. in the upper Roer Valley to ~18 m a.s.l. at the confluence with the Meuse at Roermond. The height of the terrace scarp between level E and the (highest) level A is ~10 m in the lower reach of the Roer Valley. This elevation difference decreases in the upstream direction until level E and level A are positioned at similar elevations near the transition to the middle Roer Valley (Fig. 10; profile A-A' to D-D'). Therefore, discrimination between the terraces is based on pedology and historical mapping in this middle part of the Roer Valley.

The elevation difference between level E and level A increases to ~2 m in the upper Roer Valley (Fig. 10; profile G-G' and H-H'). The gradient of level E decreases from ~3.0 m/km to ~2.0 m/km and ~1.3 m/km in the upper, middle and lower reach of the Roer Valley, respectively.

4.4.5.2 Sedimentology

Level E is characterized by a lithological sequence that contains a channel lag of poorly sorted coarse to very coarse sand, gravelly sand and gravel at the base. Gravel content and gravel size increase in the upstream direction, with clasts up to (at least) 5 cm in the middle and upper reach. This channel lag is overlain by a fining-upward sequence of silty sands, pointing to a pointbar sequence. A vertically accreted overbank unit, which becomes coarser grained towards the top (i.e., sandy loam to loamy sand), covers these pointbar sediments. This unit often shows pronounced layering in the middle Roer Valley (Schalich, 1968). The thickness of the sediment sequence decreases from ~5 m in the lower reach of the Roer to ~2 m in the middle and upper Roer Valley (Schalich, 1968; Janssens, 2011; BGR, n.d.).

4.4.5.3 Chronology

The basal infills of the Gutt Grittern (Fig. 6M) and Rurich (Fig. 6N) channels are dated to the Subatlantic based on the pollen assemblage (Fig. 7, Fig. 8). The relatively low percentage of tree pollen and high amount of upland herbs and Poaceae, together with indicator species such as *Cerealia*, *Centaurea*, *Cannabis*-type and *Fagopyrum*, indicate an agricultural landscape of probably Medieval age or younger (~0.5 ka cal BP). This is in accordance with Schalich (1968). Based on the presence of nineteenth century artefacts in the bedload and high lead and zinc concentrations in the overlying “youngest overbank sediments” he dated this sediment sequence to the beginning of the nineteenth century (~0.2 ka cal BP). No ¹⁴C dates could be retrieved from the Gutt Grittern and Rurich channels due to lack of datable organic material in these clastic channel fills.

4.5 Discussion

4.5.1 Late Pleniglacial

The fluvial planform of the Roer during the Late Pleniglacial is characterized by a broad river plain, which widens downstream (level A, Fig. 5, Fig. 12A). This widening of the lower Roer Valley was interpreted by Kasse et al. (2017) as an aggrading, sandy, fan-shaped fluvial body in the confluence area of the Roer and Meuse. Furthermore, they indicate that the planform of the lower Roer Valley was probably that of a sandy braided system because of the absence of long fining-upward sequences and thick channel fills, which are associated with meandering channels.

Farther upstream of the study area of Kasse et al. (2017), however, the bedload material consists of coarser, gravelly sediments (Schalich, 1968; BGR, n.d.) and the morphology of site Ivenhain (Fig. 6B) does show a clear meandering planform associated with a ~2 m thick channel fill. The infill of the Ivenhain channel started during the Late Pleniglacial (Fig. 7, Fig. 8). Furthermore, new data on site Haaserdriesch (Fig. 6F) shows that this channel has an infill that started during the Late Pleniglacial (Fig. 7, Fig. 8). This implies that the morphology of the Roer during the Late Pleniglacial probably consisted of both a braided and a meandering planform. A meandering planform during the Late Pleniglacial was also observed in, for example, the middle Tisza Valley and other European valleys as well (Schirmer, 1995; Kasse et al., 2010). A possible explanation for the different, co-existing planforms might be a braided to low-sinuosity planform in the valley centre, with meandering secondary channels along the valley sides (Fig. 13).

Alternatively, the differences in planform can be related to variations in gradient and lithology. Kleinhans and Van den Berg (2011) show that channel patterns might change from meandering to braided due to a decrease in grain size and/or an increase in stream power. Such reach-to-reach variations (e.g., gravel size bedload in the middle and upstream parts versus sandy bedload in the lower part) might have controlled the planform differences in the Roer Valley. The aggrading nature of the Roer, and the formation of a fan-shaped fluvial body in the lower Roer Valley, can be explained primarily by base-level control of the Meuse. The Roer followed the aggradation of the Meuse, which was caused by the climatic conditions during the (Late) Pleniglacial (Van Balen et al., 2010). The formation of the observed sandy aeolian cover in the lower Roer Valley is ascribed to a decline in fluvial activity due to the increasing climatic aridity during the Late Pleniglacial and, therefore, availability of sandy source material (Kasse et al., 2017).

4.5.2 Bølling

The Roer River had a high-sinuosity, double channel belt, meandering planform during the Bølling (Level B; Fig. 5, Fig. 6C, D, 12B and 13). The changed planform, compared to the Late Pleniglacial, can be explained by the effects of climate change. The transition from the Late Pleniglacial to the Bølling is marked by an increase in temperature and precipitation (Vandenberghe and Bohncke, 1985; Renssen and Isarin, 2001). This resulted in an increased vegetation cover, more mixed discharge regime, degrading permafrost and reduced sediment input. Consequently, discharge concentrated into a decreasing number of channels, increasing the stream power in these channels and thus initiating incision. Deposition of overbank loams stabilized floodplains and river banks, enhancing further meandering and incision of the channels.

Furthermore, incision of the Meuse during the Bølling resulted in base-level lowering of the Roer, which contributed to the incision of the Roer channels. The same process of channel reduction and overbank sedimentation during the Bølling resulted in a transitional low-sinuosity multi-channel system for the Meuse and Niers rivers (Kasse et al., 1995, Kasse et al., 2005; Woolderink et al., 2018). Such differences in fluvial planform transitions may be explained by catchment or reach-specific factors such as discharge, grain size, gradient, tectonic setting and vegetation cover (Schumm, 1981; Vandenberghe, 1995; Erkens et al., 2011; Woolderink et al., 2018).

4.5.3 Bølling-Older Dryas transition

During either the late Bølling or the early Older Dryas, the Roer abandoned the southernmost course of its, up to then, double channel belt system in the lower Roer Valley (Fig. 5, Fig. 12C and 13). The abandonment of the southern course during the Bølling to Older Dryas transition could be derived from the start of infill of multiple meander scars of this southern Roer course (e.g., Karken, Geraerds, Kapbusch; Figs. 6C, D, E, Fig. 7, Fig. 8). This moment of abandonment of the southern course is supported by the age of a meander infill more downstream, which started to infill during the early Allerød (site Posterholt [Bakels, 2017]).

The abandonment of the southern course takes place at a bifurcation ~27 km upstream of the confluence between the Roer and Meuse at Roermond (Fig. 5). The most likely scenario is that the northern branch gained more discharge due to a gradient advantage. This, in turn, led to a reduced flow in the southern branch, leaving an “underfit” river system in this southern branch (Fig. 5, Fig. 12C and 13). This “underfit” system probably remained active during the Lateglacial as a course of the Wurm tributary, and a partially connected or high-water channel of the Roer (sites Schafhausen and Kitscherholz, Figs. 6G, H, Fig. 7, Fig. 12D and E). An increase of discharge in the northern Roer branch agrees with the increased meander size of the Allerød meanders (level B1) in this branch

compared to the preceding meanders of the double channel belt Bølling system (Fig. 5; Level B).

Climate change during the onset of the Bølling is considered to be an unlikely controlling factor in the preference of the northern Roer course because such climatic changes are regional. The only way in which these regional changes may have resulted in a preferred discharge in the northern Roer branch is when the indirect effects of permafrost degradation, vegetation cover or sedimentation pattern to climate change was non-uniform within the river plain.

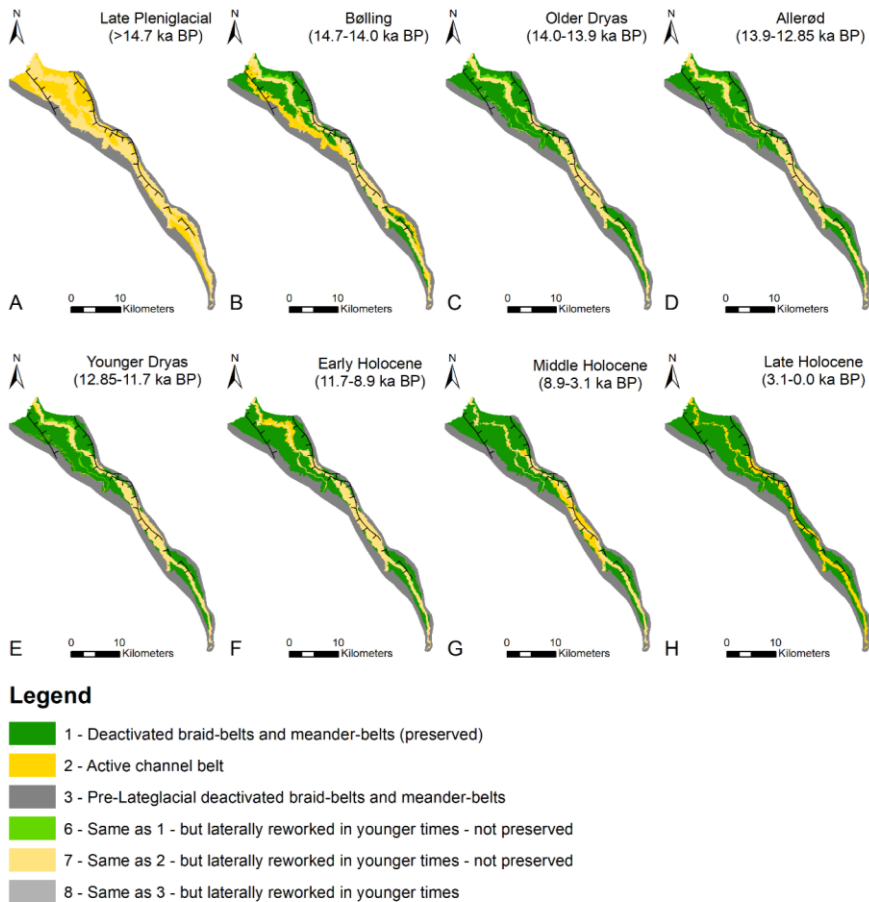


Fig. 12: Palaeogeographic evolution of the Roer River. (A) Late Pleniglacial, (B) Bølling, (C) Older Dryas, (D) Allerød, (E) Younger Dryas, (F) Early Holocene, (G) Middle Holocene, (H) Late Holocene. Fault zones in the north represent the Peel Boundary Fault Zone (PBFZ) and RR fault zone as indicated in Fig. 2. Legend after Berendsen and Stouthamer (2001) and Cohen et al. (2012).

As both courses of the Roer in the lower Roer Valley have approximately the same length and confluence location prior to the abandonment of the southern course (Fig. 12B), incision of the Meuse is also considered as an improbable cause for the observed preferred discharge in the northern Roer branch during the Bølling to Older Dryas transition. The configuration of the confluence of the Wurm and Roer (Fig. 5, Fig. 12), was already established prior to the Bølling to Older Dryas transition. It is, therefore, considered unlikely that this confluence of Roer and Wurm is responsible for the higher discharge in the northern Roer branch.

Tectonic forcing can be considered as a controlling factor on the abandonment of the southern channel of the Roer in the lower Roer Valley. Van den Berg et al. (2002) and Van Balen et al., 2018, Van Balen et al., 2019 concluded, based on trench studies, that faulting events, with associated earthquakes up to Mw 6.5–6.8, occurred along the Peel Boundary Fault Zone (PBFZ) during the Late Pleniglacial to Lateglacial period. Results of the trench study by Van Balen et al. (2019) show that the main faulting event occurred around 14.0 ka cal BP. This implies that a tectonic forcing acted on the Roer River during the late Bølling or early Older Dryas. These faulting events caused a vertical displacement along the PBFZ of approximately 1 m (Van den Berg et al., 2002; Michon and Van Balen, 2005, Van Balen et al., 2018, Van Balen et al., 2019). No displacement is inferred for the Beegden (BE) fault zone, which is located south of the Roer (Kasse et al., 2017). Thus, differential subsidence will have occurred (only displacement along the northern PBFZ). This differential subsidence will have resulted in a lateral gradient towards the northeast, i.e., in the direction of the PBFZ. Such a lateral gradient could then lead to an increased discharge to the northern Roer channel, resulting in the expanded northern and underfit southern course of the Roer. Likewise, tectonic forcing was suggested before as a possible cause for the abandonment of the southern Roer course by Kasse et al. (2017).

Another tectonic forcing that might have acted (simultaneously) on the abandonment of the southern course in the lower Roer Valley may be the presence of a zone of increased subsidence in the area of bifurcation. The study by Gold et al. (2017) shows enhanced subsidence rates around this area near Rurich (Fig. 1, Fig. 2). The increased subsidence is likely related to the fault configuration in this zone, where the PBFZ is connected to both the RR and EF faults (Fig. 2). Rivers will adapt to such a zone of subsidence by aggradation (Holbrook and Schumm, 1999). Aggradation normally occurs at the river bed, banks and floodplain. However, as the height of overbank deposition declines away from the channel, the river bed will become increasingly higher relative to the floodplain (Kleinhans et al., 2013). A gradient advantage develops towards the floodplain, which might trigger river bifurcation and avulsion (Törnqvist and Bridge, 2002; Kleinhans et al., 2013). Such an adjustment to a zone of subsidence is likely also (partially) the cause for the bifurcation of the Roer in the lower Roer Valley. This hypothesis is supported by a distinct levee complex that has formed in the area around Rurich on the present-day

terrace level E. Furthermore, elevation differences between the different terraces are minimal in this zone (Fig. 10, profile D-D'). Both the levee formation and the minimal elevation differences between the different terraces point to a zone of aggradation, making river bifurcation and avulsion a likely process in this area.

Another abandonment of one of the branches of a double channel belt Lateglacial Roer is observed in the upper reach of the Roer Valley. The younger terrace level(s) in the upper reach of the Roer Valley are positioned more to the south of the valley (Fig. 5, Fig. 12B and C). The reason for this is the position of the RR fault zone in between the Lateglacial and Holocene terraces (Fig. 5). Differential subsidence along the RR fault zone, where the Roer Valley Graben is subsiding compared to the Erft Block (Fig. 2) is, most likely, the cause for the avulsion of the Roer to the south. It should be noted, however, that age control for faulting events in the upper Roer Valley is suboptimal, which might mean that the observed southward shift of the Roer is not contemporaneous with the shift in the lower Roer Valley. More detailed age control in the upper Roer Valley might resolve this issue

4.5.4 Allerød

The Roer is characterized by a single-channel, high-sinuosity meandering planform during the Allerød (Level B1, Fig. 5, Fig. 12D and 13). With this change towards a meandering planform during the Allerød the Roer resembles most of the northwest and central European rivers (Kozarski, 1983; Szumanski, 1983; Kalicki, 1991; Berendsen et al., 1995; Kaiser et al., 2012; Woolderink et al., 2018). These Allerød meanders are larger than those that were formed during the Bølling (Fig. 5 and site Lerop 4; OSL age 13.5 ± 0.8 ka [Kasse et al., 2017]). The cause for this is, presumably, the increase in bankfull discharge following the change from a multi- to a single channel belt river system during the Bølling-Older Dryas transition. The downstream incision of the Roer can be attributed to increased discharge, reduced sediment supply and incision of the Meuse.

4.5.5 Younger Dryas

Based on the absence of braided morphology (remnants) and sedimentological characteristics, it is concluded that the Roer River continued to meander during the Younger Dryas (level B2, Fig. 5, Fig. 12E and 13). In this way the Roer River follows the fluvial development of the Warta (Poland) and Tisza (Hungary), which also continued to meander during the Younger Dryas (Kozarski et al., 1988; Vandenberghe et al., 1994; Starkel, 2003; Gábris and Nádor, 2007; Kasse et al., 2010).

Kasse et al. (2017), conversely, indicate that a SE-NW oriented straight lineament could represent a terrace scarp and remnant that was formed by a straight or possibly braided Roer River (level B2 near Roermond). This terrace remnant can probably be attributed to base-level lowering of the Roer by incision of the Meuse during the Younger Dryas (Kasse et al., 2017).

The biostratigraphically dated basal infills of palaeochannels Kitscherholz and Schafhausen (Fig. 7) indicate that the underfit system in the former southern course of the Roer was abandoned during the end of the Younger Dryas (Figs. 12E, F and 13). As a result, more developed soils (gley/pseudo-gley, [NRW, n.d.]) could form in the abandoned southern course of the Roer River during the succeeding Holocene compared to the younger and less well-developed soils (gley-vega, [NRW, n.d.]) in the still active northern Roer branch.

4.5.6 Early Holocene

During the Early Holocene, the Roer is characterized by a single-channel, meandering planform (Fig. 13). At the start of the Holocene, climate improved rapidly, leading to an increased vegetation cover and decreased sediment supply to the river (Renssen, 2001; Hoek and Bohncke, 2002). This process led to incision and a reduction of the number of active channels of the Meuse River (Woolderink et al., 2018). The incision of the Meuse resulted in a base-level lowering of the Roer River that, along with the reduced sediment supply from the Roer hinterland, forced the Roer to incise in the lower Roer Valley during the Preboreal. The resulting incised position of the Roer due to this base-level lowering is, together with continued subsidence along the PBFZ and RR, most probably the cause for the clustering of Holocene channel belts along the northern boundary of the Roer Valley Graben (RVG) (Fig. 5, Fig. 10, Fig. 12).

The incision of the Roer during the Early Holocene resulted in an increased gradient in the lower reach of the Roer Valley that might, together with the sandy subsoil, be the cause of the increase in sinuosity of the meandering planform of the Roer during this time (Level C; Fig. 11, Fig. 12F). An increase of incision rates during the start of the Holocene was also observed for other northwestern European river systems (Vandenberghé et al., 1994; Schirmer, 1995; Huisink, 1997; Kasse et al., 2005, Kasse et al., 2010; Erkens et al., 2011; Kaiser et al., 2012; Woolderink et al., 2018).

The meandering planform of the Roer led to extensive lateral erosion of older terraces in the lower Roer Valley (Fig. 5, Fig. 6I). The end of activity of the Early Holocene Roer (level C) river incision probably occurred during the (late) Boreal (e.g., start of infill of Bennebroek and Bolberg, Fig. 7, Fig. 8).

Although incision and lateral erosion prevailed during the Early Holocene in the lower Roer Valley, sedimentation of overbank fines during this period was observed in the form of a (slightly) silty clay unit, which is now strongly oxidized and compacted (Janssens, 2011). Contrary to the observed incision and extensive lateral erosion in the lower Roer Valley, deposition of the so-called “old overbank sediments” was observed to be the most important process for the middle Roer Valley during the Early Holocene (Schalich, 1968; Hindel et al., 1996). A possible reason for this reach-to-reach difference might be the upstream knickpoint migration during the Early Holocene (leading to incision and erosion in the lower part of the valley), which did not reach the middle Roer Valley (Fig. 11).

4.5.7 Middle Holocene

The morphology of the Middle Holocene level D is dominated by multiple channels that converge and diverge regularly, indicating an anastomosing river pattern (Figs. 6L, 9F and 13). This change of channel pattern is, most likely, the result of a more stable climate and continued vegetation succession. Alternatively, anthropogenic land-use changes may already have influenced river dynamics since the Neolithic Period in areas that are rich in loess (Schirmer, 1995; Gerlach et al., 2012). Remnants of level D in the lower Roer Valley have a meandering planform (Figs. 9E and 13). Furthermore, the lateral extent of the channel belt in the lower Roer Valley is less compared to the Early Holocene plain (Fig. 5).

The observed differences between the fluvial planform of the lower and middle Roer Valley might be explained by several factors such as a difference in subsurface composition and gradient. The downstream part of the Roer Valley has a sandy subsurface with a relatively low gradient (Fig. 11). The middle Roer Valley has a bedload that mainly consists of gravel, and a gradient that is higher than that of the lower Roer Valley (Fig. 11). Kleinhans and Van den Berg (2011) showed that channel patterns might change from laterally immobile to meandering with a decrease in grain size. Such a shift over the laterally immobile to meandering threshold might be the reason for the observed planform difference between the anastomosing middle and meandering lower Roer Valley. Faulting and subsidence were, most probably, important in forcing reach-specific variations such as the lateral extent of the channel belts and zones of aggradation.

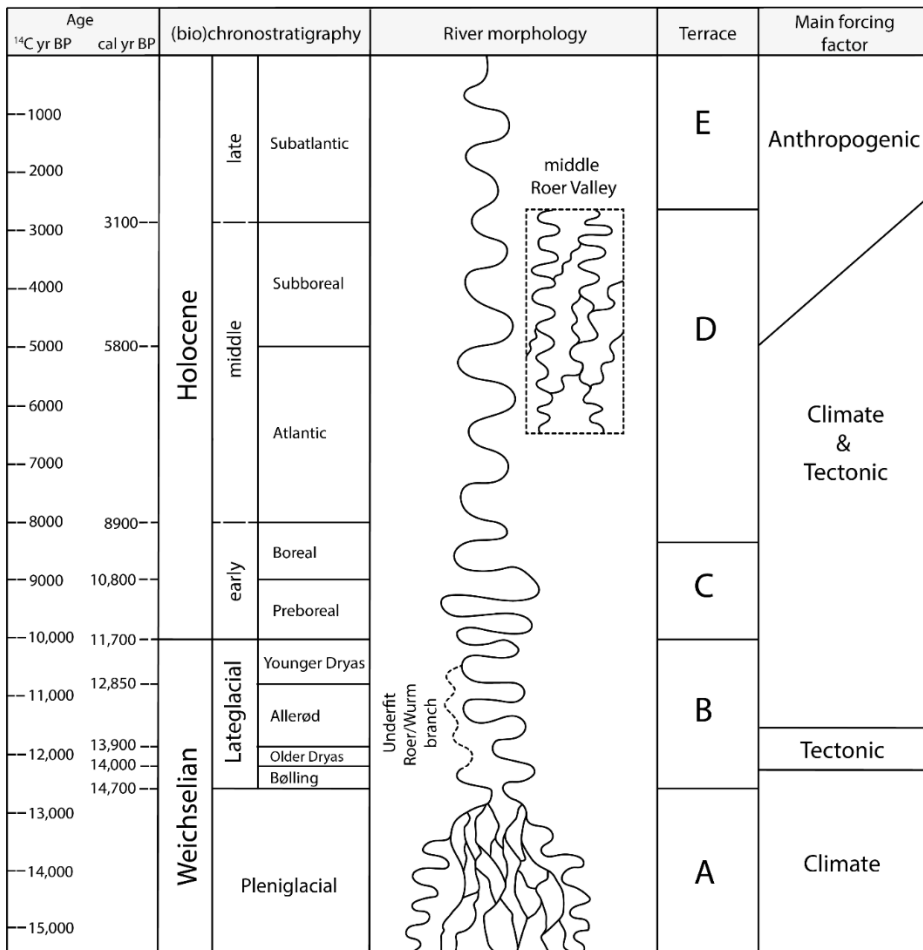


Fig. 13: Fluvial planform evolution and terrace levels of the Roer River since the Weichselian Late Pleniglacial alongside the main forcing factor(s).

4.5.8 Late Holocene

The Late Holocene Roer is characterized by a meandering planform (Fig. 13). Furthermore, overbank sedimentation increases during the Subatlantic (i.e., the “younger overbank sequences” as defined by Schalich, 1968), of which most of the deposition probably occurred between the seventh and twelfth century (Schalich, 1968; Hindel et al., 1996).

Deforestation and increased anthropogenic stresses by agriculture and mining since Roman times are, most probably, the forcing factor behind the incision that formed the lowest terrace level E (Fig. 13). Deforestation leads to higher runoff and increased discharges in the river channel(s) and, therefore, higher stream power that, in turn, forces

incision of the channels (De Moor, 2007; Ward et al., 2008). The increase in sedimentation is, most likely, also linked to the Roman and Early Middle Age deforestation in the study area between the third and fourteenth century (Schalich, 1968; Bunnik, 1999). The timing of the increased sedimentation is supported by slightly raised concentrations of lead and zinc in the lower part of the “younger overbank deposits”, which are related to the start of lead and zinc mining in the study area during Roman times (Hindel et al., 1996). The effects of increased anthropogenic stresses on river dynamics during the Late Holocene are recognized in most of the northwestern and central European river systems (Kalicki, 1991; Schirmer, 1995; Notebaert and Verstraeten, 2010; Kaiser et al., 2012).

Another possible cause for the incision of level E might be the transition from the Medieval Warm Period to the Little Ice Age (fourteenth to nineteenth century). This relatively cold period could have led to increased bankfull discharges of the Roer due to reduced evapotranspiration, frozen soils, and more snowmelt peak discharges in both the Roer Valley and the Eifel-Ardenne hinterland. Such a phase of erosion was recognized for other rivers in northwestern and central Europe as well (Kalicki, 1991; Rumsby and Macklin, 1996).

The biostratigraphically dated start of infill of the Gutt Grittern and Rurich channels (Fig. 7, Fig. 8) during or after the Middle Ages support the hypothesis that terrace level E has been active since at least the Middle Ages.

Schalich (1968) introduces an additional phase of bed aggradation and overbank deposition in his subdivision for the middle reach of the Roer Valley. This “youngest overbank sediment sequence” is dated to the beginning of the nineteenth century (~0.2 ka cal BP). These deposits contain, in the middle Roer Valley, artefacts of the eighteenth and nineteenth century and are, furthermore, characterized by an increased amount of lead and zinc pollution (Schalich, 1968; Hindel et al., 1996). The final phase of overbank sedimentation is probably caused by the intensification of zinc mining and smelting by the end of the nineteenth century (Schalich, 1968). Such increased pollution of lead and zinc was also observed in the uppermost overbank deposits in the lower Roer Valley and the Inde tributary (Schmidt-Wygasch et al., 2010; Janssens, 2011). Due to suboptimal dating resolution of parts of the Roer Valley, however, the “younger and youngest overbank sediment sequences” by Schalich (1968) were grouped into one terrace level, level E in our study.

4.6 Conclusions

The changes in fluvial dynamics and planform of the Roer River since the Weichselian Late Pleniglacial can be regarded as an interplay between tectonic, climatic and anthropogenic influences. Based on geomorphological and geological mapping of terrace levels of the Roer since the Late Pleniglacial we conclude that:

- The external forcings of the Roer River have led to five terraces with diverse fluvial planforms since the Weichselian Late Pleniglacial.
- Reach-to-reach variations in terrace formation and fluvial planform change are present in the Roer Valley. Such reach-specific phenomena can be attributed to variations in tectonic setting, subsurface lithology, base-level fluctuations or the confluence with tributary systems.
- Climatic changes during the onset of the Lateglacial were the dominant forcing factor on terrace formation and changes in fluvial planform of the Roer. During this time the Late Pleniglacial Roer had a braided to low-sinuosity planform in the valley centre with secondary meandering channels along the valley sides. This planform changed to a double channel belt meandering system during the Bølling, which evolved into a single-channel meandering system throughout the rest of the Lateglacial and Early Holocene.
- A (lateral) response of the Roer River to tectonic forcing is concluded from (i) the preferred occupation of the northern Roer channel on the down-tilted side of the Roer Valley Graben, (ii) an “underfit” river system on the up-tilted side of the Roer Valley Graben, (iii) the presence of a distinct difference between soils in the up-tilted side (gley/pseudo-gley) and those in the down-tilted side (gley-vega) of the Roer Valley Graben, (iv) an asymmetric position and clustering of Holocene channel belts along the Peel Boundary and Rurand fault zones, and (v) the (gradual) infill of a zone of subsidence around Rurich.
- The preferred occupation of the northern river course by the Roer in the lower Roer Valley during the Lateglacial and Holocene is caused by (i) differential subsidence within the Roer Valley Graben, (ii) climate-forced changes in precipitation, permafrost occurrence, vegetational cover and sediment supply, and (iii) base-level lowering of the Meuse River.
- Changes in planform (from meandering to anastomosing) and fluvial dynamics during the Middle Holocene are the result of both climatic and tectonic forcing.
- Increased anthropogenic stresses on the landscape during the Late Holocene resulted in the formation of a new terrace level in the Roer Valley with, at least, two overbank sedimentation phases.

4.7 Acknowledgments

This research is part of a PhD project “Reconstruction and Modelling of the Meuse and Rhine River. Sinuosity Response to Faulting in the Roer Valley Rift System” funded by The Netherlands Organisation for Scientific Research (NWO; project nr. 821.01.011). We would like to thank Marlies Janssens and John van der Woude for their indispensable contributions to this study. Furthermore, we would like to thank the staff members of the Sediment Laboratory of the Vrije Universiteit for their help with the sediment analysis. We thank the Centrum voor Isotopen Onderzoek (CIO) in Groningen, the Netherlands, for analysing the radiocarbon samples. Two anonymous reviewers are thanked for their constructive reviews that helped improve this paper.

4.8 References

- > AHN 2, n.d.. Retrieved May 1, 2018, from <http://www.ahn.nl/index.html>
- > Ahorner, L., 1962. Untersuchungen zur quartären Bruchtektonik der Niederrheinischen Bucht. *E&G–Quaternary Science Journal*, 13(1). <http://dx.doi.org/10.23689/figgeo-1466>
- > Alexander, J., Leeder, M.R., 1987. Active tectonic control on alluvial architecture. In: Ethridge, F.G., Flores, R.M., Harvey, M.D. (Eds.), *Recent Developments in Fluvial Sedimentology*. Soc. Econ. Paleontol Mineral. Spec. Publ. 39, 243-252.
- > Antoine, P., Lautridou, J.P., Laurent, M., 2000. Long-term fluvial archives in NW France: response of the Seine and Somme rivers to tectonic movements, climatic variations and sea-level changes. *Geomorphology* 33, 183-207. [https://doi.org/10.1016/S0169-555X\(99\)00122-1](https://doi.org/10.1016/S0169-555X(99)00122-1)
- > Bakels, C., 2017a. Posterholt, a Late Pleistocene–Holocene record of the vegetation history in and around the valley of the Vlootbeek, a tributary of the river Meuse (southeastern Netherlands). *Netherlands Journal of Geosciences* 96(2), 175-182. <https://doi.org/10.1017/njg.2016.44>
- > Bakels, C., 2017b. Medieval impacts on the vegetation around the confluence of the river Meuse and its tributary the Swalm, the Netherlands. *Netherlands Journal of Geosciences*, 96(2) 165-173. <http://dx.doi.org/10.1017/njg.2016.21>
- > Berendsen, H.J.A., Stouthamer, E., 2001. Palaeogeographic development of the Rhine-Meuse delta, the Netherlands. Koninklijke van Gorcum, Assen. http://dx.doi.org/10.1046/j.1365-3091.2002.00469_1.x
- > Berendsen, H.J.A., Cohen, K.M., Stouthamer, E., 2001. Maps and cross-sections. In: Berendsen, H.J.A., Stouthamer, E., 2001: Palaeogeographic development of the Rhine-Meuse delta, the Netherlands. Koninklijke van Gorcum, Assen. http://dx.doi.org/10.1046/j.1365-3091.2002.00469_1.x
- > Berendsen, H.J.A., Cohen, K.M., Stouthamer, E., 2007. The use of GIS in reconstructing the Holocene palaeogeography of the Rhine–Meuse delta, the Netherlands. *International Journal of Geographical Information Science* 21, 589-602. <https://doi.org/10.1080/13658810601064918>
- > Berendsen, H.J.A., Hoek, W.Z., Schorn, E., 1995. Late Weichselian and Holocene river channel changes of the rivers Rhine and Meuse in the Netherlands (land van Maas en Waal). In: Frenzel, B., Vandenberghe, J., Kasse, C., Bohncke, S.J.P., Glaser, B. (Eds.), *European river activity and climate change during the Lateglacial and early Holocene*, ‘European

- Palaeoclimate and Man 9, Palaoklimaforschung 14, Gustar Fischer Verlag, Stuttgart, pp. 151-171.
- › BGR (Bundesanstalt für Geowissenschaften und Rohstoffe), n.d.. Borehole Map Germany, Retrieved March 8, 2018, from <https://boreholemap.bgr.de/mapapps/resources/apps/boreholemap/index.html?lang=en>
 - › Blum, M.D., Törnqvist, T.E., 2000. Fluvial responses to climate and sea level change: A review and look forward. *Sedimentology* 47, 2-48. <http://dx.doi.org/10.1046/j.1365-3091.2000.00008.x>
 - › Boenigk, W., 1978. Gliederung der altquartären Ablagerungen in der Niederrheinischen Bucht. *Fortschritte Geologie Rheinland und Westfalen* 28, 135-212.
 - › Boenigk, W., Frechen, M., 2006. The Pliocene and Quaternary fluvial archives of the Rhine system. *Quaternary Science Reviews* 25(5), 550-574. doi:10.1016/j.quascirev.2005.01.018
 - › Bogaart, P.W., Van Balen, R.T., 2000. Numerical modeling of the response of alluvial rivers to Quaternary climate change. *Global and Planetary Change* 27, 147-163. [https://doi.org/10.1016/S0921-8181\(01\)00064-9](https://doi.org/10.1016/S0921-8181(01)00064-9)
 - › Bos, J.A.A., Zuidhoff, F.S., 2015. De restgeul van Well-Aijen, een reconstructie van de vegetatieontwikkeling van het noord-limburgse Maasdal gedurende het Holoceen (Mesolithicum-Vroeg-Romeinse tijd). ADC-Rapport 3599/BAAC Rapport A-12.0274, 92 pp.
 - › Bos, J.A.A., Dambeck, R., Kalis, A.J., Schweizer, A., Thiemeyer, H., 2008. Palaeoenvironmental changes and vegetation history of the northern upper Rhine Graben (southwestern Germany) since the Lateglacial. *Netherlands Journal of Geosciences/Geologie en Mijnbouw* 87, 67-90.
 - › Bridge, J.S., Leeder, M.R., 1979. A simulation model of alluvial stratigraphy. *Sedimentology* 26(5), 617-644. <https://doi.org/10.1111/j.1365-3091.1979.tb00935.x>
 - › Bridgland, D., Westaway, R., 2008. Climatically controlled river terrace staircases: A worldwide Quaternary phenomenon. *Geomorphology* 98, 285-315. <https://doi.org/10.1016/j.geomorph.2006.12.032>
 - › Bunnik, F.P.M., 1999. Vegetationsgeschichte der Lößböden zwischen Rhein und Maas von der Bronzezeit bis in die frühe Neuzeit. Published doctoral dissertation, Universiteit Utrecht.
 - › Burrato, P., Ciucci, F., Valensise, G., 2003. An inventory of river anomalies in the Po Plain, Northern Italy: evidence for active blind thrust faulting. *Annals of Geophysics* 46 (5), 865-882. <http://hdl.handle.net/2122/993>
 - › Busschers, F.S., Kasse, C., Van Balen, R.T., Vandenberghe, J., Cohen, K.M., Weerts, H.J.T., Bunnik, F.P.M., 2007. Late Pleistocene evolution of the Rhine-Meuse system in the southern North Sea basin: imprints of climate change, sea-level oscillation and glacio-isostasy. *Quaternary Science Reviews* 26(25-28), 3216-3248. <https://doi.org/10.1016/j.quascirev.2007.07.013>
 - › Camelbeeck, T., Meghraoui, M., 1998. Geological and geophysical evidence for large palaeo-earthquakes with surface faulting in the Roer Graben (northwest Europe). *Geophysical Journal International* 132(2), 347-362. <https://doi.org/10.1046/j.1365-246x.1998.00428.x>
 - › Camelbeeck, T., Alexandre, P., Vanneste, K., Meghraoui, M., 2000. Long-term seismicity in regions of present day low seismic activity: the example of western Europe. *Soil Dynamics and earthquake engineering* 20(5-8), 405-414. [https://doi.org/10.1016/S0267-7261\(00\)00080-4](https://doi.org/10.1016/S0267-7261(00)00080-4)
 - › Camelbeeck, T., Vanneste, K., Alexandre, P., Verbeeck, K., Petermans, To., Rosset, P., Everaerts, M., Warnant, R., Van Camp, M., 2007. Relevance of active faulting and seismicity

- studies to assessments of long-term earthquake activity and maximum magnitude in intraplate northwest Europe, between the Lower Rhine Embayment and the North Sea. In: Stein, S., Mazzotti, S., ed., *Continental Intraplate Earthquakes: Science, Hazard, and Policy Issues: Geological Society of America Special Paper 425*, 193–224, doi: 10.1130/2007.2425(14).
- › Cohen, K.M., 2003. Differential subsidence within a coastal prism: Late-Glacial-Holocene tectonics in the Rhine-Meuse delta, the Netherlands. Published doctoral dissertation, Universiteit Utrecht.
 - › Cohen, K.M., Stouthamer, E., Berendsen, H.J.A., 2002. Fluvial deposits as a record for late Quaternary neotectonic activity in the Rhine-Meuse delta, the Netherlands. *Netherlands Journal of Geosciences/Geologie en Mijnbouw* 81, 389–405.
 - › Cohen, K.M., Stouthamer, E., Pierik, H.J., Geurts, A.H., 2012. Rhine-Meuse delta studies' digital basemap for delta evolution and palaeogeography. Dept. Physical Geography. Utrecht University. Digital Dataset. DANS. <https://doi.org/10.17026/dans-x7g-sjtw>
 - › Dambeck, R., Thiemeyer, H., 2002. Fluvial history of the northern Upper Rhine river (southwestern Germany) during the Lateglacial and Holocene times. *Quaternary International* 93, 53-63. [https://doi.org/10.1016/S1040-6182\(02\)00006-X](https://doi.org/10.1016/S1040-6182(02)00006-X)
 - › De Moor, J.J.W., 2007. Human impact on Holocene catchment development and fluvial processes-the Geul River catchment, SE Netherlands. Published doctoral dissertation, Vrije Universiteit Amsterdam.
 - › De Moor, J. J. W., Kasse, C., Van Balen, R., Vandenberghe, J., Wallinga, J., 2008. Human and climate impact on catchment development during the Holocene-Geul River, the Netherlands. *Geomorphology* 98(3-4), 316-339. <https://doi.org/10.1016/j.geomorph.2006.12.033>
 - › Dumont, J.F., Mering, C., Parrot, J.F., Taud, H., 1996. Morphological and mathematical analysis of asymmetrical fluvial pattern: a study case from the Ucayali River (Peru). *Zeitschrift für Geomorphologie: Neue Folge* 103, 269-282.
 - › Dury, G.H., 1970. General theory of meandering valleys and underfit streams. In: Dury, G.H. (Ed.), *River and River Terraces*. MacMillan, London, pp. 264–275.
 - › Erkens, G., Hoffmann, T., Gerlach, R., Klostermann, J., 2011. Complex fluvial response to Lateglacial and Holocene allogenic forcing in the lower Rhine valley (Germany). *Quaternary Science Reviews* 30, 611-627. <https://doi.org/10.1016/j.quascirev.2010.11.019>
 - › Erkens, G., Dambeck, R., Volleberg, K.P., Bouman, M.T.I.J., Bos, J.A.A., Cohen, K.M., Wallinga, J., Hoek, W.Z., 2009. Fluvial terrace formation in the northern Upper Rhine Graben during the last 20000 years as a result of allogenic controls and autogenic evolution. *Geomorphology* 103, 476-495. <https://doi.org/10.1016/j.geomorph.2008.07.021>
 - › Faegri, K., Iversen, J., 1989. *Textbook of Pollen Analysis*, 4th edition. Wiley & Sons (Chichester): 328 pp.
 - › Gábris, G., Nádor, A., 2007. Long-term fluvial archives in Hungary: response of the Danube and Tisza rivers to tectonic movements and climatic changes during the Quaternary: a review and new synthesis. *Quaternary Science Reviews*, 26 (22-24), 2758-2782.
 - › Geluk, M.C., Duin, E.J.T., Duser, M., Rijkers, R.H.B., Van den Berg, M.W., Van Rooijen, P., 1994. Stratigraphy and tectonics of the Roer Valley Graben. *Geologie en Mijnbouw* 73, 129-129.
 - › Gerlach, R., Fischer, P., Eckmeier, E., Hilgers, A., 2012. Buried dark soil horizons and archaeological features in the Neolithic settlement region of the Lower Rhine area, NW Germany: formation, geochemistry and chronostratigraphy. *Quaternary International*, 265, 191-204.

- › Gold, R.D., Friedrich, A., Kübler, S., Salamon, M., 2017. Apparent Late Quaternary Fault-Slip Rate Increase in the Southern Lower Rhine Graben, Central Europe. *Bulletin of the Seismological Society of America* 107(2), 563-580. <https://doi.org/10.1785/0120160197>
- › Grimm, E., 1992. TILIA and TILIA-graph: pollen spreadsheet and graphics programs. *Programs and Abstracts, 8th International Palynological Congress, Aix-en-Provence*: 56.
- › Grooteman, L.P.A., 2018. Fluvial development of the Roer (the Netherlands-western Germany) during the late Weichselian to Holocene in response to climate, base-level and tectonics. Master thesis, Vrije Universiteit Amsterdam (Amsterdam): 57 pp.
- › Hijma, M.P., Cohen, K.M, Hoffmann, G., Van der Spek, A.J.F., Stouthamer, E., 2009. From river valley to estuary: The evolution of the Rhine mouth in the early to middle Holocene (western Netherlands, Rhine-Meuse delta). *Netherlands Journal of Geosciences/Geologie en Mijnbouw* 88, 13-53. <https://doi.org/10.1017/S0016774600000986>
- › Hindel, R., Schalich, J., De Vos, W., Ebbing, J., Swennen, R., Van Keer, I., 1996. Vertical distribution of elements in overbank sediment profiles from Belgium, Germany and The Netherlands. *Journal of Geochemical Exploration* 56(2), 105-122. [https://doi.org/10.1016/0375-6742\(96\)00010-6](https://doi.org/10.1016/0375-6742(96)00010-6)
- › Hoek, W.Z., 1997. Palaeogeography of Lateglacial vegetations. Aspects of Lateglacial and early Holocene vegetation, abiotic landscape and climate in the Netherlands. Published doctoral dissertation, Vrije Universiteit Amsterdam.
- › Hoek, W.Z., 1997. Atlas to Palaeogeography of Lateglacial vegetations. Maps of Lateglacial and early Holocene landscape and vegetation in The Netherlands, with an extensive review of available palynological data. Published doctoral dissertation, Vrije Universiteit Amsterdam.
- › Hoek, W.Z., Bohncke, S.J.P., 2002. Climatic and environmental events over the last termination, as recorded in the Netherlands: A review. *Netherlands Journal of Geosciences/Geologie en Mijnbouw* 81, 123-137. <https://doi.org/10.1017/S001677460002062X>
- › Hoek, W.Z., Lammertsma, E.I., Bohncke, S.J.P., Bos, J.A.A., Bunnik, F., Kasse, C., Schokker, J., Westerhoff, W., 2017. Lateglacial and Early Holocene vegetation development and fluvial system changes in the northern Meuse valley, the Netherlands: A review of palynological data. *Netherlands Journal of Geosciences/Geologie en Mijnbouw* 96, 93-114. <https://doi.org/10.1017/njg.2017.4>
- › Holbrook, J., Schumm, S.A., 1999. Geomorphic and sedimentary response of rivers to tectonic deformation: A brief review and critique of a tool for recognizing subtle epeirogenic deformation in modern and ancient settings. *Tectonophysics* 305, 287-306. [https://doi.org/10.1016/S0040-1951\(99\)00011-6](https://doi.org/10.1016/S0040-1951(99)00011-6)
- › Houben, P., 2003. Spatio-temporally variable response of fluvial systems to Late Pleistocene climate change: a case study from central Germany. *Quaternary Science Reviews* 22(20), 2125-2140. [https://doi.org/10.1016/S0277-3791\(03\)00181-1](https://doi.org/10.1016/S0277-3791(03)00181-1)
- › Houtgast, R.F., Van Balen, R.T., 2000. Neotectonics of the Roer Valley Rift System, the Netherlands. *Global and Planetary Change* 27, 131-146. [https://doi.org/10.1016/S0921-8181\(01\)00063-7](https://doi.org/10.1016/S0921-8181(01)00063-7)
- › Houtgast, R.F., Van Balen, R.T., Bouwer, L.M., Brand, G.B.M., Brijker, J.M., 2002. Late Quaternary activity of the Feldbiss Fault Zone, Roer Valley Rift System, the Netherlands, based on displaced fluvial terrace fragments. *Tectonophysics* 352, 295-315. [https://doi.org/10.1016/S0040-1951\(02\)00219-6](https://doi.org/10.1016/S0040-1951(02)00219-6)
- › Houtgast, R.F., Van Balen, R.T., Kasse, C., 2005. Late Quaternary evolution of the Feldbiss Fault (Roer Valley Rift System, the Netherlands) based on trenching, and its potential relation

- to glacial unloading. *Quaternary Science Reviews* 24(3-4), 489-508. <https://doi.org/10.1016/j.quascirev.2004.01.012>
- › Houtgast, R.F., Van Balen, R.T., Kasse, C., Vandenberghe, J., 2003. Late Quaternary tectonic evolution and post seismic near surface fault displacements along the Geleen Fault (Feldbiss Fault Zone–Roer Valley Rift System, the Netherlands), based on trenching. *Netherlands Journal of Geosciences* 82(2), 177-196. <https://doi.org/10.1017/S0016774600020734>
 - › Huisink, M., 1997. Lateglacial sedimentological and morphological changes in a lowland river in response to climatic change: The Maas, southern Netherlands. *Journal of Quaternary Science* 12, 209-223. [http://dx.doi.org/10.1002/\(SICI\)1099-1417\(199705/06\)12:3<209::AID-JQS306>3.0.CO;2-P](http://dx.doi.org/10.1002/(SICI)1099-1417(199705/06)12:3<209::AID-JQS306>3.0.CO;2-P)
 - › Janssens, M.M., 2011. Holocene floodplain development of the river Rur: allogenic or autogenic forcing mechanisms? Master thesis, Vrije Universiteit Amsterdam (Amsterdam): 53 pp.
 - › Janssens, M.M., Kasse, C., Bohncke, S.J.P., Greaves, H., Cohen, K.M., Wallinga, J., Hoek, W.Z., 2012. Climate-driven fluvial development and valley abandonment at the last glacial-interglacial transition (Oude IJssel-Rhine, Germany). *Netherlands Journal of Geosciences/Geologie en Mijnbouw* 91, 37-62. <https://doi.org/10.1017/S001677460000055X>Kaiser, K., Lorenz, S., Germer, S., Juschus, O., Küster, M., Libra, J., Bens, O. Hüttl, R. F., 2012. Late Quaternary evolution of rivers, lakes and peatlands in northeast Germany reflecting past climatic and human impact—an overview. *E&G Quaternary Science Journal*, 61(2), 103-132.
 - › Kalicki, T., 1991. The evolution of the Vistula river valley between Cracow and Niepołomice in Late Vistulian and Holocene times. In: Starkel (Eds.), *Evolution of the Vistula river valley during the last, 15000 years, Part IV, Geographical Studies, Special Issue*, 6 (1991), pp. 11-37.
 - › Kalis, A.J., Bunnik, F.P.M., 1990. Holozäne Vegetationsgeschichte in der westlichen niederrheinischen Bucht. In: Schirmer, W. (ed.): *Rheingeschichte zwischen Mosel und Maas. J. Wegener (Dormagen)*: 266–272.
 - › Kasse, C., Van Balen, R.T., Bohncke, S.J.P., Wallinga, J., Vreugdenhil, M., 2017. Climate and base-level controlled fluvial system change and incision during the last glacial–interglacial transition, Roer river, the Netherlands–western Germany. *Netherlands Journal of Geosciences* 96(2), 71-92. <https://doi.org/10.1017/njg.2016.50>
 - › Kasse, C., Bohncke, S.J.P., Vandenberghe, J., Gábris, G., 2010. Fluvial style changes during the last glacial–interglacial transition in the middle Tisza valley (Hungary). *Proceedings of the Geologists' Association* 121, 180-194. <https://doi.org/10.1016/j.pgeola.2010.02.005>
 - › Kasse, C., Hoek, W.Z., Bohncke, S.J.P., Konert, M., Weijers, J., Cassee, M., Van der Zee, R., 2005. Late glacial fluvial response of the Niers-Rhine (western Germany) to climate and vegetation change. *Journal of Quaternary Science* 20, 377-394. <http://dx.doi.org/10.1002/jqs.923>
 - › Kasse, C., Vandenberghe, J., Bohncke, S.J.P., 1995. Climatic change and fluvial dynamics of the Maas during the Late Weichselian and Early Holocene. In: Frenzel, B., Vandenberghe, J., Kasse, C., Bohncke, S.J.P., Glaser, B. (Eds.), *European river activity and climate change during the Lateglacial and early Holocene, 'European Palaeoclimate and Man 9, Palaoklimaforschung 14*, Gustav Fischer Verlag, Stuttgart, pp. 123-150.
 - › Kemna, H.A., 2005. Pliocene and lower Pleistocene stratigraphy in the lower Rhine Embayment, Germany. Published doctoral dissertation, Universität zu Köln.

- › Kiden, P., 1991. The Lateglacial and Holocene evolution of the Middle and Lower River Scheldt, Belgium. In: Starkel, L., Gregory, K.J., Thornes, J.B. (eds): *Temperate palaeohydrology*. John Wiley and Sons (Chichester): 283–299.
- › Kleinhans, M.G., Van den Berg, J.H., 2011. River channel and bar patterns explained and predicted by an empirical and a physics based method. *Earth Surface Processes and Landforms* 36, 721-738. <http://dx.doi.org/10.1002/esp.2090>
- › Kleinhans, M.G., Ferguson, R.I., Lane, S.N., & Hardy, R.J., 2013. Splitting rivers at their seams: bifurcations and avulsion. *Earth Surface Processes and Landforms* 38(1), 47-61. <https://doi.org/10.1002/esp.3268>
- › Klostermann, J., 1983. *Die Geologie der Venloer Scholle (Niederrhein)*. Geologisches Landesamt Nordrhein-Westfalen, Krefeld.
- › Kozarski, S., 1983. River channel adjustment to climatic change in west central Poland. *Background to Palaeohydrology*, 355-374.
- › Kozarski, S., Gonera, P., Antczak, B., 1988. Valley Floor Development and Paleohydrological Changes: The Late Vistulian and Holocene History of the Warta River (Poland). In: Lang, G., Schluchter, C. (Eds.), *Lake, Mire and River Environments*. Balkema, Rotterdam, pp. 185-203.
- › Land NRW, n.d.. Datenlizenz Deutschland-Namensnennung-Version 2.0 (www.govdata.de/dl-de/by-2-0). Retrieved May 1, 2018, from <https://www.opengeodata.nrw.de/produkte/geobasis/dgm/>
- › LANUV (Landesamt für Natur, Umwelt und Verbraucherschutz Nordrhein-Westfalen), n.d.. Pegel daten Stah in Hydrologische Rohdaten Online (HYGON). Retrieved September 9, 2018 from <http://luadb.lids.nrw.de/LUA/hygon/pegel.php?stationsinfo=ja&stationsname=Stah&ersterAuffrue=aktuelle%2BWerte>
- › Leeder, M.R., Alexander, J., 1987. The origin and tectonic significance of asymmetrical meander-belts. *Sedimentology* 34(2), 217-226. <https://doi.org/10.1111/j.1365-3091.1987.tb00772.x>
- › Michon, L., Van Balen, R.T., 2005. Characterization and quantification of active faulting in the Roer Valley Rift System based on high precision digital elevation models. *Quaternary Science Reviews* 24, 455-472. <https://doi.org/10.1016/j.quascirev.2003.11.009>
- › Michon, L., Van Balen, R.T., Merle, O., Pagnier, H., 2003. The Cenozoic evolution of the Roer Valley Rift System integrated at a European scale. *Tectonophysics* 367, 101-126. [https://doi.org/10.1016/S0040-1951\(03\)00132-X](https://doi.org/10.1016/S0040-1951(03)00132-X)
- › Mike, K., 1975. Utilization of the analysis of ancient river beds for the detection of Holocene crustal movements. *Developments in Geotectonics* 9, 359-368. <https://doi.org/10.1016/B978-0-444-41420-5.50043-5>
- › Moore, P.D., Webb, J.A., Collinson, M.E., 1991. *Pollen analysis*, 2nd edition. Blackwell Scientific Publications (Oxford): 216 pp.
- › Nanson, G.C., 1980. A regional trend to meander migration. *The Journal of Geology* 88(1), 100-108. <https://doi.org/10.1086/628477>.
- › Notebaert, B., Verstraeten, G., 2010. Sensitivity of West and Central European river systems to environmental changes during the Holocene: a review. *Earth-Science Reviews* 103(3-4), 163-182. <https://doi.org/10.1016/j.earscirev.2010.09.009>
- › NRW, n.d. IS BK 50 Bodenkarte von NRW 1 : 50.000 – Datensatz. Datenlizenz Deutschland-Namensnennung-Version 2.0 (www.govdata.de/dl-de/by-2-0). Retrieved June 10, 2018, from <https://www.geoportal.nrw/themenkarten>.

- › Peakall, J., 1998. Axial river evolution in response to half-graben faulting: Carson River, Nevada, USA. *Journal of Sedimentary Research* 68(5), 788-799. <https://doi.org/10.2110/jsr.68.788>
- › Peakall, J., Leeder, M., Best, J., Ashworth, P., 2000. River response to lateral ground tilting: a synthesis and some implications for the modelling of alluvial architecture in extensional basins. *Basin Research* 12(3-4), 413-424.
- › Pierik, H.J., Cohen, K.M., Stouthamer, E., 2016. A new GIS approach for reconstructing and mapping dynamic Late Holocene coastal plain palaeogeography. *Geomorphology* 270, 55-70. <https://doi.org/10.1016/j.geomorph.2016.05.037>
- › Renssen, H., 2001. The climate in The Netherlands during the Younger Dryas and Preboreal: means and extremes obtained with an atmospheric general circulation model. *Geologie en Mijnbouw / Netherlands Journal of Geosciences* 80: 19–30. <https://doi.org/10.1017/S0016774600022289>
- › Renssen, H., Isarin, R.F., 2001. The two major warming phases of the last deglaciation at 14.7 and 11.5 ka cal BP in Europe: Climate reconstructions and AGCM experiments. *Global and Planetary Change* 30, 117-153. [https://doi.org/10.1016/S0921-8181\(01\)00082-0](https://doi.org/10.1016/S0921-8181(01)00082-0)
- › Rose, J., 1995. Lateglacial and Early Holocene river activity in lowland Britain. In: Frenzel, B., Vandenberghe, J., Kasse, C., Bohncke, S.J.P., Glaser, B. (Eds.) *European river activity and climate change during the Lateglacial and early Holocene, 'European Palaeoclimate and Man 9, Palaoklimaforschung 14*, Gustar Fischer Verlag, Stuttgart, pp. 51-74.
- › Rumsby, B.T., Macklin, M.G., 1996. River response to the last neoglaciation (the 'Little Ice Age') in northern, western and central Europe. Geological Society, London, *Special Publications* 115(1), 217-233. <https://doi.org/10.1144/GSL.SP.1996.115.01.17>
- › Schäfer, A., Siehl, A., 2002. Preface: Rift tectonics and syngenetic sedimentation—the Cenozoic Lower Rhine Basin and related structures. *Netherlands Journal of Geosciences*, 81(2), 145-147. <https://doi.org/10.1017/S001677460002237X>
- › Schäfer, A., Utescher, T., Klett, M., Valdivia-Manchego, M., 2005. The Cenozoic Lower Rhine Basin—rifting, sedimentation, and cyclic stratigraphy. *International Journal of Earth Sciences* 94(4), 621-639. <https://doi.org/10.1007/s00531-005-0499-7>
- › Schäfer, A., Hilger, D., Gross, G., Von der Hocht, F., 1996. Cyclic sedimentation in Tertiary Lower-Rhine Basin (Germany)—the 'Liegendrücken' of the brown-coal open-cast Fortuna mine. *Sedimentary Geology* 103(3-4), 229-247. [https://doi.org/10.1016/0037-0738\(95\)00091-7](https://doi.org/10.1016/0037-0738(95)00091-7)
- › Schalich, J., 1968. Die Spätpleistozäne und Holozäne Tal- und Bodenentwicklung an der mittleren Rur. *Fortschritte Geologie Rheinland und Westfalen* 16, 339–370.
- › Schirmer, W., 1995. Valley bottoms in the late Quaternary. *Zeitschrift für Geomorphologie Supplement*, 100, 27-51.
- › Schirmer, W., 1990. Rheingeschichte zwischen Mosel und Maas. *Deuqua-Führer*, 1, 295pp.
- › Schmidt-Wygasch, C., Schamuhn, S., Meurers-Balke, J., Lehmkuhl, F., Gerlach, R., 2010. Indirect dating of historical land use through mining: Linking heavy metal analyses of fluvial deposits to archaeobotanical data and written accounts. *Geoarchaeology* 25(6), 837-856. <https://doi.org/10.1002/gea.20334>
- › Schokker, J., Cleveringa, P., Murray, A.S., Wallinga, J., Westerhoff, W.E., 2005. An OSL dated middle and Late Quaternary sedimentary record in the Roer Valley Graben (southeastern Netherlands). *Quaternary Science Reviews* 24 (20-21), 2243-2264. <https://doi.org/10.1016/j.quascirev.2005.01.010>

- › Schumm, S.A., 1986. Alluvial river response to active tectonics. *Active tectonics*, pp. 80-94.
- › Schumm, S.A., 1985. Patterns of alluvial rivers. *Annual Review of Earth and Planetary Sciences* 13(1), 5-27.
- › Schumm, S.A., 1981. Evolution and response of the fluvial system, sedimentologic implications. *Society of Economic Paleontologists and Mineralogists, Special Publication* 31, 19-29.
- › Schumm, S.A., 1973. Geomorphic thresholds and complex response of drainage systems. *Fluvial Geomorphology* 6, 69-85.
- › Starkel, L., 2003. Younger Dryas – Preboreal transition documented in the fluvial environment of Polish rivers. *Global and Planetary Change* 35, 157–167. [https://doi.org/10.1016/S0921-8181\(02\)00133-9](https://doi.org/10.1016/S0921-8181(02)00133-9)
- › Starkel, L., Michczyńska, D. J., Gębica, P., Kiss, T., Panin, A., Perşoiu, I., 2015. Climatic fluctuations reflected in the evolution of fluvial systems of Central-Eastern Europe (60–8 ka cal BP). *Quaternary International* 388, 97-118. <https://doi.org/10.1016/j.quaint.2015.04.017>
- › Starkel, L., Ge, P., Superson, J., 2007. Last Glacial–Interglacial cycle in the evolution of river valleys in southern and central Poland. *Quaternary Science Reviews* 26, 2924-2936. <https://doi.org/10.1016/j.quascirev.2006.01.038>
- › Stouthamer, E., Berendsen, H. J., 2007. Avulsion: the relative roles of autogenic and allogenic processes. *Sedimentary Geology* 198(3-4), 309-325. <https://doi.org/10.1016/j.sedgeo.2007.01.017>
- › Szumanski, A., 1983. Paleochannels of large meanders in the river valleys of the Polish Lowland. *Quaternary Studies in Poland*, 4, 207-216.
- › Tebbens, L.A., Veldkamp, A., Westerhoff, W., Kroonenberg, S.B., 1999. Fluvial incision and channel downcutting as a response to Late-glacial and Early Holocene climate change: The lower reach of the river Meuse (Maas), the Netherlands. *Journal of Quaternary Science* 14, 59-75.
- › Törnqvist, T.E., Bridge, J.S., 2002. Spatial variation of overbank aggradation rate and its influence on avulsion frequency. *Sedimentology* 49(5), 891-905. <https://doi.org/10.1046/j.1365-3091.2002.00478.x>
- › Van Balen, R.T., Bakker, M.A.J., Kasse, C., Wallinga, J., Woolderink, H.A.G., 2019. A Late Glacial surface rupturing earthquake at the Peel Boundary fault zone, Roer Valley Rift System, the Netherlands, *Quaternary Science Reviews* 218, 254-266. <https://doi.org/10.1016/j.quascirev.2019.06.033>
- › Van Balen, R.T., Bakker, M.A.J., Kasse, C., 2018. Evidence for a large Late Glacial large earthquake, Peel Boundary Fault zone, The Netherlands. In: *NAC (Nederlands Aardwetenschappelijk Congres)*; 15-16 March 2018, Veldhoven.
- › Van Balen, R.T., Busschers, F.S., Tucker, G.E., 2010. Modeling the response of the Rhine–Meuse fluvial system to Late Pleistocene climate change. *Geomorphology* 114(3), 440-452.
- › Van Balen, R.T., Houtgast, R.F., Cloetingh, S.A.P.L., 2005. Neotectonics of the Netherlands: A review. *Quaternary Science Reviews* 24, 439-454. <https://doi.org/10.1016/j.quascirev.2004.01.011>
- › Van den Berg, M.W., 1996. Fluvial sequences of the Maas: A 10 ma record of neotectonics and climate change at various time-scales. Published doctoral dissertation, Landbouwniversiteit Wageningen.
- › Van den Berg, M., Vanneste, K., Dost, B., Lokhorst, A., Van Eijk, M., Verbeeck, K., 2002. Paleoseismic investigations along the Peel Boundary Fault: geological setting, site selection

- and trenching results. *Netherlands Journal of Geosciences* 81(1), 39-60. <https://doi.org/10.1017/S0016774600020552>
- › Vandenberghe, J., 2003. Climate forcing of fluvial system development: An evolution of ideas. *Quaternary Science Reviews* 22, 2053-2060. [https://doi.org/10.1016/S0277-3791\(03\)00213-0](https://doi.org/10.1016/S0277-3791(03)00213-0)
 - › Vandenberghe, J., 2002. The relation between climate and river processes, landforms and deposits during the Quaternary. *Quaternary International* 91, 17-23. [https://doi.org/10.1016/S1040-6182\(01\)00098-2](https://doi.org/10.1016/S1040-6182(01)00098-2)
 - › Vandenberghe, J., 1995. Timescales, climate and river development. *Quaternary Science Reviews* 14, 631-638. [https://doi.org/10.1016/0277-3791\(95\)00043-0](https://doi.org/10.1016/0277-3791(95)00043-0)
 - › Vandenberghe, J., Bohncke, S.J.P., 1985. The Weichselian Late Glacial in a small lowland valley (Mark River, Belgium and The Netherlands). *Quaternaire* 22(2), 167-175. <https://doi.org/10.3406/quate.1985.1541>
 - › Vandenberghe, J., Kasse, C., Bohncke, S., Kozarski, S., 1994. Climate-related river activity at the Weichselian-Holocene transition: a comparative study of the Warta and Maas rivers. *Terra nova* 6(5), 476-485. <https://doi.org/10.1111/j.1365-3121.1994.tb00891.x>
 - › Vanneste, K., Verbeeck, K., 2001. Paleoseismological analysis of the Rurand fault near Julich, Roer Valley graben, Germany: Coseismic or aseismic faulting history?. *Geologie en Mijnbouw*, 80(3/4), 155-170. <https://doi.org/10.1017/S0016774600023817>
 - › Vanneste, K., Verbeeck, K., Petermans, T., 2008. Pseudo-3D imaging of a low-slip-rate, active normal fault using shallow geophysical methods: The Geleen fault in the Belgian Maas River valley. *Geophysics* 73(1), B1-B9. <https://doi.org/10.1190/1.2816428>
 - › Verstraeten, G., Lang, A., Houben, P., 2009. Human impact on sediment dynamics-quantification and timing. *Catena* 77(2), 77-80. <http://dx.doi.org/10.1016/j.catena.2009.01.005>
 - › Vreugdenhil, M., 2011. Fluvial and vegetational development during the Late Pleniglacial, Lateglacial and Holocene in the Rur valley. Master thesis, Vrije Universiteit Amsterdam (Amsterdam): 53 pp.
 - › Wang, X., Van Balen, R., Yi, S., Vandenberghe, J., Lu, H., 2014. Differential tectonic movements in the confluence area of the Huang Shui and Huang He rivers (Yellow River), NE Tibetan Plateau, inferred from fluvial terraces. *Boreas* 43, 469-484. <http://dx.doi.org/10.1111/bor.12054>
 - › Ward, P.J., Renssen, H., Aerts, J.C.J.H., Van Balen, R.T., Vandenberghe, J., 2008. Strong increases in flood frequency and discharge of the river Meuse over the Late Holocene: Impacts of long-term anthropogenic land use change and climate variability. *Hydrology and Earth System Sciences Discussions* 12, 159-175.
 - › Ward, P.J., Van Balen, R.T., Verstraeten, G., Renssen, H., Vandenberghe, J., 2009. The impact of land use and climate change on Late Holocene and future suspended sediment yield of the Meuse catchment. *Geomorphology* 103, 389-400. <https://doi.org/10.1016/j.geomorph.2008.07.006>
 - › Westerhoff, W. E., Kemna, H.A., Boenigk, W., 2008. The confluence area of Rhine, Meuse, and Belgian rivers: Late Pliocene and Early Pleistocene fluvial history of the northern Lower Rhine Embayment. *Netherlands Journal of Geosciences-Geologie en Mijnbouw* 87(1), 107. <https://doi.org/10.1017/S0016774600024070>
 - › Woolderink, H.A.G., Cohen, K.M., 2018. Digital Basemap for the Lower Meuse Valley Palaeogeography. *DANS*. <https://doi.org/10.17026/dans-xkk-f29b>
 - › Woolderink, H.A.G., Kasse, C., Cohen, K.M., Hoek, W.Z., Van Balen, R.T., 2018. Spatial and temporal variations in river terrace formation, preservation, and morphology in the Lower

Meuse Valley, The Netherlands. *Quaternary Research*, 1-22.
<https://doi.org/10.1017/qua.2018.49>

- > Zagwijn, W.H., 1989. The Netherlands during the Tertiary and the Quaternary: a case history of coastal lowland evolution. In *Coastal Lowlands*. Springer, Dordrecht. pp. 107-120.
- > Zagwijn, W.H., 1986. Nederland in het Holoceen. *Geologie van Nederland*, Rijks Geologische Dienst, Haarlem.
- > Ziegler, P.A., 1994. Cenozoic rift system of western and central-Europe, an overview. *Geologie en Mijnbouw* 73(2-4), 99-127
- > Ziegler, P.A., 1992. Plate tectonics, plate moving mechanisms and rifting. *Tectonophysics* 215(1-2), 9-34. [https://doi.org/10.1016/0040-1951\(92\)90072-E](https://doi.org/10.1016/0040-1951(92)90072-E)

Chapter 5

Patterns in river channel sinuosity of the Meuse, Roer and Rhine rivers in the Lower Rhine Embayment rift-system, are they tectonically forced?

Abstract

The tectonic and fluvial setting of the Rhine-Meuse river system in the Lower Rhine Embayment rift system is exceptionally well known. The 19th century, pre-regulation river courses of three rivers are used to study a postulated sinuosity response to faulting. The fault-perpendicular Meuse River shows patterns of sinuosity changes at different spatial scales. The large-scale (>5 km) sinuosity changes are related mainly to the faulting-induced changes of the subsurface lithology, determining the bed and bank characteristics. However, at a smaller scale, some fault-related channel sinuosity anomalies are observed. The fault-parallel Roer River shows sinuosity changes related to a normal, non-tectonic longitudinal gradient change. Sinuosity patterns of the Rhine River are predominantly related to lithological differences and reduced incision rates. Sinuosity can thus be an indicator of tectonic motions, but gradient, subsurface lithology and river bank composition determine sinuosity as well. Therefore, a sinuosity change is no proof for fault activity. On the other hand, the absence of a sinuosity change does not imply inactivity of a fault at geological time-scales.

Published as: Woolderink, H. A. G., Cohen, K. M., Kasse, C., Kleinhans, M. G., Van Balen, R. T. (2021). Patterns in river channel sinuosity of the Meuse, Roer and Rhine rivers in the Lower Rhine Embayment rift-system, are they tectonically forced? Geomorphology, 375.

5.1 Introduction

The effect of tectonic vertical motions on (alluvial) river response has been a matter of interest over the past decades (Burnett and Schumm, 1983; Ouchi, 1985; Leeder and Alexander, 1987; Holbrook and Schumm, 1999; Marple and Talwani, 2000; Buratto et al., 2003; Jain and Sinha, 2005; Holbrook et al., 2006; Aswathy et al., 2008; Taha and Anderson, 2008; Petrovski and Timar, 2010, Arcos, 2012; Lahiri and Sinha, 2012; Mack et al., 2012; Whitney and Hengesh, 2015). One of the commonly observed effects is a change in sinuosity. A sinuosity change is a means for the river to maintain a constant channel gradient. Via changes in the amount and size of the individual meander loops, the river channel is presumed to dynamically alter its channel length in such a way that the channel gradient remains unchanged despite the tectonic tilting (Holbrook and Schumm, 1999). The sinuosity response to active faulting depends on the relation between the sense of movement and the flow direction. A normal fault with the hanging wall in the downstream direction (i.e. downstepping in downstream direction) will enhance the fluvial gradient and, as a result, an increased sinuosity will occur at the fault trace. In contrast, a normal fault that is downstepping in upstream direction may lead to a reduced gradient and, hence, sinuosity (Ouchi, 1985; Holbrook and Schumm, 1999). Both physical scale experiments and numerous field examples show that an increase of valley floor gradient results in increased sinuosity of the river channel or vice versa (Adams, 1980; Schumm and Harvey, 1985; Ouchi 1985; Gomez and Marron, 1991; Schumm et al., 1994; Smith et al., 1997; Holbrook and Schumm, 1999; Schumm et al., 2002; Timár, 2003; Zámolyi et al., 2010; Petrovski and Timár, 2010; Petrovski et al., 2012). Most of the studies on the effects of tectonic vertical motions and river response show that sinuosity changes provide a means, as a geomorphic indicator, to identify active deformation from fluvial stratigraphic and -morphologic archives, which can be of large value for earthquake studies as demonstrated by Holbrook et al. (2006).

Sinuosity changes in meandering rivers, however, depend on many more factors than structural controls alone such as changes in discharge regime, erodibility of the river banks and channel bed, balance of bed load vs. suspended load, groundwater seepage and dominant mode of meander cut-off (chute or neck) (Baker, 1978; Schumm, 1963; Dade, 2000; Van Balen et al., 2008; Stouthamer et al., 2011; Kleinhans and van den Berg, 2011; Pierik et al., 2017; Candel et al., 2020). Therefore, in the absence of independent constraints for tectonics, the attribution of observed sinuosity changes to either tectonic or other controlling factors is challenging. Moreover, case studies that do use sinuosity changes as indications of differential tectonic control are often restricted to the analyses of motions of fault-bounded blocks at the reach scale (Burnett, 1982; Burnett and Schumm, 1983; Jorgensen, 1990; Jain and Sinha, 2005; Lahiri and Sinha, 2012). Alternations in sinuosity, however, can also be induced across fault zones at the sub-reach scale (i.e. just upstream vs. just downstream a fault trace). These more local responses to individual active faults may occur superimposed on regional-scale block-

wise tilting caused by the tectonic structure at large. These aspects of scale complicate attributing sinuosity changes to tectonic controls and quantifying them against non-tectonic variations even further.

The aim of this study is to investigate the possible role of tectonics (at multiple scales) as a forcing factor on river channel sinuosity. In this study we combine the well-known tectonic and sedimentary setting of three rivers (Meuse, Roer and Rhine) in the rift system of the Lower Rhine Embayment in NW Europe (SE Netherlands and adjacent Belgium and Germany) with morphometric sinuosity analyses of their pre-regulation courses (i.e. 19th cy). The rivers have diverse positions in the active rift system (i.e. transverse and lateral [Fig. 1 and section 2]) and, for the Meuse and Roer rivers, the displacement history of the faults in their courses are well-known from independent data. Moreover, variations in river bed and bank characteristics over the course of the rivers, which determine sinuosity as well, are also well known. The Lower Rhine Embayment rift system, therefore, provides a natural laboratory to unravel tectonically-forced responses of channel sinuosity from other forcing factors for rivers that are subjected to various degrees of faulting, both at the scale of fault-bounded blocks (> 5 km) and fault zones. The Meuse (transverse) and Roer (lateral) rivers are used to study the effect(s) of tectonic faulting on river sinuosity. The results of these rivers will help interpret sinuosity changes of the Rhine River as possible geomorphic indicators of (active) faulting at the rift margin (Fig. 1).

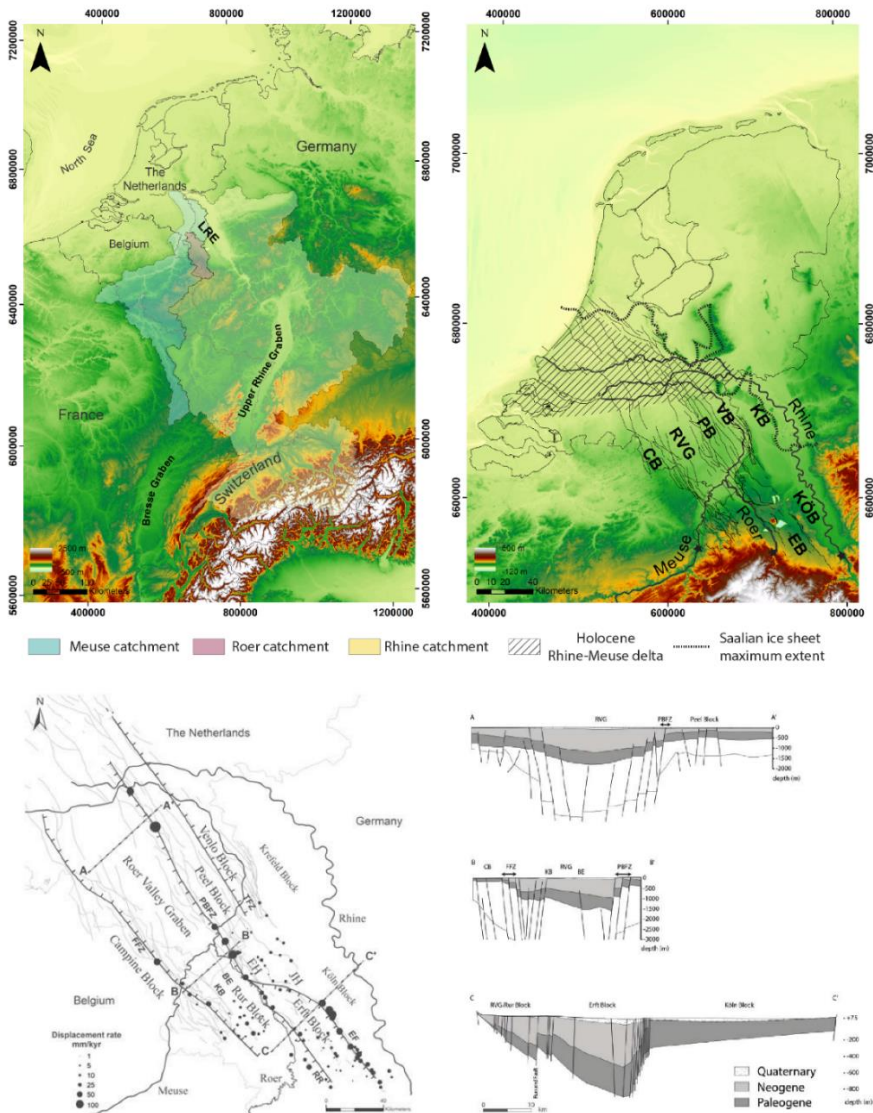


Fig. 1: The Lower Rhine Embayment (LRE) as part of the European Cenozoic rift system. The Meuse, Roer and Rhine rivers flow through the LRE. The Meuse crosses the rift system, the Roer parallels the Roer Valley Graben (RVG) and the Rhine occupies the rift margin. Tectonic displacements are the highest along the north-eastern boundary faults of the Roer Valley Graben (RVG) and Erft Block (EB). Displacement rates are adapted from Gold et al. (2017), Cohen (2003), Van Balen et al. (2019), Michon and Van Balen et al. (2005), Van den Berg et al. (2002), Houtgast et al. (2005) (after Woolderink et al. 2019).

5.2 Fluvial and tectonic setting

5.2.1 Present-day characteristics of the Meuse, Roer and Rhine rivers

The Meuse River is a circa 900 km long rainfed river that has its headwaters in northeastern France (Fig. 1). The Meuse then flows along the rims of the Paris Basin and crosses the Ardennes Massif before it enters the tectonic system of this study at Eijsden (Fig. 1). The Meuse River crosses multiple fault zones of the Lower Rhine Embayment (LRE). Because it crosses the main graben of the rift system (i.e. the Roer Valley Graben [RVG]), rather than following it, its geomorphology (floodplain width, flanking terrace flights) is substantially affected by differential tectonics (Fig. 1 [Van den Broek and Maarleveld, 1963; Van den Berg, 1996; Huisink, 1998, Woolderink et al., 2019]). The Meuse enters its Holocene deltaic reaches where it turns westward in the central Netherlands (Fig. 1). The present-day mean annual discharge is circa $250 \text{ m}^3/\text{s}$ and its bankfull discharge is approximately equal to mean annual flood, which is around $1500 \text{ m}^3/\text{s}$ at Maaseik (Belgium; Table 1). The catchment size of the Meuse river system is $33,000 \text{ km}^2$. Gradients of the Meuse valley range between ~ 60 and 10 cm/km on average. The adaption length of the backwater curve lies between 7.5 and 52.5 km . The adaption length represents the upstream length up to which the effects of a downstream perturbation can propagate, which is an important factor when considering the effects of faulting on river morphodynamics.

The Roer River is the main tributary of the Meuse River in the study area, and has a catchment size of circa 2354 km^2 . The Roer has its source in the Hautes Fagnes (Belgium) and has a length of 165 km . In the upstream $\sim 85 \text{ km}$ bedrock is dominant as it flows through the uplifting Eifel region. The downstream alluvial reach, circa 80 km , flows through the subsiding RVG (Fig. 1). The Roer enters the RVG at Düren and flows parallel to the direction of the graben and fault zones (Fig. 1). The mean annual discharge of the Roer River is $\sim 21.8 \text{ m}^3/\text{s}$ (at Stah, Germany) and discharge varies between 8 and $124 \text{ m}^3/\text{s}$ (LANUV, n.d.; Table 1). Valley gradient varies between circa 230 and 90 cm/km and the adaption lengths of the backwater curves range between 0.8 and 2.9 km .

The Rhine River is the largest river passing through the rift system. It has a length of 1230 km and flows from the Alps in Switzerland, through Germany and the Netherlands to the North Sea (Fig. 1). The Rhine river is a snowmelt and rainfed river and its catchment is circa $185,000 \text{ km}^2$. The Rhine River enters the Lower Rhine Embayment at Bonn and takes a north westerly course along the eastern margin of the tectonic system, avoiding the rift system depocentres (Fig. 1). The river enters its deltaic reach in the Dutch-German border region. The mean annual discharge is around $2200 \text{ m}^3/\text{s}$ at Rees (Germany [Erkens, 2009]) and the mean annual flood discharge is $\sim 6500 \text{ m}^3/\text{s}$. The adaption length for the backwater effect is around 29 km (Table 1) and valley gradient average lies between 35 and 20 cm/km .

Table 1: Main river characteristics of the gravel and sand reaches of the Meuse, Roer and Rhine rivers.

	Meuse Gravel	Meuse Sand	Roer Gravel	Roer Sand	Rhine Gravel
Q _{flood} (M ³ /S)	1500			85	6500
Width (m)	125	150	40	30	425
Depth (m)	4.5	5.3	1.9	2.6	7.3
Width/depth	27.8	28.6	21.1	11.5	58.2
Gradient Valley (m/km)	0.6	0.1	2.3	0.9	0.35 - 0.20
Grainsize (m)	0.02 - 0.04	0.0005 - 0.001	0.04	0.0005 - 0.001	0.015 - 0.02
Sinuosity range	1.07 - 2.77	1.03 - 3.39	1.05 - 1.42	1.17 - 2.20	1.03 - 1.93
Shields number	0.05	0.40	0.06	1.61	0.06
Adaption length backwater effect (km)	7.5	52.5	0.8	2.9	29.2

5.2.2 Tectonic structure and depositional record

The Lower Rhine Embayment (LRE) forms the northern segment of the European Cenozoic Rift System (ECRIS). The ECRIS spans from the North Sea to the Mediterranean and also includes the Eger Graben (Czech Republic), Leinegraben (Germany), the Bresse, Limagne, Saône grabens, gulf of Lyon (France) and the Valencia Trough (Spain [Ziegler, 1992]). The Roer Valley Rift System (RVRS) is part of the LRE (Fig. 1). The LRE is situated in the southern Netherlands and adjacent parts of Belgium and Germany (Fig. 1). The RVRS developed upon Palaeozoic to Mesozoic fault structures and has been reactivated multiple times in both reverse and normal faulting modes (Geluk et al., 1994; Van Balen et al., 2019). The last extension phase, which is still ongoing, started during the Late Oligocene. This extension can be related to the (ongoing) stresses exerted by the Alpine orogeny on its forelands (Ziegler, 1992).

The tectonic evolution of the LRE has been studied extensively (Fig. 1 [Ahorner, 1962; Klostermann, 1983; Zagwijn, 1989; Schirmer, 1990; Ziegler, 1992, 1994; Geluk et al., 1994; Van den Berg, 1996; Houtgast and Van Balen, 2000; Houtgast et al., 2002; Cohen et al., 2002; Schäfer and Siehl, 2002; Michon et al., 2003; Van Balen et al., 2005; Kemna, 2005; Westerhoff et al., 2008]). The horst-graben structure of the LRE consist of asymmetric (half) grabens and symmetric (full) grabens (Fig. 1 [Schäfer et al., 2005; Michon and Van Balen, 2005; Westerhoff et al., 2008]). The main fault zones of the LRE have a NW-SE orientation (Fig. 1). The most important grabens in the LRE are the Erft Block (EB) and the Roer Valley Graben (RVG)/Rur Block (RB) respectively. The RVG is bounded by the relatively uplifting Campine Block (CB) in the south and the Peel Block (PB) in the north (Van Balen et al., 2005; Westerhoff et al., 2008). The upstream part of the CB consists of relatively cohesive Cretaceous and Paleogene limestone (hard) rocks. A transition to unconsolidated sands occurs near Maastricht. The shallow subsurface of the RVG consist mainly of relatively coarse-grained (older) Rhine-Meuse deposits. The PB is characterized by (cohesive) fine marine and coastal deposits of

Miocene age. The Venlo Block (VB) consist predominantly of fluvial sediments (Woolderink et al., 2018 and references herein). The fault systems also continue in the subsurface of the Rhine-Meuse delta (Cohen et al., 2002), but are not considered a direct control to Late Holocene deltaic river reaches and hence these are left out of our sinuosity analysis.

The LRE has a general northwest tilting direction, which is a result of subsidence in the North Sea Basin (Kooi et al., 1991,1998) and the Quaternary uplift of the Rhenish Shield (Van Balen et al., 2000; Demoulin and Hallot, 2009). A secondary tilt direction to the northeast was observed for the tectonic blocks of the RVRS, based on lithostratigraphic mapping of the basin fill (Van Balen et al., 2000). A superimposed regional-scale, glacio-isostatic northward tilting component is reckoned to have been in play in the youngest 20,000 years (Kiden et al., 2002; Cohen, 2003; Busschers et al., 2007; Hijma et al., 2009), owing to the near-field peripheral position of the region to land ice masses (forebulge collapse). However, the subsidence due to isostatic movements becomes insignificant during the past few thousand years compared to the tectonic component (Kiden et al., 2002).

The NE-SW directed extension led to a maximum of circa 1200– 1500 m of subsidence in the RVG since the Late Oligocene (Geluk et al., 1994; Van Balen et al., 2005; Schäfer et al., 2005; Kemna, 2005; Schokker et al., 2005; Westerhoff et al., 2008). An overview of the displacement rates of the (main) fault zones of the LRE is shown in Fig. 1. The highest displacement rates, and maximum sediment accumulation, occurs along the north-eastern boundary faults of the RVG and EB (Ahorner, 1962; Schäfer et al., 1996; Camelbeeck and Meghraoui, 1998; Van den Berg et al., 2002; Houtgast et al., 2002; Michon and Van Balen, 2005; Gold et al., 2017; Woolderink et al., 2019).

The Feldbiss Fault Zone (FFZ) separates the RVG from the CB in the south, while the Peel Boundary Fault Zone (PBFZ) forms the boundary between the RVG and PB in the north (Fig. 1). The river Meuse at present traverses these faults, and has had such a course since ~300.000 years ago (Van den Berg, 1996; Houtgast et al., 2002; Schokker et al., 2007). The FFZ is downstepping in the flow direction of the Meuse River, while the PBFZ is downstepping in upstream direction. Both the FFZ and PBFZ reach to the surface and are visible as fault scarps and in seismic and geo-electric profiles (DINoloket, 2019; Paulissen, 1985; Vanneste et al., 2002). The Koningsbosch (KB) and Beegden (BE) faults delineate a small horst within the subsiding RVG (Fig. 1). The KB fault reaches up to the Meuse river bed, is visible on shallow river seismic sections and on geo-electric profiles, and is downstepping in upstream direction (Demco, 1998; Tigrek et al., 2000). The BE fault has not been surveyed and it is unknown whether this fault reaches up to the river bed. According to borehole data (DINoloket, 2019), the fault seems not to have affected deposits of the Meuse River of the last ~300.000 years and there is no morphological expression of the BE.

The BE normal fault steps down in downstream direction. Present-day and Holocene displacement rates of the KB and BE faults are unknown.

In the southeastern part of the LRE, the PBFZ splits into the Rur (RR) and Erft (EFZ) fault zones. The Rur Fault (RR) separates the RVG/RB from the EB. The Köln Block (KÖB) forms the hanging wall in the eastern part of the LRE, where it is separated from the EB by the Ville horst and Erft Fault Zone (EFZ) (Fig. 1 [Schäfer et al., 2005]). The Ville horst continues to the northwest into the Jackerather and Erkelenz horsts respectively (cf. Ahorner, 1962). The continuation of these horst structures form the Peel Block in the Netherlands (Fig. 1). The PB is bordered by the Venlo Block (VB) that lies to the north (Fig. 1).

The VB and PB are separated by the Tegelen Fault Zone (TFZ). The TFZ consist of three faults that are all downstepping in downstream direction of the Meuse (Fig. 1). The faults reach up to the river bed according to shallow-seismic river profiles (Tigrek et al., 2000). The displacement rates of the faults have not been constrained in the study area. However, since these faults have no morphologic expression, their average rates should be less than those of the historically seismically active FFZ and the PBFZ. An estimation of displacement rates, between ~ 0.02 mm/yr (± 0.01) and 0.11 (± 0.02), of the TFZ more to the north was given by Cohen et al. (2002). In the northeast a relatively high block, the Krefeld Block (KB), borders the subsiding VB area (Geluk et al., 1994). The shallow subsurface of the KB consist mainly of Pleistocene fluvial gravel and sand of the Rhine River (NRW 2019).

The LRE main fault zones are seismically active with the 1756 Düren (Mw 5.7) and 1992 Roermond (Mw 5.4) earthquakes as the most significant examples (Geluk et al., 1994; Camelbeeck et al., 2007). Palaeoseismological data from trench studies over the PBFZ and FFZ shows that fault displacement has been episodic, especially during the Lateglacial period (Vanneste and Verbeeck, 2001; Vanneste et al., 2001; Van den Berg et al., 2002; Camelbeek et al., 2007; Vandenberghe et al., 2009; Vanneste et al., 2018; Van Balen et al., 2019).

5.3 Methods

Both the longitudinal profiles and sinuosity calculations are based on the early 19th century courses of the Meuse, Roer and Rhine rivers as these courses pre-date most regulations (e.g. dykes, weirs, groins, channelization) of the rivers. The Meuse channel was digitized from the georeferenced Topografische en Militaire kaart van het Koninkrijk der Nederlanden 1850–1864 (Kadaster 1850). The river channels of the Roer and Rhine were derived from the Tranchot Maps 1801–1828.

5.3.1 Longitudinal profiles

In a GIS, points were placed along the digitized 19th cy. river channels with a spacing of 100 m. For each of the points the height was extracted from a 1 m (horizontal) resolution contemporary Digital Elevation Model [AHN2, n.d.; Land NRW, n.d.]. Hereafter the height was plotted against the distance along the river channel (Fig. 2).

A considerable bandwidth of height points is generated by this method due to (gravel/sand) mining, inclusion of water-bodies and presence of anthropogenic (infra) structures along certain stretches of the rivers. This is especially the case for the Meuse River in the RVG (Fig. 2). Therefore, median values were established, where each median is calculated over a sliding window across neighbouring elevation points, for the longitudinal channel profile of each of the rivers. The window size was determined by incrementally increasing the window size until the inflection point, after which an increase in window size did not contribute to a smoother profile anymore. The window sizes used for the Meuse, Roer and Rhine are 101, 51 and 161 points (or 10, 5 and 16 km) respectively. By using this method, the median elevation values become dependent on the sinuosity of the river channel, which varies spatially over the longitudinal profile of the rivers.

Valley gradients were calculated by $S_v = P * S_c$, where S_c = channel slope and P is the sinuosity, in order to retrieve them separately for each sinuosity zone. Hereafter the potential specific stream power ω_{pv} (W/m^2), which is a parameter for the potential maximum of the available flow energy for a river stretch with a sinuosity of 1 (Kleinhans and van den Berg, 2011), was calculated for each sinuosity reach of the rivers. It is defined as $\omega_{pv} = \frac{\rho g Q S_v}{W_r}$, where ρ = water density ($kg\ m^{-3}$), g = gravitational acceleration ($m\ s^{-2}$), Q = channel forming discharge (m^3/s), S_v = valley slope (-) and W_r = reference channel width. The channel reference width is predicted by $W_r = \alpha \sqrt{Q}$ where $\alpha = 4.7$ for sand ($D_{50} < 2\ mm$) and 3.0 for gravel ($D_{50} > 2\ mm$) reaches of the rivers (Van den Berg, 1995; Kleinhans and van den Berg, 2011). The calculation of streampower per sinuosity-reach used in this study is a relatively crude approach and is hence mostly suited to indicate relatively large-scale variations in streampower over the length of the longitudinal river profiles. However, this sinuosity-reach approach is very well-suited to compare the reach-specific streampower and sinuosity of the river channel to fault locations, which is the focus of this study.

5.3.2 Sinuosity

Sinuosity is defined as the ratio of channel length over valley length. Sinuosity can be computed at the largest scale, using the valley length corresponding to the whole river stretch, as well as to shorter parts of river valley stretches. Therefore, sinuosity is

analysed and presented as a function of length-scale in this study (e.g. Lancaster and Bras, 2002; Van Balen et al., 2008). The average sinuosity for the whole range of potential lengths was calculated, (zero to fifteen kilometres), to determine the most suitable length-scale. The minimum length resulting in the maximum average sinuosity was selected as lengths above this minimum value have no significant contribution to sinuosity (Appendix A). The length scales used for the Meuse, Roer and Rhine sinuosity calculations are respectively 7.5, 3 and 12.5 km (Appendix A).

5.4 Results and interpretation

5.4.1 Longitudinal profiles

The Meuse River shows a distinct break in the gradient of the longitudinal profile, and associated peak in gradient change, around 15 km along the river channel (Fig. 2). Relatively high changes in gradient occur around the FFZ (i.e. HH, GF, FF), KB, BE and just in front of the PBFZ I (Fig. 2). However, the overall channel gradient over the CB and RVG remains relatively stable around 0.35 m/km. A peak in the change of gradient occurs at ~105 km along the river channel. The average channel gradient over the PB and VB reduces to ~8 cm/km (90–175 km). The Roer River has a concave river profile with a gradual change in gradient around 46 km along the river channel profile (Fig. 2). Here the channel gradient reduces from ~204 cm/km in the upstream part to ~70 cm/km in the reach downstream of the concavity (Fig. 2). The change in gradient reduces in the downstream direction (Fig. 2). The change in gradient of the Roer River is relatively peaked compared to the Meuse and Rhine rivers. The channel gradient of the Rhine River between ~8 and 85 km is ~19 cm/km (Fig. 2). Between ~85 and 135 km this gradient steepens to ~24 cm/km. The gradient of the channel changes relatively abruptly around 158 km, this is, however, due to an anomaly in the Digital Elevation Model and has no natural cause. From 135 to 208 km the gradient of the Rhine channel reduces to ~13 cm/km.

5.4.2 Sinuosity patterns

5.4.2.1 *Meuse*

The early 19th century course of the Meuse can be visually subdivided into three sinuosity zones, labelled M1-M3 (Fig. 3). In sinuosity reach M1 the Meuse River is relatively straight with sinuosity values of ~1.07–1.13. In the next downstream stretch, M2, the sinuosity is larger, ranging between 1.19 and 2.76 (Fig. 3). Despite the increase in sinuosity from zone M1 to M2, the coarseness of the bed load (gravel) and the discharge remain constant. However, the erodibility of the bed and banks is different in stretch M1. Here the subsurface consists of relatively cohesive Cretaceous and Paleogene limestone, while in the upstream part of zone M2 the bed and banks consist of unconsolidated sands (<https://www.dinoloket.nl>, 2019). The relatively hard limestone

likely reduces vertical erosion and lateral movement and hence sinuosity of the river channel in zone M1 (Figs. 3 and 4). The peak in change of gradient around 15 km along the river channel (Fig. 4) coincides with the lithological transition (from limestone to sands) of the subsurface. This increases erodibility of bed and banks downstream of the lithological transition and hence a larger gradient is observed in zone M2 (Fig. 4). This results in an enhanced lateral displacement and, consequently, a sinuosity increase (Figs. 3 and 4). More downstream, in the RVG the lithology changes to coarse-grained gravel and sands of older Rhine-Meuse fluvial deposits that are still relatively easily reworked and, therefore, promote lateral dynamics of the river and thus sinuosity.

Zone M3 is characterized by sinuosity values between 1.08 and 1.30, which shows that the river in this reach is rather straight (Fig. 3). This is in line with a reduction of the gradient and associated stream powers in this reach (Fig. 4). However, the change in subsurface lithology over the PBFZ I is an additional factor to be taken into account for the sinuosity change. In the upstream part of zone M3, on the PB, the subsurface lithology consists of cohesive Miocene, Pliocene and Early Pleistocene fine-grained sands and clays (Woolderink et al. 2018 and references herein). This reduces bank erosion and, hence, lateral movement and sinuosity. Moreover, bank height increases over the PB and VB due to ongoing incision during the Holocene. These factors hamper lateral dynamics of the river channel. Vertical incision thus prevails over lateral movement, resulting in a low-sinuosity channel of the Meuse River in zone M3 (Fig. 4; [Woolderink et al. 2018]).

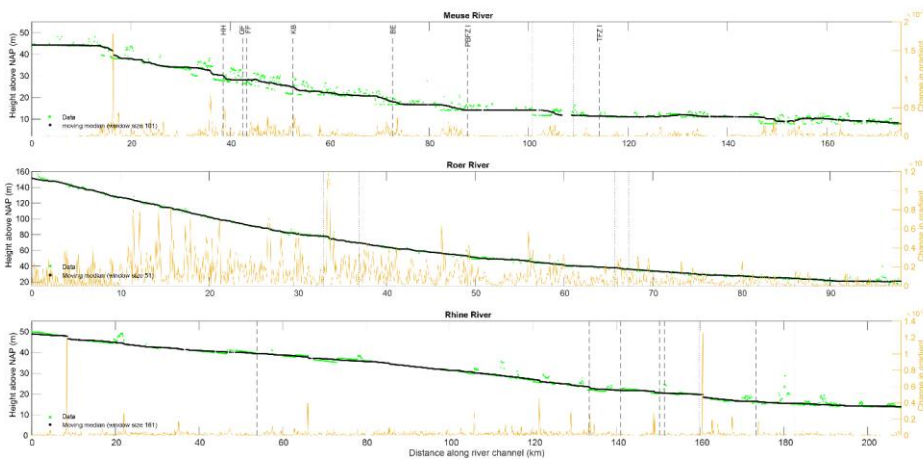


Fig. 2: Early 19th century longitudinal river channel profiles of the Meuse, Roer and Rhine rivers. Dashed lines represent (semi)perpendicular crossing by the river channels of the (postulated) faults of the Lower Rhine Embayment. Dotted lines indicate a parallel course of the river channel and the fault zone. NAP is the dutch ordnance datum.

5.4.2.2 Roer

The early 19th century course of the Roer River can be divided into two reaches based on the sinuosity of the river channel (Fig. 3). Zone R1 is characterized by relatively low sinuosity values between 1.04 and 1.40. Sinuosity increases in zone R2 with values ranging between ~1.20 and 2.20 (Fig. 3). The increase in sinuosity values at ~46 km along the river channel of the Roer (Fig. 3) coincides with a decrease in gradient from ~204 cm/km in zone R1 to ~70 cm/km in zone R2 (Fig. 4). A reduced gradient results in a reduced potential specific stream power (Fig. 4) and, therefore, in a shift from a chute-dominated meandering pattern to a scroll-bar dominated meandering river pattern (cf. Kleinhans and van den Berg, 2011 [Fig. 5D]). Frequent chute cut offs will result in a decrease in sinuosity of the channel, while increased scroll-bar formation enhances lateral migration and sinuosity. The threshold between chute-dominated to scroll-bar dominated meandering for the Roer River lies around a ω_{pv} value of ~60 (Fig. 5D). Although exact grainsize measurements were not available for the upstream part of the Roer River, a general classification of so-called “Grobkies and Mittelkies”, corresponding to a grainsize of $6.3 \cdot 10^{-3}$ – $6.3 \cdot 10^{-2}$ m, was derived for the bedload in this reach (NRW 2019).

For this grainsize range our threshold in stream power between scroll-bar dominated and chute-dominated meandering for the Roer River falls within the empirically derived threshold shown by Kleinhans and van den Berg, 2011 [Appendix B]). The negative correlation between stream power and sinuosity for the Roer River is shown by Figs. 4 and 5F. It is striking that sinuosity reaches of the Roer River that are outside the trend can be explained by a change in lithology (Fig. 5F). Furthermore, the sinuosity zone in which the Roer River “crosses” fault zones of the LRE parallelly, fits the trend of sinuosity versus stream power, indicating that the sinuosity of the Roer River is not influenced by tectonics (Fig. 5F). The results for the Roer River show that sinuosity is dependent on other factors than tectonics (i.e. grain-size, chute and neck cut-off, bank strength and height [Baker, 1978; Schumm, 1963; Dade, 2000; Kleinhans and van den Berg, 2011; Candel et al., 2020]).

5.4.2.3 Rhine

The early 19th century course of the Rhine River can be subdivided into four sinuosity zones (Fig. 3 zones Rh1-Rh4). Zone Rh1 is relatively straight with sinuosity values between 1.04 and 1.10 (Fig. 3). This low sinuosity is not the result of a reduced gradient, which is relatively high in this upstream reach (with corresponding high streampowers [Fig. 4]), or a change in discharge. Bedrock lithology, however, offers an explanation for the relatively straight river channel in zone Rh1 compared to a more sinuous channel in zone Rh2 (Fig. 3, Fig. 4). The relatively resistant Palaeozoic bedrock of the Rhenish Massif hampers lateral movement of the Rhine River and, therefore, sinuosity in reach Rh1.

Within zone Rh2 sinuosity increases to values ranging between 1.13 and 1.60 (Fig. 3). The subsurface lithology changes from the Palaeozoic slates in zone Rh1 to Quaternary sand and gravel of older Rhine deposits in zone Rh2 (NRW 2019). This change in subsurface lithology, together with the transition from a confined to a more unconfined setting, results in a sinuosity increase in zone Rh2 due to more easily lateral erodible banks.

Zone Rh3 is the part of the Rhine with the highest sinuosity values; these vary between 1.26 and 1.91 (Fig. 3). The erodibility of the subsurface does not change between zone Rh2 and Rh3, as the river channel remains in the alluvial sediments of older Rhine deposits (NRW 2019). There is, however, a slight increase in gradient in zone Rh3, to ~24 cm/km, and associated stream powers (Fig. 2, Fig. 4).

This increase in gradient is, most likely, the cause of the higher sinuosity of zone Rh3. The increase in sinuosity between zone Rh2 and Rh3 does not coincide with any known fault structure of the LRE (Fig. 3). In fact, the most sinuous part of the river channel in Rh3 flows more or less parallel to the strike of the known fault zones of the rift system (Fig. 3), making a fault related forcing unlikely.

Attributing changes in sinuosity in the Lower Rhine, e.g. into and out of reach Rh3, to tectonic controls at this stage of research can only be speculative. In zone Rh3 the Rhine course is positioned relatively closer to the LRE margin and the flanking Rhenish Massif and outside the Quaternary depocentre (which lies somewhat to the west). Such could explain why both the sinuosity and gradient increases in zone Rh3 (Fig. 1, Fig. 3). If so, the gradient increase is the result of touching the very margin of the rift system in the area, and not so much controlled by neotectonically active faults, but by inherited structures from before Oligocene-Miocene rift system reactivation.

Downstream, in zone Rh4, sinuosity decreases to between 1.23 and 1.57 (Fig. 3). The reduced sinuosity in zone Rh4 (compared to zone Rh3) coincides with a decreased gradient of the longitudinal profile in this zone (Fig. 2, Fig. 4). Such a reduced gradient might be caused by active tectonics (Schumm et al. 2002) and the transition coincides with postulated fault locations (Ahorner 1962). It is, however, unlikely that this reduced gradient is a result of active tectonics because the faults do not have a surface expression in the (older) floodplain(s) of the Rhine River. Moreover, remnants of slightly older Rhine channels are highly sinuous (Erkens et al. 2011; Cohen et al. 2012). A more likely cause for the reduced gradient is a reduced incision rate (as proposed by Erkens et al. 2011), which is caused by aggradation of fines in this reach, similar to the deltaic reaches downstream. Moreover, the transition between zone Rh3 and Rh4 coincides with the maximum extent of the Saalian ice-sheet (Fig. 1), resulting in a local depocentre and hence reduced gradients in zone Rh4.

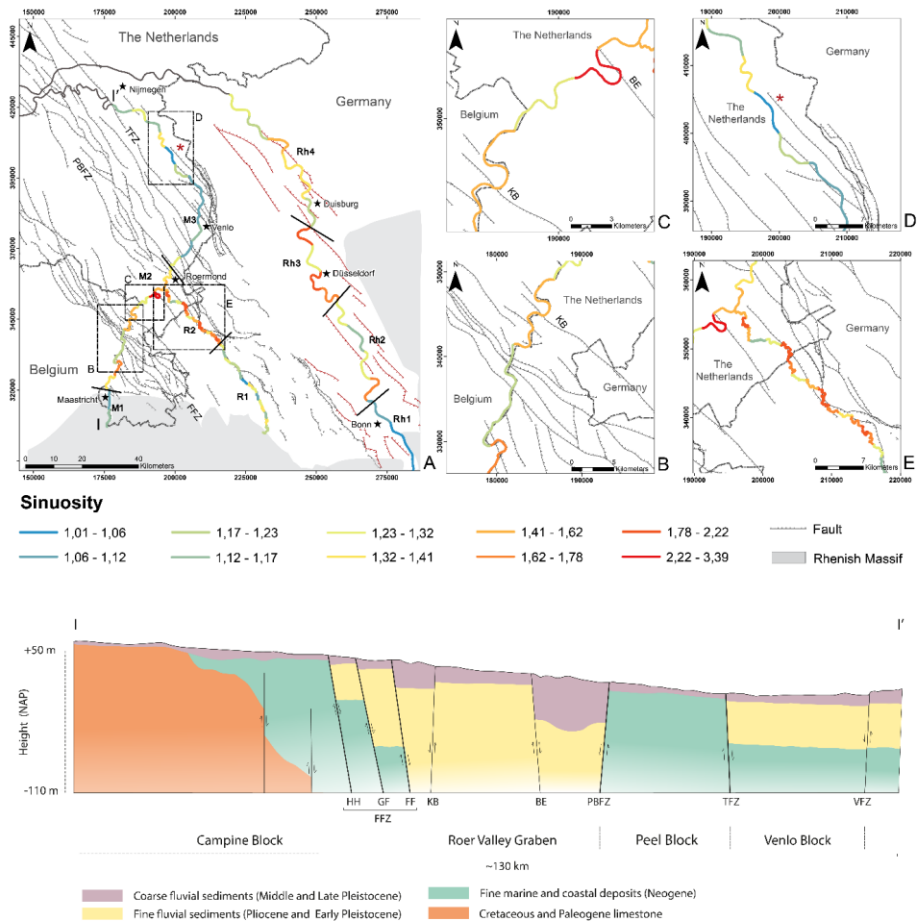


Fig. 3: A: Sinuosity analysis (per reach) of the early 19th century Meuse, Roer and Rhine rivers. The presence of the red coloured fault zones is uncertain. The transition from Cretaceous and Paleogene limestone to unconsolidated sands roughly coincides with the division between M1 and M2. B: Sinuosity changes of the Meuse over the Feldbiss and Koningsbosch fault zones. C: Sinuosity changes of the Meuse over the downstepping in upstream direction Koningsbosch and downstepping in downstream direction Beegden fault zones. D: Meanders (yellow) in zone M3 with a relatively high sinuosity that occur above strike-extrapolated strands of the TFZ I (indicated by the red asterisk). E: High-sinuosity reach R2 of the Roer River. Transect I-I' shows a schematic representation of the lithology of the (faulted) shallow subsurface along the longitudinal profile of the Meuse River in the LRE.

5.5 Discussion

5.5.1 Large-scale sinuosity patterns

The analyses of sinuosity changes suggest that large-scale sinuosity characteristics of the Meuse River are closely related to the location of faults, but not to faulting. The sinuosity of the Meuse River is indirectly (or passively) controlled by faulting as the faulted subsurface of the LRE causes differences in channel bed lithology, gradient and bank height along the river profile. This is shown in Fig. 4 which shows the stream power plotted over the longitudinal channel profile. The high sinuosity zone M2 coincides with a relatively high gradient, while zone M3 has low-sinuosity values due to the flattened gradient and cohesive and fine-grained lithology in the relatively uplifting PB and VB (Fig. 4). The same passive tectonic control was also observed for the previously investigated fluvial terraces of the Meuse river (Woolderink et al., 2018). A reach-specific tectonic control on river sinuosity was, for instance, also observed in the Mississippi River (Schumm et al., 1994) and Baghmata River (Jain and Sinha, 2005). From this it could be concluded that a faulted subsurface influences the large-scale sinuosity patterns of alluvial rivers in active tectonic (rift) systems.

However, the Roer River shows that different sinuosity zones along a river can be the result of a concave river profile with associated changes in streampower and bedload grainsize, without tectonic forcing or faults along the longitudinal river profile (Fig. 4). For the Pannagon River (India) it was shown that the style and degree of river channel sinuosity also depends not solely on tectonics but on a number of other (geological) factors and riparian vegetation as well (Aswathy et al., 2008). Furthermore, the experiments by Schumm and Khan (1972) showed that sinuosity only increases with gradient up to a threshold, a further increase leads to a braided river pattern in which sinuosity is lower. The Roer River shows that it is not necessary to have a channel pattern shift to a braided style to accomplish a sinuosity decrease with increasing gradient, but that frequent chute cut-offs within the self-organized meandering domain lead to a similar result (Figs. 4 and 5B, D).

The sinuosity changes of the Rhine River, positioned at the rift margin, also show large scale sinuosity patterns (Fig. 2). A trend of increasing sinuosity and gradient seems apparent for zone Rh3 in Fig. 4. This is supported by Fig. 5C and G that show a general positive trend between valley gradient/stream power and sinuosity (cf. Holbrook and Schumm, 1999; Timár, 2003; Petrovski et al., 2012), albeit for a certain range of valley gradient and stream power (i.e. in the meandering with scroll bar domain cf. Kleinhans and Van den Berg, 2011 [Appendix B]). Overall, the variations in river sinuosity of the early 19th century course of the Rhine River do not seem to be actively tectonically forced as sinuosity zones can be attributed to other causes such as inherited lithological differences, downstream reduced incision rates and changes in bank height and

composition. Moreover, the sinuosity zones in which the river channel crosses fault zones fall within the positive trend that can be observed for the Rhine, indicating that sinuosity changes are not bounded to fault zones. Sinuosity is, therefore, not considered to be a valid indicator of tectonic activity for the Rhine River.

The above illustrates that an indirect relation between faulting, subsurface lithology and sinuosity exists for the Meuse river in the Lower Rhine Embayment rift system, but not for the Roer and Rhine rivers. Therefore, specific relations between faulting, valley slope and sinuosity cannot be generalized (cf. Kleinhans and van den Berg, 2011).

5.5.2 Local sinuosity anomalies at fault zones

A local change in sinuosity occurs in zone M2, around the Feldbiss Fault Zone (FFZ) (Figs. 3 and 4). Here sinuosity first decreases to ~ 1.2 , when the Meuse river approaches the FFZ, after which sinuosity increases to ~ 1.6 when entering the RVG (Fig. 3). The FFZ consist of three faults that are downstepping in the downstream direction (e.g. Heerlerheide, Geleen and Felbiss faults). The faults of the FFZ are active and fault scarps occur on the late Middle Pleistocene terraces next to the Holocene floodplain (Houtgast et al., 2005; Camelbeeck et al., 2007). Relatively high changes in gradient occur around the FFZ (Figs. 2 and 4). A local sinuosity increase at fault-zone scale at the FFZ might thus be expected, in response to the downstepping normal faults and associated increase in gradient (Holbrook and Schumm, 1999). Such an increase in sinuosity was evidenced for rivers in the Pannonian Basin and the Mississippi River (Schumm et al., 1994; Holbrook and Schumm, 1999; Petrovski et al., 2012). However, a sinuosity decrease is observed at the FFZ (Fig. 3).

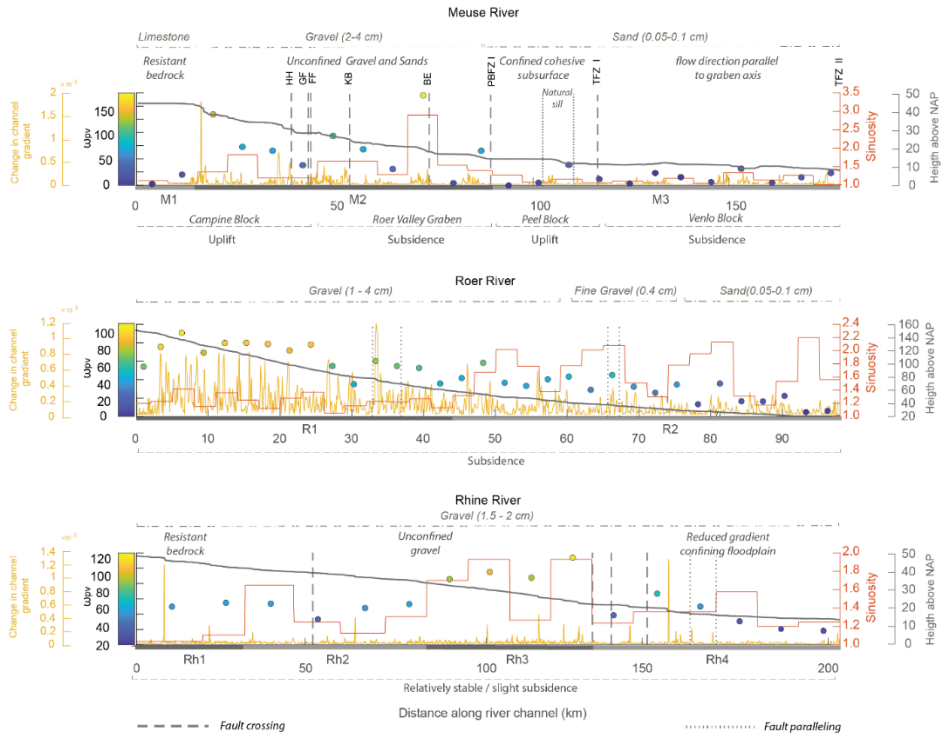


Fig. 4: Sinuosity, potential specific stream power and (change) in channel gradient along the longitudinal channel profiles and sinuosity zones of the early 19th century Meuse, Roer and Rhine rivers. Dashed lines represent (semi) perpendicular crossing by the river channels of (postulated) faults of the Lower Rhine Embayment. Dotted lines indicate a parallel course of the river channel and the fault zone.

The lack of a sinuosity increase around the FFZ implies that either the rate of faulting (and associated increase in gradient) is not high enough to force a sinuosity change, or that in-channel erosion and sedimentation has levelled height differences to such an extent that a sinuosity change was not established. Alternatively, a sinuosity decrease, as observed for the FFZ, can be explained by a gradient increase. The Roer River shows that higher gradients upstream lead to more chute cutoffs of the channel which reduces channel sinuosity (Fig. 4). This is considered as a likely cause for the relatively low-sinuosity reaches over the FFZ as local increased channel gradients are still observed in the channel profile and because the Meuse is near the threshold to a chute cut-off dominated meandering river (cf. Kleinhans and van den Berg, 2011 [Appendix B]) at the FFZ (Table 1). This is supported by remnants of phases of higher sinuosity and the presence of chute-channels in the adjacent floodplain at the FFZ.

A notable alignment of two relatively high-sinuosity meanders occurs along the Koningsbosch Fault (KB) and the Beegden Fault (BE), which delineate a small horst within the RVG (Figs. 1 and 3C). A reduced sinuosity is expected at the KB fault due to its upstream directed down stepping (Fig. 1) and resulting decrease in gradient. An increase in sinuosity is expected at the BE fault (Fig. 1) because of an increase in gradient at a fault that is downstepping in downstream direction (Holbrook and Schumm, 1999). There is no change in subsurface lithology over the KB fault which could account for the increased sinuosity at this fault zone. A local increase in channel gradient is, however, observed for the KB (Fig. 2). This might be the cause of the increased sinuosity of the KB fault, though this is the opposite of the expected sinuosity decrease from the downstepping in upstream direction of the KB fault. The sinuosity increase at the downstepping Beegden fault (BE) could imply that the fault reaches upon the river bed and is tectonically active. Alternatively, the high sinuosity might be the result of the confluence with the Roer River which would lead to a knickpoint and increased valley gradient and, hence, a larger sinuosity of the meandering Meuse in this area than both upstream and downstream (Fig. 3).

Sinuosity of the channel decreases over the PBFZ, which is downstepping in the upstream direction, when transitioning from the RVG to the PB (Fig. 3). However, the gradient, stream power and sinuosity remain relatively high up to the PBFZ (Figs. 3 and 4). This shows that the tectonic configuration of a fault-bounded horst exerts a substantially different form of forcing on river channels than dome-shaped warping (cf. Holbrook and Schumm, 1999). In the latter, a sinuosity decrease is to be expected in front of the axis of uplift where the gradient decreases. Uplift may expose more resistant substrates underneath otherwise alluvial rivers, resulting in channel profile anomalies (Holbrook and Schumm, 1999). This is also observed for the Meuse River between ~100 and 110 km (Figs. 2 and 4). Here resistive layers of clay and lignite are locally exposed in the Meuse channel (causing a natural sill), leading to an increased gradient of the longitudinal profile (Figs. 2 and 4). This does, however, not mean that there is active deformation present at this location, but rather implies a passive tectonic control on the longitudinal profile. Our results, therefore, concur with Holbrook and Schumm (1999) who stated that such complexities and profile adjustments can rarely be used to indicate uplift without other evidence.

The faults of the TFZ I reach up to the river bed at the transition between the PB and VB, but no effect of fault displacement (i.e. an expected sinuosity increase) is noticeable in the channel gradient or the sinuosity (Figs. 2, 3 and 4). This implies that either no displacement has occurred along the TFZ I for, at least, the last two centuries or that slip rates were minor enough for the river channel to adjust to by in channel erosion and sedimentation.

Two relatively high-sinuosity meanders occur in M3, but no fault is known at this location (Fig. 3D). However, the meanders occur above strike-extrapolated strands of the TFZ I, 6 km to the northwest, which could imply our current fault data base is incomplete (Fig. 3D, red asterisk).

A possible correlation between fault zones and sinuosity and stream power for the Meuse River can be observed from Fig. 5E. Almost all fault zones that reach upon the surface have a relatively high stream power. There is, however no relationship between stream power and sinuosity for the fault zones (Fig. 5E). Moreover, all the high stream power segments fall within large-scale sinuosity zone M2 (Figs. 3 and 4), which is characterized by a relatively high gradient and unconfined floodplain and gravel/sand lithology of the subsurface. This endorses our previous observation that the sinuosity of the Meuse river is influenced by fault bounded blocks (Fig. 3), but that there is no uniform relation between fault zone scale vertical tectonic movements and sinuosity (Fig. 5E).

From the above it can be concluded that sinuosity change as an indicator of abrupt tectonic vertical motions along fault zones is not straightforward. Therefore, unless the different forcing factors can be unravelled by detailed morphometric analysis and a well constrained tectonic and sedimentary framework, (local) sinuosity anomalies should be interpreted as an indicator of possible tectonic deformation at best. In this our results coincide with Schumm (1986) and Holbrook and Schumm (1999) who mention that alternative explanations must be addressed before sinuosity change can be considered valid as an indicator of tectonic deformation. Moreover, the rate at which fluvial morphodynamics occur might be much higher than that of tectonic faulting. This can lead to reworking of fluvial response(s) to faulting by subsequent river dynamics. It is, therefore, important to be aware of such transient river response when interpreting the geomorphological and sedimentological record for fault related sinuosity anomalies.

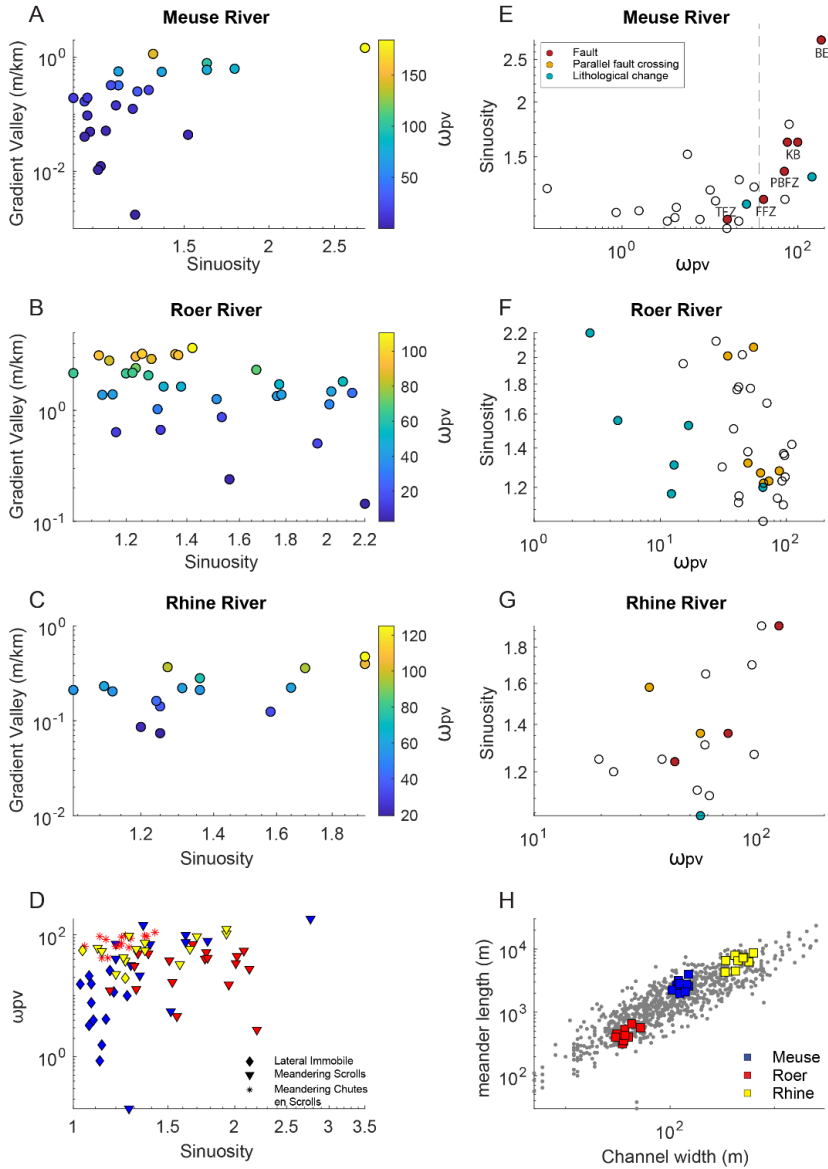


Fig. 5: A–C: Valley gradient vs sinuosity for the Meuse, Roer and Rhine, respectively. The circles represent the sinuosity reaches of the rivers. The Meuse river shows no clear relationship between valley gradient and sinuosity. The Roer has a negative correlation while the Rhine shows a positive correlation between sinuosity and gradient of the valley D: Potential specific stream power versus sinuosity for the different fluvial planforms of the Meuse, Roer and Rhine. E–G: Sinuosity versus potential specific stream power for the Meuse, Roer and Rhine, respectively. Open circles represent null conditions. The legend for the Meuse applies to the panels of the Roer and Rhine as well. The Meuse shows no clear relationship, while the Roer and Rhine show a negative and positive correlation respectively. Sinuosity zones that coincide with fault locations, parallel fault crossings or lithological changes of the subsurface are indicated by colour. H: Relation between meander length and channel width of the meandering reaches of the Meuse, Roer and Rhine rivers. Grey points are adapted from Leuven et al. (2018).

5.6 Conclusions

The effects of tectonic vertical motions on the Meuse (crossing the faults), Roer (parallel to the faults) and Rhine (rift margin) rivers have been investigated and the following can be concluded:

- The sinuosity of the early 19th century course of the Meuse river is (indirectly) controlled by tectonics on a block-scale as this determines the large-scale differences in valley gradient and subsurface lithology, and hence the erodibility of the river bed and banks.
- Downstream sinuosity increases along the Roer River are the result of a decreasing gradient along the concave river profile and associated change from a chute-dominated to scroll-bar dominated meandering system.
- The early 19th century course of the Rhine River does not reveal any tectonic controls or fault zone activity. Changes in sinuosity are mostly related to lithological differences, reduced incision rates and changes in bank height and composition.
- The relation between fault motions, river gradient and sinuosity is not straightforward as sinuosity is also controlled by (o.a.) river bed and bank characteristics, intrinsic fluvial dynamics, meandering style and because sinuosity varies over time.
- Sinuosity change as an indicator of tectonic motions can only be used in combination with a well-known tectonic and sedimentary framework. The absence of a sinuosity change does not imply inactivity of the fault at geological time-scales, nor is a deviating sinuosity value proof of fault activity.

5.7 Acknowledgements

This research is part of a PhD project “Reconstruction and Modelling of the Meuse and Rhine River. Sinuosity Response to Faulting in the Roer Valley Rift System” funded by Netherlands Organisation for Scientific Research (NWO; project nr. 821.01.011). We would like to thank John Holbrook, Gábor Timár and an anonymous reviewer for their constructive comments and review that helped improve this manuscript

5.8 References

- › Adams, J., 1980. Active tilting of the United States midcontinent: geodetic and geomorphic evidence. *Geology* 9, 442–446.
- › Ahorner, L., 1962. Untersuchungen zur quartären Bruchtektonik der Niederrheinischen Bucht. *Quaternary Science Journal* 13 (1), 24–105.
- › Arcos, M.E.M., 2012. A Holocene sedimentary record of tectonically influenced reduced channel mobility, Skokomish River delta, Washington State, USA. *Geomorphology* 177, 93–107.
- › Aswathy, M.V., Vijith, H., Satheesh, R., 2008. Factors influencing the sinuosity of Pannagon River, Kottayam, Kerala, India: an assessment using remote sensing and GIS. *Environ Monit. Assess.* 138 (1–3), 173–180.
- › Baker, V., 1978. Adjustment of fluvial systems to climate and source terrain in tropical and subtropical environments. In: Miall, A.D. (Ed.), *Fluvial Sedimentology*. 5. Memoir Canadian Society of Petroleum Geologists, pp. 211–230.
- › Burnett, A.W., 1982. Alluvial Stream Response to Neotectonics in the Lower Mississippi Valley. Doctoral dissertation, Colorado State University.
- › Burnett, A.W., Schumm, S.A., 1983. Alluvial-river response to neotectonic deformation in Louisiana and Mississippi. *Science* 222 (4619), 49–50.
- › Burrato, P., Ciucci, F., Valensise, G., 2003. An inventory of river anomalies in the Po Plain, Northern Italy: evidence for active blind thrust faulting. *Ann. Geophys.* 46 (5), 865–882.
- › Busschers, F.S., Kasse, C., Van Balen, R.T., Vandenberghe, J., Cohen, K.M., Weerts, H.J.T., Wallinga, J., Johns, C., Cleveringa, P., Bunnik, F.P.M., 2007. Late Pleistocene evolution of the Rhine-Meuse system in the southern North Sea basin: imprints of climate change, sea-level oscillation and glacio-isostasy. *Quat. Sci. Rev.* 26 (25–28), 3216–3248.
- › Camelbeeck, T., Meghraoui, M., 1998. Geological and geophysical evidence for large palaeo-earthquakes with surface faulting in the Roer Graben (northwest Europe). *Geophys. J. Int.* 132 (2), 347–362. <https://doi.org/10.1046/j.1365-246x.1998.00428.x>.
- › Camelbeeck, T., Vanneste, K., Alexandre, P., Verbeeck, K., Petermans, T., Rosset, P., Mazzotti, S., 2007. Relevance of active faulting and seismicity studies to assessments of long-term earthquake activity and maximum magnitude in intraplate Northwest Europe, between the Lower Rhine Embayment and the North Sea. In: Stein, S., Mazzotti, S. (Eds.), *Continental Intraplate Earthquakes: Science, Hazard, and Policy Issues*, Special Paper 425. Geological Society of America, Boulder, Colorado, pp. 193–224.
- › Candel, J.H.J., Kleinhans, M.G., Makaske, B., Wallinga, J., 2020. Predicting river channel pattern based on stream power, bed material and bank strength. *Progress in Physical Geography: Earth and Environment*. 1 (26), 1–26. <https://doi.org/10.1177/0309133320948831>.

- › Cohen, K.M., 2003. Differential Subsidence within a Coastal Prism: Late-Glacial-Holocene Tectonics in the Rhine-Meuse Delta, the Netherlands. Doctoral dissertation, Utrecht University.
- › Cohen, K.M., Stouthamer, E., Berendsen, H.J.A., 2002. Fluvial deposits as a record for late Quaternary neotectonic activity in the Rhine-Meuse delta, the Netherlands. *Netherlands Journal of Geosciences - Geologie en Mijnbouw* 81, 389–405.
- › Cohen, K.M., Stouthamer, E., Pierik, H.J., Geurts, A.H., 2012. Rhine-Meuse Delta Studies' Digital Basemap for Delta Evolution and palaeogeography. Department of Physical Geography, UNIVERSITEIT Utrecht, Digital Dataset, DANS, (November 10, 2016). doi:10.17026/dans-x7g-sjtw.
- › Dade, W., 2000. Grain size, sediment transport and alluvial channel pattern. *Geomorphology* 35, 119–126.
- › Demco, 1998. Geo-elektrische metingen op de Grensmaas. Report R980110A. Projektbureau Maaswerken, Maastricht, The Netherlands, pp. 1–13.
- › Demoulin, A., Hallot, E., 2009. Shape and amount of the Quaternary uplift of the western Rhenish shield and the Ardennes (western Europe). *Tectonophysics* 474 (3–4), 696–708.
- › Erkens, G., 2009. Sediment Dynamics in the Rhine Catchment: Quantification of Fluvial Response to Climate Change and Human Impact. Doctoral dissertation, Utrecht University.
- › Erkens, G., Hoffmann, T., Gerlach, R., Klostermann, J., 2011. Complex fluvial response to late glacial and Holocene allogenic forcing in the lower Rhine valley (Germany). *Quat. Sci. Rev.* 30, 611–627.
- › Geluk, M.C., Duin, E.T., Duser, M., Rijkers, R.H.B., Van den Berg, M.W., Van Rooijen, P., 1994. Stratigraphy and tectonics of the Roer Valley Graben. *Geol. Mijnb.* 73, 129.
- › Gold, R.D., Friedrich, A., Kübler, S., Salamon, M., 2017. Apparent Late Quaternary Fault-Slip Rate Increase in the Southern Lower Rhine Graben, Central Europe. *Bulletin of the Seismological Society of America* 107 (2), 563–580.
- › Gomez, B., Marron, D.C., 1991. Neotectonic effects on sinuosity and channel migration, Belle Fourche River, western South Dakota. *Earth Surface Processes and Landforms* 16, 227–235.
- › Hijma, M.P., Cohen, K.M., Hoffmann, G., Van der Spek, A.J.F., Stouthamer, E., 2009. From river valley to estuary: the evolution of the Rhine mouth in the early to middle Holocene (western Netherlands, Rhine-Meuse delta). *Netherlands Journal of Geosciences-Geologie en Mijnbouw* 88, 13–53.
- › Holbrook, J., Schumm, S.A., 1999. Geomorphic and sedimentary response of rivers to tectonic deformation: a brief review and critique of a tool for recognizing subtle epeirogenic deformation in modern and ancient settings. *Tectonophysics* 305 (1–3), 287–306.
- › Holbrook, J., Autin, W.J., Rittenour, T.M., Marshak, S., Goble, R.J., 2006. Stratigraphic evidence for millennial-scale temporal clustering of earthquakes on a continental-interior fault: Holocene Mississippi River floodplain deposits, New Madrid seismic zone, USA. *Tectonophysics* 420 (3–4), 431–454.
- › Houtgast, R.F., Van Balen, R.T., 2000. Neotectonics of the Roer Valley rift system, the Netherlands. *Glob. Planet. Chang.* 27 (1–4), 131–146.
- › Houtgast, R.F., Van Balen, R.T., Bouwer, L.M., Brand, G.B.M., Brijker, J.M., 2002. Late Quaternary activity of the Feldbiss Fault Zone, Roer Valley Rift System, the Netherlands, based on displaced fluvial terrace fragments. *Tectonophysics* 352, 295–315. [https://doi.org/10.1016/S0040-1951\(02\)00219-6](https://doi.org/10.1016/S0040-1951(02)00219-6).

- › Houtgast, R.F., Van Balen, R.T., Kasse, C., 2005. Late Quaternary evolution of the Feldbiss Fault (Roer Valley Rift System, the Netherlands) based on trenching, and its potential relation to glacial unloading. *Quat. Sci. Rev.* 24 (3–4), 489–508.
- › AHN 2, n.d.. <http://www.ahn.nl/index.html> (accessed 1 February 2020).
- › Data en Informatie van Nederlandse Ondergrond (DINOloket), (2019). DINOloket, <https://www.dinoloket.nl>. (accessed November 11, 2019).
- › Huisink, M., 1998. Tectonic versus climatic controls on the River Maas dynamics during the Late Glacial. In: Baker, V.R., Gregory, K.J. (Eds.), Benito, G. John Wiley and Sons *Palaeohydrology and Environmental Change*, pp. 99–109.
- › Jain, V., Sinha, R., 2005. Response of active tectonics on the alluvial Baghmata River, Himalayan foreland basin, eastern India. *Geomorphology* 70 (3–4), 339–356.
- › Jorgensen, D.W., 1990. Adjustment of Alluvial River Morphology and Process to Localized Active Tectonics. Doctoral dissertation, Colorado State University.
- › Kadaster, 1850. Topografische Militaire Kaart van het Koninkrijk der Nederlanden. 1850. TMK. DANS. <https://doi.org/10.17026/dans-zrx-wz6e>.
- › Kemna, H.A., 2005. Pliocene and Lower Pleistocene Stratigraphy in the Lower Rhine Embayment, Germany, Doctoral dissertation. Universität Köln.
- › Kiden, P., Denys, L., Johnston, P., 2002. Late Quaternary sea-level change and isostatic and tectonic land movements along the Belgian–Dutch North Sea coast: geological data and model results. *J. Quat. Sci.* 17 (5–6), 535–546.
- › Kleinhans, M.G., van den Berg, J.H., 2011. River channel and bar patterns explained and predicted by an empirical and a physics-based method. *Earth Surf. Process. Landf.* 36 (6), 721–738.
- › Klostermann, J., 1983. Die Geologie der Venloer Scholle (Niederrhein). Geologisches Landesamt Nordrhein-Westfalen, Krefeld.
- › Kooi, H., Hettema, M., Cloetingh, S., 1991. Lithospheric dynamics and the rapid Pliocene-Quaternary subsidence phase in the southern North Sea basin. *Tectonophysics* 192 (3–4), 245–259.
- › Kooi, H., Johnston, P., Lambeck, K., Smither, C., Molendijk, R., 1998. Geological causes of recent (~100 yr) vertical land movement in the Netherlands. *Tectonophysics* 299 (4), 297–316.
- › Lahiri, S.K., Sinha, R., 2012. Tectonic controls on the morphodynamics of the Brahmaputra River system in the upper Assam valley, India. *Geomorphology* 169, 74–85.
- › Lancaster, S.T., Bras, R.L., 2002. A simple model of river meandering and its comparison to natural channels. *Hydrol. Process.* 16 (1), 1–26.
- › Land NRW, (n.d.). Datenlizenz Deutschland-Namensnennung-Version 2.0 (www.govdata.de/dl-de/by-2-0). <https://www.opengeodata.nrw.de/produkte/geobasis/dgm/> (accessed 1 February 2020).
- › Leeder, M.R., Alexander, J.A.N., 1987. The origin and tectonic significance of asymmetrical meander-belts. *Sedimentology* 34 (2), 217–226.
- › Leuven, J.R., van Maanen, B., Lexmond, B.R., van der Hoek, B.V., Spruijt, M.J., Kleinhans, M.G., 2018. Dimensions of fluvial-tidal meanders: are they disproportionately large? *Geology* 46 (10), 923–926.
- › Mack, G.H., Leeder, M., Perez-Arlucea, M., Durr, M., 2012. Tectonic and climatic controls on Holocene channel migration, incision and terrace formation by the Rio Grande in the Palomas half graben, southern Rio Grande rift, USA. *Sedimentology* 58 (5), 1065–1086.

- › Marple, R.T., Talwani, P., 2000. Evidence for a buried fault system in the Coastal Plain of the Carolinas and Virginia—implications for neotectonics in the southeastern United States. *Geol. Soc. Am. Bull.* 112 (2), 200–220.
- › Michon, L., Van Balen, R.T., 2005. Characterization and quantification of active faulting in the Roer valley rift system based on high precision digital elevation models. *Quat. Sci. Rev.* 24 (3–4), 455–472.
- › Michon, L., Van Balen, R.T., Merle, O., Pagnier, H., 2003. The Cenozoic evolution of the Roer Valley Rift System integrated at a European scale. *Tectonophysics* 367, 101–126 [https://doi.org/10.1016/S0040-1951\(03\)00132-X](https://doi.org/10.1016/S0040-1951(03)00132-X).
- › NRW, 2019. IS GK 100 (WMS)– Datensatz. Datenlizenz Deutschland-Namensnennung Version 2.0 (www.govdata.de/dl-de/by-2-0). <https://www.geoportal.nrw/themenkarten> (accessed 15 Oktober 2019).
- › Ouchi, S., 1985. Response of alluvial rivers to slow active tectonic movement. *Geol. Soc. Am. Bull.* 96 (4), 504–515.
- › Paulissen, E., Vandenberghe, J., Gullentops, F., 1985. The Feldebiss fault in the Maas valley bottom (Limburg, Belgium). *Geol. Mijnb.* 64, 79–87.
- › Petrovski, J., Timár, G., 2010. Channel sinuosity of the Körös River system, Hungary/Romania, as a possible indicator of the neotectonic activity. *Geomorphology* 122 (3–4), 223–230.
- › Petrovski, J., Székely, B., Timár, G., 2012. A systematic overview of the coincidences of river sinuosity changes and tectonically active structures in the Pannonian Basin. *Glob. Planet. Chang.* 98, 109–121.
- › Pierik, H.J., Stouthamer, E., Cohen, K.M., 2017. Natural levee evolution in the Rhine-Meuse delta, the Netherlands, during the first millennium CE. *Geomorphology* 295, 215–234.
- › Schäfer, A., Siehl, A., 2002. Preface: Rift tectonics and syngenetic sedimentation—the Cenozoic Lower Rhine Basin and related structures. *Neth. J. Geosci.* 81 (2), 145–147. <https://doi.org/10.1017/S001677460002237X>.
- › Schäfer, A., Hilger, D., Gross, G., Von der Hocht, F., 1996. Cyclic sedimentation in Tertiary Lower-Rhine Basin (Germany)—the ‘Liegendrücken’ of the brown-coal open-cast Fortuna mine. *Sedimentary Geology*, 103(3–4), 229–247. doi:[https://doi.org/10.1016/0037-0738\(95\)00091-7](https://doi.org/10.1016/0037-0738(95)00091-7).
- › Schäfer, A., Utescher, T., Klett, M., Valdivia-Manchego, M., 2005. The Cenozoic Lower Rhine Basin—rifting, sedimentation, and cyclic stratigraphy. *Int. J. Earth Sci.* 94 (4), 621–639. <https://doi.org/10.1007/s00531-005-0499-7>.
- › Schirmer, W., 1990. Rheingeschichte zwischen Mosel und Maas. *Deuqua-Führer* 1, 295.
- › Schokker, J., Cleveringa, P., Murray, A.S., Wallinga, J., Westerhoff, W.E., 2005. An OSL dated middle and Late Quaternary sedimentary record in the Roer Valley Graben (southeastern Netherlands). *Quaternary Science Reviews* 24 (20–21), 2243–2264. <https://doi.org/10.1016/j.quascirev.2005.01.010>.
- › Schokker, J., Weerts, H.J.T., Westerhoff, W.E., Berendsen, H.J.A., Otter, C.D., 2007. Introduction of the Boxtel Formation and implications for the Quaternary lithostratigraphy of the Netherlands. *Netherlands Journal of Geosciences/Geologie en Mijnbouw* 86 (3).
- › Schumm, S.A., 1963. Sinuosity of alluvial rivers on the Great Plains. *Geol. Soc. Am. Bull.* 74 (9), 1089–1100.
- › Schumm, S.A., 1986. Alluvial river response to active tectonics. *Active tectonics* 80–94.

- > Schumm, S.A., Khan, H.R., 1972. Experimental study of channel patterns. *Geol. Soc. Am. Bull.* 83 (6), 1755–1770.
- > Schumm, S.A., Harvey, M.D., 1985. Preliminary geomorphic evaluation of the Sacramento River (Red Bluff to Butte Basin). Unpublished report to Sacramento District. Corps of Engineers, p. 57.
- > Schumm, S.A., Rutherford, I.D., Brooks, J., 1994. Pre-cutoff morphology of the lower Mississippi River. In: Schumm, S.A., Winkley, B.R. (Eds.), *The Variability of Large Alluvial Rivers*. American Society of Civil Engineers Press, New York, pp. 13–44.
- > Schumm, S.A., Dumont, J.F., Holbrook, J.M., 2002. *Active Tectonics and Alluvial Rivers*. Cambridge University Press.
- > Smith, N.D., McCarthy, T.S., Ellery, W.N., Merry, C.L., Rütger, H., 1997. Avulsion and anastomosis in the panhandle region of the Okavango Fan, Botswana. *Geomorphology* 20, 49–65.
- > Stouthamer, E., Cohen, K.M., Gouw, M.J., 2011. Avulsion and its implications for fluvialdeltaic architecture: insights from the Holocene Rhine-Meuse delta. *SEPM Spec. Publ.* 97, 215–232.
- > Taha, Z.P., Anderson, J.B., 2008. The influence of valley aggradation and listric normal faulting on styles of river avulsion: a case study of the Brazos River, Texas, USA. *Geomorphology* 95 (3–4), 429–448.
- > Tigrek, S., Kiden, P., Houtgast, R.F., Van Kuijk, J.M., 2000. A high-resolution seismic survey on the river Maas. *Petrophysics meets Geophysics*, 6–8 November, Paris.
- > Timár, G., 2003. Controls on channel sinuosity changes: a case study of the Tisza River, the Great Hungarian Plain. *Quat. Sci. Rev.* 22 (20), 2199–2207.
- > Van Balen, R.T., Houtgast, R.F., Van der Wateren, F.M., Vandenberghe, J., Bogaart, P.W., 2000. Sediment budget and tectonic evolution of the Meuse catchment in the Ardennes and the Roer Valley Rift System. *Glob. Planet. Chang.* 27, 113–129.
- > Van Balen, R.T., Houtgast, R.F., Cloetingh, S.A.P.L., 2005. Neotectonics of the Netherlands: a review. *Quat. Sci. Rev.* 24 (3–4), 439–454.
- > Van Balen, R.T., Kasse, C., De Moor, J., 2008. Impact of groundwater flow on meandering; example from the Geul River, the Netherlands. *Earth Surf. Process. Landf.* 33 (13), 2010–2028.
- > Van Balen, R.T., Bakker, M.A.J., Kasse, C., Wallinga, J., Woolderink, H.A.G., 2019. A late Glacial surface rupturing earthquake at the Peel Boundary fault zone, Roer Valley Rift System, the Netherlands. *Quat. Sci. Rev.* 218, 254–266.
- > Van den Berg, J., 1995. Prediction of alluvial channel pattern of perennial rivers. *Geomorphology* 12, 259–279.
- > Van den Berg, M., Vanneste, K., Dost, B., Lokhorst, A., Van Eijk, M., Verbeeck, K., 2002. Paleoseismic investigations along the Peel Boundary Fault: geological setting, site selection and trenching results. *Neth. J. Geosci.* 81 (1), 39–60. <https://doi.org/10.1017/S0016774600020552>.
- > Van den Berg, M.W., 1996. *Fluvial Sequences of the Maas: A 10 Ma Record of Neotectonics and Climate Change at Various TimeScales*. Doctoral dissertation, Landbouwniversiteit Wageningen.
- > Van den Broek, J.M.M., Maarleveld, G.C., 1963. The late Pleistocene terrace deposits of the Meuse. *Mededelingen Geologische Stichting NS* 16, 13–24.

- › Vandenberghe, D., Vanneste, K., Verbeeck, K., Paulissen, E., Buylaert, J.P., De Corte, F., 2009. Late Weichselian and Holocene earthquake events along the Geleen fault in NE Belgium: OSL age constraints. *Quat. Int.* 199 (1–2), 56–74.
- › Vanneste, K., Verbeeck, K., 2001. Paleoseismological analysis of the Rurand fault near Julich, Roer Valley graben, Germany: Coseismic or aseismic faulting history? *Geol. Mijnb.* 80 (3/4), 155–170.
- › Vanneste, K., Verbeeck, K., Camelbeeck, T., Paulissen, E., Meghraoui, M., Renardy, F., Jongmans, D., Frechen, M., 2001. Surface-rupturing history of the Bree fault scarp, Roer Valley graben: evidence for six events since the late Pleistocene. *J. Seismol.* 5 (3), 329–359.
- › Vanneste, K., Verbeeck, K., Camelbeeck, T., 2002. Exploring the Belgian Maas valley between Neeroeteren and Bichterweert for evidence of active faulting. *Aardkundige Mededelingen* 12, 5–8.
- › Vanneste, K., Camelbeeck, T., Verbeeck, K., Demoulin, A., 2018. Morphotectonics and past large earthquakes in Eastern Belgium. In: Demoulin, A. (Ed.), *Landscapes and Landforms of Belgium and Luxembourg*. World Geomorphological Landscapes. Springer Cham, pp. 215–236 https://doi.org/10.1007/978-3-319-58239-9_13.
- › Westerhoff, W.E., Kemna, H.A., Boenigk, W., 2008. The confluence area of Rhine, Meuse, and Belgian rivers: Late Pliocene and Early Pleistocene fluvial history of the northern Lower Rhine Embayment. *Netherlands Journal of Geosciences-Geologie en Mijnbouw* 87 (1), 107.
- › Whitney, B.B., Hengesh, J.V., 2015. Geomorphological evidence for late Quaternary tectonic deformation of the Cape Region, coastal west Central Australia. *Geomorphology* 241, 160–174.
- › Woolderink, H.A.G., Kasse, C., Cohen, K.M., Hoek, W.Z. Van Balen, R.T., 2018. Spatial and temporal variations in river terrace formation, preservation, and morphology in the lower Meuse Valley, the Netherlands. *Quat. Res.* 91 (2), 548–569.
- › Woolderink, H.A.G., Kasse, C., Grooteman, L.P.A., Van Balen, R.T., 2019. Interplay between climatic, tectonic and anthropogenic forcing in the Lower Rhine Graben, the Roer River. *Geomorphology* 344, 25–45.
- › Zagwijn, W.H., 1989. The Netherlands during the Tertiary and the Quaternary: a case history of coastal lowland evolution. *Geol. Mijnb.* 68, 107–120.
- › Zámolyi, A., Székely, B., Draganits, E., Timár, G., 2010. Neotectonic control on river sinuosity at the western margin of the Little Hungarian Plain. *Geomorphology* 122 (3–4), 231–243.
- › Ziegler, P.A., 1992. European Cenozoic rift system. *Geodynamics of rifting* 1, 91–111.
- › Ziegler, P.A., 1994. Cenozoic rift system of western and Central-Europe, an overview. *Geol.Mijnb.* 73 (2–4), 99–127.

Chapter 6

Modelling the effects of normal faulting on alluvial river morphodynamics.

Abstract

Normal faulting forces the morphodynamics of alluvial rivers by changing the topographic gradient of the river valley and channel at and near the fault zone. Normal faulting can affect river morphodynamics instantaneously, by surface-rupturing earthquakes, and gradually, by relatively slow vertical displacement relative to an appropriate timescale of morphological change. The effects of faulting on river morphodynamics and morphology are, however, complex as they depend on numerous non-tectonic characteristics as well. The resulting time-dependent river responses change the relationships between faulting and river dynamics behind reconstruction from morphological and sedimentological records. To enhance our understanding of river channel response to tectonic faulting we used the physics-based, two-dimensional morphodynamic model Nays2D to simulate the responses of a laboratory-scale alluvial river with vegetated floodplain to various faulting and offset scenarios. Results of a model with a normal fault downstepping in the downstream direction show that channel sinuosity and bend radius increase up to a maximum as a result of the faulting enhanced valley gradient, after which a chute cutoff reduces channel sinuosity to a new dynamic equilibrium value that is generally higher than the pre-faulting sinuosity. A scenario involving a normal fault downstepping in the upstream direction shows that it leads to reduced fluvial activity upstream of the fault due to a backwater effect. The position within a meander bend at which faulting occurs has a profound influence on the evolution of sinuosity; fault locations that enhance flow velocities over the point bar result in a faster sinuosity increase and subsequent chute cutoff than locations that enhance flow velocity directed towards the floodplain. This upward causation from the bend scale to the reach and floodplain scale arises from the complex interactions between meandering and floodplain and the nonlinearities of the sediment transport and chute cutoff processes and has ramifications for reconstructions.

Submitted (in revised form) to Earth Surface Processes and Landforms as: H.A.G. Woolderink, S.A.H. Weisscher, M.G. Kleinhans, C. Kasse, R.T. Van Balen. Modelling the effects of normal faulting on alluvial river morphodynamics.

6.1 Introduction

Faulting acts as a forcing factor on the morphodynamics of rivers by (locally) changing the topographic gradient of the river valley and channel. Faulting will change the elevation of the river bed and floodplain at the fault zone, depending on the fault configuration (Fig.1). Such changes in the topography of the river valley can trigger a morphodynamic response of the river in order to restore the altered gradient. This morphodynamic response can be in the form of solely a longitudinal (bed) profile adjustment or in combination with a planform change of the river channel. For a normal fault that is downstepping in the downstream direction, degradation of the river bed will occur upstream of the fault and aggradation downstream (Fig.1; [Holbrook and Schumm, 1999]). The opposite is expected for a fault that is downstepping in the upstream direction (Fig.1). Because of this, the preservation of longitudinal river bed deformations of alluvial rivers by faulting in the sedimentary record is rare (Holbrook and Schumm, 1999). This complicates our understanding of the interactions between faulting and subsequent longitudinal profile adjustment of alluvial rivers.

Channel adjustment patterns in response to faulting may range from a (local) shift in channel pattern (e.g. from scroll bar dominated to chute dominated meandering) to an intrapattern adjustment such as a change in sinuosity of a meandering river channel (Ouchi, 1985, Timar, 2003; Holbrook and Schumm, 1999). Moreover, faulting can alter the cross-section (e.g. width-to-depth ratio) of a river via a change in gradients (Holbrook and Schumm, 1999). Such changes in channel width will result in a changing bar pattern which might, in turn, alter floodplain morphology and channel migration (Kleinhans, 2010; Kleinhans et al., 2013). Alluvial rivers may thus respond in various ways to faulting. However, each of these morphodynamic responses can also be the result of other causes (Ouchi; 1985; Holbrook and Schumm, 1999; Kleinhans, 2010), complicating derived relationships between faulting and river dynamics from the sedimentary and geomorphological record.

Faulting can offset a river valley and channel both instantaneously by e.g. surface rupturing earthquakes, and gradually by relatively slowly continuing vertical displacement. The reoccurrence interval of large surface rupturing earthquakes that are able to produce co-seismic vertical displacements of the earth's surface are often relatively large. This hampers the possibility of collecting observational data of river response to co-seismic vertical displacements. Slow tectonic deformation such as creep may force river morphodynamics on a time scale of thousands of years, obstructing collection of observational data as well. Finally, the response of a river is often transient, which implies that a river might not yet have completed the full response to faulting when observations are made.

Most numeric modelling studies of alluvial river response focus on the long-term basin-scale effects of tectonics on alluvial architecture (Allen, 1978; Bridge and Leeder, 1979; Alexander and Leeder, 1987; Bryant et al., 1995; Mackey and Bridge, 1995). In contrast, model studies on the effects of more local faulting on alluvial river morphodynamics and morphology (e.g. on the scale of multiple meander bends) are currently lacking. Therefore, in this study, we use a physics-based two-dimensional morphodynamic model Nays2D (Shimizu et al., 2013). Our study will focus on the sinuosity and longitudinal response of a laboratory-scale alluvial river to various faulting and offset scenarios. Both instant and gradual faulting scenarios are simulated to study their effects on river morphodynamics. Furthermore, both a footwall to hanging wall transition and a hanging wall to footwall configuration of the normal fault are studied. In addition, the effect of the position of a fault along a meander bend will be investigated to study a possible differential morphodynamic response.

By excluding the natural, co-acting processes of e.g. changing sediment loads, climatic change in discharge and vegetation cover, and variations in bank characteristics on river morphodynamics, this study will contribute to the understanding of river channel response to merely tectonic faulting.

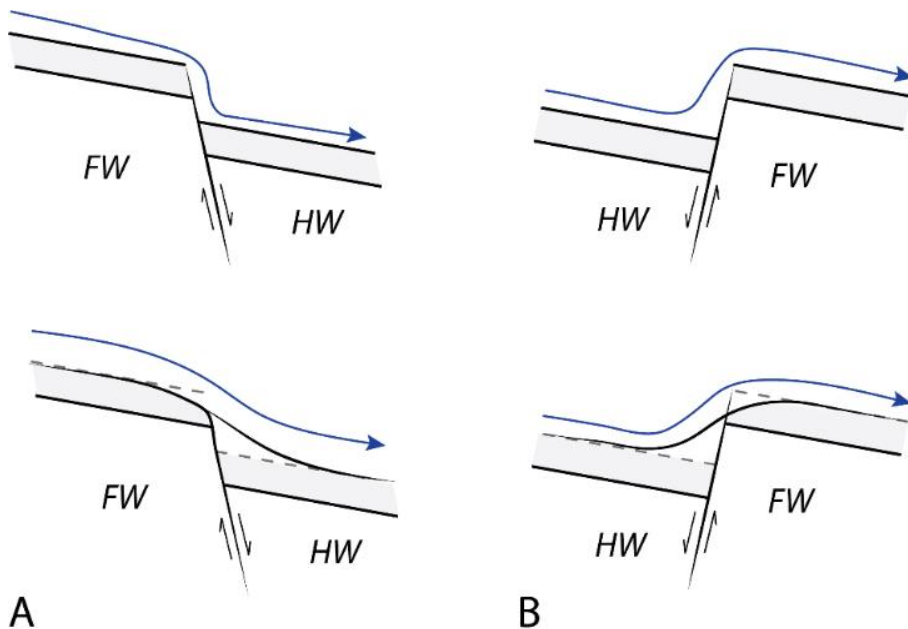


Fig. 1: Potential effects of normal faulting on river bed and flow deformation. A) Normal fault that is downstepping in downstream direction (increases gradient). B) Normal fault that is downstepping in upstream direction (reduces gradient). Figure is based on Holbrook and Schumm, 1999.

6.2 Methods

6.2.1 Model description

Nays2D solves the depth-averaged, nonlinear shallow water equations as well as the equations for bed load transport and bed level change (Shimizu et al., 2013). In this study, we used a model setup after Weisscher et al. (2019) who modelled a dynamic meandering river on a laboratory scale in which the idealized model settings (table 1) were inspired by the Allier River (France) and Otofuke River (Japan). We used this model setup because it could accurately model the river pattern and dynamics of a chute-cutoff-dominated meandering river with self-formed floodplain (Weisscher et al., 2019).

The model consists of a fixed rectilinear computational grid with 0.1 m square grid cells, representing a domain of a 4.5 m wide and 60 m long. The initial straight channel was 0.5 m wide and 0.004 m deep. An initial lateral offset of +0.4 m was used for the 0.5 m fixed-width inlet to steer morphological change. The slope of the banks was 45 degrees (Weisscher et al., 2019). The model setup calculates bedload transport only (Meyer-Peter and Müller, 1948).

A sustained periodic inflow perturbation (e.g. movement of the inlet) was applied to ensure the initiation and persistence of dynamic meandering. Weisscher et al. (2019) added colonization and mortality of vegetation to Nays2D. In this sub-model, vegetation colonizes dry cells and is removed from drowned cells and from cells in which the erosion depth exceeds the rooting depth (table 1). The settlement of (riparian) vegetation is used as a bar-floodplain conversion agent (Weisscher et al. 2019). Vegetation colonization is tested year-round (300 seconds). For a more extensive model description we refer to Weisscher et al., (2019).

For our study a normal fault was added to Nays2D. Grid cells downstream of the fault were displaced vertically to mimic fault movement. The amount of vertical displacement and the rate of deformation were varied to enable modelling of both instant and gradual faulting. To reduce computing time, we used the topography output of an original model run at 200 years (~167 hours) as the initial meandering planform for our faulting scenarios.

For all model scenarios we applied a minimum of 100 cycles of a 50 min hydrograph, representing a time span of 100 (hydrological) years. The hydrograph varied between 1 and 6.4 Ls-1. The initial topography was run 3 cycles to re-establish hydrodynamics and vegetation cover on the loaded initial planform before a faulting perturbation was applied to the model.

Table 1: Model settings for the scenarios in this study (after Weisscher et al., 2019)

Parameter	Value	Unit
Discharge Q (low-high)	1 – 6.4	L s ⁻¹
Time step hydrodynamics/bed level change	0.02	s
Time step vegetation settling	300	s
Channel width	0.5	m
Channel depth	0.04	m
Aspect ratio (width/depth)	12.5	-
Grain size	0.76 x 10 ⁻³	m
Valley slope	2 x 10 ⁻³	m m ⁻¹
Inflow migration period T	42.5	h
Inflow migration amplitude	0.75	m
Drag coefficient vegetation C _D	1	-
Vegetation stem thickness D	0.5 x 10 ⁻³	m
Rooting depth	0.03	m
Manning's n	0.02	s m ^{1/6}
Shields number	0.07	-
Froude number	0.4	-

6.2.2 Model scenarios

Depending on the dip direction of the fault, normal faulting results in a relatively subsiding and uplifting river bed in the part of the model downstream of the fault. In the description of the model scenarios, we therefore apply the terms subsidence and uplift. The applied fault offsets are inspired on the reconstructed maximum vertical surface deformation along a fault of the Peel Boundary Fault Zone in the Lower Rhine Embayment (LRE) rift system (Van Balen et al., 2019). Therefore, an offset of 0.4 and 1.2 m was used for the instant scenarios, which corresponds with an approximate earthquake magnitude of ~6.5 to 6.8 (Wells and Coppersmith, 1994). The offsets are 1/8th and 3/8th of the channel depth respectively. The same total offsets were used for the gradual faulting scenarios, although these exceed the displacement rates of gradual faulting rates in the LRE, in order to compare the morphodynamic responses. Assuming a 100 yr time-interval, this results in offset rates of 4 and 12 mm/yr.

A scenario without any faulting was conducted as a reference (L0). Multiple model scenarios were designed to study the effects of fault orientation, fault position and displacement rates. The first set of model scenarios was designed to model a meandering river that flows from a hanging-wall to a footwall of a normal fault (i.e. a relative uplift occurs at the downstream part of the model [Fig.1]).

The second set was designed to study the effect of meandering river flow from footwall to hanging-wall (these are relative subsidence scenarios). Both sets of scenarios were applied to study instant ([L1, 3, 5, and 7]) and gradual ([L2, 6, 8 and 4]) displacement

(Table 2). Also, in both sets the effects of a small (0.005 cm or 1/8th of the channel depth) and a large offset (0.015 cm or 3/8th of the channel depth) along the fault were studied. The fault was positioned at the same location (32 m) for all these scenarios.

Four extra scenarios were performed to investigate the effect of variable fault offset for the subsidence scenarios in more detail (RC2,4,5,6). With these four extra runs a total set of six subsidence scenarios was established, for which the fault offset was increased incrementally with 0.005 m between each scenario (RC 1-6). To test the influence of fault position with respect to the meanders, two additional simulations (i.e. instant large subsidence scenarios) were performed for which the fault was located at 31.0 and 31.6 m along the model domain respectively (Table 2).

6.2.3 Data analysis

The bathymetry of the model runs (detrended with the initial valley gradient) was used for both qualitative and quantitative map comparison. The main channel was determined using the method described by Weisscher et al. (2019), which is calculated as the detrended bed elevation times flow velocity to the power of three. This was empirically found to be the best indicator of channel position that excludes deep but abandoned channels and fast overbank flow (Weisscher et al., 2019). Sinuosity of the main channel was determined in a zone extending from 10 m upstream to 10 m downstream of the fault, in order to exclude potential boundary effects. Sinuosity was computed by dividing the distance along the main channel by the valley length. The initial and maximum meander amplitude and wavelength were measured using the main channel across the fault zone. Longitudinal profiles were determined using the bed elevation along the main channel.

6.3 Results

The results of the faulting scenarios will be presented and subsequently interpreted and discussed below. First, the subsidence scenarios will be presented, followed by the uplifting scenarios. Hereafter, the effects of increasing fault offset will be discussed, followed by the effects of fault location within a meander on river morphodynamics.

6.3.1 Subsidence scenarios

The effect of a normal fault downstepping in the downstream direction is a gradient increase over the fault. This gradient increase leads to higher flow velocities which cause change in the longitudinal bed profile and morphology of the river.

Table 2: Overview of deformation style, rate and fault location for the different scenarios in this study.

Deformation style	Instant or Gradual	Deformation rate (m/yr or instant)	Total offset (m)	Total offset Channel depth (m)	Fault location(m)	Scenario
Uplift	Gradual	0.00015	0.015	3/8 th	32.0	L2
Uplift	Instant	0.015	0.015	3/8 th	32.0	L1
Uplift	Gradual	0.00005	0.005	1/8 th	32.0	L6
Uplift	Instant	0.005	0.005	1/8 th	32.0	L5
No deformation	-	-	-	-	-	L0
Subsidence	Gradual	-0.00005	-0.005	1/8 th	32.0	L8
Subsidence	Instant	-0.005	-0.005	1/8 th	32.0	L7/RC1
Subsidence	Gradual	-0.00015	-0.015	3/8 th	32.0	L4
Subsidence	Instant	-0.015	-0.015	3/8 th	32.0	L3/F0/RC3
Subsidence	Instant	-0.010	-0.010	2/8 th	32.0	RC2
Subsidence	Instant	-0.020	-0.020	4/8 th	32.0	RC4
Subsidence	Instant	-0.025	-0.025	5/8 th	32.0	RC5
Subsidence	Instant	-0.030	-0.030	6/8 th	32.0	RC6
Subsidence	Instant	-0.015	-0.015	3/8 th	31.0	F1
Subsidence	Instant	-0.015	-0.015	3/8 th	31.6	F2

6.3.1.1 Longitudinal profiles

The subsidence scenarios show incision of the river bed at and just upstream of the fault, which increases the channel depth relative to the floodplain (Figs 2 and 3). The lowering of the bed level is larger near the fault zone than more upstream (Fig.2). Especially the pools in the outer bends are subjected to vertical erosion. The eroded sediment is deposited downstream of the fault, which increases the channel bed and channel width (Figs. 2 and 3). There is a difference in how the bed level changes between the instant and gradual displacement scenarios. Where the gradual subsidence scenarios show a slight lowering of the bed level at the riffle just after the fault (i.e. at around 33m) the instant scenarios show aggradation at this position. For the first outer bend after the fault zone (i.e. at about 34 m) all subsidence scenarios show an increase in bed level and reduced channel depth (Fig.2). Aggradation of the bed level occurs to ~ 3 m (0.7 meander wavelength) downstream of the fault for the gradual subsidence scenarios. For the instant subsidence scenarios this aggradation continuous to ~ 6.5 m (1.5 meander wavelength) downstream of the fault (Fig.2).

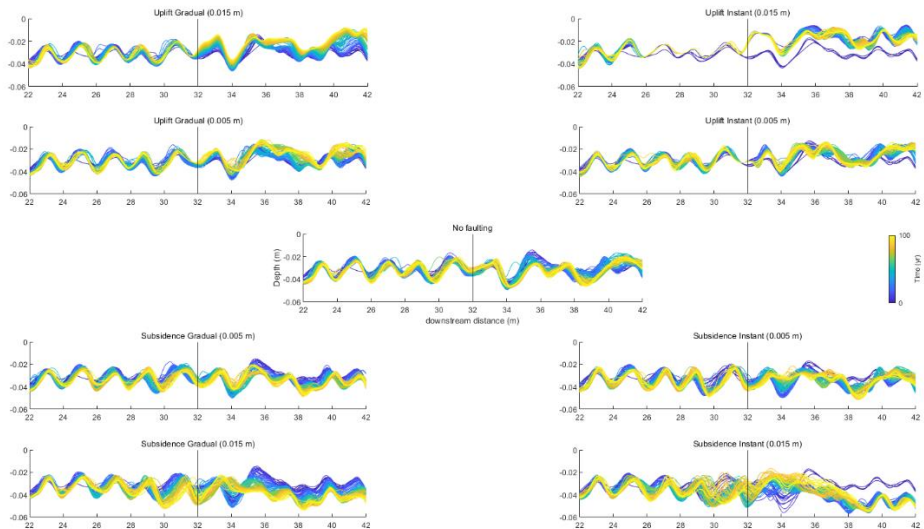


Fig. 2: Longitudinal bed profiles of the faulting scenarios over time. Note that the subsidence scenarios (bottom panels) show a clear adjustment of the river bed to the faulting perturbation where erosion takes place upstream of the fault and sedimentation downstream of the fault. The uplift scenarios (top panels) show a less clear adjustment to faulting.

The longitudinal bed profile responds to the faulting in the subsidence scenarios by incision upstream and aggradation downstream of the fault (Fig.2). The incision upstream of the fault is the result of an increased fluvial gradient and, hence, increased flow velocity and sediment transport capacity. Deposition downstream of the fault is the result of a decreasing gradient. The extent of the adaption of the longitudinal profile is dependent on the rate of fault movement (Fig. 2). This can be explained by the increase in gradient per unit time and the non-linearity of sediment transport. The sudden increase in gradient, and thus flow velocity, leads to a larger amount of eroded and deposited sediment, and hence downstream extent of channel bed aggradation, than in the continuous faulting scenarios.

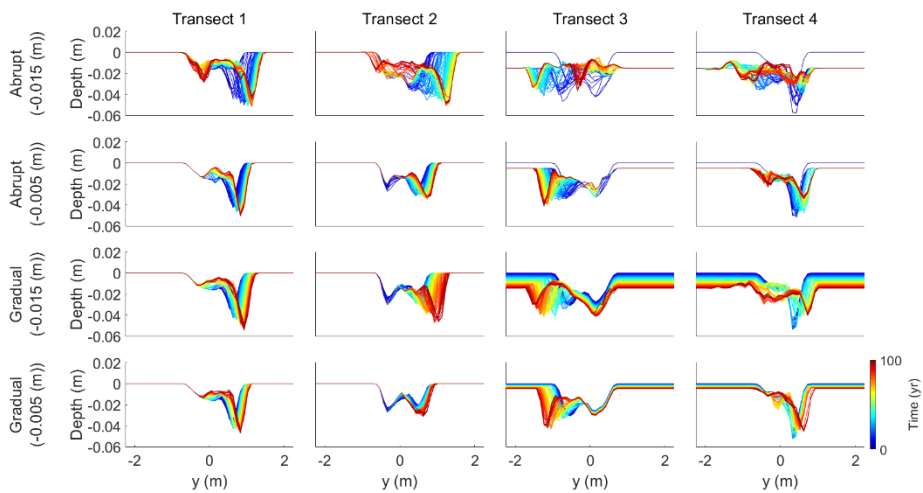


Fig. 3: Cross-sections over the floodplain at different distances to the fault for all of the subsidence scenarios (see fig.4 for locations of the transects). Panels show erosion upstream of the fault (Transects 1 and 2) and sedimentation downstream (Transects 3 and 4).

Table 3: Changes in meander amplitude for the model scenarios.

	Vertical displacement	Amplitude (m)	Change amplitude (m)	Change amplitude (%)	Normalized change amplitude
L02	Uplift Gradual (0.015 m)	0.66	0.01	1.6	0.1
L01	Uplift Instant (0.015 m)	0.60	-0.05	-7.8	-0.7
L06	Uplift Gradual (0.005 m)	0.68	0.04	5.4	0.5
L05	Uplift Instant (0.005 m)	0.66	0.02	2.3	0.2
L0	No faulting	0.72	0.07	11.2	1.0
L08	Subsidence Gradual (-0.005 m)	0.77	0.12	18.6	1.7
L07	Subsidence Instant (-0.005 m)	0.85	0.21	32.4	2.9
L04	Subsidence Gradual (-0.015 m)	0.98	0.34	52.0	4.6
L03	Subsidence Instant (-0.015 m)	1.21	0.56	87.4	7.8
RC1	Subsidence Instant (-0.005 m)	0.85	0.21	32.4	2.9
RC2	Subsidence Instant (-0.01 m)	1.20	0.55	85.7	7.7
RC3	Subsidence Instant (-0.015 m)	1.21	0.56	87.4	7.8
RC4	Subsidence Instant (-0.02 m)	1.13	0.48	74.7	6.7
RC5	Subsidence Instant (-0.025 m)	1.88	1.23	191.3	17.1
RC6	Subsidence Instant (-0.03 m)	2.33	1.68	261.1	23.3

6.3.1.2 Morphology and sinuosity

The control scenario without any faulting (L0) shows an 11% increase in meander amplitude over the model run (Figs 4 and 5; Table 3). The scenarios with relatively small subsidence (i.e. 0.005 m or 1/8th channel depth) show that the meander amplitude increases with ~20-30% at the fault zone due to lateral migration. The same is observed for the large gradual offset (0.015 m or 3/8th channel depth), although here the amount of the meander amplitude change is higher (i.e. 52 % [Figs. 4 and 5; Table 3]).

The results of the large instant offset simulations show a different pattern. In these results, the meander amplitude increases with a maximum of 87% of its original size, and the location shifts downstream till ~75 years. Hereafter, a chute cutoff occurs and the main channel is straightened just downstream of the fault zone, which reduces the meander amplitude with ~20% and doubles the wavelength (Figs. 4 and 5; Table 3). The sinuosity increases from ~1.17 to 1.3 for all subsidence runs, except for the large gradual subsidence. In this simulation, sinuosity increases to 1.35 (Fig. 6), at the location mainly centered around the fault zone (Fig. 4). The observed lateral migration and sinuosity response can be explained by two complementing processes that control river channel sinuosity, namely bank erosion and bar accretion, although the former is the dominant forcing factor for scroll-bar migration (van de Lageweg et al., 2014). Enhanced bank erosion occurs in response to the erosion and scouring at the pools in the outer part of the meander bends, which increases the outer bank slope (Fig. 7B). In turn, this increases the stress on the bank material and hence causes bank erosion by mass failure of the river banks.

The enhanced erosion of the outer banks leads to enhanced lateral bend migration and an increase of meander amplitude. This increases the sinuosity of the river channel. For the gradual subsidence scenarios, bank erosion and pointbar accretion result in a more or less linear adaption of the sinuosity of the river channel (Fig. 6). However, for the instant subsidence scenarios, sinuosity change shows a relatively fast increase in sinuosity after which a new (dynamic) equilibrium is reached (Fig. 6). This difference can be explained by the amount of gradient increase, which is much larger (100x) in the instant scenarios compared to the gradual scenarios.

Over time, erosion and sedimentation around the fault zone reduce the gradient over the fault. In turn, this reduces the lateral displacement rate and change in channel sinuosity. Moreover, by lengthening of the river channel by a sinuosity increase the channel gradient is also reduced, complementing the in-channel erosion and sedimentation. These processes can explain the limitation of further sinuosity increase of the river channel (Crosato, 2007) beyond a certain threshold (which is ~1.3 for the presented model runs). Another explanation for this threshold in natural settings might be flow separation due

to secondary flow cells near the outer bank in very sharp bends, which prevents further lateral erosion and displacement (Hickin, 1977; c.f. Crosato, 2009).

The river channel may also reduce its sinuosity due to a chute cutoff. As the sinuosity of the river channel increases due to outer bank erosion and lateral migration of the channel, sedimentation occurs in the channel (Fig.7). Moreover, overbank flow occurs over the point bar during floods because of a gradient advantage compared to the main channel. As a result, a chute channel develops over the point bar, forming a bifurcation (Van Dijk et al., 2012; 2014). The division of flow and sediment at such a bifurcation can result in sedimentation in the main channel, which is then eventually closed off, and a transformation of the chute channel to the new main channel may occur (Kleinhans et al., 2008; Van Dijk et al., 2014). This chute cutoff reduces the sinuosity of the river channel over the fault instantly (Figs. 4 and 6). Over time, the former main channel can be completely filled with (overbank) sediments (Toonen et al., 2012) and hence hidden from the floodplain morphology.

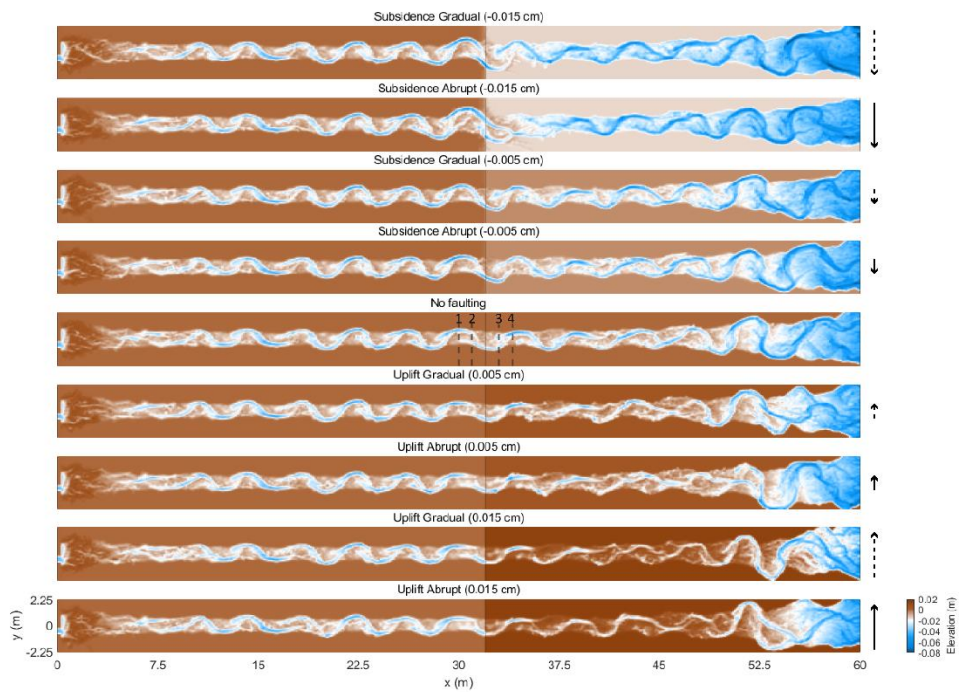


Fig. 4: Morphology of the (detrended) river bed and floodplain for the model scenarios at the end of the model run ($t = 100$ years).

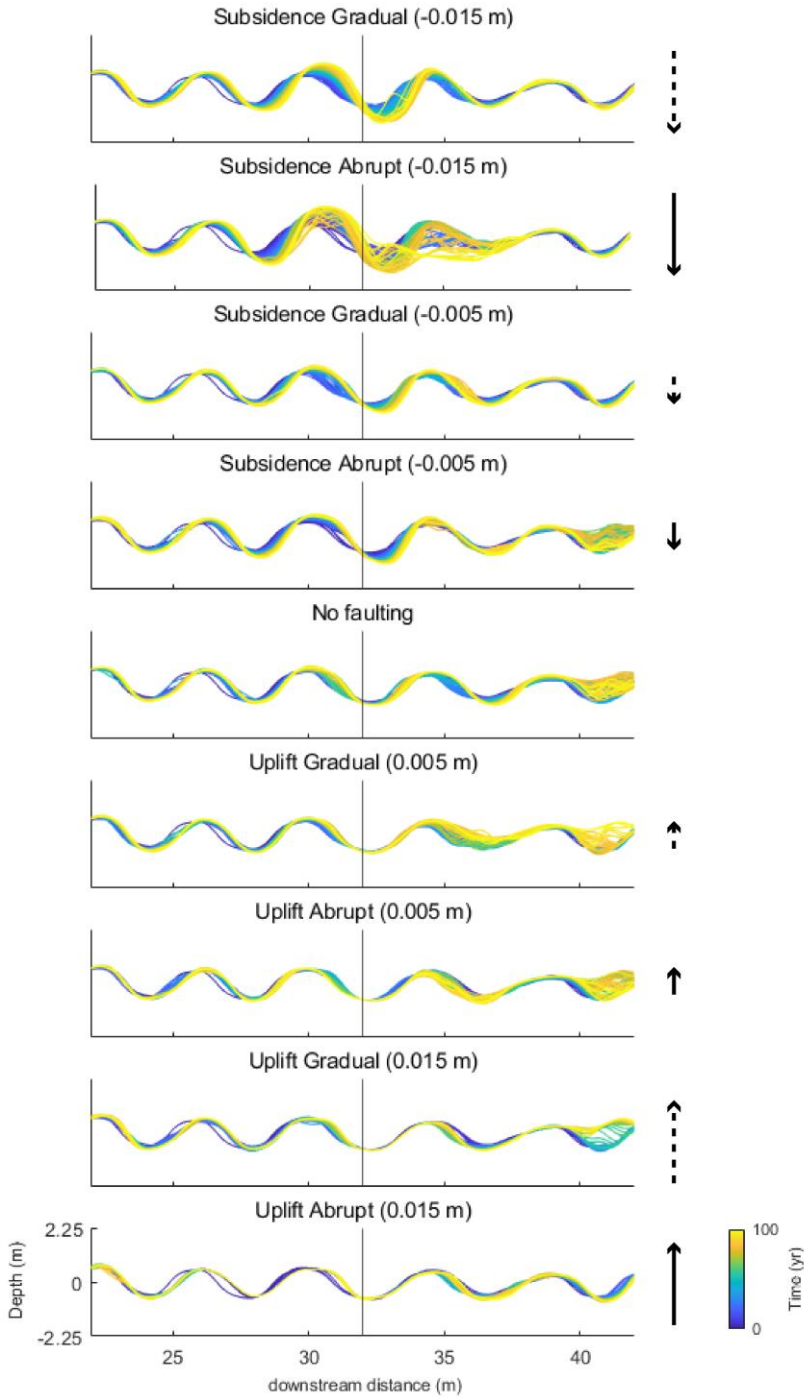


Fig. 5: Position of the main channel over time for the model scenarios. Note that the change of (or lack of) the main channel position occurs predominantly within 2 meander wavelengths around the fault.

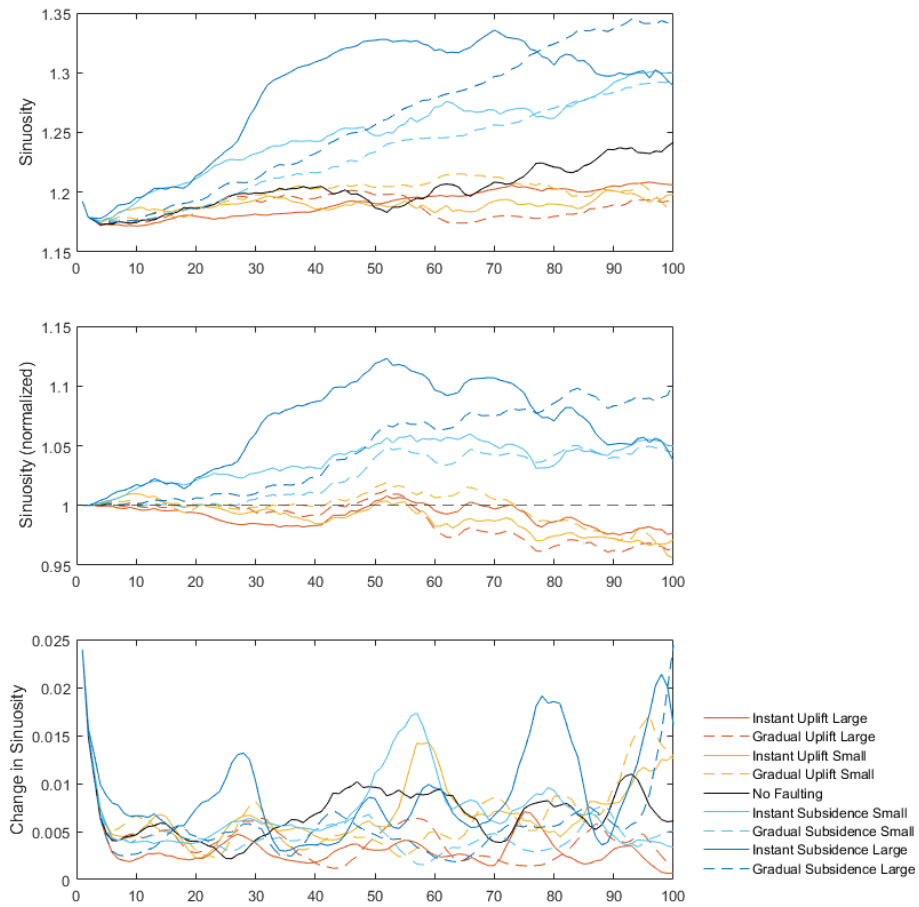


Fig. 6: Sinuosity of the main channel over time for the model scenarios. Top Panel shows the sinuosity profiles of model runs. Middle panel shows the sinuosity profiles normalized to the reference run (L0). Bottom panel shows the change in sinuosity over time for the model scenarios.

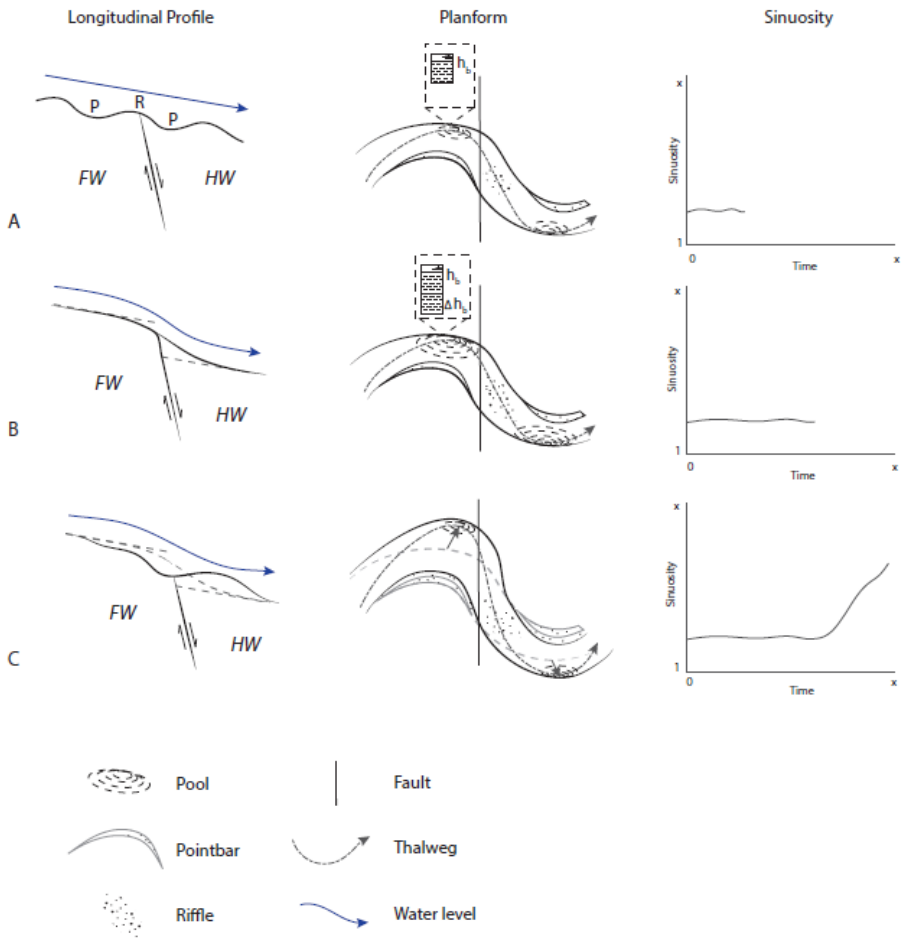


Fig. 7: Conceptual model of the effects of the subsidence faulting scenarios on the longitudinal river bed profile and sinuosity increase. A) Pre-faulting scenario with riffle-pool morphology in the river channel. B). Adaption of the longitudinal bed profile just after faulting with erosion of the bed upstream of the fault and sedimentation downstream. Scouring in the outer bend increases the height of the river bank at these locations. C) Further erosion and sedimentation in the longitudinal bed profile. The increase in bank height due to scouring in the outer bend leads to bank-collapse and lateral migration of the river channel which increases sinuosity of the channel.

6.3.2 Uplift scenario's

Scenarios adopting a relative uplift of the river (bed) downstream of the fault (i.e. the fault is downstepping in the upstream direction) will result in a gradient decrease over the fault. Moreover, the uplift will pose an obstruction to flow of the river which might cause change in the longitudinal bed profile and morphology of the river.

6.3.2.1 Longitudinal profiles

The effects of the uplift scenarios on the bed topography can be inferred from longitudinal and perpendicular cross sections (Figs. 2 and 9). Almost no change in bed level occurs just upstream of the fault on the hanging wall (Fig. 2; Table 3). Moderate vertical erosion occurs in the outer meander bends on the footwall. On this uplifted block the width of the channel does not change and, hence, the width-to-depth ratio decreases slightly (Fig. 9). In general, the amount of vertical erosion increases further downstream of the fault location (i.e. within several meters of the fault [Fig. 9]). However, the incision is smaller than the applied uplift in the scenarios. An exception is the result of the small instant uplift scenario, in which the incision is nearly equal to the amount of uplift.

The lack of change in bed topography can be attributed to the development of a backwater in front of the fault in these scenarios, which is caused by the obstruction to flow posed by the uplifted downstream footwall. The backwater effect reduces flow velocities in the channel on the hanging wall and, during floods, over the pointbar and floodplain (Fig.8). The decrease in flow velocity reduces morphodynamics of the river channel in this reach. This process is most pronounced for the instant faulting scenarios (Fig. 8), as this results in the most pronounced obstruction to flow in the river channel. The upstream length to which the backwater reaches depends on the amount of fault offset. For the relatively large instant faulting scenario (0.015 m or $3/8^{\text{th}}$ channel depth), this is ~ 8 m upstream of the fault, which is approximately 2 meander wavelengths (Figs. 4, 8). On the footwall, not affected by a backwater effect, flow velocities are not altered, resulting in moderate vertical erosion in the outer meander bends on this block.

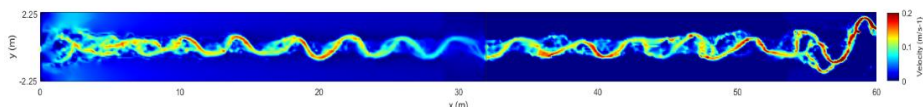


Fig. 8: Example of the backwater that develops in front of the fault in the uplift scenarios. Velocities are reduced over a zone of ~ 2 meander wavelengths.

6.3.2.2 Morphology and sinuosity

The scenarios with relative uplift show that the main channel remains at a fixed position around the fault (Fig.5). An exception is the meander at ~ 27.5 m, which experiences a minor downstream displacement (Fig.5). Compared to the control run, the uplift scenarios show a smaller amplitude change (Table 3). As in the control run, the meander wavelength remains constant (Fig.5).

The sinuosity of the channel remains fairly constant over time (i.e. between ~ 1.17 and 1.20) (Fig.6), especially for the first 40 years. After 50 years, the sinuosity of the reference run increases from 1.19 to 1.24. The uplift scenarios, however, show sinuosity values that remain more or less stable (Fig.6).

The lack of sinuosity increase in the uplift scenarios can partly be attributed to the backwater effect, which reduces flow velocity and hence decreases the amount of bank erosion and thus lateral migration rate of the channel. On the footwall sediment concentrations are less than the transport capacity due to the reduced flow velocities in the backwater on the hanging wall. This leads to erosion of sediment in the channel and hence to slight channel straightening (Fig. 5). The fault displacement makes the backwater reach on the relatively subsiding hanging wall more prone to flooding. In extreme cases even a lake might develop, as in the instant large offset scenario (Fig. 8).

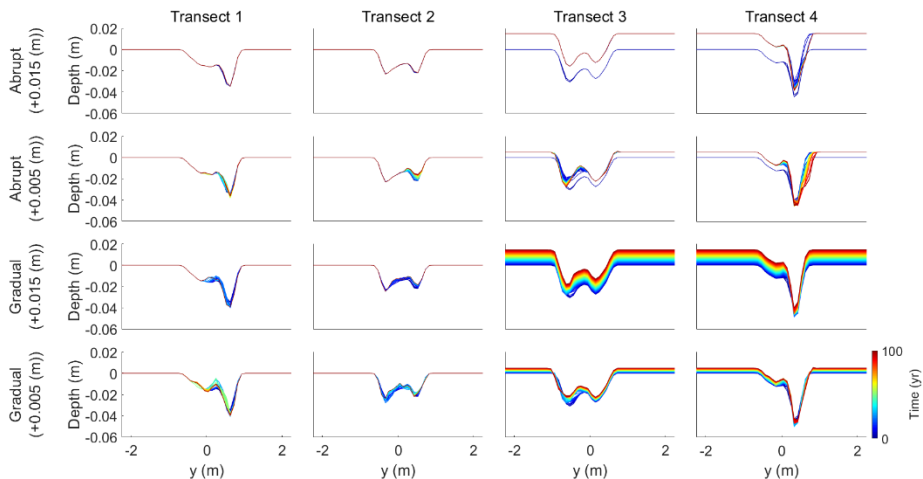


Fig. 9: Cross-sections over the floodplain at different distances to the fault for all of the uplift scenarios (see fig.4 for locations of the transects). Note the lack of change, especially for the instant scenarios, in front of the fault.

6.3.3 Fault offset

The instant subsidence scenario is used to test the effect of different amounts of fault offset as this scenario results in the most obvious sinuosity change (Fig. 10). The amount of offset is incrementally increased with 0.005 m (1/8th channel depth) to a maximum offset of 0.03 m (6/8th channel depth). Fig. 11 shows that the fault offsets of 0.005 m and 0.010 m have a relatively constant sinuosity increase to ~60 and 80 years respectively before sinuosity stabilizes. The amount of faulting offset influences the rate of sinuosity increase where larger offsets result in faster increase of sinuosity (Fig. 11). The critical value of river sinuosity of our model runs lies, with exception of the 0.030 m scenario, around 1.3 (Fig. 12). Further increase of the channel sinuosity leads to instability of channel sinuosity. As discussed above, this might lead to a chute cutoff and hence sinuosity decrease on a somewhat longer timescale.

The rate of sinuosity increase with increasing fault offsets can be explained by the fact that a larger offset results in a higher gradient and, therefore, a larger flow velocity. In turn, this leads to increased bank erosion, lateral displacement and thus a sinuosity increase of the channel.

The exception of the 0.030 m model run is probably the result of the large amount of sediment that is deposited at the foot of the fault (Figs. 11 and 12). This sedimentation forms a fluvial fan, which forces the flow of the channel towards the side of the model domain. In an unconfined setting, this process might have led to a channel avulsion because the gradient advantage towards the floodplain is significantly higher than that of the fluvial fan.

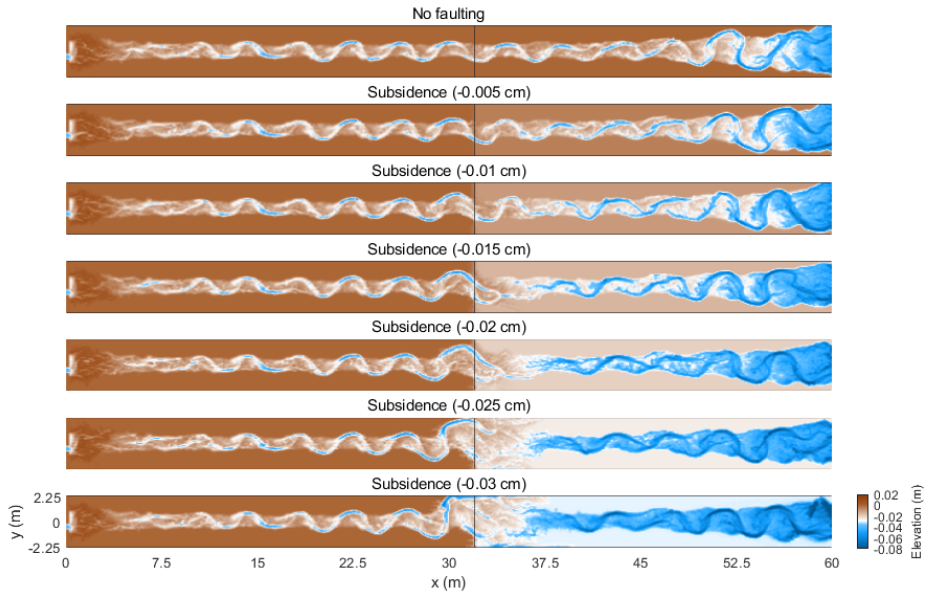


Fig. 10: Morphology of the detrended bed elevation at the end of the model run for the scenarios that simulate incremental increase of subsidence. Morphodynamic change of the river channel increases with vertical offset.

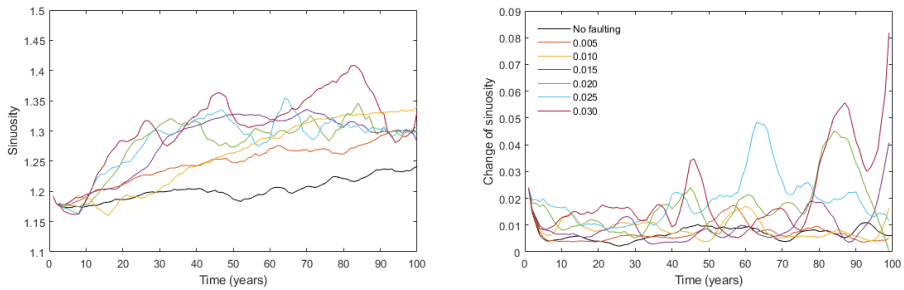


Fig. 11: Sinuosity of the main channel over time for the incrementally increasing subsidence scenarios. Top panel shows the sinuosity profiles of model scenarios while the bottom panel shows the change of sinuosity over time.

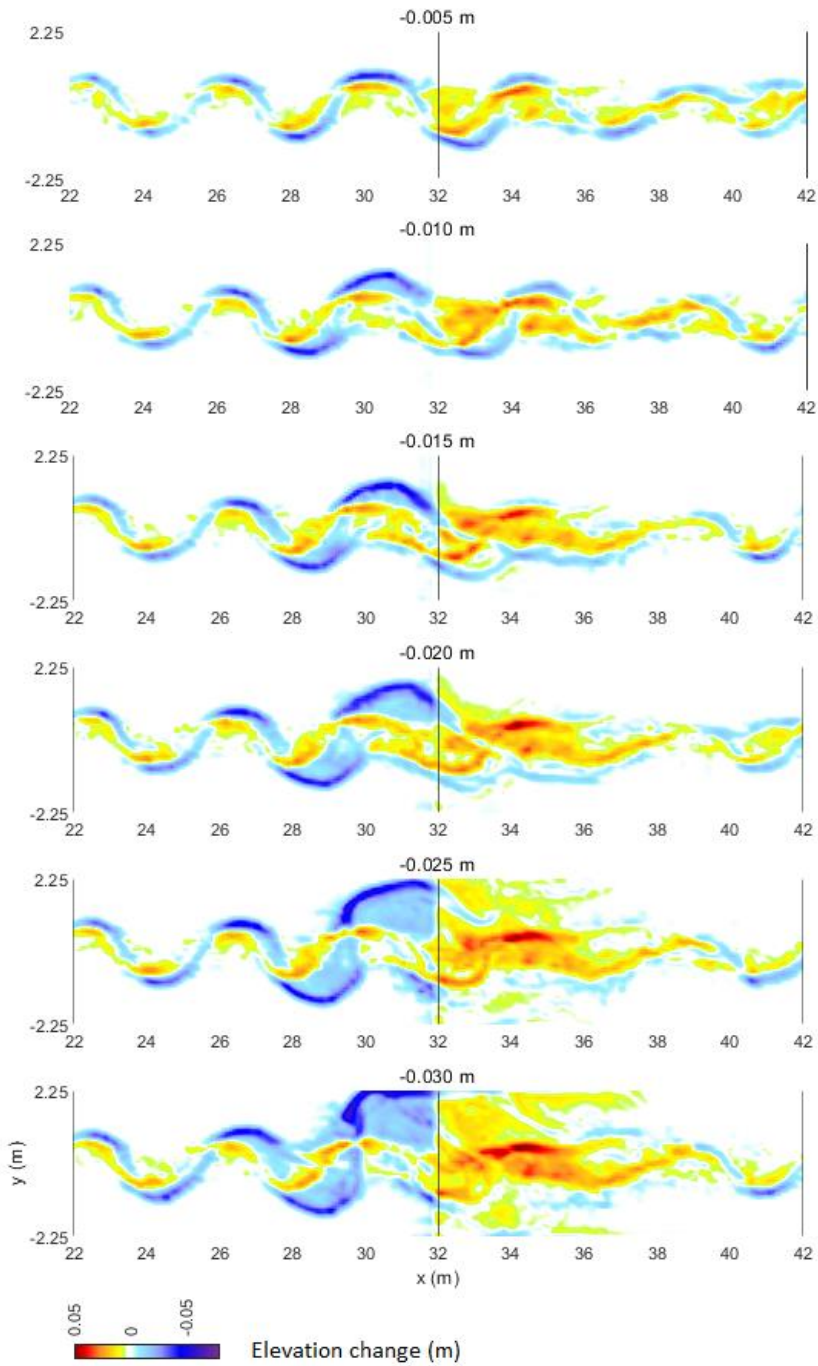


Fig. 12: Change of morphology and bed elevation over the course of the model runs for the incrementally increasing subsidence scenarios (i.e. $t_{100} - t_0$). Note that the largest subsidence scenarios result in a fluvial fan downstream of the fault that forces the channel to the side of the model domain.

6.3.4 Fault location

The effect of fault location was studied by using two additional scenarios (i.e. fault location at 31.0 and 31.6 m) with an instant fault offset of 0.015 m (3/8th channel depth) using the subsidence setup. The first ~50 years of both scenarios show a similar increase in sinuosity from ~1.18 to 1.33. However, hereafter the sinuosity changes of the different scenarios start to deviate (Fig. 13).

The scenario with a fault at 31.0 m shows a chute cutoff of the channel occurring at ~55 years, which reduces the sinuosity to 1.27 within 10 years. Subsequently, sinuosity increases again to 1.31 at the end of the model run. The scenarios with the fault at 31.6 m predict sinuosity to increase for ~70 years, and then the change in sinuosity decreases and sinuosity stabilizes around 1.39. However, at 92 years a chute cutoff reduces the sinuosity of the channel to 1.31. The standard fault location at 32.0 m shows a relatively stable sinuosity of 1.33 up to ~72 years after which it decreases to 1.29 to return to a sinuosity of ~1.33 at the end of the run. Overall the different positions of the fault locations lead to a similar end result. However, substantial differences are observed for the time-progressive evolution.

The cause for the observed differences is best explained by the velocity maps of the flow after the fault displacement (Fig.14). The local increase in velocity (left panels Fig.14) is the result of an increased gradient. The location of 31.0 m positions the fault at the downstream end of the bend apex. Subsidence of the right-hand side of the model domain therefore leads to a superposition of the upstream meander compared to the meander bend downstream of the fault (Fig.14). The combination of these factors makes that the flow after fault displacement is largely directed over the downstream pointbar of the fault (Fig.14, right panels). This overbank flow, which has an increased velocity due to the increased gradient, leads to erosion of the pointbar and chute-channel development. Therefore, the sinuosity profile of the fault location at 31.0 m shows a relatively fast chute-cutoff development (i.e. after ~55 years [Fig.13, bottom panel]).

The fault position at 31.6 m is located at the inflection point of the meandering channel. Although the same response as for the fault location at 31.0 m is partially observed for this fault position, a large part of the flow is directed into the main channel towards the next meander bend (Fig. 14).

This results in a longer period of bank erosion, lateral migration and hence meander curvature before the gradient advantage over the pointbar becomes high enough for a chute cutoff to occur.

The fault location at 32.0 m positions the fault at the start of the bend apex of the meander (Fig. 14). In this case the fault offset results in a direction of the flow (with increased flow velocity) towards the outer bank of the meander. Here, scouring takes places which

eventually leads to a sinuosity increase (Fig. 13, bottom panel). However, the flow direction towards the outer bend is to the vegetated, erosion resistant floodplain instead of the pointbar and does therefore not contribute to the development of a chute channel. The fact that such a chute cutoff does eventually develop for the scenario with the fault location at 32.0 m can be attributed to the increased gradient advantage over the pointbar which forms as a result of increased bend curvature and downstream bar formation (Van Dijk et al., 2014).

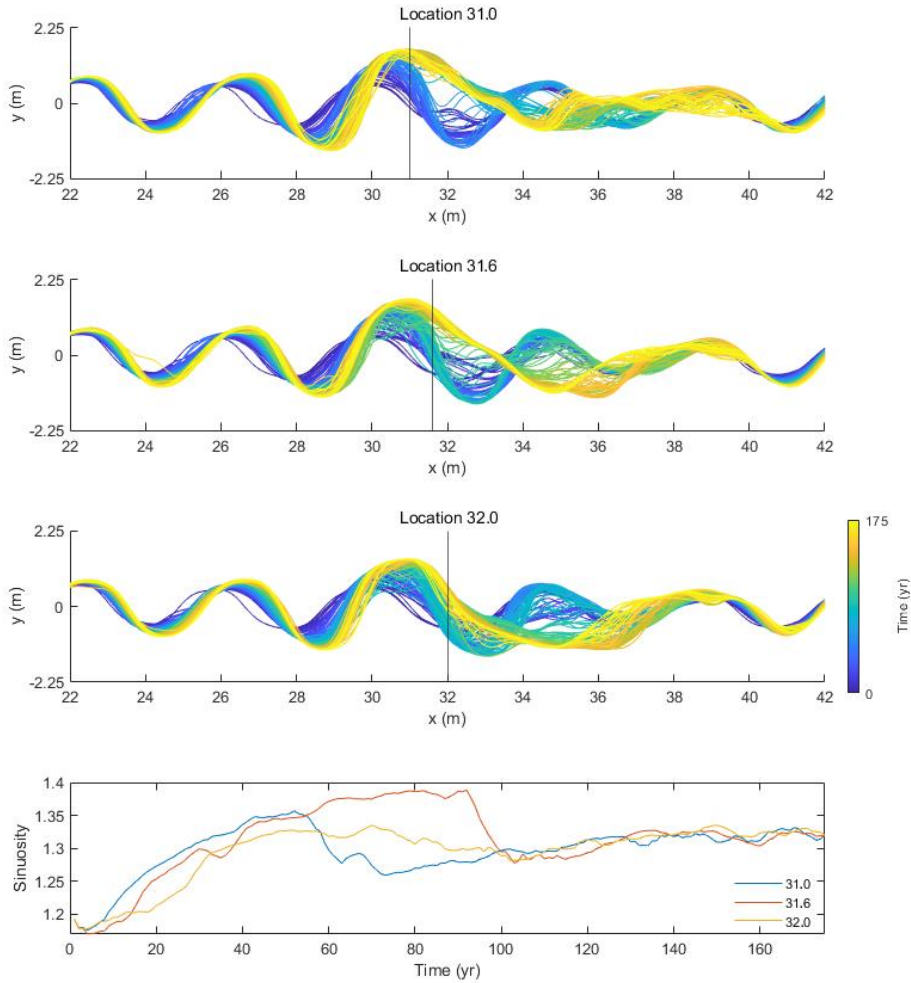


Fig. 13: Evolution of the position and sinuosity of the main channel over time for the scenarios with different fault locations.

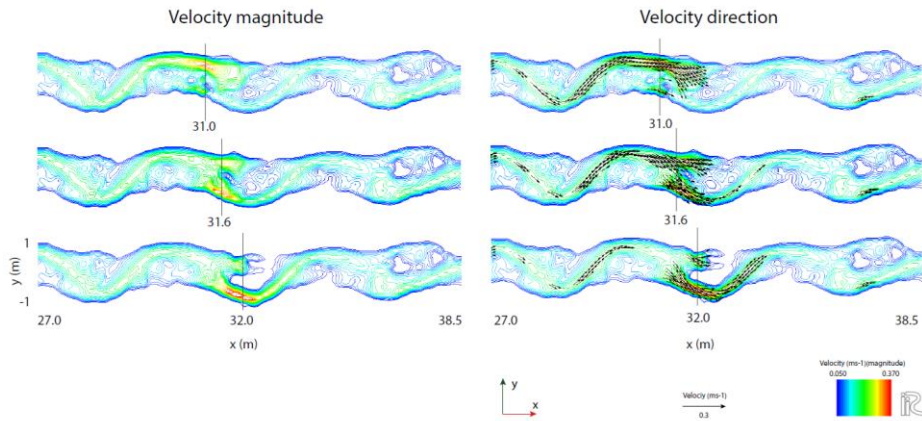


Fig. 14: Maps that show the velocity magnitude and direction of flow in the model during high for the different fault location scenarios.

6.4 Discussion

6.4.1 Comparison to field studies

The model results show that a changing valley gradient over a fault leads to both longitudinal erosion and aggradation of the river bed and lateral adaption such as increased lateral displacement or chute cutoff. Erosion of the footwall and aggradation on the hanging wall of a fault are commonly observed responses to a gradient increase, i.e. a normal fault downstepping in the downstream direction (cf. Holbrook and Schumm, 1999; Parker, 2004). The shallowing and widening of the channel just downstream of this kind of fault were also observed in both experimental and field studies for zones of relative subsidence and lowered slopes (Ouchi, 1985; Jin and Schumm, 1987; Jorgensen, 1990; Holbrook and Schumm, 1999).

An increase in sinuosity in response to a faulting-induced steepening of the valley floor, as shown for the subsidence scenarios, is observed frequently in the geomorphological record as well (Ouchi, 1985; Schumm et al., 2002; Timar, 2003; Petrovszki et al., 2012). However, the model shows that a continued increase in sinuosity might eventually lead to a chute cutoff which reduces channel sinuosity (Fig.13). Therefore, the posed relationship between gradient and river channel sinuosity increase is only valid up to a maximum threshold of bend sharpness (c.f. Schumm and Khan, 1972; Holbrook and Schumm, 1999; Woolderink et al., 2021). Moreover, if faulting rates become too high relative to the sediment transport capacity of the river, excess sedimentation on the footwall may lead to channel avulsion (Fig. 12). These results are in agreement with

Schumm et al. (2000), showing that the rate of deformation (i.e. faulting) appears to influence river response.

Flooding of the backwater reach was observed as a response to a normal fault downstepping in the upstream direction, like observed in field studies (Van Arsdale, 1994; Holbrook and Schumm, 1999). Such flooding or lake development will often result in increased accumulation of (fine) sediments, due to the reduced flow and sediment transport capacity, at the river bed and floodplain in the backwater reach (Holbrook and Schumm, 1999). However, this effect of increased aggradation was less pronounced as the modelling of fines was not included in our model.

Increased incision and decreased width-to-depth ratios, such as in the predictions for the uplift scenarios, are frequently observed responses of river channels that transverse zones of uplift (Jorgensen, 1990; Holbrook and Schumm, 1999; Woolderink et al., 2018). A decreased channel sinuosity over a zone of relative uplift was, for example, observed in the geomorphological record of the Meuse River in the Lower Rhine Embayment rift system (Woolderink et al., 2018). However, it should be noted that anomalies in channel width, depth and width-to-depth ratios alone are not sufficient indicators for tectonic perturbation in field studies as these characteristics are also dependent on variables such as bankfull discharge, sediment load and type, vegetation patterns, floodplain and bank material and confluences or bifurcations (Schumm, 1977; Holbrook and Schumm, 1999).

Finally, our model does not include all processes that may influence the response of a river to a faulting perturbation. For instance, co-seismic displacement may very well lead to bank failure or sand wells in the river channel (Fuller, 1912; Schumm et al., 2002). These perturbations will influence morphodynamics and morphology by the local increase of sediment input to the river channel, or in the form of a temporary blockage of the flow. It was, for instance, shown for the Baghmata river in India that faulting lead to the formation of compressed meanders upstream of the fault (Jain and Sinha, 2005). These compressed meanders were subsequently abandoned as a result of channel straightening due to hydrological adjustments of the river channel (Jain and Sinha, 2005). Moreover, vertical displacement can lead to juxtaposition of different lithologies, causing variability in erosion resistance of the river bed and banks over a fault (zone). Jin and Schumm (1987) showed, based on an experiment with a resistant clay block in the middle of the flume, that the presence of lithological differences can also lead to compression of meander bends, in this case upstream of the clay plug. Although such differential erodibility due to juxtaposition were not included in our model setup they can provide valuable opportunities for future modelling studies.

6.4.2 Tectonic deformation rates

The faulting offsets that were used for the modelling scenarios are relatively large. The vertical displacement of $1/8^{\text{th}}$ and $3/8^{\text{th}}$ of the channel depth correspond to offsets of 0.4 and 1.2 meters. These offsets relate to a Moment Magnitude of $\sim 6.5 - 6.8$ (Wells and Coppersmith, 1994). These vertical displacements and earthquake magnitudes form, for example, the upper limit of the earthquakes in the Lower Rhine Embayment (Camelbeeck et al., 2007) which is the area on which our modelling scenarios are based. The displacement rates of 4 and 12 mm/yr for the gradual displacement scenarios are very high compared to natural deformation rates at intraplate fault systems. Long-term vertical displacement rates in the Lower Rhine Embayment did not exceed 0.1 mm/yr (Vanneste et al., 2013). Nevertheless, the offset rates used in this model study are within the range of summarized worldwide rates of Quaternary vertical deformation, which lie between 0.1 and 10 mm/yr (Kaizuka, 1967; Ouchi, 1985; Schumm et al., 2000). Therefore, the used gradual offset rates can be regarded as a reasonable upper estimation for active aseismic deformation to study the effects on river morphodynamics.

Our model results suggest that a vertical displacement of $1/8^{\text{th}}$ of the river channel depth is sufficient to cause a morphodynamic response that is retraceable in the geological record. Similar relative offsets in an analogue experiment by Ouchi (1985) resulted in a response of the meandering channel as well. Their results showed that an increase in slope resulted in an increased sinuosity of the experimental river. However, observations of geomorphological records showed that natural river systems may already respond to deformation rates of ~ 1 mm/yr (Zámolyi et al., 2010). It is, however, not solely the faulting rate that affects alluvial rivers, but the total accumulated deformation of a river valley in a period of several decades to centuries. This will inevitably change the channel gradient (Ouchi, 1985) and hence lead to morphodynamic and morphological changes.

6.4.3 Relative time scales

Our model results show that the vertical adaption of the river bed occurs relatively fast (within ~ 5 years after the displacement [Fig. 15]) compared to the lateral adaption process (between $\sim 20-90$ years). This discrepancy can best be explained by the relations between the characteristic spatial scale and formative time scale of the morphological phenomena (Kleinhans et al., 2015), where in-channel morphodynamics might be an order of magnitude faster than bend migration and planform changes. For example, ten Brinke (2004) showed that erosion of the IJssel River (NL) river bed of ~ 0.5 to 1.5 meter occurred within a few years after channel canalization that cut off several meander bends. For the subsidence scenarios, it was shown that lateral channel migration rates might be increased by 1.5 to 23 times compared to the reference scenario without faulting (Table 3).

Relatively reduced vertical and lateral displacement rates are linked to the uplift scenarios (Table 3). Thus, faulting may increase or decrease both the vertical and lateral dynamics of a river channel by an order of magnitude compared to a non-affected river reach.

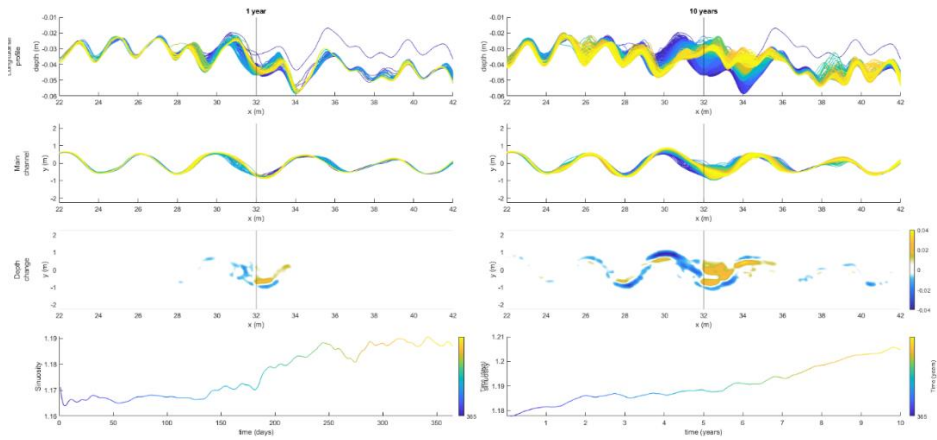


Fig. 15: Evolution of the longitudinal bed profile, main channel position and sinuosity during the first year (left panels) and after 10 years (right panels) subsequent to a subsidence faulting perturbation.

6.4.4 Transient response, fault location and preservation potential

Our model results show that a fault displacement of an alluvial river can result in multiple, time-dependent, morphological adjustments of the river channel such as erosion and sedimentation along the longitudinal river profile, sinuosity increase or (chute) cutoff of the channel (Figs. 2, 6, 13). Therefore, the response is transient. This time-dependent river response is important when deriving relationships between faulting and river dynamics from morphological and sedimentological record. It is crucial to understand if an observed morphological response is the final outcome of the morphodynamic adaption or that it is part of an ongoing transient response. For example, sediment aggradation at the hanging wall will normally lead to a locally increased preservation potential. However, only the lower parts of the prior sedimentation succession might be preserved if aggradation occurs alongside lateral migration. (Lewin and Macklin, 2003). This process can hence lead to a burial and masking of the geomorphology of the initial part of the sequence of responses to faulting. Alternatively, if a chute cutoff leads to incision of the new chute channel, the initial sinuosity increase may be partially preserved in the sedimentological and morphological record.

However, these possible preservation situations also depend on the difference in relative time-scales of river dynamics and faulting. A highly dynamic river is more likely to rework potential geomorphic indicators between successive faulting events than a river that is less dynamic. Moreover, the relative position at which a meander bend crosses a fault influences the river response to faulting (Figs. 13 and 14). This is important to consider when analyzing the geomorphological record for possible fault presence and evidence of faulting.

The above indicates that without a detailed reconstruction of the response of a meandering channel our abductive inferences from the morphological or sedimentological records might lead to erroneous conceptual models of the relation between faulting and alluvial river response. Our model results can hence provide a guideline to include process-based reasoning in the interpretation of geomorphological and sedimentological observations of fluvial response to faulting. The combination of these approaches will help understand the natural processes involved in more detail and might therefore lead to better predictions of possible effects of faulting on river morphodynamics.

6.5 Conclusions

The following can be concluded from our numerical modelling study of the morphodynamic response to various faulting scenarios:

- Channel sinuosity increases as a result of the faulting enhanced valley gradient, which leads to enhanced bank erosion and lateral displacement. Moreover, relative subsidence of the downstream part of the river over a normal fault (fault downstepping in downstream direction) leads to incision of the river bed at the footwall and sedimentation on the hanging wall. Both the longitudinal and lateral adaptations are restricted to a zone of approximately 2 meander wavelengths around the fault and diminish both upstream and downstream.
- Relative uplift of the downstream part of the river over a fault (normal fault downstepping in upstream direction) leads to reduced fluvial activity upstream of the fault due to a backwater effect. The uplift results in (minor) thalweg incision and channel straightening downstream of the fault.
- Sinuosity increase as a response to faulting can continue to a maximum bend radius. Hereafter a chute cutoff will reduce channel sinuosity to a new dynamic equilibrium that is generally higher than the pre-faulting sinuosity.
- Instant faulting leads to a faster morphodynamic response of the river channel than gradual faulting
- The relative position within a meander bend at which faulting occurs has a profound influence on the evolution of sinuosity. Fault locations that enhance flow velocities over the point bar result in a faster sinuosity increase and subsequent chute cutoff than locations that enhance flow velocity towards the floodplain.
- Fault displacement will lead to a transient river response which should be considered in the interpretation of morphological and sedimentological observations.

6.6 References

- › Allen, J. R. L., 1978. Studies in fluvial sedimentation: an exploratory quantitative model for the architecture of avulsion-controlled alluvial suites. *Sedimentary Geology*, 21(2), 129-147.
- › Alexander, J., Leeder, M. R., 1987. Active tectonic control on alluvial architecture. In: Ethridge, F.G., Flores, R.M., Harvey, M.D., (Eds.) *Recent Developments in Fluvial Sedimentology*. Spec. Publ. Soc. Econ. Paleont. Miner., 39, 243-252
- › Bryant, M., Falk, P., Paola, C., 1995. Experimental study of avulsion frequency and rate of deposition. *Geology*, 23, 365-368.
- › Bridge, J. S., Leeder, M. R., 1979. A simulation model of alluvial stratigraphy. *Sedimentology*, 26(5), 617-644.
- › Camelbeeck, T., Vanneste, K., Alexandre, P., Verbeeck, K., Petermans, T., Rosset, P., Mazzotti, S., 2007. Relevance of active faulting and seismicity studies to assessments of long-term earthquake activity and maximum magnitude in intraplate northwest Europe, between the Lower Rhine Embayment and the North Sea. In: Stein, S., Mazzotti, S., (Eds.), *Continental Intraplate Earthquakes: Science, Hazard, and Policy Issues*, Special Paper 425, Geological Society of America, Boulder, Colorado, 193–224.
- › Crosato, A., 2009. Physical explanations of variations in river meander migration rates from model comparison. *Earth Surface Processes and Landforms*, 34(15), 2078-2086.
- › Crosato, A., 2007. Variations of channel migration rates in two meander models. In *Proc. 5th IAHR Symp. on River, Coastal and Estuarine Morphodynamics*, Enschede, the Netherlands (pp. 17-21).
- › Fuller, M.L., 1912. The New Madrid earthquake. *U.S. Geol. Surv. Bull.*, 494 119 pp.
- › Gomez, B., Marron, D.C., 1991. Neotectonic effects on sinuosity and channel migration, Belle Fourche River, western South Dakota. *Earth Surface Processes and Landforms*, 16, 227-235
- › Hickin, E.J. 1977. Hydraulic factors controlling channel migration. *Research in Fluvial Systems*, Dacidsen-Aenott, R. & Nicking W. (Eds.), *Proceedings of the 5th Guelph Geomorph. Symp.*, Geobooks, Norwich, pp. 59-72.
- › Holbrook, J., Schumm, S. A., 1999. Geomorphic and sedimentary response of rivers to tectonic deformation: a brief review and critique of a tool for recognizing subtle epeirogenic deformation in modern and ancient settings. *Tectonophysics*, 305(1-3), 287-306.
- › Jain, V., Sinha, R., 2005. Response of active tectonics on the alluvial Baghmati River, Himalayan foreland basin, eastern India. *Geomorphology*, 70(3-4), 339-356.
- › Jin, D., Schumm, S.A., 1987. A new technique for modeling river morphology. In: Gardner, V. (Ed.), *International Geomorphology*. Wiley, Chichester, pp. 681-690.
- › Jorgensen, D.W., 1990. Adjustment of alluvial river morphology and process to localized active tectonics. (Doctoral Dissertation, Colorado State University).
- › Kleinhans, M. G., 2010. Sorting out river channel patterns. *Progress in physical geography*, 34(3), 287-326.
- › Kleinhans, M. G., Braudrick, C., van Dijk, W. M., Van de Lageweg, W. I., Teske, R., Van Oorschot, M., 2015. Swiftiness of biomorphodynamics in Lilliput-to Giant-sized rivers and deltas. *Geomorphology*, 244, 56-73.
- › Kleinhans, M. G., Ferguson, R. I., Lane, S. N., Hardy, R. J., 2013. Splitting rivers at their seams: bifurcations and avulsion. *Earth Surface Processes and Landforms*, 38(1), 47-61.

- › Kleinhans, M. G., Jagers, H. R. A., Mosselman, E., Sloff, C. J., 2008. Bifurcation dynamics and avulsion duration in meandering rivers by one-dimensional and three-dimensional models. *Water resources research*, 44(8).
- › Lewin, J., & Macklin, M. G., 2003. Preservation potential for Late Quaternary river alluvium. *Journal of Quaternary Science: Published for the Quaternary Research Association*, 18(2), 107-120.
- › Mackey, S.D., Bridge, J.S., 1995. Three-dimensional model of alluvial stratigraphy: theory and application. *Journal of Sedimentary Research*. B65, 7-31.
- › Meyer-Peter E, Müller R. 1948. Formulas for bed-load transport, In IAHSR 2nd Meeting, Stockholm: Appendix 2 IAHR: Beijing;39–64
- › Ouchi, S., 1985. Response of alluvial rivers to slow active tectonic movement. *Geological Society of America Bulletin*, 96(4), 504-515.
- › Parker, G., 2004. 1D sediment transport morphodynamics with applications to rivers and turbidity currents. E-book available at Gary Parker's Morphodynamics Web Page, last update April, 13, 2006.
- › Petrovski, J., Székely, B., Timár, G., 2012. A systematic overview of the coincidences of river sinuosity changes and tectonically active structures in the Pannonian Basin. *Global and Planetary Change*, 98, 109-121.
- › Shimizu Y, Inoue T, Hamaki M, Iwasaki T., 2013. iRIC Software, Changing River Science: Nays2D Solver Manual. International River Interface Cooperative: Sapporo, Hokkaido, Japan.
- › Schumm, S.A., 1977. *The fluvial system*. John Wiley and Sons, New York, 338 pp.
- › Schumm, S. A., Khan, H. R., 1972. Experimental study of channel patterns. *Geological Society of America Bulletin*, 83(6), 1755-1770.
- › Schumm, S. A., Dumont, J. F., Holbrook, J. M., 2002. *Active tectonics and alluvial rivers*. Cambridge University Press.
- › Ten Brinke, W., 2004. *The Dutch Rhine, a Restrained River*. Veen Magazines B.V.
- › Timár, G., 2003. Controls on channel sinuosity changes: a case study of the Tisza River, the Great Hungarian Plain. *Quaternary Science Reviews*, 22(20), 2199-2207.
- › Toonen, W. H., Kleinhans, M. G., Cohen, K. M., 2012. Sedimentary architecture of abandoned channel fills. *Earth surface processes and landforms*, 37(4), 459-472.
- › Van Balen, R.T., Bakker, M.A.J., Kasse, C., Wallinga, J. Woolderink, H.A.G., 2019. A Late Glacial surface rupturing earthquake at the Peel Boundary fault zone, Roer Valley Rift System, the Netherlands. *Quaternary Science Reviews*, 218, 254-266.
- › Vanneste, K., Camelbeeck, T., Verbeeck, K., 2013. A model of composite seismic sources for the Lower Rhine Graben, Northwest Europe. *Bulletin of the Seismological Society of America*, 103(2A), 984-1007.
- › Van Dijk, W. M., Schuurman, F., Van de Lageweg, W. I., Kleinhans, M. G., 2014. Bifurcation instability and chute cutoff development in meandering gravel-bed rivers. *Geomorphology*, 213, 277-291.
- › Van Dijk, W. M., Van de Lageweg, W. I., Kleinhans, M. G., 2012. Experimental meandering river with chute cutoffs. *Journal of Geophysical Research: Earth Surface*, 117(F3).
- › van de Lageweg, W. I., van Dijk, W. M., Baar, A. W., Rutten, J., Kleinhans, M. G., 2014. Bank pull or bar push: What drives scroll-bar formation in meandering rivers?. *Geology*, 42(4), 319-322.

- › Weisscher, S. A., Shimizu, Y., Kleinhans, M. G., 2019. Upstream perturbation and floodplain formation effects on chute-cutoff-dominated meandering river pattern and dynamics. *Earth surface processes and landforms*, 44(11), 2156-2169.
- › Wells, D. L., Coppersmith, K. J., 1994. New empirical relationships among magnitude, rupture length, rupture width, rupture area, and surface displacement. *Bulletin of the seismological Society of America*, 84(4), 974-1002.
- › Woolderink, H.A.G., Cohen, M.K., Kleinhans, M.G., Van Balen, R.T., 2021. Patterns in river channel sinuosity of the Meuse, Roer and Rhine rivers in the Lower Rhine Embayment rift system, are they tectonically forced? *Geomorphology*.
- › Woolderink, H.A.G., Kasse, C., Cohen, K.M., Hoek, W.Z. Van Balen, R.T., 2018. Spatial and temporal variations in river terrace formation, preservation, and morphology in the Lower Meuse Valley, The Netherlands. *Quaternary Research*, 91(2), 548-569.
- › Zámolyi, A., Székely, B., Draganits, E., Timár, G., 2010. Neotectonic control on river sinuosity at the western margin of the Little Hungarian Plain. *Geomorphology*, 122(3-4), 231-243.

Chapter 7

The effects of faulting on river channel sinuosity; a review, evaluation and application of concepts.

H.A.G. Woolderink

7.1 Introduction

Faulting can lead to a vertical displacement of the earth's surface and, hence, locally change the gradient of a river valley floor. Alluvial rivers are susceptible to changes in the slope of their valley and respond by altering their morphodynamics and morphology. A widely used indicator of these changes is the sinuosity of the river channel, which is the ratio between the lengths of the river channel and valley, which has been shown in physical scale experiments and field examples (Burnet and Schumm, 1983; Ouchi, 1985; Jin and Schumm, 1987; Holbrook and Schumm, 1999; Timar, 2003; Petrovski et al., 2012). Via changes in the amount and size of the individual meander loops, the river channel is presumed to dynamically alter its channel length in such a way that the channel gradient remains unchanged despite the tectonic tilting (Holbrook and Schumm 1999).

The sinuosity response to active faulting depends on the relation between the sense of movement and the flow direction. A normal fault with the hanging wall in the downstream direction (i.e. downstepping in downstream direction) will enhance the fluvial gradient and, as a result, an increased sinuosity will occur at the fault trace. In contrast, a normal fault that is downstepping in upstream direction may lead to a reduced gradient and, hence, sinuosity (Ouchi 1985; Holbrook and Schumm 1999). Thus, changes in sinuosity can be an indicator of tectonic activity. However, sinuosity is also a function of multiple other factors, such as variability in stream-power, sediment load and composition, (riparian) vegetation cover, erodibility of the river banks and channel bed, and dominant mode of meander cutoff (chute or neck) (Baker, 1978; Schumm, 1963; Dade, 2000; Kleinhans and Van den Berg, 2011; Candel et al., 2020). Disentangling the effects of these forcing factor(s) is difficult. The use of sinuosity change as an indicator of tectonic activity may, therefore, lead to erroneous interpretations.

This paper aims to review and evaluate conceptual models of the effects of tectonic vertical motions, and in particular faulting, on the channel sinuosity of alluvial rivers, and the implications for application of sinuosity anomalies to determine tectonic vertical motions, using results and observations of previously performed physical scale experiments, combined with new numerical modelling results and field studies from the (palaeo) geomorphic record of the Meuse River.

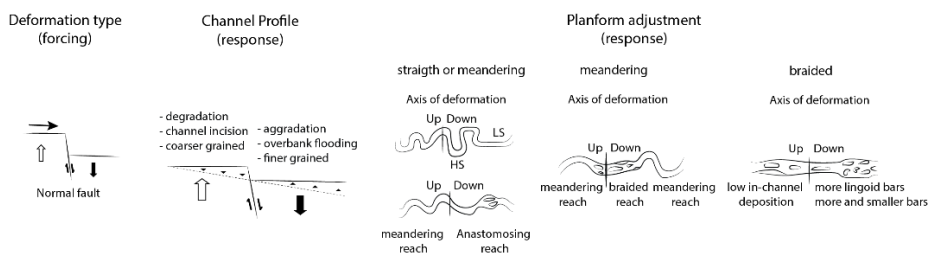


Fig. 1: Possible responses of alluvial rivers to normal faulting (redrawn from Schumm et al., 2002).

7.2 Normal faulting as a factor causing sinuosity changes

Schumm et al. (2002) show that surficial movements in an alluvial valley can have many forms. Both, gradual tilting and warping of the valley floor as well as abrupt faulting occur, and displacements can be horizontal, vertical or a combination of both. For this review we will, however, focus on vertical displacements along normal faults only (Fig. 1). According to Schumm et al. (2002), “Faults with vertical displacement may have the uplifted block upstream of the fault with the result that gradient is steepened. In the opposite case, the gradient will be decreased. The effect will resemble monoclinical tilting. Pairs of faults may produce uplifted (horst) or down dropped blocks (graben) that will both steepen and reduce gradient. This has the same effects as domes and anticlines or basins and syncline. . . . The possibilities are great, but in reality the result will be local steepening or reduction of gradient or cross-valley tilting”.

However, the vertical displacement along normal fault zones can be less straight-forward than proposed. For example, co-seismic displacements along normal faults are often asymmetric, where subsidence on the hanging wall is typically greater than the uplift of the footwall (Burbank and Anderson, 2012). Furthermore, distribution of vertical displacement may vary along a fault and will decay in a direction perpendicular to a fault during a displacement of a surface rupturing earthquake (Fig. 2). This differential distribution of vertical motions leads to numerous scenarios of altered gradients (Fig. 2). Moreover, normal fault zones may consist of multiple (linked) faults or fault segments, each of which have their own specific slip and vertical displacements distributions. Hence, vertical displacements vary spatially and temporally along a normal fault zone. In addition, rotational back-tilting of fault-bounded blocks leads to decreased gradients downstream of the fault in the situation of a normal fault that is downstepping in downstream direction.

All of these factors complicate the distribution of vertical displacement along and near normal fault zones, and thus the morphodynamic and morphological responses of rivers. Therefore, the distribution of vertical displacements along a fault zone should be taken into account when interpreting faulting related fluvial anomalies in the sedimentological or geomorphological record.

7.3 Experimental studies

In the past decades several experimental studies were performed to study the effects of (tectonically induced) vertical motions on channel pattern change and morphodynamics of alluvial rivers (Ouchi, 1983, 1985; Jin, 1983, Jin and Schumm, 1987; Dykstra, 1988; Germanowski and Schumm, 1993; Kim et al., 2010). These studies focussed on the effects of uplift and subsidence on alluvial rivers, most commonly by using a flume with an adjustable bottom.

The experiments by Ouchi (1985) showed that on the upstream side of an uplift axis a sinuosity decrease occurs, caused by a decreased gradient of the valley floor. Moreover, due to flood-induced inundation of the floodplain in front of the uplift axis, deposition of fine sediments takes place. Even a swamp environment can develop. This might, in turn, result in an anastomosing channel pattern in the backwater zone (Ouchi, 1985; Schumm et al., 2002). The same processes were postulated or observed for the downstream part of synclinal subsidence. Channel sinuosity increased in response to the steepened valley floor on the downstream side of the uplift axis (Fig. 1) or the upstream side of the subsidence axis respectively (Ouchi, 1983; 1985).

Jin and Schumm (1987) showed, based on an experiment with a resistant clay block in the middle of the flume, that the presence of lithological differences can lead to compression of meander bends upstream of the clay plug. This indicates that juxtaposition of different lithologies due to faulting may influence meandering of a river.

The experiments by Ouchi were also conducted in sand, without a floodplain of finer, cohesive materials. Jin and Schumm (1987) performed a series of experiments that did have a floodplain, which consisted of kaolinite and fine sand, providing enhanced stability of the channel by limiting (bank) erosion. The importance of a cohesive floodplain for (sustained) meandering in flume experiments was endorsed by, o.a. Peakall et al. (2007), Braudrick et al. (2009) and Van Dijk et al. (2013).

The experiments by Jin and Schumm (1987) showed that the effects of the uplifted part of the flume were relatively local around the zone of uplift. The reach in front of the uplift showed a straightening and thus sinuosity decrease of the channel for a short period of time (~50 hours [Jin and Schumm, 1987]), after which the channel sinuosity restored to almost the original value (Jin and Schumm, 1987; Schumm et al., 2002). Only the reach just downstream of the uplift was severely impacted by the vertical motions, resulting in an increased sinuosity at the end of the experiment. Overall the experiments by Jin and Schumm (1987) confirmed those of Ouchi (1985) where an increase or decrease in valley floor gradient resulted in a change in sinuosity of the river channel.

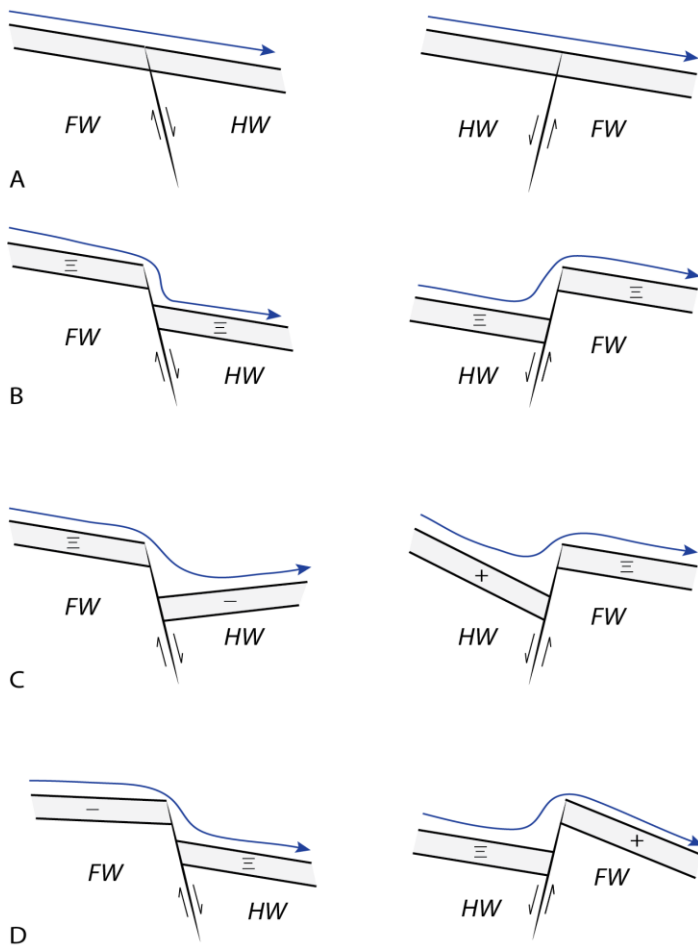
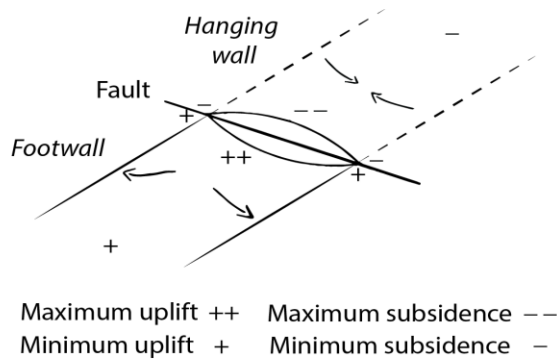


Fig. 2: Scenarios of vertical displacement distributions along normal faults and their effects on river (valley) gradients around the fault zone. A) pre-faulting, B) faulting with uniform vertical displacement, C) Increased vertical displacement on hanging wall, D) Increased vertical displacement on the footwall.

Although the experiments of Jin and Schumm had a floodplain, their experiments did not incorporate the effects of vegetation distribution. It was shown that, besides cohesive fines, the presence of vegetation in physical models has a profound influence on both flow resistance and on floodplain and bank strength (Braudrick et al., 2009; Tal and Paola, 2010; Van Dijk et al., 2013). It would, therefore, be desirable to perform a set of experiments with uplift and subsidence of an adjustable flume bottom in a self-sustaining physical meander experiment that includes both (overbank) fines and vegetation, as these factors best resemble the natural environment of most meandering rivers. Moreover, from the experiments of Dykstra (1988) it seems critical to adjust the uplift /subsidence rate in physical models to such an extent that deformation is able to force a morphodynamic response, but does not limit lateral dynamics.

7.4 Numerical modelling

The effects of various tectonic deformation rates and styles along normal fault zones on alluvial meandering river morphodynamics and morphology were numerically modelled by Woolderink et al., (in prep). Their results showed a positive relation between a tectonically increased gradient of the valley floor and sinuosity of a bed-load dominated meandering river on laboratory-scale. However, the model results also indicated that the sinuosity response was limited to a bend curvature maximum, after which channel sinuosity was reduced by a chute-cutoff. For a model adopting a relative uplift of the downstream block, a backwater (effect) in front of the fault was the result. In this zone flow velocities decreased substantially which decreased morphodynamic and morphological change of the channel. Comparing results of abrupt versus gradual faulting scenarios revealed that the former leads to a faster morphodynamic and sinuosity response than the latter. The relative position within a meander bend at which faulting occurs showed to have a profound influence on the evolution of river channel sinuosity, as this determines the location of the increased flow (i.e. over the downstream pointbar or against the outer bend floodplain).

7.5 Case studies

The conceptual models of faulting and river channel sinuosity have been applied in several case studies like the Belle Fourche river (South Dakota; Gomez and Marron, 1991), rivers in the US (Missouri, Kansas, Illinois, Mississippi, Sacramento; [Adams, 1980; Schumm and Harvey, 1985; Schumm et al., 1994]), the Tisza river (Timar, 2003) and its tributaries in the Pannonian basin (Zamolyi et al., 2010; Petrovski and Timar, 2010) and the Okavango Fan (Botswana; Smith et al., 1997). These studies show that the sinuosity response to tectonic motions provide a means to identify active tectonic vertical motions from fluvial stratigraphic and -morphologic archives. In some cases, these can

be of large value for studies on surface rupturing earthquakes, as demonstrated by Holbrook et al. (2006).

However, there are also field studies that showed that the relationship between sinuosity and valley gradient is not straightforward. The Meuse River, for instance, showed a complex relation between faulting and channel sinuosity. Changes in sinuosity of the Meuse river showed to be related to the location of faults, but not to faulting. The faulted subsurface of the Lower Rhine Embayment causes differences in channel bed lithology, gradient and river bank height and resistivity which, in turn, determine fluvial dynamics. Moreover, large-scale (>10km) sinuosity changes of the Roer River, a major tributary of the Meuse, show an inverse relationship between valley gradient and sinuosity (Woolderink et al., 2021). This increase in sinuosity with decreasing gradient can be explained by a transition from a chute to a scroll-bar dominated meandering river along the river.

A similar relationship was found for the Pannagon River (India) by Aswathy et al. (2008). According to these authors, “Overlay analysis shown that more sinuosity exists at the gentle slope areas (5-15°), where they tend to erode their sides and move back and forth across the land area”. Moreover, the study of the Pannagon River showed that sinuosity changes are controlled by lithology of the subsurface and riparian vegetation as well (Aswathy et al., 2008). From the field studies above it can be concluded that changes in river channel sinuosity along a river are the result of an interplay between multiple factors.

7.6 Combining the evidence

As Holbrook and Schumm (1999) mention “The tectonic effects discussed in this paper should be viewed as a collection of tectonic indicators. Like most indicators used in the geosciences, these have caveats and alternative explanations that must be addressed before application of the indicator can be considered valid.”. It is, therefore, that the combination of physical scale experiments, numerical morphodynamic modelling and detailed field-examples can provide a valuable contribution to our concepts of faulting induced changes in river dynamics and morphology as they complement each-other biases and limitations.

Both the physical scale experiments and numerical modelling show that an increase of valley floor gradient results in increased sinuosity of the river channel (Ouchi, 1985; Holbrook and Schumm, 1999; Schumm et al., 2000; Woolderink et al., in prep). These observations are supported by numerous field examples (Gomez and Marron, 1991; Adams, 1980; Schumm and Harvey, 1985; Schumm et al., 1994; Smith et al. 1997; Timar, 2003; Zamolyi et al., 2010; Petrovszki and Timar, 2010; Petrovszki et al., 2012). However, when the valley gradient is too high relative to the channel (bed)

characteristics, sinuosity will decrease as a result of a shift to a more chute-dominated meandering style (Kleinhans and Van den Berg, 2011; Woolderink et al., 2021) or even (weakly) braided (Schumm et al., 2002). Moreover, other factors also affect meandering, such as variability in stream-power, sediment load and composition, (riparian) vegetation cover, erodibility of the river banks and channel bed, and dominant mode of meander cutoff (chute or neck) (Baker, 1978; Schumm, 1963; Dade, 2000; Aswathy, 2008; Kleinhans and Van den Berg, 2011; Candel et al., 2020). The combination of the different approaches shows that, when circumstances are right, an increase of valley floor gradient will indeed result in higher sinuosity as a result of increased flow velocities, enhanced bank erosion and lateral migration of the river channel. However, this is only valid for the scroll-bar dominated meandering rivers.

The numerical model results indicated that a sinuosity increase in response to normal faulting in the downstream direction will not always result in a new dynamic equilibrium of a higher sinuosity river channel. Over time the bend curvature may become too high, resulting in a (chute) cutoff. It is, therefore, crucial to consider the morphodynamic and morphological response of an alluvial river to faulting as transient. This implies that our derived relations from the sedimentological and geomorphological record are biased by the moment we observe them. For instance, an initial channel straightening or change to a braided planform might be erased or overprinted (and hence hidden from the surface) by a subsequent change to a regime of increased lateral movement of a meandering channel, as a response to decreasing gradients due to footwall erosion and hanging wall sedimentation. In the same manner a sinuosity change of a river channel to faulting at the present day might only be a first step of a transient morphodynamic and morphological response that is not yet completed.

The above shows that specific relations between sinuosity and valley slope cannot be generalized (Kleinhans and Van den Berg, 2011). Therefore, sinuosity anomalies should only be used as a geomorphic indicator for tectonics in combination with a well-known sedimentary, vegetational and temporal setting.

7.7 Application to palaeoseismology and river response

The combined lessons of the physical and numerical modelling and field examples can be used to postulate hypotheses of alluvial river response(s) to faulting preserved in the geomorphological and sedimentary record. Below we use morphodynamic and morphological responses of the Meuse River to (palaeo) faulting events along two major fault zones of the Lower Rhine Embayment as an example.

7.7.1 Feldbiss Fault Zone (Lower Rhine Embayment, the Netherlands)

The FFZ consists of three normal faults that are downstepping in the downstream direction (e.g. Heerlerheide, Geleen and Felbiss faults [Fig. 3]). The FFZ is crossed by the meandering Meuse. Faults of the FFZ are active: fault scarps occur on the late Middle Pleistocene terraces next to the Holocene floodplain of the Meuse River (Houtgast et al., 2005; Camelbeeck et al., 2007). The reconstructed Younger Dryas channels at the FFZ show a meandering planform while both upstream and downstream of the fault zone the river has a wandering/braided planform (Woolderink et al., 2018). A shift from braided to meandering would indicate a decrease of flow velocity, decreased sediment load or an increase of sediment grainsize. There is no increase of sediment grainsize over the fault zone, and a decreased sediment load is unlikely as an increase in gradient would promote erosion and sediment uptake rather than deposition. Therefore, a local decrease in flow velocity is the most likely cause for the shift to a meandering planform.

However, this is the opposite to what is expected from a series of downstream downstepping normal faults. An explanation for a decrease of gradient and hence flow velocity might be rotational back-tilting of the tectonic blocks at the FFZ. It can be derived from the older Pleistocene Meuse terrace surfaces over the FFZ that this process occurs, and that it reduces the valley gradient on a block scale. This local change in river planform implies that the Meuse River was near the transition of (moderately) braided and chute cut-off dominated meandering (cf. Kleinhans and Van den Berg, 2011) during the Younger Dryas, where only relatively minor changes in gradient are needed to (locally) force a change in fluvial planform.

The dated and reconstructed late Holocene (< 3.1 ka BP) channels show a deflection towards the east just upstream of the FFZ (Fig. 3 [Woolderink et al., 2018]). This can be explained by an along strike gradient in fault offset. A conceptual model of the morphodynamic response of a river to such a gradient is shown in Fig. 3. For the FFZ such a gradient is likely because of the youngest surface rupturing event along the FFZ. Palaeoseismological trenching along the Geleen Fault (part of the FFZ) in Belgium showed that the last surface rupturing earthquake occurred between 2.5 ± 0.3 and 3.1 ± 0.3 ka BP (Camelbeek et al., 2007; Vanneste et al., 2018). The displacement varies between 0.5 to 0.85 m along the investigated trenches (Fig. 3, Bree 1, 1bis, 2 and Rotem

2, 3 [Vanneste et al., 2018]). However, little Holocene offset was recognized along the continuation of this Geleen fault zone in the Netherlands (Fig. 3, Geleen trench [Houtgast et al., 2003]). This implies that mostly the western segment(s) of the Geleen fault experienced vertical displacement during the late Holocene. With a maximum displacement at the western edge of the Meuse floodplain and a decreasing offset towards the east, a gradient advantage to the (north) east developed. In this situation a deflection of the river directed from the relatively updoming to the subsiding area is indeed to be expected (Schumm et al., 2002).

Furthermore, a local sinuosity increase at fault-zone scale at the FFZ might be expected in response to the Late Holocene displacement event. However, this is not observed (Fig. 3). The lack of sinuosity response around the FFZ implies that: i) there was no (significant) height difference in the longitudinal profile as a result of deflection of the river channel, ii) aggradation and incision of the floodplain was able to level height differences in the longitudinal profile caused by fault motions, iii) the sinuosity response was not preserved due to subsequent erosion, iv) there was a sinuosity decrease due to an enhanced gradient instead of the expected increase. In the latter it is important to note that the Meuse is a chute cut-off dominated meandering river (cf. Kleinhans and Van den Berg, 2011) at the FFZ. Therefore, a local increase in gradient might lead to chute cut-off of the channel, which reduces sinuosity.

On the other hand, a reduced sinuosity at the FFZ could also be explained by a decreased gradient over the FFZ due to rotational back-tilting of the fault-bounded blocks, as was suggested for the Younger Dryas change in fluvial planform in this zone.

Nevertheless, we cannot rule out the possibility that an enhanced sinuosity has existed in the past as a result of displacement along this fault zone and that there is no remnant left in the floodplain because of the transient nature of sinuosity of river channels. If such a sinuosity increase did occur, it was present for a maximum of ~3.0 ka, indicating the importance of preservation potential of morphodynamic river responses to a tectonic deformation.

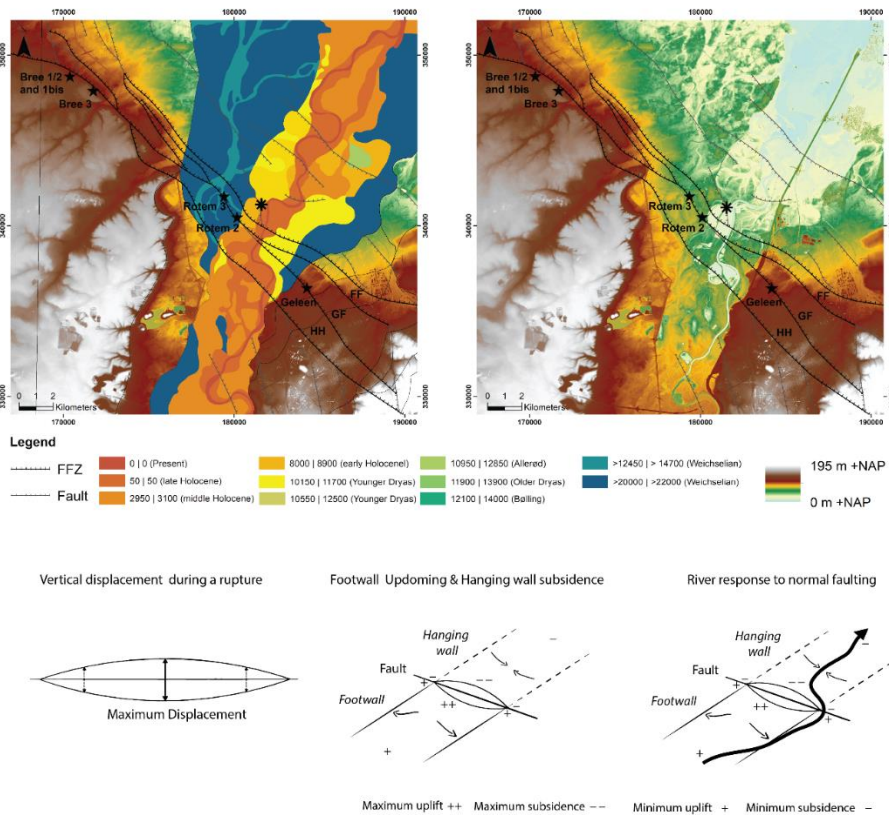


Fig. 3: Deflection of the Meuse river channel in response to local updoming and subsidence due to normal faulting induced vertical surface displacement.

7.7.2 Peel Boundary Fault Zone (Lower Rhine Embayment, the Netherlands)

The PBFZ is the major fault zone of the Lower Rhine Embayment. The last earthquake event, in 1992, had a moment magnitude of 5.3 and did not cause surface rupture. Palaeoseismological trenching studies of the PBFZ showed a large (Mw 6.5-6.8) surface rupturing earthquake with a vertical offset of ~1m at the beginning of the Allerød period and a smaller seismic event with a displacement of ~0.3 m during the latter part of the Allerød (Van den berg, 2002; Van Balen et al., 2019). Due to the downstepping of the PBFZ in upstream direction, the vertical displacement along the fault elevated the river bed downstream of the fault, relative to the riverbed at the upstream side of the fault (Fig. 4).

A highly sinuous meander positioned along the strike of the PBFZ (Fig. 4) formed during the Allerød and locally scrolls in upstream direction, while all other meanders on the same river terrace show a downstream meander migration. Palaeogeographic

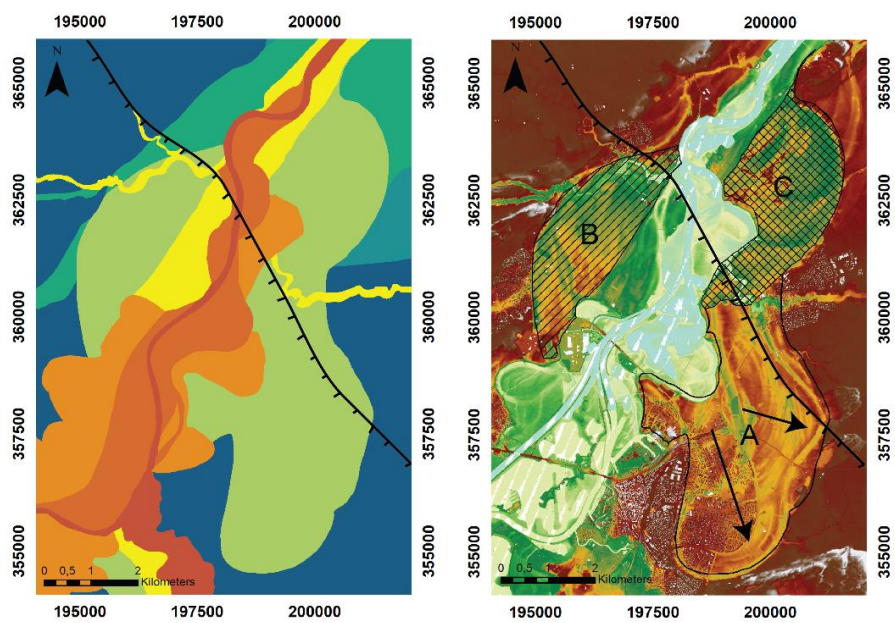
reconstructions show that the Allerød river terrace consists of three different sub-levels, something that is only observed at this fault zone (Woolderink et al., 2018).

Anomalous or compressed meanders in response to active faulting as described above were also recognized for the Nile and Bagmati river (Schumm and Galay, 1994, Jain and Sinha, 2005). In these cases, the compressed meanders were abandoned by channel straightening, due to hydrological adjustments of the river channel, over time as well. It seems, therefore, that anomalously high sinuosity because of compression is a possible marker of a faulting perturbation (Holbrook and Schumm, 1999, Schumm et al., 2002, Jain and Sinha, 2005).

A highly sinuous meander in response to a normal fault downstepping in upstream direction is, however, opposite to what was observed in the morphodynamic modelling of Woolderink et al. (in prep), which showed a decrease in river dynamics. For this scenario the discrepancy can be the result of multiple factors. First, the distribution of vertical motions caused by the surface rupturing earthquake might have locally increased the gradient towards the PBFZ (Fig. 4). Such an increase will have led to enhanced meander migration and sinuosity increase in front of the fault zone.

Another possible explanation might be enhanced sediment deposition in the river channel in the backwater reach that formed as a result of the fault displacement (c.f. Parker, 2004). In that scenario in-channel sedimentation will have enhanced bar-formation and hence lateral displacement and sinuosity increase.

In either way, the increase in sinuosity of the Allerød river channel will have resulted in a gradient advantage over the pointbar over time. A cutoff of the channel occurred as a result (Fig. 4). The new channel had a steeper gradient than the original channel which implies a higher flow velocity and sediment transport capacity. This resulted in the formation of terrace sublevels B and C at a lower elevation (~1 meter lower for each sublevel) as a secondary response. In turn, this leads to the preservation of the primary sinuosity response of the Allerød river channel. Thus, the faulting event led to two different time-progressive morphodynamic responses, meandering followed by terrace formation. Together, both responses represent a transient response.



Legend

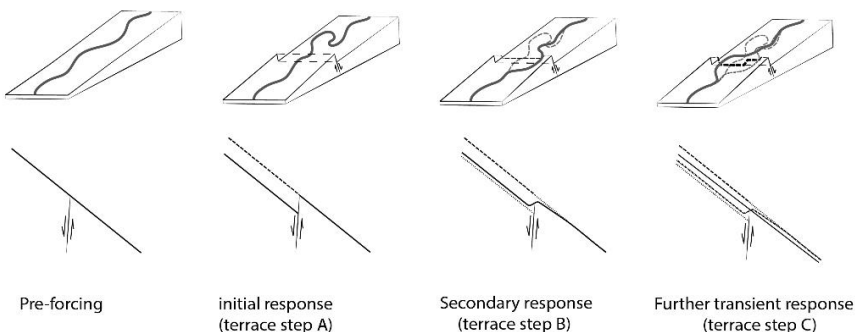


Fig. 4: Conceptual model of transient river response of the Meuse River, and subsequent preservation, to early Lateglacial faulting at the Peel Boundary Fault Zone

7.8 Conclusions

The review, evaluation and application of concepts concerning the effects of faulting on river channel sinuosity in this study lead to the following conclusions:

- An increase of the valley floor gradient will, when circumstances are right, result in a higher sinuosity of the river channel for scroll-bar dominated meandering rivers. The relation between fault motions, river gradient and sinuosity is, however, not straightforward and should only be used in combination with a well-known tectonic, sedimentary and temporal framework.
- The distribution of vertical displacements along a fault zone should be taken into account when interpreting faulting related fluvial anomalies in the sedimentological or geomorphological record, as the distribution patterns of vertical deformation may vary spatially and temporally along fault zones.
- It is crucial to consider the morphodynamic response of an alluvial river to faulting as transient when interpreting the sedimentary record.
- The combination of physical scale experiments, numerical morphodynamic modelling and detailed field examples can provide a valuable contribution to our concepts of faulting induced changes in river dynamics and morphology as they complement each-other biases and limitations.

7.9 References

- › Adams, J. 1980. Active tilting of the United States midcontinent: geodetic and geomorphic evidence. *Geology*, 8, 442-446.
- › Aswathy, M. V., Vijith, H., Satheesh, R., 2008. Factors influencing the sinuosity of Pannagon River, Kottayam, Kerala, India: an assessment using remote sensing and GIS. *Environmental monitoring and assessment*, 138(1-3), 173-180.
- › Baker V., 1978. Adjustment of fluvial systems to climate and source terrain in tropical and subtropical environments. In: Miall, A.D. (Ed.), *Fluvial Sedimentology*, vol. 5. *Memoir-Canadian Society of Petroleum Geologists*, 211–230
- › Braudrick, C. A., Dietrich, W. E., Leverich, G. T., Sklar, L. S., 2009. Experimental evidence for the conditions necessary to sustain meandering in coarse-bedded rivers. *Proceedings of the National Academy of Sciences*, 106(40), 16936-16941.
- › Burbank, D. W., Anderson, R. S., 2012. *Tectonic geomorphology*. John Wiley & Sons.
- › Burnett, A. W., & Schumm, S. A., 1983. Alluvial-river response to neotectonic deformation in Louisiana and Mississippi. *Science*, 222(4619), 49-50.
- › Candel, J. H. J., Kleinhans, M.G., Makaske, B., Wallinga, J., 2020. Predicting river channel pattern based on stream power, bed material and bank strength. *Progress in Physical Geography: Earth and Environment*. 1(26), 1-26, <https://doi.org/10.1177/0309133320948831>
- › Camelbeeck, T., Vanneste, K., Alexandre, P., Verbeeck, K., Petermans, T., Rosset, P., Mazzotti, S., 2007. Relevance of active faulting and seismicity studies to assessments of long-term earthquake activity and maximum magnitude in intraplate northwest Europe, between the Lower Rhine Embayment and the North Sea. In: Stein, S., Mazzotti, S., (Eds.), *Continental Intraplate Earthquakes: Science, Hazard, and Policy Issues*, Special Paper 425, Geological Society of America, Boulder, Colorado, 193–224.
- › Dade, W., 2000. Grain size, sediment transport and alluvial channel pattern. *Geomorphology*, 35, 119–126.
- › Dykstra, S., 1988. The effects of tectonic deformation on laboratory drainage basins. Unpublished report, Colorado State University.
- › Gomez, B., Marron, D.C., 1991. Neotectonic effects on sinuosity and channel migration, Belle Fourche River, western South Dakota. *Earth Surface Processes and Landforms*, 16, 227-235
- › Holbrook, J., Schumm, S. A., 1999. Geomorphic and sedimentary response of rivers to tectonic deformation: a brief review and critique of a tool for recognizing subtle epeirogenic deformation in modern and ancient settings. *Tectonophysics*, 305(1-3), 287-306.
- › Holbrook, J., Autin, W. J., Rittenour, T. M., Marshak, S., Goble, R. J., 2006. Stratigraphic evidence for millennial-scale temporal clustering of earthquakes on a continental-interior fault: Holocene Mississippi River floodplain deposits, New Madrid seismic zone, USA. *Tectonophysics*, 420(3-4), 431-454.
- › Houtgast, R. F., Van Balen, R. T., Kasse, C., 2005. Late Quaternary evolution of the Feldbiss Fault (Roer Valley Rift System, the Netherlands) based on trenching, and its potential relation to glacial unloading. *Quaternary Science Reviews*, 24(3-4), 489-508.
- › Houtgast, R. F., Van Balen, R. T., Kasse, C., & Vandenberghe, J., 2003. Late Quaternary tectonic evolution and postseismic near surface fault displacements along the Geleen Fault (Feldbiss Fault Zone–Roer Valley Rift System, the Netherlands), based on trenching. *Netherlands Journal of geosciences*, 82(2), 177-196.

- › Jain, V., Sinha, R., 2005. Response of active tectonics on the alluvial Baghmata River, Himalayan foreland basin, eastern India. *Geomorphology*, 70(3-4), 339-356.
- › Jin, D. 1983. Unpublished report on experimental studies. Colorado State Univ., 15 pp.
- › Jin, D., Schumm, S.A., 1987. A new technique for modeling river morphology. In: Gardner, V. (Ed.), *International Geomorphology*. Wiley, Chichester, pp. 681-690.
- › Kim, W., Sheets, B. A., & Paola, C. (2010). Steering of experimental channels by lateral basin tilting. *Basin Research*, 22(3), 286-301.
- › Kleinhans, M. G., van den Berg, J. H., 2011. River channel and bar patterns explained and predicted by an empirical and a physics-based method. *Earth Surface Processes and Landforms*, 36(6), 721-738.
- › Ouchi, S., 1985. Response of alluvial rivers to slow active tectonic movement. *Geological Society of America Bulletin*, 96(4), 504-515.
- › Ouchi, S., 1983 Response of alluvial rivers to slow active tectonic movement. (Doctoral Dissertation, Colorado State University).
- › Parker, G., 2004. 1D sediment transport morphodynamics with applications to rivers and turbidity currents. E-book available at Gary Parker's Morphodynamics Web Page, last update April, 13, 2006.
- › Peakall, J., Ashworth, P. J., Best, J. L., 2007. Meander-bend evolution, alluvial architecture, and the role of cohesion in sinuous river channels: a flume study. *Journal of Sedimentary Research*, 77(3), 197-212.
- › Petrovski, J., Timár, G., 2010. Channel sinuosity of the Körös River system, Hungary/Romania, as possible indicator of the neotectonic activity. *Geomorphology*, 122(3-4), 223-230.
- › Petrovski, J., Székely, B., Timár, G., 2012. A systematic overview of the coincidences of river sinuosity changes and tectonically active structures in the Pannonian Basin. *Global and Planetary Change*, 98, 109-121.
- › Schumm, S. A., 1963. Sinuosity of alluvial rivers on the Great Plains. *Geological Society of America Bulletin*, 74(9), 1089-1100.
- › Schumm, S.A., Harvey, M.D., 1985. Preliminary geomorphic evaluation of the Sacramento River (Red Bluff to Butte Basin). Unpublished report to Sacramento District, Corps of Engineers, 57 pp.
- › Schumm, S. A., Dumont, J. F., Holbrook, J. M., 2002. *Active tectonics and alluvial rivers*. Cambridge University Press.
- › Schumm, S. A., Rutherford, I. D., Brooks, J., 1994. Pre-cutoff morphology of the lower Mississippi River. In *The variability of large alluvial rivers*. 13-44.
- › Smith, N. D., McCarthy, T. S., Ellery, W. N., Merry, C. L., Ruther, H., 1997. Avulsion and anastomosis in the panhandle region of the Okavango Fan, Botswana. *Geomorphology*, 20(1-2), 49-65.
- › Tal, M., Paola, C., 2010. Effects of vegetation on channel morphodynamics: results and insights from laboratory experiments. *Earth Surface Processes and Landforms*, 35(9), 1014-1028.
- › Timár, G., 2003. Controls on channel sinuosity changes: a case study of the Tisza River, the Great Hungarian Plain. *Quaternary Science Reviews*, 22(20), 2199-2207.
- › Vanneste, K., Camelbeeck, T., Verbeeck, K., Demoulin, A., 2018. Morphotectonics and past large earthquakes in Eastern Belgium. In: Demoulin, A. (Eds) *Landscapes and Landforms of*

- Belgium and Luxembourg. *World Geomorphological Landscapes*. (215-236). Springer, Cham. https://doi.org/10.1007/978-3-319-58239-9_13.
- › Van Balen, R.T., Bakker, M.A.J., Kasse, C., Wallinga, J. Woolderink, H.A.G., 2019. A Late Glacial surface rupturing earthquake at the Peel Boundary fault zone, Roer Valley Rift System, the Netherlands. *Quaternary Science Reviews*, 218, 254-266.
 - › Van den Berg, M., Vanneste, K., Dost, B., Lokhorst, A., Van Eijk, M., Verbeeck, K., 2002. Paleoseismic investigations along the Peel Boundary Fault: geological setting, site selection and trenching results. *Netherlands Journal of Geosciences*, 81(1), 39–60. <https://doi.org/10.1017/S0016774600020552>.
 - › Van Dijk, W. M., Teske, R., Van de Lageweg, W. I., Kleinhans, M. G., 2013. Effects of vegetation distribution on experimental river channel dynamics. *Water Resources Research*, 49(11), 7558-7574.
 - › Woolderink, H.A.G., Cohen, M.K., Kleinhans, M.G., Van Balen, R.T., 2021. Patterns in river channel sinuosity of the Meuse, Roer and Rhine rivers in the Lower Rhine Embayment rift system, are they tectonically forced? *Geomorphology*, 107550.
 - › Woolderink, H.A.G., Kasse, C., Cohen, K.M., Hoek, W.Z. Van Balen, R.T., 2018. Spatial and temporal variations in river terrace formation, preservation, and morphology in the Lower Meuse Valley, The Netherlands. *Quaternary Research*, 91(2), 548-569.
 - › Zámolyi, A., Székely, B., Draganits, E., Timár, G., 2010. Neotectonic control on river sinuosity at the western margin of the Little Hungarian Plain. *Geomorphology*, 122(3-4), 231-243.

Chapter 8

Conclusions and Synthesis

8.1 Summary of the main conclusions

This thesis aims to study the effects of faulting on the morphodynamics and morphology of alluvial meandering rivers. The combination of the exceptionally well known tectonic setting of the Lower Rhine Embayment rift system and palaeogeographic evolution of the Meuse river system is used as a natural laboratory for detailed case-studies. Palaeogeographic reconstructions and morphometric analyses reveal multiple tectono-morphological indicators in the study area. The numerical meander simulation model Nays2D is used to study the effects of various tectonic faulting scenarios on an alluvial meandering river to help better understand the processes that result in observed morphodynamic and morphological river responses. The conceptual models of numerical process-modelling and detailed case studies are combined to gain a better understanding of the effects of faulting on morphodynamic and morphological river response.

8.1.1 Morphological indicators of faulting from palaeogeographic reconstructions

8.1.1.1 *Meuse River*

- Terrace formation, preservation and morphology is reach-specific for the Lower Meuse river. Lateglacial terrace fragments are best preserved on the relative uplifting PB and VB downstream in the study area, owing to a combination of low gradients and channel-belt width reduction of the incisional reach traversing the PB. Lateglacial morphology is, on the other hand, poorly preserved in the RVG and on the CB, owing to a relatively high gradient and greater sediment supply, driving Holocene channels to erode them by lateral migration and avulsions.
- Longitudinal profiles of the Lateglacial Meuse river terraces show evidence for differential uplift.
- Local morphodynamic responses of the Meuse River, such as the Younger Dryas channel pattern change, Early Holocene avulsion and Late Holocene deflection are related to local displacements along the Feldbiss Fault Zone.
- The late Holocene course of the Meuse river shows a deflection from the area of maximum vertical deformation along the Feldbiss Fault Zone.

- Vertical displacement along the Peel Boundary Fault Zone during the early Lateglacial caused a transient response with sinuosity increase of the channel followed by channel cut-off, incision and terrace formation by lateral migration.
- Holocene channel belts are narrow with low-sinuosity to straight channel patterns on the uplifting PB and VB, while channel-belt activity occurred in a broader zone by channels of greater sinuosity in the RVG and the north of the CB.

8.1.1.2 Roer River

- Reach-to-reach variations in terrace formation and fluvial planform change are present in the Roer Valley. Such reach-specific phenomena can be attributed to variations in tectonic setting, subsurface lithology, base-level fluctuations or the confluence with tributary systems.
- A (lateral) response of the Roer River to tectonic vertical motions is concluded from (i) the preferred occupation of the northern Roer channel on the down-tilted side of the Roer Valley Graben, (ii) an “underfit” river system on the up-tilted side of the Roer Valley Graben, (iii) the presence of a distinct difference between soils in the up-tilted side (gley/ pseudo-gley) and those in the down-tilted side (gley-vega) of the Roer Valley Graben, (iv) an asymmetric position and clustering of Holocene channel belts along the Peel Boundary and Rurand fault zones, and (v) the (gradual) infill of a zone of subsidence around Rurich.
- The preferred occupation of the northern river course by the Roer in the lower Roer Valley during the Lateglacial and Holocene is caused by (i) differential subsidence within the Roer Valley Graben, (ii) climate-forced changes in precipitation, permafrost occurrence, vegetational cover and sediment supply, and (iii) base-level lowering of the Meuse River.

8.1.2 Morphometric indicators

- Tilt directions of the fault-bounded blocks of the Lower Rhine Embayment had a pronounced influence on the drainage pattern of the Meuse river catchment in this area by forcing streams to follow both the along strike and rotational tilt directions and by deflecting away from and into zones of (relative) uplift and subsidence respectively.
- The sinuosity of the early 19th century course of the Meuse river is (indirectly) controlled by tectonics on a block-scale as this determines the large-scale differences in valley gradient and subsurface lithology, and hence the erodibility of the river bed and banks.

- The early 19th century course of the Rhine River is not influenced by fault motions. Changes in sinuosity are mostly related to lithological differences, reduced incision rates and changes in bank height and composition. Changes in sinuosity of the Roer river are the result of a shift from a chute- to scroll-bar dominated meandering style along the river.
- The relation between fault motions, river gradient and sinuosity is not straightforward as sinuosity is also controlled by intrinsic fluvial dynamics, meandering style and because sinuosity varies over time.

8.1.3 Modelling the effects of tectonic deformations on alluvial river morphodynamics.

The following can be concluded from the numerical modelling study of the morphodynamic response(s) of a laboratory-scale alluvial channel to various faulting scenarios (i.e. instant vs gradual), offsets and fault locations;

- Relative subsidence of the downstream part of the river over a fault (footwall to hanging wall) leads to increased erosion of the river bed at the footwall and sedimentation on the hanging wall. Moreover, channel sinuosity increases as a result of the morphodynamic responses due to the faulting-induced enhanced valley gradient. Both the longitudinal and lateral adaptations are restricted to a zone around the fault and diminish both upstream and downstream.
- Relative uplift of the downstream part of the river over a fault (hanging wall to footwall) leads to reduced morphodynamic and morphological changes in front of the fault due to a developing backwater. The uplift results in (minor) thalweg incision and channel straightening downstream of the fault.
- Sinuosity increase as a response to faulting can continue to a maximum bend radius after which a (chute) cutoff will reduce channel sinuosity again.
- Abrupt faulting leads to faster morphodynamic and morphological responses of the river channel to the perturbation than gradual fault displacement
- The relative position within a meander bend at which faulting occurs has a profound influence on the time-progressive river channel sinuosity.
- Faulting can lead to a transient river response which should be considered in the interpretation of morphological and sedimentological observations.

8.2 Synthesis

Tectonics can force alluvial river morphodynamics on a range of spatial and temporal scales (Schumm et al., 2002). However, every tectonic forcing can, in essence, be reduced to changes in the balance between streampower and erosion resistance of the river bed and bank. Tectonic faulting leads to either an increase or decrease of gradient, and hence streampower, near a fault zone (Holbrook and Schumm, 1999; Schumm et al., 2002). When streampower increases, and the erosion resistance of river bed and bank remain unaltered, erosion will take place until the transport capacity of the river is reached. Especially the erosion at the outside of the meander bend is of importance for the lateral migration of a river channel. Scouring of the channel bed leads to increased bank heights which will collapse if stresses become too high (Hudson and Kesel, 2000). This bank erosion leads to lateral displacement of the channel and thus a sinuosity increase. It is, therefore, that an increased gradient due to tectonic faulting can lead to an enhanced sinuosity of the river channel, as was frequently observed in geomorphological records. Examples of this have been shown for rivers in the US (Missouri, Kansas, Illinois, Mississippi, Sacramento, Belle Fourche (south Dakota); Adams, 1980; Schumm and Harvey, 1985; Gomez and Marron, 1991; Schumm et al., 1994), the Tisza river (Timar, 2003) and its tributaries in the Pannonian basin (Zamolyi et al., 2010; Petrovski and Timar, 2010) and the Okavango Fan (Botswana; Smith et al., 1997). However, the above is only applicable for a certain range of streampowers and bed-load sediment size (i.e. scroll-bar dominated meandering rivers). If faulting changes the gradient at a fault zone to such an extent that the river crosses a threshold to a chute-cutoff dominated meandering, or even (weakly) braided, sinuosity may decrease instead of increase as a result of the faulting perturbation (Schumm et al. 2002; Woolderink et al., 2021). Moreover, if the rate of faulting is too high, vertical incision of the river bed will constrain lateral migration, and hence sinuosity, by the greater thickness of alluvial deposits that needs to be removed (Lewin and Macklin, 2003).

A decreased gradient as a result of faulting will generally lead to decreased morphological change (Ouchi, 1985; Holbrook and Schumm, 1999). Moreover, faulting can lead to a downstream elevated river bed that forms a depth constriction in the river channel, resulting in a change to non-uniform flow and geometry along the river.

A backwater can develop in response to such a situation. The backwater reduces flow velocity and thus morphodynamic and morphological change in the backwater reach. In this way a relative uplift of the downstream block of a normal fault can result in reduced morphological change of the river channel. Such a situation may even lead to enhanced (overbank) deposits or swamp development in the backwater reach (Holbrook and Schumm, 1999; c.f. Parker, 2004).

However, it was shown that, for example, the Baghmata river formed anomalous or compressed meanders in front of a fault zone in response to active faulting (Jain and Sinha, 2005). A similar observation was made for the Meuse River. Here an Allerød meander at the Peel Boundary Fault Zone near Roermond has an anomalously high sinuosity and has locally migrated in upstream direction. The most likely scenario for the formation of this meander is that sedimentation in the backwater reach, that formed in response to faulting, caused enhanced lateral displacement of the river channel. Sedimentation in the river channel leads to bar formation which can cause flow to be directed to the outer bank of a river channel and hence lead to bank erosion, lateral displacement and sinuosity increase.

The situations above assume no lithological change of river bed and banks over a fault zone. This is, however, an oversimplification of the natural situation. Faulting will, for example, often juxtapose different lithologies, which means different erosive resistance of river bed and banks, on either side of the fault zone(s). For instance, it was shown in experimental studies that the transition from an easily erodible lithology (e.g. sand and gravel) to a more erosive resistant lithology like clay, will also lead to compressed and highly sinuous meanders upstream of the lithological transition (Jin, 1983; Jin and Schumm, 1987). Such a situation could also occur in nature, due to juxtaposition as a result of faulting. Although a lithological transition occurs at the Peel Boundary Fault Zone, it is unlikely that this will have had a major influence in the formation of the compressed Allerød meander, as lithological transects show that the juxtaposed lithologies were, at that time, most probably below the base of the river channel. Juxtaposition due to faulting did, however, play a role in case of the Meuse River on a more regional scale, as it has led to a reach-specific morphological evolution of the river channel and floodplain in other areas. With this the example of the Meuse River shows that faulting can form a passive control on river morphodynamics and morphology (Woolderink et al., 2018).

The anomalous meander near Roermond does also show the importance of preservation potential when considering the morphodynamic and morphological response(s) of rivers to faulting. Over time lateral channel migration, incision, aggradation and other subsequent river activity will determine the preservation potential of alluvial units (Lewin and Macklin; 2003). Lateral migration will, for example, decrease the preservation potential of an initial morphodynamic response while incision might lead to isolation, and hence increased preservation, of the same response of the river to faulting. The latter resulted in the preservation of the transient response of the anomalous meander near Roermond.

Besides the longitudinal changes in gradient, faulting can also lead to a predominantly lateral directed gradient change, and thus river response, if a river flows parallel to the fault zone. The most common responses to such a lateral tilting of the floodplain are avulsion (sudden change of the river channel to a new course over the floodplain) and combing (i.e. slow migration by preferential downslope erosion and meander cutoff to the downthrown part of the floodplain [Leeder and Alexander, 1987; Leeder and Gawthorpe, 1987]). The former was observed for the early Lateglacial Roer River in the study area (Woolderink et al., 2019).

Overall this study shows that tectonics can both actively and passively force river morphodynamics and morphology. It is, therefore, important to consider faulting not only as a constant external forcing factor but also recognize the potential short-term and local effects on river dynamics. The effects of faulting on river morphodynamics and morphology are, however, complex as they depend on numerous local, non-tectonic, characteristics of flow, river bed/bank and vegetation cover as well. Sinuosity change as an indicator of tectonic motions can hence only be used in combination with a well-known tectonic and sedimentary framework. The absence of a sinuosity change does not imply inactivity of the fault at geological time-scales. On the other hand, a deviating sinuosity value is no proof for fault activity. Moreover, slip distribution along the fault zone should be incorporated when interpreting faulting related fluvial anomalies in the sedimentological or geomorphological record as non-uniform slip distributions along faults may influence local gradients.

8.3 Future research

Although the potential effects of tectonic vertical motions on river morphodynamics and morphology is already a well-studied subject, significant progress can still be made, especially in the effects of local gradient deformations at fault zones due to differential distribution of vertical displacement. This can best be done by combining field-examples with numerical and physical modelling. Numerical modelling of tectonic faulting and river response can be improved by including mixed-load sediment types and the effects of juxta-position. Extending numerical models to account for differential vertical displacement distribution and local effects of surface rupturing seismic faulting such as river bank collapse, sand-boils and fluidisation processes may improve our ability to model river responses to faulting more accurately. The conceptual models that were derived from the physical scale experiments of tectonic deformation and alluvial rivers in the past decades may benefit from more recent advances in physically modelling (meandering) river systems. Including both cohesive (floodplain) sediments and vegetation in the physical flume models may lead to a better representation of natural processes. The physical scale experiments may be extended by performing actual (normal) faulting scenarios instead of the previous doming experiments, as faulting may influence river dynamics in a significantly different way than doming, due to its local and instant nature. Simulating the effects of both instant and gradual faulting in flume experiments may provide additional knowledge about the effects of faulting on river morphodynamics and morphology, as was demonstrated for the numerical model study in this dissertation. Considering field studies, it is important to perform a thorough study of the sedimentary, vegetational and anthropogenic setting as these factors should be omitted as a forcing factor for (local) fluvial anomalies in the geomorphic and sedimentary record. Overall, combining field-studies, numerical modelling and physical experiments may improve our understanding of the effects of tectonic forcing on alluvial dynamics as they complement each-other biases and limitations.

8.4 References

- › Adams, J., 1980. Active tilting of the United States midcontinent: geodetic and geomorphic evidence. *Geology* 9, 442–446.
- › Gomez, B., Marron, D.C., 1991. Neotectonic effects on sinuosity and channel migration, Belle Fourche River, western South Dakota. *Earth Surface Processes and Landforms* 16, 227–235.
- › Holbrook, J., Schumm, S.A., 1999. Geomorphic and sedimentary response of rivers to tectonic deformation: a brief review and critique of a tool for recognizing subtle epeirogenic deformation in modern and ancient settings. *Tectonophysics* 305 (1–3), 287–306.
- › Holbrook, J., Schumm, S.A., 1999. Geomorphic and sedimentary response of rivers to tectonic deformation: a brief review and critique of a tool for recognizing subtle epeirogenic deformation in modern and ancient settings. *Tectonophysics* 305 (1–3), 287–306.
- › Hudson, P. F., Kesel, R. H., 2000. Channel migration and meander-bend curvature in the lower Mississippi River prior to major human modification. *Geology*, 28(6), 531-534.
- › Jain, V., Sinha, R., 2005. Response of active tectonics on the alluvial Baghmati River, Himalayan foreland basin, eastern India. *Geomorphology* 70 (3–4), 339–356.
- › Jin, D. 1983. Unpublished report on experimental studies. Colorado State Univ., 15 pp.
- › Jin, D., Schumm, S.A., 1987. A new technique for modeling river morphology. In: Gardner, V. (Ed.), *International Geomorphology*. Wiley, Chichester, pp. 681-690.
- › Leeder, M. R., Alexander, J. A. N., 1987. The origin and tectonic significance of asymmetrical meander-belts. *Sedimentology*, 34(2), 217-226.
- › Leeder, M. R., Gawthorpe, R. L., 1987. Sedimentary models for extensional tilt-block/half-graben basins. *Geological Society, London, Special Publications*, 28(1), 139-152.
- › Lewin, J., Macklin, M. G., 2003. Preservation potential for Late Quaternary river alluvium. *Journal of Quaternary Science: Published for the Quaternary Research Association*, 18(2), 107-120.
- › Ouchi, S., 1985. Response of alluvial rivers to slow active tectonic movement. *Geol. Soc. Am. Bull.* 96 (4), 504–515.
- › Parker, G., 2004. 1D sediment transport morphodynamics with applications to rivers and turbidity currents. E-book available at Gary Parker’s Morphodynamics Web Page, last update April, 13, 2006.
- › Petrovski, J., Székely, B., Timár, G., 2012. A systematic overview of the coincidences of river sinuosity changes and tectonically active structures in the Pannonian Basin. *Global and Planetary Change*, 98, 109-121.
- › Schumm, S.A., Harvey, M.D., 1985. Preliminary geomorphic evaluation of the Sacramento River (Red Bluff to Butte Basin). Unpublished report to Sacramento District. Corps of Engineers, p. 57.
- › Schumm, S.A., Rutherford, I.D., Brooks, J., 1994. Pre-cutoff morphology of the lower Mississippi River. In: Schumm, S.A., Winkley, B.R. (Eds.), *The Variability of Large Alluvial Rivers*. American Society of Civil Engineers Press, New York, pp. 13–44.
- › Schumm, S. A., Dumont, J. F., Holbrook, J. M., 2002. *Active tectonics and alluvial rivers*. Cambridge University Press.
- › Smith, N.D., McCarthy, T.S., Ellery, W.N., Merry, C.L., Rütger, H., 1997. Avulsion and anastomosis in the panhandle region of the Okavango Fan, Botswana. *Geomorphology* 20, 49–65.

- › Timár, G., 2003. Controls on channel sinuosity changes: a case study of the Tisza River, the Great Hungarian Plain. *Quaternary Science Reviews*, 22(20), 2199-2207.
- › Woolderink, H.A.G., Cohen, M.K., Kleinhans, M.G., Van Balen, R.T., 2021. Patterns in river channel sinuosity of the Meuse, Roer and Rhine rivers in the Lower Rhine Embayment rift system, are they tectonically forced? *Geomorphology*, 107550.
- › Woolderink, H. A. G., Kasse, C., Grooteman, L. P. A., Van Balen, R. T., 2019. Interplay between climatic, tectonic and anthropogenic forcing in the Lower Rhine Graben, the Roer River. *Geomorphology*, 344, 25-45.
- › Woolderink, H.A.G., Kasse, C., Cohen, K.M., Hoek, W.Z. Van Balen, R.T., 2018. Spatial and temporal variations in river terrace formation, preservation, and morphology in the Lower Meuse Valley, The Netherlands. *Quaternary Research*, 91(2), 548-569.
- › Zámolyi, A., Székely, B., Draganits, E., Timár, G., 2010. Neotectonic control on river sinuosity at the western margin of the Little Hungarian Plain. *Geomorphology* 122 (3-4), 231–243.

Summary

Rivers tend to maintain a gradient that is more or less constant, and that fits the discharge and sediment supply of that river. Vertical motions along normal faults in the subsurface can, temporarily, alter this gradient of the river. This can occur on the relatively large scale of tectonic blocks (>5 km), or on a the more locale scale of fault zones. The altered gradient of the river leads to adaption processes in the river channel in order to restore the faulting induced change in gradient. Such responses to normal faulting range from longitudinal bed profile adjustments to channel pattern changes. One of the commonly observed responses is a change in sinuosity of the river channel. Via changes in the amount and size of the individual meander loops, the river channel is presumed to dynamically alter its channel length in such a way that the channel gradient remains unchanged despite the tectonic tilting. Numerous field examples show that an increase of valley floor gradient results in increased sinuosity of the river channel or vice versa. However, sinuosity changes and erosion and sedimentation patterns in meandering rivers depend on many more factors than faulting alone. These different forcing factors can operate simultaneously, making disentanglement of the effects of the different forcing factors difficult. The proposed relationships between tectonics and meandering remain to a large extent hypothetical due to a lack of physical modeling, and because of the small number of detailed case studies that are able to disentangle the different forcing factors. In addition, the hypothetical meandering river responses are based on block-wise tectonic motions (e.g. tilting of fault-bounded blocks, doming) and do not include local tectonic movements, at and near the fault trace.

The aim of this research is to unravel the morphodynamic and morphological response(s) of alluvial rivers to faulting induced vertical motions. Both case study's and numerical modelling will be used to achieve this aim. Because both the Meuse and the Roer river flow through the tectonically active Roer Valley Rift System, whose tectonic activity is exceptionally well known, and these river have formed a series of relatively well-preserved remnants of former river plains (river terraces) in the past circa 50.000 years, this in an ideal study area to investigate how river dynamics are influenced by faulting.

The objectives are to; i) Reconstruct the palaeogeographic evolution of the downstream part of the Meuse and Roer rivers in order to disentangle the influence of climatic, tectonic and anthropogenic forcings on river morphodynamics and morphology, ii) Determine the relation(s) between (transient) morphodynamic river response and tectonic movements at different spatial scales (fault-bounded blocks and faults) and on long and short (earthquake) time-scales, using the Meuse-Roer river system and Roer Valley Rift System (RVRS) data on river morphology and fault activity, iii) Use a numerical meander simulation model (Nays2D) to study the effects of various tectonic deformation rates and styles along normal fault zones on alluvial meandering river

morphodynamics and morphology, and test the conceptual models based on the reconstructions.

The reconstruction of the palaeogeographic development of the Meuse River has led to the insight that the development and preservation of river terraces varies greatly along the length profile of the river. These reach-specific characteristics of the river terraces of the Meuse are determined by the faulted subsurface. The different tectonic blocks cause regional differences in the gradient of the Meuse, and in the lithological composition of the subsurface. The latter has effects on the extent to which the Meuse can move laterally or incise vertically. This balance between lateral displacement and vertical incision is also influenced by the relative uplift or subsidence of the various tectonic blocks, with the Meuse mainly incising into the relatively uplifting blocks. In general, the Late Glacial (~14,700 – 11,700 years ago) terrace fragments of the Meuse are predominantly preserved on the Peel-Block and on the Venlo-Block. The younger, Holocene, terrace remnants on these tectonic blocks are relatively limited in extent compared to the Campine-Blok and the Roer Valley Graben, where the Holocene deposits cover a wide plain. Sinuosity analysis of the 19th century course of the Meuse River has shown that there are also clear differences in the sinuosity of the river channel across the different tectonic blocks. These can also be explained by differential subsidence which, among other things, cause differences in gradient and composition of the subsurface.

The reconstructions of the Meuse River also show that differential subsidence on the scale of individual fault zones has had an important influence on the dynamics of the Meuse. River terraces from the Younger Dryas (~12,900 to 11,700 years ago) at the Feldebiss fault zone, for example, show a meandering river pattern while the terraces both upstream and downstream mainly show a braiding river pattern. The early Holocene (~11,700-10,000 years ago) river terraces show an avulsion of the Meuse river channel just downstream of the Feldebiss fault zone. This avulsion is the result of local sedimentation on the downstream side of the fault zone. Late Holocene (younger than 3000 years) Meuse deposits show that the river channel upstream of the Feldebiss fault zone has moved mainly in a north-easterly direction. The most likely explanation for this is a difference in the amount of vertical movement along the different segments of the Feldebiss fault zone. Palaeoseismological research has shown that vertical movements occurred mainly along the western segments of the Feldebiss fault zone, and much less in the eastern edge of this part of the Meuse valley. This lead to a gradient advantage towards the northeast, after which the river channel of the Meuse River has (gradually) moved in this direction.

Another exceptional situation occurs at the Peel Boundary Fault Zone near Roermond. At this location an "abnormal" meander has formed just upstream of the fault zone. The meander is abnormal because it has a very high sinuosity and even (briefly) migrated in upstream direction, while all other meanders from this period show a downstream

migration. This characteristic meander has formed as a result of vertical movements along the Peel Boundary Fault Zone during severe earthquakes at the beginning of the Late Glacial. During this time, the surface along the fault, and therefore also the bottom of the Maas channel, has moved by approximately 1 meter. This offset has had important consequences for the flow in the river channel. It influenced the sedimentation patterns in the river channel and, hence, also the sinuosity of the river. By temporarily increasing the sinuosity of the river channel, and locally eroding and depositing sediments, the Meuse River adapted to the faulting induced change in gradient, after which the Meuse River was able to recover to its 'normal' dynamics.

The development of the Roer River, a tributary of the Meuse that flows into the Meuse near Roermond, has also clearly been influenced by differential subsidence in the Roer Valley Rift System. The Roer River runs more or less parallel to the strike of the Peel Boundary Fault Zone. At the time of the increased fault activity and the relatively large offset along the Peel Boundary Fault Zone at the beginning of the Late Glacial, the downstream part of the Roer consisted of two courses, with the bifurcation point just across the border with Germany. Because vertical movements, as a result of the heavy earthquake (s), were predominantly along the Peel Boundary Fault Zone and not (or to a much lesser extent) along the southern boundary fault zone (Beegden fault zone), a gradient advantage developed to the north in the Roer Valley Graben. As a result, the discharge in the northern course of the Roer increased, while it decreased in the southern (now higher elevated) course. Consequently, the southern course of the Roer River was abandoned during the early Late Glacial and has subsequently been preserved in the landscape as a fossil river plain.

In addition to the aforementioned reconstructions, this research also used a numerical meander simulation model (Nays2D) to study the effects of different styles and rates of fault displacement on river dynamics, and to test the conceptual models obtained from the reconstructions and existing literature. Modelling results show that the sinuosity of a meandering river channel increases with a transition from a relatively uplifting tectonic block to a subsiding block. This can be explained by the fact that the increased gradient results in a faster flow, which erodes strongly, especially in the outer bends of a river channel. This causes the outer banks of the river channel to collapse, causing the channel to migrate laterally and thus increasing the sinuosity of the river at the fault zone. This effect mainly takes place in a limited zone around a fault, approximately within the distance of 2 meander wavelengths. An increase in fault offset leads to an increase of the river channel sinuosity. However, when the sinuosity increase has reached a critical value, a decrease of the sinuosity will often take place due to a so-called 'chute cutoff'. The gradient over the inner bend of the river meander has been increased by the sinuosity increase to such an extent that the water flows over the inner bend during high discharges. This erodes sediments of the inner meander bend, creating a new channel with a more direct route along the valley axis, which reduces the sinuosity. The model scenarios show

that the sinuosity of the river channel after the cut off is often still higher than in the initial situation, before the vertical displacement at the fault.

In the opposite situation, simulating a transition from a subsiding tectonic block to an uplifting block, the model outputs show a different trend. River dynamics upstream of the fault decrease in these cases. The decrease in dynamics in a zone before the fault can be explained by the backwater effect that forms in response to the faulting perturbation. Flow velocity decreases in this backwater reach. In turn, this reduces erosion and can even lead to sedimentation if the sediment load of the river is too high for the discharge. These factors hamper the lateral dynamics of the river channel.

Finally, the influence of the relative position of a fault along a meander bend was modelled to study a possible differential morphodynamic response. Results show that the different positions of the fault lead to a similar end result. However, substantial differences are observed for the time-progressive evolution. For example, a fault at the so-called "apex" of a meander bend causes a chute cutoff to take place relatively quickly after the initial increase of the sinuosity, which reduces the sinuosity again. This is caused by the fact that a large part of the flow is directed over the inner meander bend during high discharges. The scenario in which the position of the fault causes a faster flow towards the relatively erosion resistant outer bend results in a longer period of sinuosity increase. This situation persists until the point is reached when the curvature of the bend causes such a gradient advantage over the pointbar that here too the flow takes the shortcut over inner bend.

When the results of the reconstructions and numerical modelling are combined, it appears that the effects of faulting on river dynamics, and sinuosity in particular, are not unambiguous. On a local scale, a river channel will often show an increase in sinuosity in response to the faulting induced increased gradient. This is, however, only the case if the threshold to a chute cutoff, or even braiding river type, is not reached. In addition, other factors such as river bed / bank strength, vegetation cover and sediment type also play an important role in the sinuosity of a river channel. In short, a sinuosity anomaly can only be used as an indicator for faulting when the influence of other, non-tectonic, factors at that location are also known. The absence of a sinuosity change does not imply inactivity of the fault at geological time-scales, nor is a deviating sinuosity value proof of fault activity.

It can also be concluded that vertical movements along faults can indirectly force river dynamics on a larger, block scale. This is because they cause differences in the subsurface lithology and can also influence the large-scale gradients of tectonic blocks. The combination of detailed reconstructions that allow unravelling of the effects of faulting in relation to other factors, and the use of a numerical simulation model have shown that inclusion of process-based reasoning in the interpretation of

geomorphological and sedimentological observations of fluvial response to faulting improves our understanding of the natural processes involved and, therefore, contributes to better prediction of faulting effects on river morphodynamics.

Finally, it can be concluded that tectonics should not only be seen as a constant, continuous and large-scale forcing on river dynamics, but that vertical motions along fault zones are also an important forcing factor on river dynamics on local and short time scales.

Samenvatting

Rivieren stromen over het algemeen met een zo constant mogelijk gradiënt die past bij de waterafvoer en sedimenttoevoer van de rivier. Verticale verplaatsingen langs breuken in de ondergrond zorgen ervoor dat de steilte van de gradiënt van een rivier (tijdelijk) wordt veranderd. Dit kan plaatsvinden op een relatief grote schaal van tektonische blokken (> 5 km), of een meer lokale schaal van breukzones. Als een reactie op de veranderde gradiënt vinden er processen plaats in de riviergeul, die ervoor zorgen dat de oorspronkelijke gradiënt zoveel mogelijk wordt hersteld. Dit kan variëren van (lokale) erosie en afzetting van sedimenten in de geul van de rivier, maar kan ook leiden tot een veranderend rivierpatroon. Eén van de meest voorkomende aanpassing is dat het bochtige karakter van de riviergeul (sinuositeit) verandert. Door een verandering van de sinuositeit wordt de lengte van de riviergeul ten opzichte van een vaste afstand langs de as van een rivier, verlengd (hogere sinuositeit) of verkort (lagere sinuositeit). Op deze manier kan de oorspronkelijke gradiënt ook gedeeltelijk hersteld worden. Dat dit proces plaatsvindt is al geruime tijd bekend uit verschillende voorbeelden in riviersystemen wereldwijd. Echter, veranderingen in sinuositeit en erosie- en sedimentatiepatronen binnen rivier systemen zijn ook afhankelijk van vele andere, niet tektonische factoren. Doordat deze factoren vaak simultaan optreden is het moeilijk om de effecten van de verschillende sturende factoren uit elkaar te halen. Tevens zijn de huidige ideeën over de effecten van verticale breukbewegingen op rivieren voor een groot deel hypothetisch. Dit komt door een gebrek aan gedetailleerde studies waarbij de verschillende forcerende factor onderscheiden kunnen worden en het ontbreken van het gebruik van (geschikte) numerieke modellen. Verder beperken deze theorieën zich veelal tot grootschalige veranderingen in riviergedrag (tektonische blokken) en worden de lokale effecten, op de schaal van individuele breukzones, niet meegenomen.

Het doel van dit onderzoek is om de effecten van verticale bodembewegingen langs breuken op rivierdynamiek beter te begrijpen en te kwantificeren. Hiervoor wordt gebruik gemaakt van veldstudies en numeriek modellering. Omdat zowel de rivier de Maas als de Roer door het tektonisch actieve Roer Valley Rift System stromen, waarvan de tektonische activiteit uitzonderlijk goed bekend is, en deze rivieren een serie van relatief goed bewaarde restanten van een vroegere riviervlaktes (rivierterrassen) hebben gevormd in de afgelopen circa 50.000 jaar, is dit een ideaal studiegebied om te onderzoeken hoe rivierdynamiek wordt beïnvloed door breuken en bodembewegingen in de ondergrond.

De doelstellingen van het onderzoek zijn: i) De palaeogeografische ontwikkeling van het benedenstroomse deel van de rivier de Maas en de Roer te reconstrueren om zo de invloeden van klimatologische, tektonische en menselijke factoren op rivierdynamiek te

ontrafelen, ii) Het bepalen van de effecten van bodembewegingen op rivierdynamiek op verschillende ruimtelijke en temporele schalen door gebruik te maken van de uitgebreide dataset van de rivieren Maas en Roer en het tektonische riftgebied van de ‘Roer Valley Rift System’, iii) Het gebruik maken van een numeriek meandersimulatiemodel (Nays2D) om de effecten van verschillende vormen en snelheden van breukverplaatsing op rivierdynamiek te bestuderen en zo de bestaande en ontwikkelde conceptuele modellen te testen.

De reconstructie van de palaeogeografische ontwikkeling van de Maas heeft tot het inzicht geleid dat het ontstaan en de preservatie van rivierterrassen sterk varieert over het lengteprofiel van de rivier. Deze ‘reach-specific’ kenmerken van de rivierterrassen van de Maas worden bepaald door de tektonische structuur van de ondergrond. De verschillende tektonische blokken zorgen voor regionale verschillen in de gradiënt van de Maas, en in de samenstelling van de ondergrond. Dit laatste heeft een weerslag op de mate waarin de Maas zich zijdelings kan verplaatsen of juist verticaal insnijdt. Deze balans tussen zijdelingse verplaatsing en verticale insnijding wordt tevens beïnvloed door het relatief omhoogkomen of dalen van de verschillende tektonische blokken, waarbij de Maas zich vooral in de relatief omhoogkomende blokken heeft ingesneden. In het algemeen zijn de Laatglaciale (~14.700-11.700 jaar geleden) terrasfragmenten van de Maas het best bewaard gebleven op het Peel-Blok en op het Venlo-Blok. De jongere, Holocene, afzettingen zijn op deze tektonische blokken relatief beperkt in oppervlakte vergeleken met het Kempisch-Blok en de Roerdalslenk, waar de Holocene afzettingen een brede vlakte beslaan. Uit analyse van de sinuositeit van de 19^e -eeuwse loop van de Maas is gebleken dat er ook duidelijke verschillen zijn in de mate van het bochtige karakter van de riviergeul over de verschillende tektonische blokken. Ook deze kunnen verklaard worden door relatieve bodembewegingen die onder andere zorgen voor verschillen in gradiënt en samenstelling van de ondergrond.

De reconstructies van de dynamiek van de Maas laten ook zien dat bodembewegingen op de schaal van individuele breukzones een belangrijke invloed hebben gehad op de dynamiek van de Maas. Rivierterrassen uit het Jonge Dryas (~12.900 tot 11.700 jaar geleden) bij de Feldbiss breukzone laten bijvoorbeeld een meanderend rivierpatroon zien terwijl zowel bovenstrooms als benedenstrooms terrassen uit deze tijd voornamelijk een vlechtend rivierpatroon hebben. Tevens heeft er net benedenstrooms van de Feldbiss breukzone aan het begin van het Holoceen (~11.700-10.000 jaar geleden) een verlegging van de riviergeul van de Maas plaatsgevonden. Deze zogenaamde avulsie is het gevolg geweest van lokale sedimentatie aan de benedenstroomse zijde van de breukzone. Afzettingen van de Maas rond de Feldbiss breukzone uit het late deel van het Holoceen (jonger dan 3000 jaar geleden) laten zien dat de rivier zich bovenstrooms van de breukzone voornamelijk in noordoostelijke richting heeft verplaatst. De meest aannemelijke verklaring voor deze observatie is een verschil in de mate van verticale bodembeweging langs de Felbiss breukzone. Uit palaeoseismologisch onderzoek is

gebleken dat er voornamelijk beweging heeft plaatsgevonden langs de westelijke segmenten van de Feldebiss breukzone, en veel minder aan de oostelijke rand van dit deel van de Maasvallei. Dit zorgt ervoor dat er een gradiënt voordeel is ontstaan richting het noordoosten, waarna de geul van de Maas (geleidelijk) in deze richting is verplaatst.

Een andere uitzonderlijke situatie doet zich voor bij de Peelrand breukzone nabij Roermond. Hier heeft zich een 'abnormale' meander gevormd bovenstrooms van de breukzone. De meander is afwijkend omdat deze een erg hoge sinuositeit heeft en zelfs (kortstondig) in bovenstroomse richting heeft gemigreerd terwijl alle andere meanders uit deze periode zich juist benedenstrooms verplaatsten. Deze kenmerkende meander heeft zich gevormd als gevolg van verticale bewegingen langs de Peelrand breukzone, die ontstaan zijn als gevolg van zware aardbevingen langs deze breukzone aan het begin van het Laatglaciaal. In deze tijd is het oppervlak langs de breuk, en dus ook de bodem van de Maasgeul, met circa 1 meter verzet. Dit verzet heeft belangrijke gevolgen gehad voor de stroming in de rivier, welke doorwerken in de sedimentatie in de riviergeul en hierdoor ook de sinuositeit van de rivier beïnvloeden. Door de sinuositeit van de loop tijdelijk te vergroten en plaatselijk sedimenten te eroderen en af te zetten heeft de Maas zich aangepast aan de veranderde gradiënt als gevolg van de beving(en), waarna de loop van de Maas zich kon herstellen naar haar 'normale' dynamiek.

De ontwikkeling van de rivier de Roer, een zijrivier van de Maas, die nabij Roermond in de Maas uitkomt, heeft ook een duidelijke invloed ondervonden van differentiële bodembewegingen in het Roer Valley Rift System. De Roer loopt min of meer parallel aan de strekking van de Peelrand breukzone. Ten tijde van de toegenomen activiteit en het relatief grote verzet langs de Peelrand breukzone aan het begin van het Laatglaciaal bestond de benedenstroomse deel van de Roer uit twee lopen, waarbij het splitsingspunt (bifurcatie) net over de grens met Duitsland lag. Doordat er wel bodembewegingen optraden als gevolg van de zware beving(en) langs de Peelrand breukzone en niet (of in veel mindere mate) langs de zuidelijke begrenzende breukzone (Beegden breukzone), ontstond er een gradiënt voordeel naar het noorden in de Roerdalslenk. Als gevolg hiervan is de afvoer in de noordelijke loop van de Roer toegenomen terwijl deze in de zuidelijke (nu hoger gelegen) loop juist afnam. Op deze manier is de zuidelijke loop van de Roer ten tijde van het vroege deel van het Laatglaciaal verlaten en is deze afgedankte loop als een fossiele rivierlakte achtergebleven in het landschap.

Naast de genoemde reconstructies is er voor dit onderzoek ook gebruik gemaakt van een numeriek meandersimulatiemodel (Nays2D) om de effecten van verschillende vormen en snelheden van breukverplaatsing op rivierdynamiek te bestuderen en om de conceptuele modellen opgedaan uit de reconstructies en bestaande literatuur te testen. Resultaten van de modellering laten zien dat de sinuositeit van een meanderende riviergeul toeneemt bij een overgang van een relatief omhoogkomend tektonisch blok naar een dalend blok. Dit is te verklaren doordat de toegenomen gradiënt zorgt voor een

snellere stroming, die vooral in de buitenbochten van een riviergeul sterk eroderend is. Hierdoor bezwijken de buitenste banken van de riviergeul, waardoor de geul in de loop van de tijd zijdeling migreert en zo de sinuositeit van de rivier rond de breukzone toeneemt. Wat opvalt uit de modellering is dat dit effect voornamelijk plaatsvindt in een beperkte zone rond een breuk, circa binnen de afstand van 2 riviermeanderlengtes. Naarmate het verzet langs de breuk wordt vergroot neemt de mate van sinuositeitverandering toe. Echter, wanneer de sinuositeittoename een kritieke waarde heeft bereikt zal er na verloop van tijd veelal weer een afname van de sinuositeit plaatsvinden door een zogenaamde ‘chute cutoff’. Hierbij is de gradiënt over de binnenbocht van de riviermeander, door de sinuositeittoename, dusdanig vergroot dat het water tijdens hoge afvoeren over de binnenbocht stroomt en hier sedimenten erodeert en er zo een nieuwe geul ontstaat met een kortere route langs de vallei-as, waardoor de sinuositeit weer afneemt. De model scenario’s laten zien dat de sinuositeit van de riviergeul na afsnijding door deze chute cutoffs veelal nog wel hoger is dan in de beginsituatie voordat de bodembeweging heeft plaatsgevonden.

In de omgekeerde situatie, waarbij er een rivierpassage van een dalend tektonisch blok naar een omhoogkomend blok wordt gesimuleerd, laten de modelberekeningen een andere trend zien. In deze gevallen neemt de rivierdynamiek bovenstrooms van de breuk juist af. Deze afname van dynamiek in een zone voor de breuk is te verklaren door de opstuwende werking van het water in de rivier dat een verzet langs een breuk in deze situatie veroorzaakt. Door de stuwende werking neemt de stroomsnelheid van het water in de riviergeul voor de breuk af. Een afname van de stroomsnelheid zorgt voor een gereduceerde mate van erosie, en kan zelfs voor sedimentatie zorgen als de sedimentlast van de rivier te hoog is voor de afvoer, waardoor de (zijdelingse) dynamiek van de rivier ook afneemt in deze zone.

Als laatste is de invloed van de relatieve positie van een breuk binnen een riviermeanderbocht op de dynamiek onderzocht in de numerieke modelstudie. Hieruit blijkt dat de simulaties met verschillende breuklocaties leiden tot een vergelijkbaar eindresultaat, maar dat het verloop van de aanpassing aan de bodembeweging langs de breuk wel heel verschillend verloopt. Zo zorgt een breuk aan de zogenaamde ‘apex’ van een meanderbocht ervoor dat er na de initiële toename van de sinuositeit relatief snel een chute cutoff plaatsvindt die de sinuositeit weer reduceert. Dit komt doordat veel van de stroming tijdens hoge afvoeren over de binnenbocht wordt gestuurd. Het scenario waarbij de positie van de breuk zorgt voor een snellere stroming richting de relatief erosiebestendige buitenbocht zorgt voor een langere periode van sinuositeittoename, totdat het punt bereikt wordt dat de kromming van de bocht voor een dusdanig gradiëntverschil zorgt dat ook hier de stroming de kortere weg over de meanderbocht neemt.

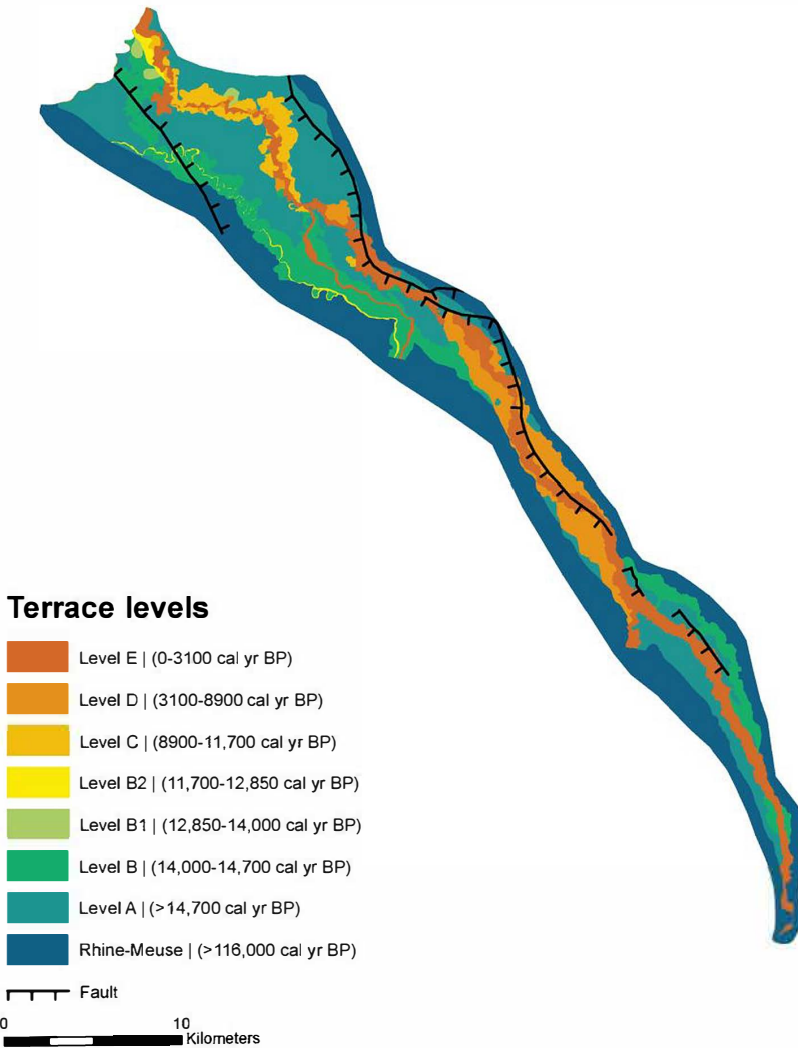
Wanneer de resultaten van de reconstructies en numerieke modellering worden samengenomen blijkt dat de effecten van bodembewegingen langs breuken op rivierdynamiek, en sinuositeit in het bijzonder, niet eenduidig zijn. Op lokale schaal zal een riviergeul veelal een toename in sinuositeit laten zien als reactie op de toegenomen gradiënt, maar dit is alleen het geval als het kritieke omslagpunt naar een chute-cutoff, of zelfs vlechtend riviertype, niet wordt bereikt. Daarbij komt ook dat andere factoren zoals geulbedding- en oeversterkte, vegetatiebedekking en sedimenttype ook een belangrijke rol spelen bij riviersinuositeit. Kortom, een sinuositeit anomalie kan alleen als een indicator voor tektonische bodembewegingen gebruikt worden, wanneer de invloed van andere, niet-tektonische, factoren op die locatie ook bekend zijn. Een afwijkende sinuositeit is geen direct bewijs voor activiteit van een breuk, en een afwezigheid van een sinuositeit anomalie is geen zekere indicatie voor inactiviteit van een breuk op geologische tijdschaal.

Verder kan geconcludeerd worden dat bewegingen langs breuken in de ondergrond rivierdynamiek op grotere schaal indirect kunnen forceren. Dit komt doordat ze voor verschillen in de samenstelling van de ondergrond zorgen en ook de grootschalige gradiënt kunnen beïnvloeden. De combinatie van gedetailleerde reconstructies, die het ontrafelen van de effecten van een tektonische component ten opzichte van andere sturende factoren mogelijk maken, en het gebruik van een numeriek simulatiemodel hebben laten zien dat het meenemen van procesmatig-gebaseerde redenering in de interpretatie van geomorfologische archieven een belangrijke toevoeging kan vormen voor onze ideeën over de invloed van bewegingen langs breuken op rivierdynamiek. Tenslotte is gebleken dat tektoniek niet alleen gezien moet worden als een constante, continue en grootschalige forcering op rivierdynamiek, maar dat bodembewegingen langs breukzones ook op lokale en korte tijdschalen een belangrijke sturende factor zijn op rivierdynamiek.

Appendices

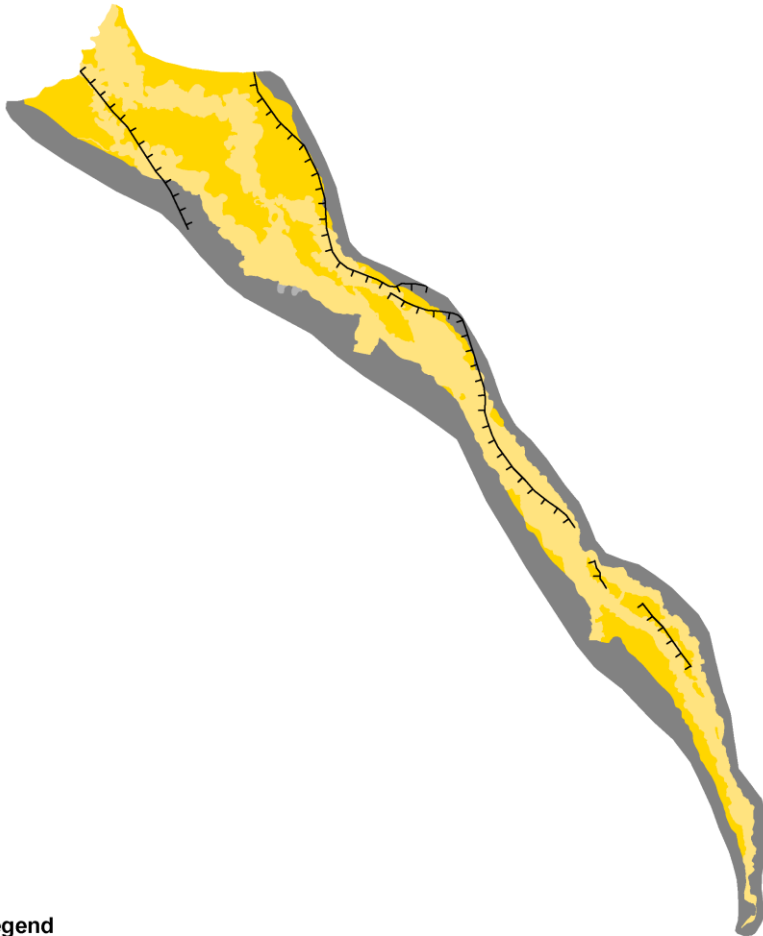
Appendices to Chapter 4

Terrace map Roer











Late Pleniglacial (>14.7 ka BP)



Legend

-  1 - Deactivated braid-belts and meander-belts (preserved)
-  2 - Active channel belt
-  3 - Pre-Lateglacial deactivated braid-belts and meander-belts
-  6 - Same as 1 - but laterally reworked in younger times - not preserved
-  7 - Same as 2 - but laterally reworked in younger times - not preserved
-  8 - Same as 3 - but laterally reworked in younger times

0 10 Kilometers

Bølling (14.7-14.0 ka BP)



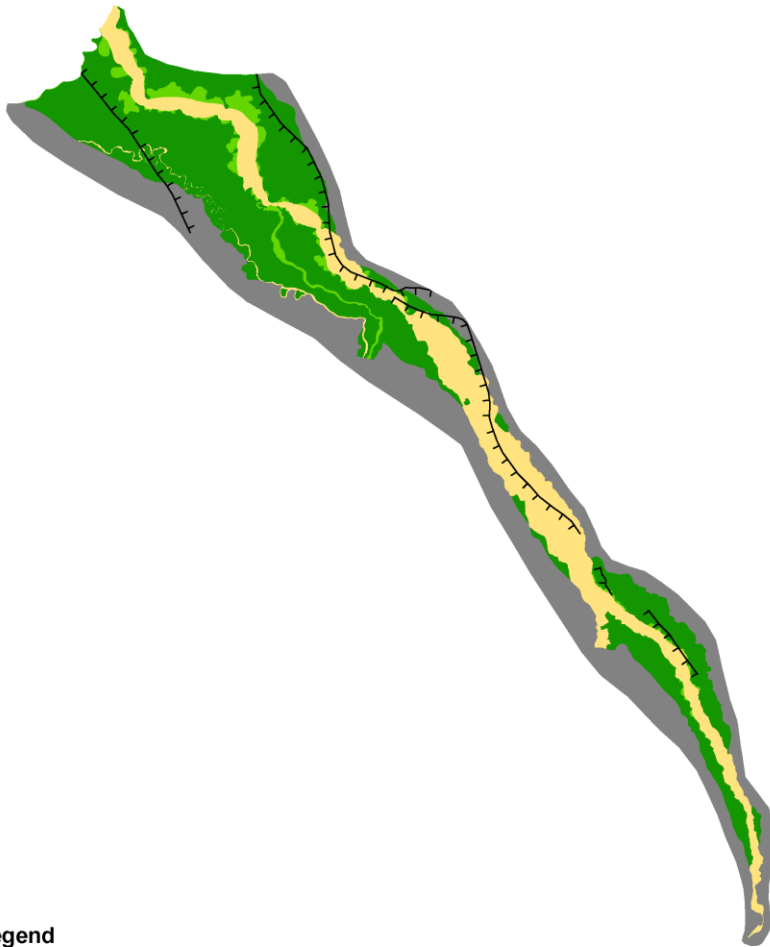
Legend

- 1 - Deactivated braid-belts and meander-belts (preserved)
- 2 - Active channel belt
- 3 - Pre-Lateglacial deactivated braid-belts and meander-belts
- 6 - Same as 1 - but laterally reworked in younger times - not preserved
- 7 - Same as 2 - but laterally reworked in younger times - not preserved
- 8 - Same as 3 - but laterally reworked in younger times











Older Dryas (14.0-13.9 ka BP)

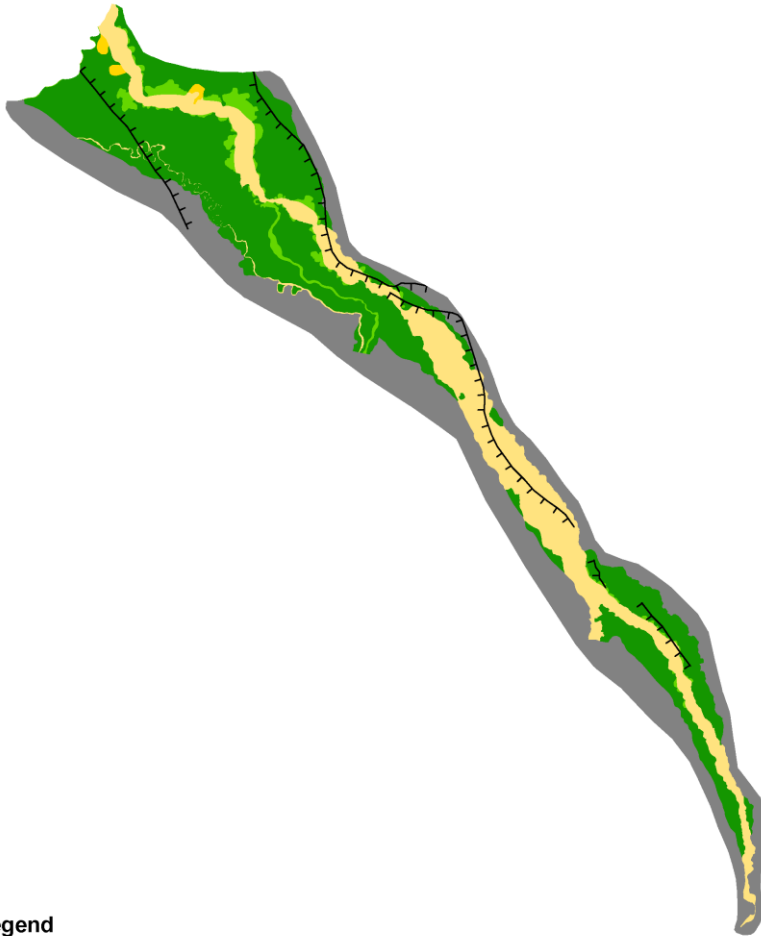


Legend







-  1 - Deactivated braid-belts and meander-belts (preserved)
-  2 - Active channel belt
-  3 - Pre-Lateglacial deactivated braid-belts and meander-belts
-  6 - Same as 1 - but laterally reworked in younger times - not preserved
-  7 - Same as 2 - but laterally reworked in younger times - not preserved
-  8 - Same as 3 - but laterally reworked in younger times

0 10
Kilometers

Allerød (13.9-12.85 ka BP)



Legend

-  1 - Deactivated braid-belts and meander-belts (preserved)
-  2 - Active channel belt
-  3 - Pre-Lateglacial deactivated braid-belts and meander-belts
-  6 - Same as 1 - but laterally reworked in younger times - not preserved
-  7 - Same as 2 - but laterally reworked in younger times - not preserved
-  8 - Same as 3 - but laterally reworked in younger times







0 10 Kilometers



Younger Dryas (12.85-11.7 ka BP)

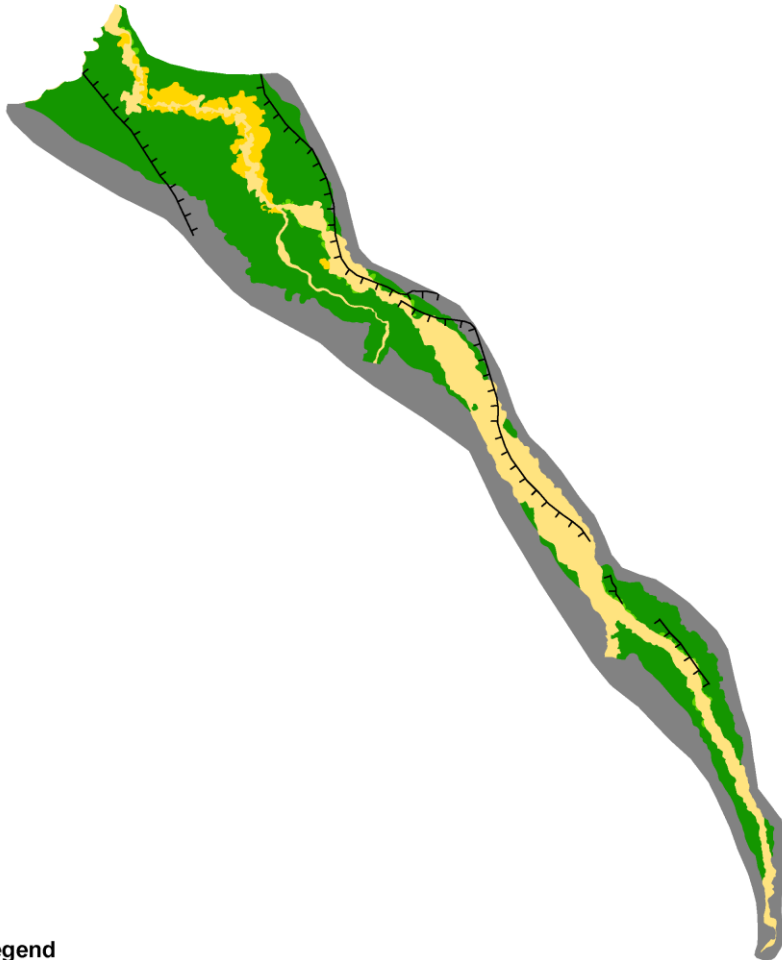


Legend






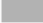
-  1 - Deactivated braid-belts and meander-belts (preserved)
-  2 - Active channel belt
-  3 - Pre-Lateglacial deactivated braid-belts and meander-belts
-  6 - Same as 1 - but laterally reworked in younger times - not preserved
-  7 - Same as 2 - but laterally reworked in younger times - not preserved
-  8 - Same as 3 - but laterally reworked in younger times

0 10
Kilometers

Early Holocene (11.7-8.9 ka BP)



Legend

-  1 - Deactivated braid-belts and meander-belts (preserved)
-  2 - Active channel belt
-  3 - Pre-Lateglacial deactivated braid-belts and meander-belts
-  6 - Same as 1 - but laterally reworked in younger times - not preserved
-  7 - Same as 2 - but laterally reworked in younger times - not preserved
-  8 - Same as 3 - but laterally reworked in younger times







0 10
Kilometers



Middle Holocene (8.9-3.1 ka BP)



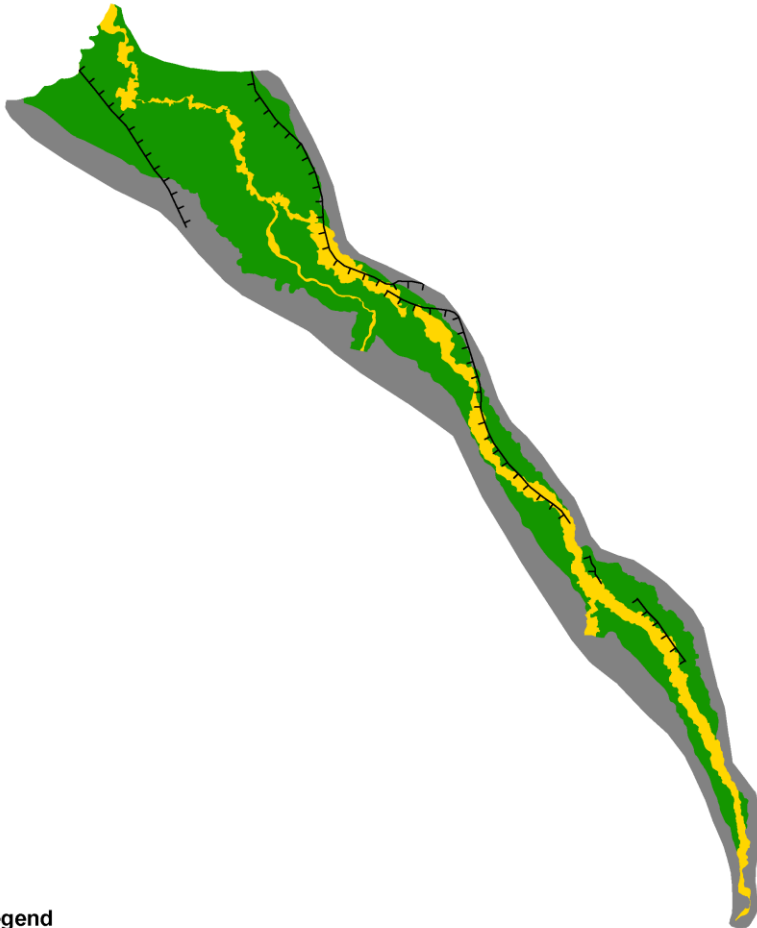
Legend

-  1 - Deactivated braid-belts and meander-belts (preserved)
-  2 - Active channel belt
-  3 - Pre-Lateglacial deactivated braid-belts and meander-belts
-  6 - Same as 1 - but laterally reworked in younger times - not preserved
-  7 - Same as 2 - but laterally reworked in younger times - not preserved
-  8 - Same as 3 - but laterally reworked in younger times







0 10
Kilometers



Late Holocene (3.1-0.0 ka BP)



Legend

-  1 - Deactivated braid-belts and meander-belts (preserved)
-  2 - Active channel belt
-  3 - Pre-Lateglacial deactivated braid-belts and meander-belts
-  6 - Same as 1 - but laterally reworked in younger times - not preserved
-  7 - Same as 2 - but laterally reworked in younger times - not preserved
-  8 - Same as 3 - but laterally reworked in younger times

0 10
Kilometers

Appendix B

This appendix shows the full pollen diagrams of the investigated sites. The pollen diagrams presented are a combination of previously published sites, in both journal articles and student thesis's and newly investigated sites. Each description of the pollen diagrams shows the source from which the pollen diagrams are retrieved and the credentials of the analyser. All diagrams were re-drawn from the original pollen-counting in Talia (version 2.0.60; Eric C. Grimm). Newly analysed radiocarbon dates are added to a number of the previously published sites to improve age control. Based on these radiocarbon dates the interpretation of the pollen diagrams might deviate from the interpretation of the original authors.

The pollen diagrams were subdivided into Local Pollen Assemblage Zones (LPAZ). LPAZ were differentiated based on changes in the main pollen taxa. Successively, the LPAZ were correlated to the Pollen Assemblage Zones (PAZ) of the biostratigraphic framework for the Lower Meuse Valley, the Netherlands (Figure 3 ,[Zagwijn, 1986; Hoek, 1997; Bos and Zuidhoff, 2015; Hoek et al., 2017; Woolderink et al., 2018]). In the pollen diagram descriptions the abbreviation AP stands for Arboreal Pollen and NAP for Non Arboreal Pollen. The dashed background in the diagrams represent an exaggeration of 5 times. The depth represented in the pollen diagrams is in centimeters below surface level. The pollen diagrams presented below are solely used for biostratigraphic dating in this study and do, therefore, not include a description of the local/regional climatic and ecological conditions.

Ivenhain

(Modified after Grooteman, 2018 / Analysis by L.P.A.

Grooteman)

LPAZ1 (200-170 cm; (humic) clay) consist of about 50% Arboreal pollen, such as *Betula* (~9%), *Pinus* (~20%), *Salix* (~30%), *Juniperus* (~2%) and *Alnus* and *Corylus* less than one percent. The prominent Upland herbs in LPAZ1 are Asteraceae (~4%), *Artemisia* (~9%), *Galium* (~2%), Apiaceae (~3%) and *Thalictrum* (~3%). Poaceae are present around 20% with in the bottom sample an occurrence of 45%. LPAZ 1 is correlated to PAZ 0 based on the relatively high amount of AP and high percentages of Poaceae, heliophilous herbs, *Salix* and *Juniperus* in this zone. PAZ 0 coincides with the Late Pleniglacial. This is supported by a radiocarbon date at 180 cm which gave an age of $13,495 \pm 40$ ^{14}C yr BP.

LPAZ2 (170-130 cm; (humic) clay) shows an increase in Poaceae, to ~32%. The trees *Salix* (~26%) and *Pinus* (between 2 and 16%) are somewhat lower in this zone. *Betula* (~15%) rises, while *Juniperus* is still present around 2%. Asteraceae (~1%), *Artemisia* (~4%), *Galium* (~1%) and *Thalictrum* (~1%) have decreased in this zone. LPAZ2 is correlated to PAZ 1 (Bølling) based on the relative importance of *Salix*, *Juniperus*, and increase in *Betula* and presence of *Helianthemum*.

LPAZ 3 (130-110 cm; peat) is marked by a distinct increase in *Betula* (~38%), while *Salix* gradually increases from 15% to 30% at the end of this zone. *Pinus* and *Juniperus* are less than one percent in this zone. In the topmost sample in this zone, *Corylus* rises to 5%. Poaceae decrease to values around 18%. The aquatic genus of *Myriophyllum* is most prominent in this zone. LPAZ 3 is correlated to PAZ 2(a) based on the strong increase in *Betula*. PAZ 2a represents the *Betula* phase of the Allerød.

LPAZ 4 (110-60 cm; humic clay) is characterized by a decrease in *Betula* (~20%) and *Salix* (~11%) while *Pinus* (~11%) increases. *Alnus* appears with values around 9% and *Corylus* is present with 5% as well as *Quercus* (~2%). The upland herbs Asteraceae (~2%) and *Filipendula* (~2%) show an increase while *Artemisia* and Apiaceae decrease to around 2%. Poaceae increases to values around 35%.

LPAZ 4 is correlated to PAZ 3 (Younger Dryas) based on the decrease in *Betula*, high values of Poaceae and low occurrences of *Salix* and *Pinus*. The occurrence of *Alnus*, *Corylus*, *Quercus* and *Fraxinus* is attributed to reworking of older deposits.

LPAZ 5 (60-45 cm; oxidized peat) shows a decline in *Betula* (5%) and *Salix* (5%), while *Pinus* (23%) increases. *Alnus* (~5%) and *Corylus* (~5%) are also present in the tree fraction. The upland herbs *Artemisia* (5%) and *Filipendula* (5%) are present. Poaceae are prominently present with values of ~50%. LPAZ 5 is correlated to PAZ 4 (Preboreal)

based on the distinct peak in Poaceae.

LPAZ 6 (45-30 cm; oxidized peat) is marked by the dominance of AP, *Pinus* (~71%), and a rise in *Corylus* up to 14%. Poaceae are lower around 9%, and the local wet vegetation is dominated by Polypodiaceae. LPAZ 6 is correlated to PAZ 5 (Boreal) based on the rise in *Pinus* and the occurrence of *Corylus*.

Haaserdriesch

(Modified after Kasse et al., 2017 | Analysis by M.Vreugdenhil)

LPAZ 1 (258–218 cm; clayey gyttja) is characterised by relatively low tree values (with the exception of *Salix*) and high percentages of Poaceae (40%) and heliophilous herbs (Asteraceae). Furthermore, *Helianthemum*, *Plantago* and *Rumex* are also present in this zone. The high value of aquatics, mainly *Potamogeton*, demonstrates the presence of lake conditions in the former channel. LPAZ 1 is correlated to PAZ 0 based on the high amount of Poaceae, NAP and relative importance of heliophilous herbs. PAZ 0 represents the Late Pleniglacial.

LPAZ 2 (218–195 cm; calcareous gyttja) shows decrease in heliophilous herbs and Poaceae (~20%), and an increase in *Betula* (~40%). LPAZ 2 is correlated to PAZ 1b based on the first rise in *Betula*, decrease in heliophilous herbs and relative importance of *Salix*. PAZ 1b corresponds to the Bølling. This correlation is supported by a radiocarbon date of 12,235±35 yr BP.

LPAZ 3 (195–181 cm; clay) is characterized by a drop in *Salix* (~15%) and *Betula* (~10%) values and an increase of NAP and Poaceae. The presence of *Alnus* and *Quercus* can be explained by reworking, which is supported by the siliciclastic character of the sediment. LPAZ 3 is correlated to PAZ 1c (Older Dryas) based on the decrease in *Betula* and increase in NAP values.

LPAZ 4 (181-160 cm; clay) shows a strong increase of AP to values of 80% and in particular *Betula* (~60%) values increase strongly. LPAZ 4 is correlated to PAZ 2 (Allerød) based on the strong increase in AP and distinct *Betula* peak.

LPAZ 5 (160-150 cm; gyttja and peat) is characterized by a decrease in *Betula* (~10%) values and an increase of NAP percentages. Furthermore, *Juniperus* and *Empetrum* are present in this zone as well. LPAZ 5 is correlated to PAZ 3 based on the increase in NAP, occurrence of *Empetrum* and relative importance of heliophilous herbs in this zone. PAZ 3 represents the Younger Dryas.

LPAZ 6 (150-125 cm; peat and clay) shows an increase in *Betula* (60%), increase in *Pinus* (~20%) and the first occurrence of *Corylus* and *Quercus*. NAP values decrease to a maximum of ~10%. LPAZ 6 is correlated to PAZ 5 based on the rise in *Betula*, *Pinus* and the appearance of *Corylus*. PAZ 5 represents the Boreal.

Kapbusch

(Modified after Grooteman, 2018 / Analysis by L.P.A.

Grooteman)

LPAZ 1 (165-155 cm; clay) is dominated by arboreal pollen (AP) around 40 to 45% and Poaceae around 30%. The arboreal pollen consist of *Betula* (~9%), *Pinus* (~11%), *Salix* (~16%) and *Juniperus* (~6%). *Salix* peaks to values of ~20% at the end of this zone. *Alnus* and *Corylus* are also present but below 5% and can, most probably, be attributed to reworking of older deposits. The upland herb fraction is dominated by Asteraceae (~7%) and *Artemisia* (~9%). LPAZ 1 is correlated to PAZ 1c based on the distribution of ~40% AP, ~30% Poaceae and ~30% other NAP. This correlation is, furthermore, based on the relatively high percentage of *Salix* at the end of this zone, which dominates over *Betula*. The correlation to PAZ 1 indicates an Older Dryas age for this zone.

LPAZ 2 (155-124 cm; humic clay-peat) is marked by an abrupt increase in AP (up to 80%) which is mostly due to a rise in *Betula* (up to 65%). The tree fraction decreases towards the top of this zone, mostly because of a lowering in *Betula* to 20%, while *Salix* increases from 5 to 20%. *Pinus*, *Alnus* and *Corylus* are below 2%. Poaceae have a percentage of ~15%. The Upland herbs consist mainly of *Artemisia* (~18%) and *Filipendula* increasing towards 12% at the top of the LPAZ. Furthermore, Asteraceae, Apiaceae and *Thalictrum* are present in minor percentages. *Equisetum* is very prominent in this zone. LPAZ 2 is correlated to PAZ 2a based on the distinct peak in *Betula*. PAZ 2(a) resembles the Allerød phase of the Lateglacial. This Allerød interpretation of LPAZ 2 is supported by a radiocarbon date of 11,915±20 ¹⁴C yr BP.

The transition to LPAZ 3 (124-87 cm; peat-humic clay) is defined by the reappearance of *Juniperus* (~4%), a decline in *Artemisia* (~5%) and high *Filipendula* (~16%) and *Saxifraga* percentages (up to 12%). Poaceae are present in somewhat lower percentages of ~8%. *Betula* percentages lie around 33%, *Pinus* is higher (~5%) than in LPAZ 2. *Salix* increases from 10% to 38%. In this zone, *Equisetum* is somewhat lower and the aquatic *Menyanthes* appears. LPAZ 3 is correlated to PAZ 3 based on the relatively low percentage of AP and high percentages of *Juniperus*. Additionally, the presence of

thermophilous trees such as *Alnus*, *Corylus* and *Carpinus* are attributed to reworking of older deposits, which is often seen in PAZ 3 (Hoek, 1997). PAZ 3 represents the Younger Dryas.

LPAZ 4 (87-77 cm; clay) is marked by an increase of Poaceae up to 50%. *Betula* (~22%), *Pinus* (~10%) and *Salix* (~10%) percentages are generally low. Upland herb percentages are low with *Artemisia* (~3%), *Filipendula* (~3%) and *Saxifraga* (~2%). The aquatic taxa *Myriophyllum* appears and peaks in this zone. Based on the distinct rise in Poaceae LPAZ 4 is correlated to PAZ 4(b), the (Rammelbeek phase of the) Preboreal.

The upper zone, LPAZ 5 (77-65 cm; clay), is characterized by an increase in trees, mostly caused by the appearance of *Corylus* (~14%) and a rise in *Pinus* (~36%) and *Salix* (up to 34%). *Betula*, however, decreases towards 4%. Poaceae decrease to around 11% and upland herbs are almost absent, apart from Asteraceae (~2%). Based on the rise in *Pinus* and the presence of *Corylus* LPAZ 5 is correlated to PAZ 5. PAZ 5 represents the Boreal.

Geraerds

(Modified after Kasse et al., 2017 | Analysis by M.Vreugdenhil)

LPAZ 1 (135-127; clay) shows high NAP percentages (~50%) and low *Betula* values (~30%). Furthermore, *Juniperus* (~5%), *Empetrum*, *Plantago*, *Thalictrum* and Asteraceae are present in this zone. LPAZ 1 is correlated to PAZ 1c based on the relatively high percentages of NAP which consist mainly of heliophilous herbs and high values of *Juniperus*. PAZ 1c represents the Older Dryas.

LPAZ 2 (127-105 cm, humic clay and gyttja) is characterized by an increase of *Betula* up to 60% and a decrease of grasses and heliophilous herbs like *Helianthemum*, *Plantago* and *Empetrum*. *Pinus* values increase slightly towards the end of this zone.

LPAZ 2 is correlated to PAZ 2 based on a distinct peak in *Betula* values in this zone, in combination with an increase in wetland herbs and aquatics. PAZ 2 is the Allerød. This correlation is confirmed by a radiocarbon date of 11,720±30 yr BP at a depth of 117-114 cm.

LPAZ 3 (105-86 cm, clay) is characterized by a decrease in AP and strong increase in Poaceae (~35%), heliophilous herbs and *Juniperus*. The presence of *Quercus* is ascribed to fluvial reworking of older deposits which is supported by the clastic nature of the deposits in this zone. LPAZ 3 is correlated to PAZ 3 based on the increase of NAP and heliophilous herbs. PAZ 3 is known as the Younger Dryas.

LPAZ 4 (86-76 cm, clay and peat) shows a strong increase in AP and decrease in heliophilous herbs and Poaceae. Furthermore, *Corylus* values are high (~70%) and low percentage of *Quercus* (5%) are present. LPAZ 4 is correlated to PAZ 5 based on the high AP percentages and high amount of *Corylus*. PAZ 5 represents the Boreal.

Karken

(Modified after Kasse et al., 2017 | Analysis by M.Vreugdenhil)

LPAZ 1 (145-123 cm; clay) shows low AP (~40%) and high values of Poaceae (40%) and heliophilous herbs (~15%), in particular *Artemisia* (5%) and Asteraceae (~10%). Combined with the presence of *Empetrum* (5%) and *Saxifraga* (~2%), this indicates a relatively cold and dry period. The presence of *Corylus*, *Alnus*, *Quercus* and Tertiary pollen in the clastic basal fill of the channel can be attributed to reworking of older sediments. LPAZ 1 is correlated to PAZ 1(c) (Older Dryas) based on the relatively low percentages of AP, together with high Poaceae values and the relatively abundant heliophilous herbs.

LPAZ 2 (123-91 cm; gyttja) is characterised by a rise in *Betula* up to 60%, wetland herbs and aquatics. *Koenigia* is present and, as a typical arctic-alpine species, it is associated with the Lateglacial. LPAZ2 is correlated to PAZ2(a) based on the distinct peak in *Betula*. PAZ2(a) represents the *Betula* phase of the Allerød. This correlation is supported by a radiocarbon date of $11,525 \pm 20$ ^{14}C yr BP at 110 cm.

LPAZ 3 (91-82 cm; oxidised peat) shows an increase in *Pinus* (~40%), a decrease in Poaceae and low values of aquatic species. LPAZ 3 is correlated to PAZ2(b) based on the increase in *Pinus* and decrease in *Betula*. PAZ2(b) represents the Pine-phase of the Allerød.

LPAZ 4 (82-77 cm; clay) shows a decrease in AP, and an increase in Poaceae and heliophilous herbs, like *Potentilla*, Brassicaceae and Asteraceae. The presence of *Carya* and *Quercus* and the clastic character of the sediment suggest reworking of sediment in the upstream catchment. LPAZ4 is correlated to PAZ 3 based on the decrease in AP and increase in Poaceae and heliophilous herbs. PAZ 3 represents the Younger Dryas. Furthermore, steppe elements, like *Ephedra*, are typical for the Younger Dryas.

LPAZ 5 (77-62 cm; clay with soil formation) shows a decrease in Poaceae (~5%) and upland herbs (5%), a strong increase in *Pinus* (~40%) and *Corylus* (~15%) and low values of *Quercus*. LPAZ 5 is correlated to PAZ 5 based on the rise in *Pinus* and the occurrence of *Corylus* and *Quercus*. PAZ 5 represents the Boreal. The upper part of zone 5 (70–62 cm; peat) may also represent the Atlantic as it is characterised by high values of *Alnus*, *Corylus* and *Tilia*.

Kitscherholz

(Modified after Kasse et al., 2017 | Analysis by M. Vreugdenhil)

LPAZ 1 (148–140 cm; gyttja and clay) has low *Betula* (~40%) values and high values of *Artemisia* (~5%), *Thalictrum* (~3%) and Asteraceae (~5%). Furthermore, *Juniperus* is present and Poaceae values are high (~30%). LPAZ 1 is correlated to PAZ 3 based on the presence of *Juniperus* and high NAP values. PAZ 3 is known as the Younger Dryas.

LPAZ 2 (140–117 cm; gyttja and peat) is characterised by high *Betula* values (40–60%), *Pinus* (10–20%) and Poaceae. LPAZ 2 is correlated to PAZ 4 based on the rise of *Betula* in the beginning of this zone in combination with a distinct peak in NAP which might represent the Rammelbeek phase of the Preboreal.

LPAZ 3 (117–112 cm; clay) shows the presence of *Corylus*, and low amount of *Quercus*. LPAZ 3 is correlated to PAZ 5 based on the appearance of *Corylus*. PAZ 5 is correlated to the Boreal.

Schafhausen

(Analysis by J.D.van der Woude, 2018)

LPAZ 1 (155-60 cm; clay) is characterized by relatively high percentages of NAP (10%) and Poaceae (~20%). *Pinus* percentages are high (~40%) and *Betula* values (~30%) increase towards the end of this zone. Furthermore, *Alnus*, *Corylus* and *Quercus* are present in this zone but this is considered to be the effect of reworking of older deposits. This is supported by the occurrence of *Carya*, *Ostrya*, *Pterocarya* and *Tsuga* in this zone, which was only present in this area during the Tertiary and early Pleistocene. LPAZ 1 is correlated to PAZ 3 based on the relatively high percentages of NAP and heliophilous herbs. PAZ 3 represents the Younger Dryas. This correlation is supported by a radiocarbon date on organic residue in the humic clay to peat transition at a depth of 80-75 cm. This radiocarbon date gave an age of 10,475 yr BP.

LPAZ 2 (60-55 cm; peat) shows a strong increase in *Alnus* (~80 %) and the presence of *Tilia*, *Fagus*, and *Corylus*. LPAZ 2 is correlated to PAZ 6 (Atlantic) based on the high percentage of *Alnus* and the presence of *Tilia*.

Turfkoelen

(Modified after Janssens, 2011 | Analysis by M.M. Janssens)

LPAZ 1 (251-231 cm; gyttja and peat) shows high values for upland herbs (~30%) and Poaceae (50%) and low values for AP (~20%). *Salix* and *Populus* are the main tree taxa registered in this zone while *Corylus* values (~10%) are low. LPAZ 1 is correlated to PAZ 4 based on the occurrence of *Corylus* in low values, the presence of *Populus*, relatively high NAP and the absence of a closed forest. PAZ 4 represents the Preboreal. This is supported by a radiocarbon date of a pine cone which gave an age of 9420 ± 30 ^{14}C yr BP (~10.7 ka BP [IntCal13 calibrated]).

LPAZ 2 (231-150 cm; (oxidized) peat) shows that *Populus* and *Salix* (<5%) values have decreased and *Corylus* values (~15%) are increasing. Furthermore, the appearance of *Ulmus* and *Quercus* are characteristic for this zone. NAP values (~60%) are still high in this zone, especially Poaceae, but this most probably a local signal. LPAZ 2 is correlated to PAZ 5 based on the increase in *Corylus* and appearance of *Ulmus* and *Quercus*. PAZ 5 represents the Boreal.

LPAZ 3 (150-120 cm; oxidized peat) is characterized by the presence of *Tilia* (25%), *Ulmus* (~40%), *Corylus* (~10%) and the start of *Alnus* (~10%). LPAZ 3 is correlated to PAZ 6 based on the occurrence of *Quercus*, *Alnus*, *Tilia* and *Ulmus*. PAZ 6 represents the Atlantic.

LPAZ 4 (120-110 cm; peat), is characterized by the lower percentages of *Ulmus* (~15%), the presence of *Alnus* and the decrease in *Tilia*. LPAZ 4 is correlated to PAZ 7 based on the decline in *Ulmus* and *Tilia* which represent the Atlantic-Subboreal transition.

Bennebroek

(Modified after Janssens, 2011 | Analysis by M.M Janssens)

LPAZ 1 (362,5- 285 cm; humic clay) at the base of the diagram is characterized by the presence of *Quercus* (~20%), *Ulmus* (~15%) and *Tilia* (~50%) and the absence of *Alnus*. Furthermore, relatively high amounts of *Betula* and *Corylus* occur in this zone. *Tilia* is the most dominant tree taxon (up to 70 %) in the latter part of this zone followed by *Ulmus* (~30 %) and *Quercus* (10-20%). LPAZ 1 is correlated to PAZ 5 based on the presence of *Tilia*, *Quercus*, *Corylus* and *Ulmus* and the absence of *Alnus*. PAZ 5 represents the Boreal.

LPAZ 2 (285-250 cm; humic clay and loamy clay) shows a distinct dip in *Tilia* percentages and peaks in *Corylus*, *Alnus* and *Betula*. LPAZ 2 is correlated to PAZ 6 based on the distinct peak in *Alnus* in favour of other tree species. PAZ 6 represents the Atlantic.

LPAZ 3 (250-170 cm; loamy clay and silty clay) is characterized by an increase in the amount of NAP and herbs and the first occurrence of cerealia. *Tilia* percentages remain high (up to ~70%). *Ulmus* shows a sudden drop at the base of this zone. LPAZ 3 is correlated to PAZ 7 (Subboreal) based on the sudden decline in *Ulmus* and relatively high amounts of *Tilia*.

LPAZ 4 (170-140 cm; loamy clay) is characterized by an increase in NAP. Furthermore, *Tilia* values are still very high (~70%) and *Alnus* percentages decrease to the end of this zone. *Corylus* and *Quercus* are still present in relatively high percentages. LPAZ 4 is also correlated to PAZ 7 based on the relatively high *Tilia* values and absence of (high percentages of) *Fagus*. PAZ 7 represents the Subboreal.

Bolberg

(Modified after Janssens, 2011 | Analysis by M.M. Janssens)

LPAZ 1 (160-115 cm; clay and peat) is characterised by relatively high NAP percentages (~30%), with Poaceae, *Artemisia* and Asteraceae as the most important upland herb taxa, at the start of the zone. The dominant tree species is *Betula* in this lower part of LPAZ1. Furthermore, *Corylus* is present and *Pinus* is an important taxon. Towards the end of this zone *Betula* (~10%) and *Salix* (<5%) have decreased and *Corlyus* (~50%) becomes the dominant tree species. Furthermore *Quercus*, *Tilia*, and *Ulmus* appear while *Betula* diminishes.

LPAZ 1 is correlated to PAZ 5 (Boreal) based on the abundant presence of *Corylus* and the presence of *Quercus*, *Tilia* and *Ulmus* in the latter part of this zone. A radiocarbon date of 3200 ¹⁴C yr BP, at 157-155 cm below surface level, is considered too young based on these palynological results. The absence of *Alnus*, *Fagus*, *Cereale*, *Secale* and the relatively high percentages of *Pinus* and NAP percentages at the depth of the radiocarbon date all point to an age that is older than the Subboreal-Subatlantic transition. It is, however, possible that roots of a younger vegetation cover penetrated into this depth. The dated material was a piece of unidentifiable wood as no suitable terrestrial macro-remains could be retrieved from the core. Most probably this piece of wood was a part of a root, explaining the young age of the radiocarbon date at this depth interval.

LPAZ 2 (115-95 cm; clay) is characterized by the strong increase of arboreal pollen (>90%). *Alnus* appears at the base of this zone and becomes a very important tree species. Furthermore, *Tilia* remains high (~15%) and *Ulmus* and *Quercus* remain relatively important taxa. LPAZ 2 is correlated to PAZ 6 (Atlantic) based on the strong increase in *Alnus* and relatively high values of *Quercus* and *Ulmus*.

LPAZ 3 (95-75 cm; peat) shows a sudden decrease in *Ulmus*. This zone is strongly dominated by *Alnus* (~70%) and *Tilia* and *Ulmus* become less important. *Quercus* percentages (~10%) are slightly higher than in the previous zone. LPAZ 3 is correlated to PAZ 7 (Subboreal) based on the sudden decline in *Ulmus*, representing the Atlantic-Subboreal transition.

LPAZ 4 (75-70 cm; peat) shows another increase of NAP, together with the appearance of cultivated species like *Cereale*, *Secale* and *Fagopyrum*. Other human indicators like *Artemisia* and *Plantago lanceolata* increase and *Fagus* appears. LPAZ 4 is correlated to PAZ 8 based on presence of *Fagus* and increasing number of Cerealia. PAZ 8 represents the Subatlantic.

Erzelbach

(Analysis by J.D.van der Woude, 2018)

LPAZ 1 (140-119 cm; humic gravel) is characterized by high AP percentages of ~90%, and high values of *Alnus* (70%) at the base of the zone which decrease to ~45% at the top of LPAZ 1. Furthermore, *Fraxinus* is present and *Corylus* has relatively high values of ~35%. LPAZ 1 is correlated to PAZ 7 based on the high values of *Corylus*, *Alnus* and the (final) occurrence of *Fraxinus*. PAZ 7 represents the Subboreal. This correlation is supported by a radiocarbon date on a hazelnut fragment found at the bedload to channel fill contact, which gave an age of 3373±17 yr BP.

LPAZ 2 (119-93 cm; humic clay) shows a strong increase in *Alnus* (~85%), indicating that alder was growing locally. *Corylus* values decrease (~5%) although this might also be due the major increase in *Alnus*. Nevertheless, LPAZ 2 is correlated to PAZ 8 based on the decrease of *Corylus* and *Fraxinus*. PAZ 8 represents the Subatlantic.

LPAZ 3 (93-61 cm; humic clay and peat) shows a decrease in *Alnus* (~30%) and increase in NAP and Poaceae (~30%). LPAZ 3 is correlated to PAZ 8 (Subatlantic) based on the decrease in AP and increase in NAP and Poaceae. This decrease in trees and increase in grasses and upland herbs can, most probably, be attributed to deforestation and human occupation.

LPAZ 4 (61-55 cm; peat) is characterized by a further increase in NAP, upland herbs and the presence of *Fagus*. LPAZ 4 is also part of PAZ 8, the Subatlantic.

Rurich

(Modified after Grooteman, 2018 / Analysis by L.P.A.

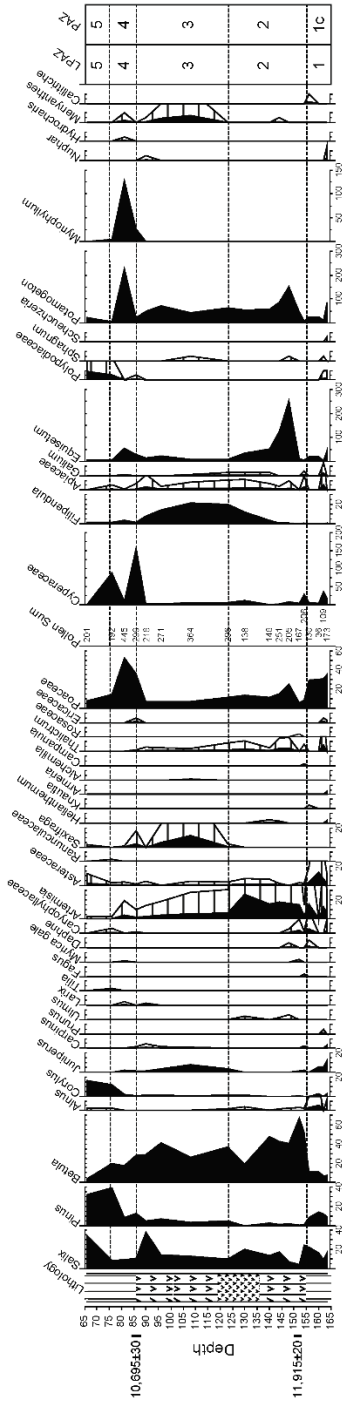
Grooteman)

LPAZ 1 (257-220 cm; clay) shows low occurrences of trees (~25%) and relatively high values of Upland herbs (~45%) and Poaceae (~30%). The tree pollen consist of predominantly thermophilous trees. Agricultural indicators such as *Cerealia* (~5%) and *Centaurea* (~2%) are present as well. LPAZ 1 is correlated to PAZ 8 based on the relatively low percentage of tree pollen and high amount of upland herbs and Poaceae, together with some indicator species such as *Cerealia* and *Centaurea*, indicating an agricultural landscape. This agricultural landscape is probably Medieval age or younger as persistent occurrence of *Cerealia* is thought to have started around 1000 BP (Bakels, 2017b).

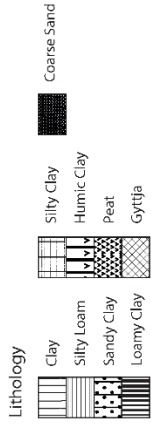
Gutt Grittern

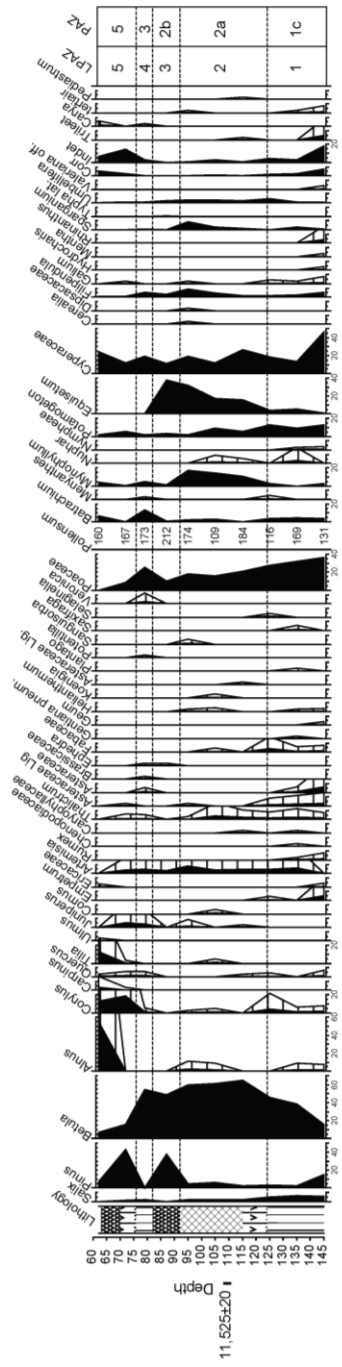
(modified after Grooteman, 2018 / Analysis by L.P.A.
Grooteman)

LPAZ 1 (275-230 cm; silty loam and clay) is dominated by Upland herbs, Poaceae (~40%) and Cerealia (~10%). The most abundant upland herb is Asteraceae (~26%), while Brassicaceae (~2%), Caryophyllaceae (~1%), *Rumex* (~1%), Ranunculaceae (~1%) are consistent throughout but present in small numbers. Cannabis-type (either *Cannabis Sativa* or *Humulus lupulus*) is also present throughout the zone. *Fagopyrum* is present in one of the pollen spectra. *Alnus* (~9%) is the most abundant of the trees, followed by *Betula* (~2%), *Corylus* (~2%), *Salix* (~1%), *Quercus* (~1%) and *Pinus* (~1%). *Tilia*, *Carpinus* and *Juglans* are also present. LPAZ 1 is correlated to PAZ 8 (Subatlantic) based on the low AP values and high values of Poaceae and Asteraceae together with the high occurrence of *Cerealia* and the presence of the Cannabis-type and *Fagopyrum*. *Juglans* has been introduced to NW Europe in the Roman Period (Bakels, 2017b). All these indicators combined suggests an age for this zone of Medieval or younger.

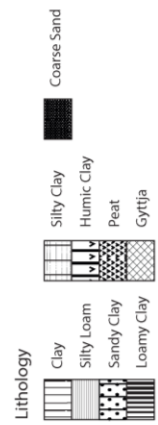


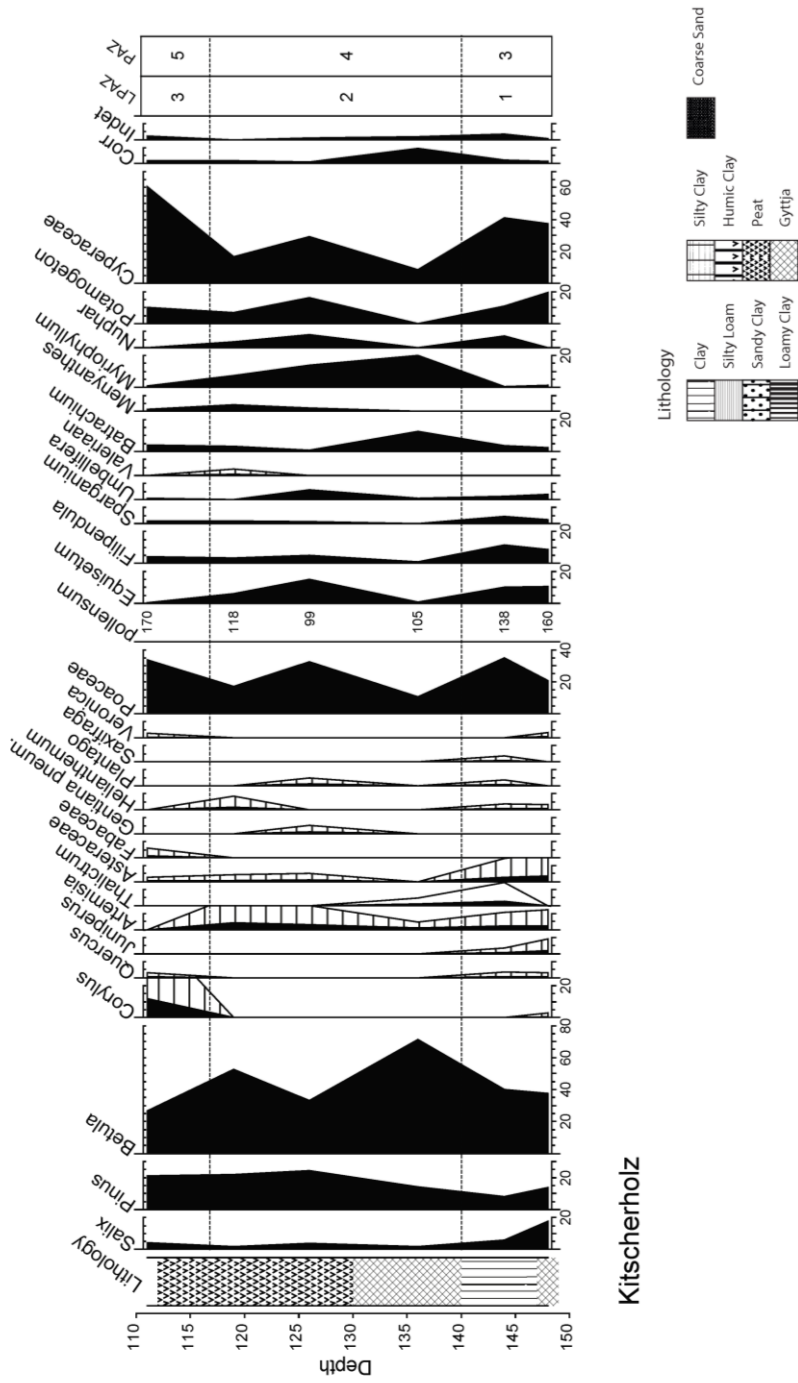
Kapbusch



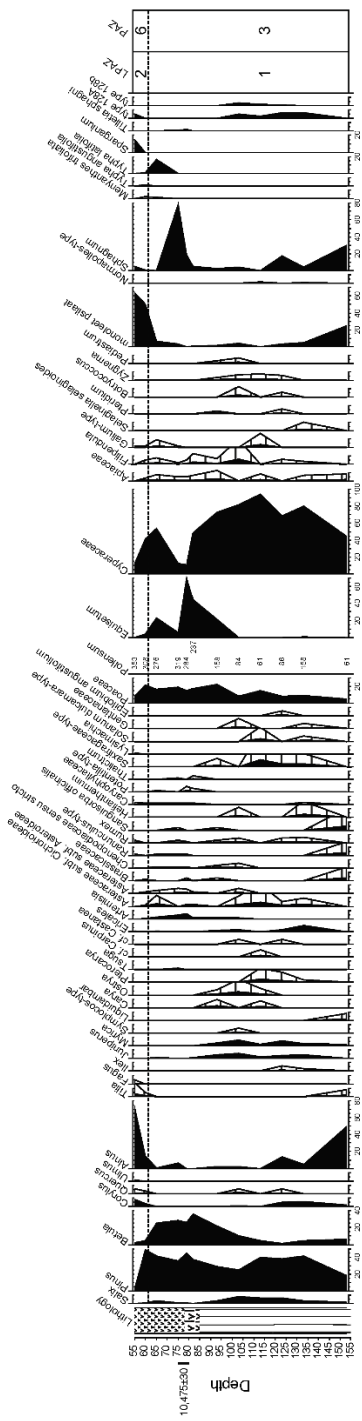


Karken

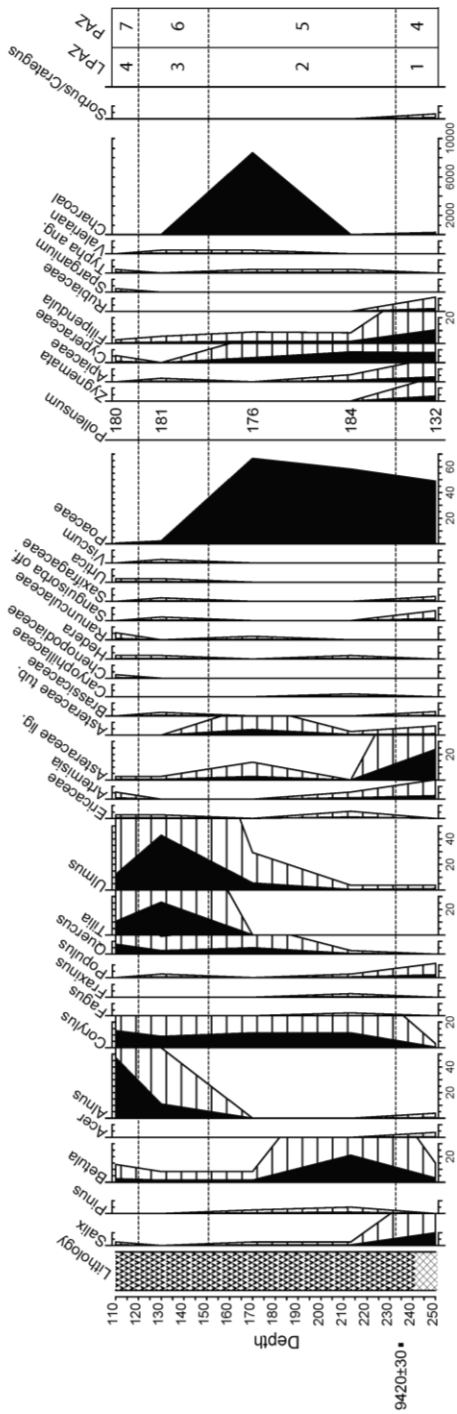




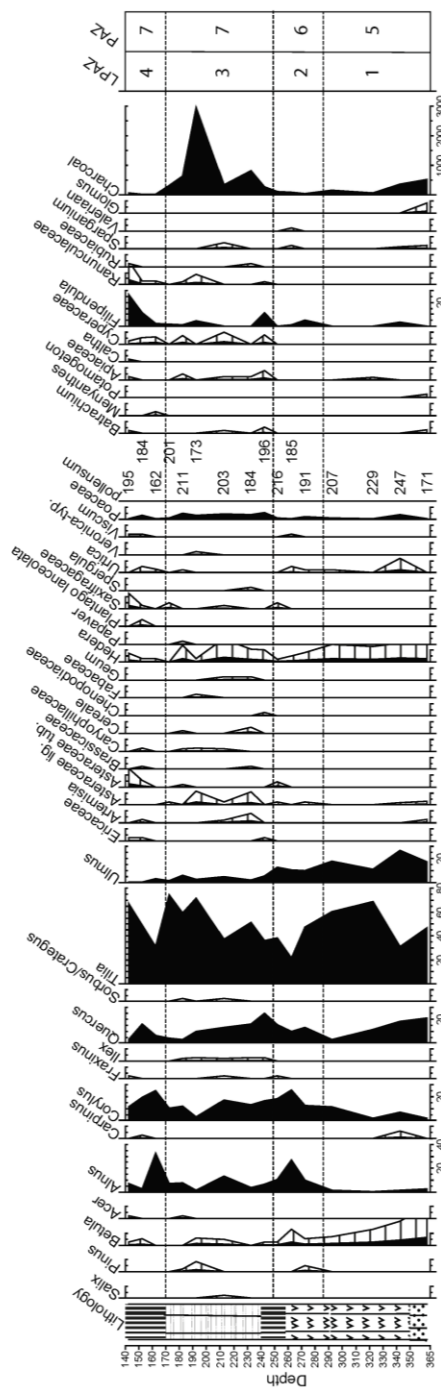
Kitscherholz



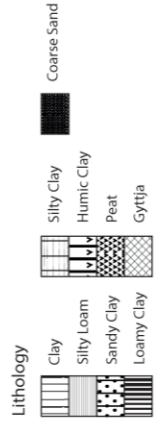
Schafhausen

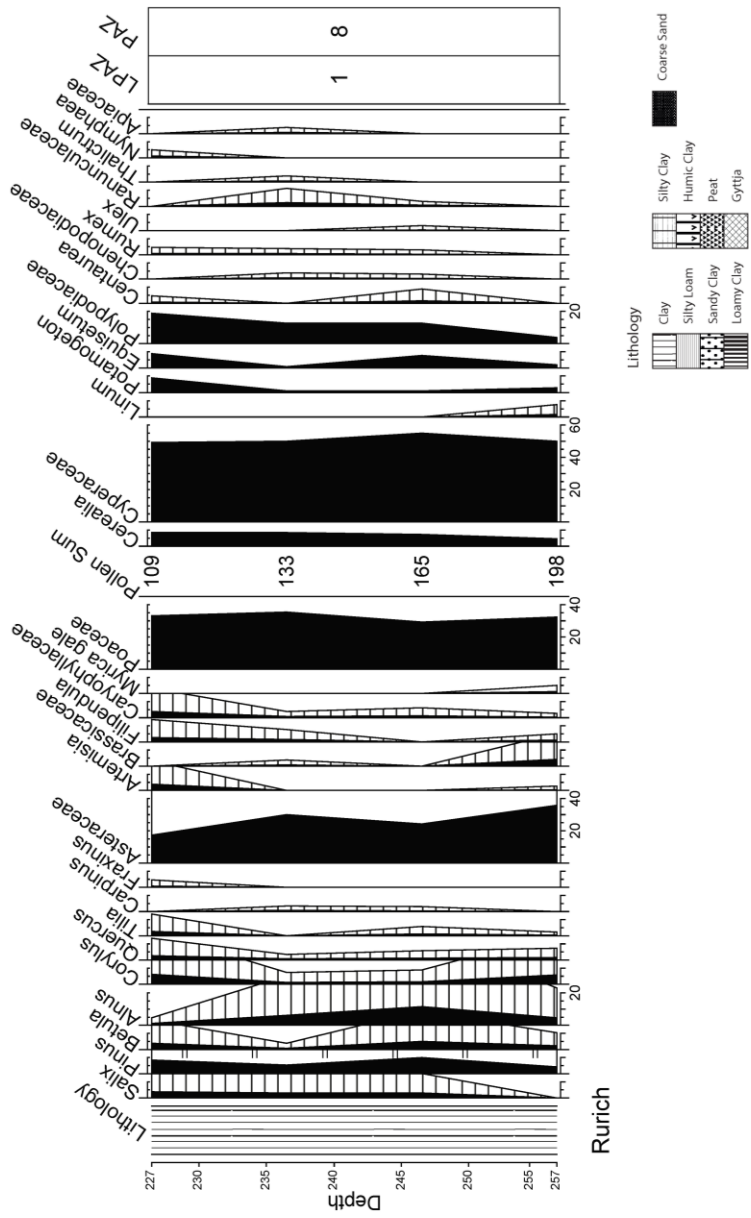


Turkkoelen

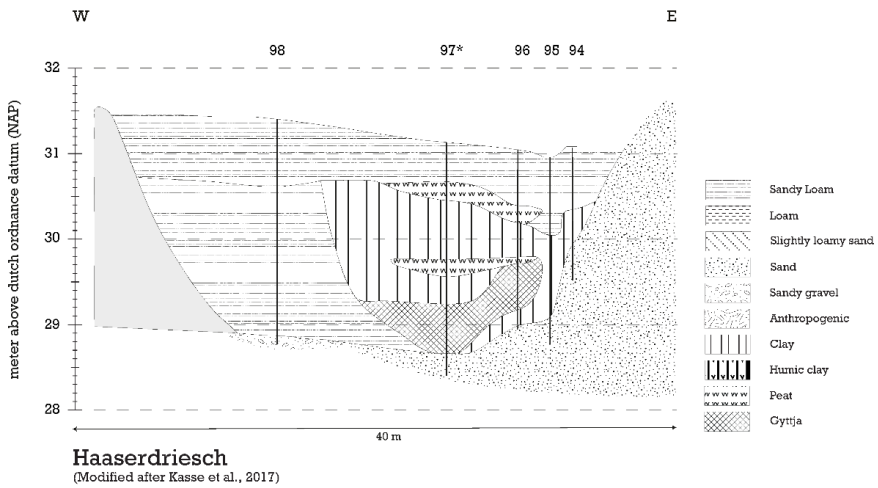
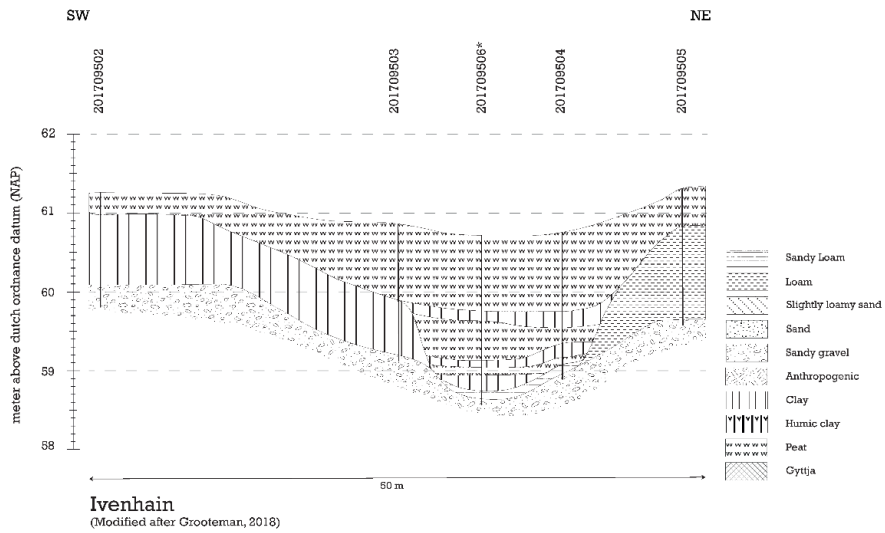


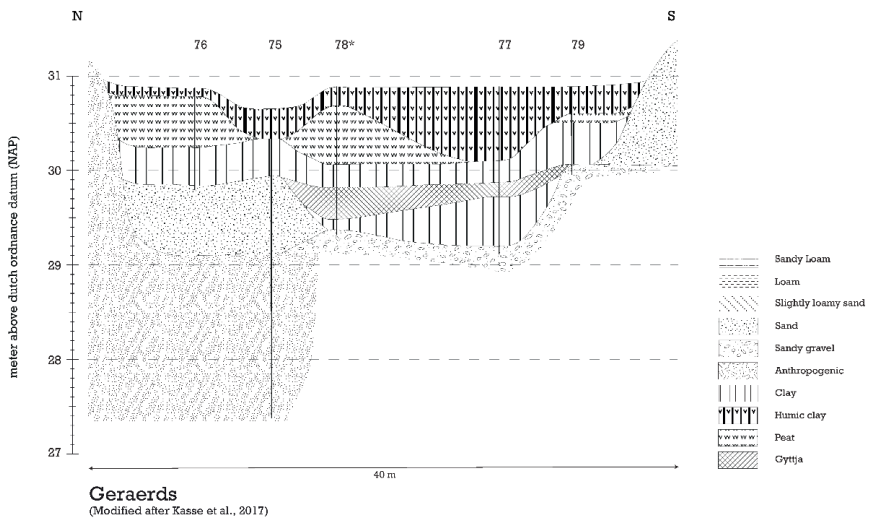
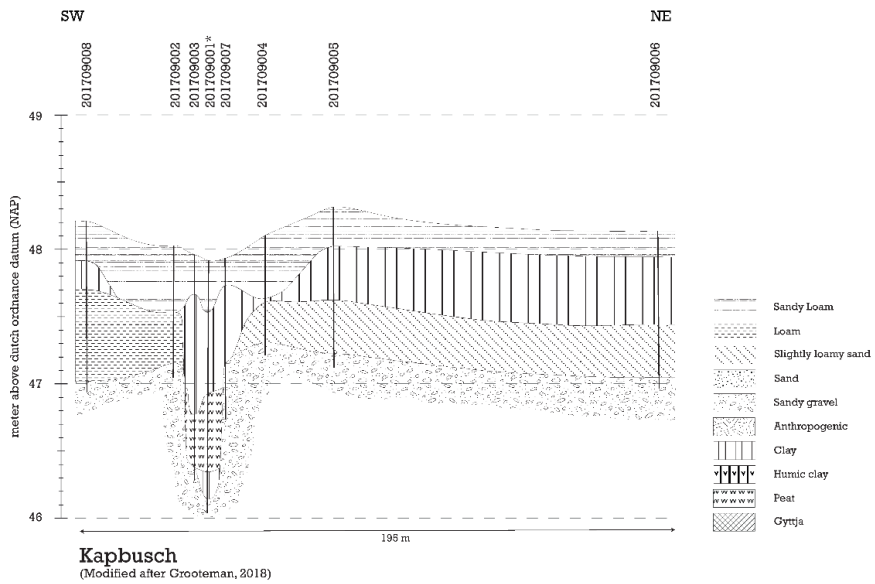
Bennebroek

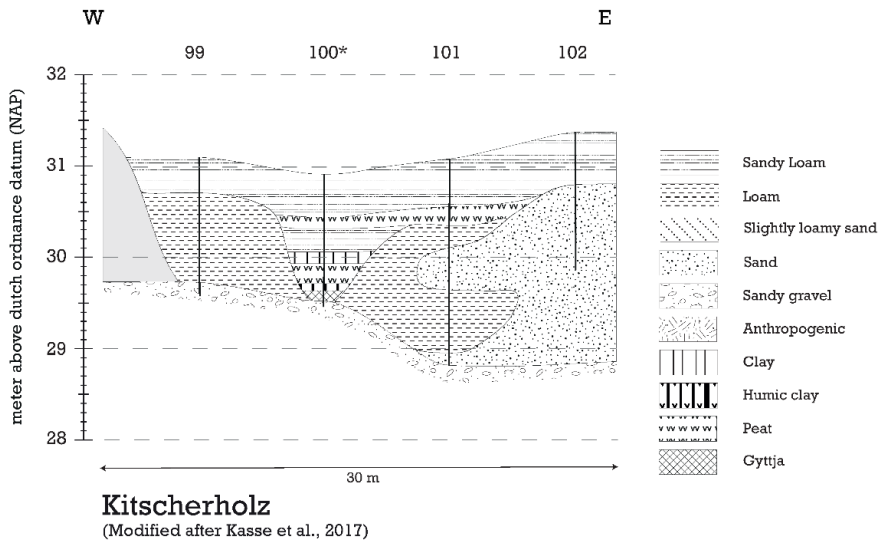
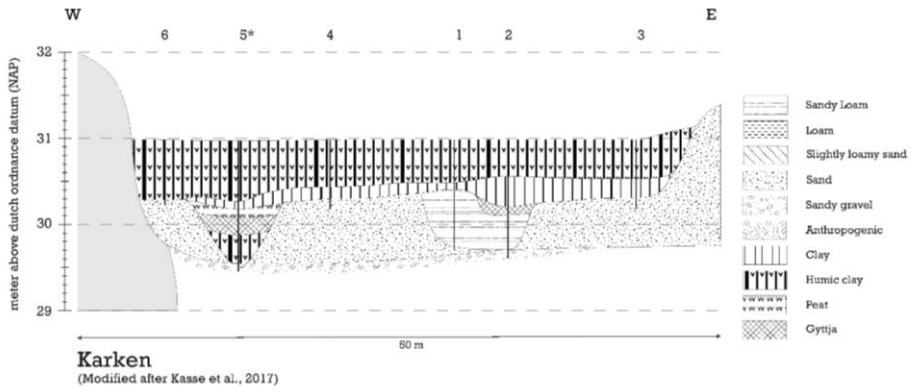


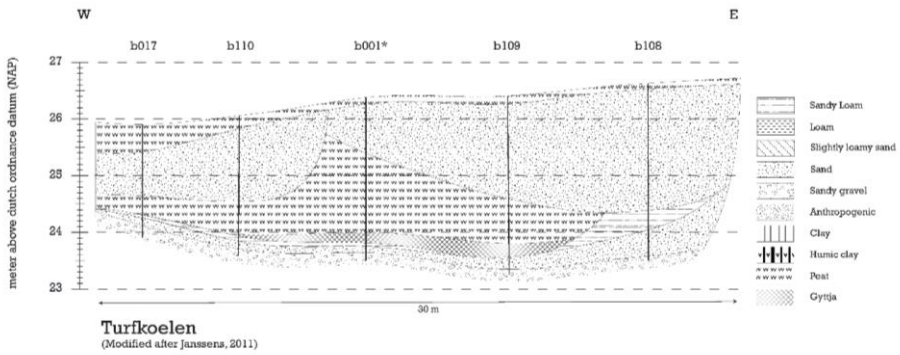
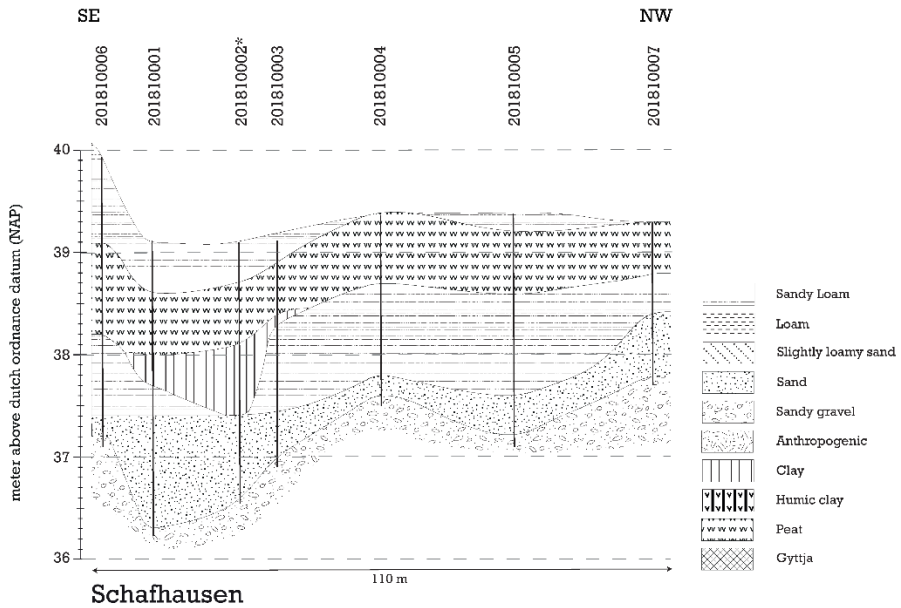


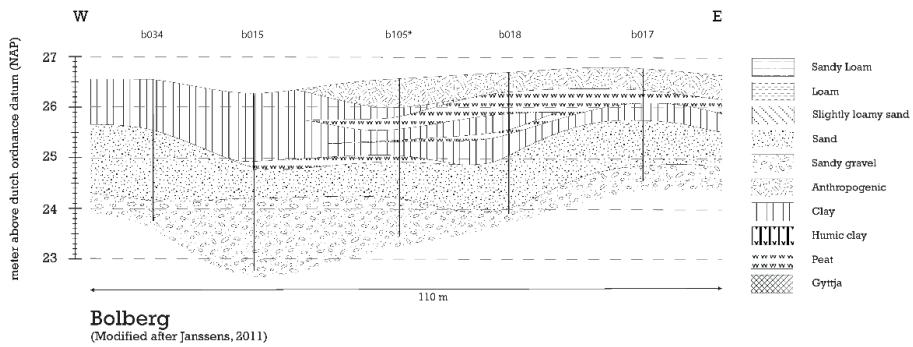
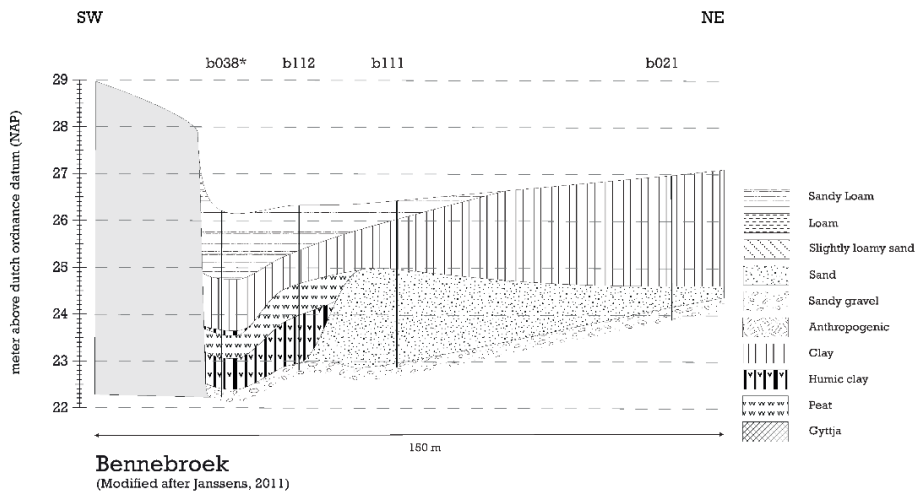
Appendix C

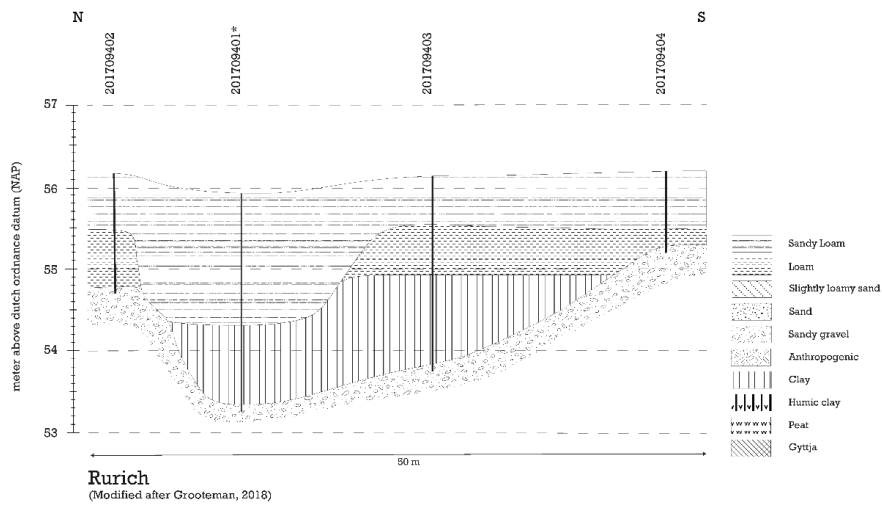
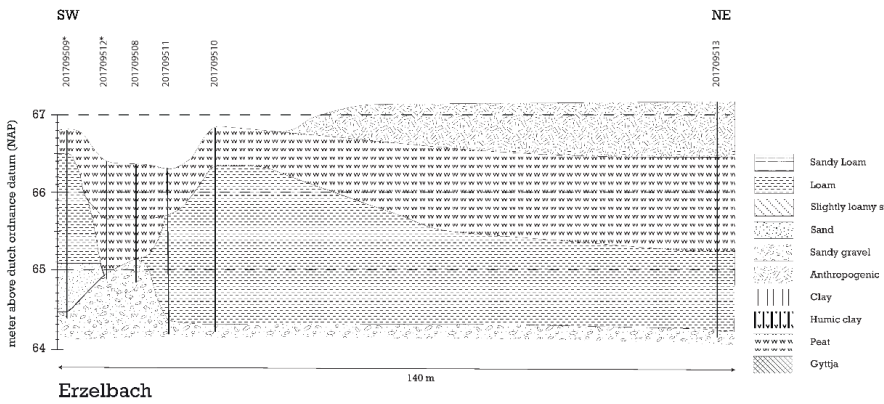


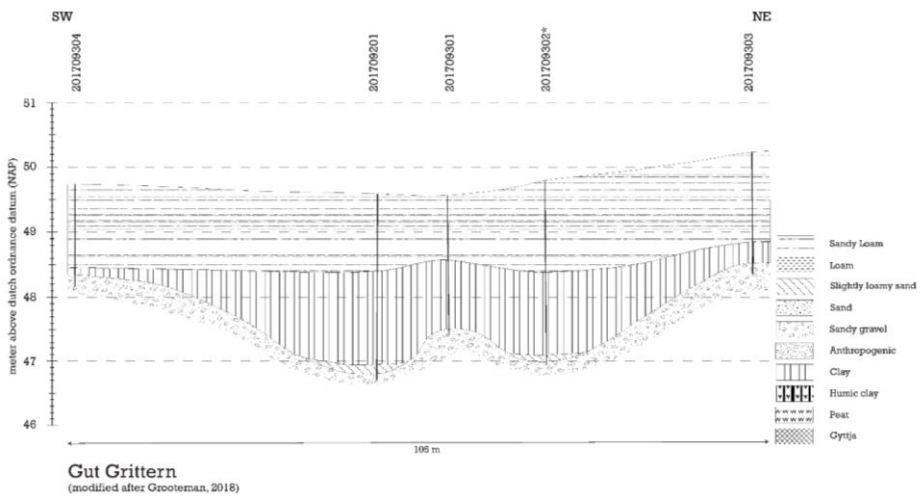




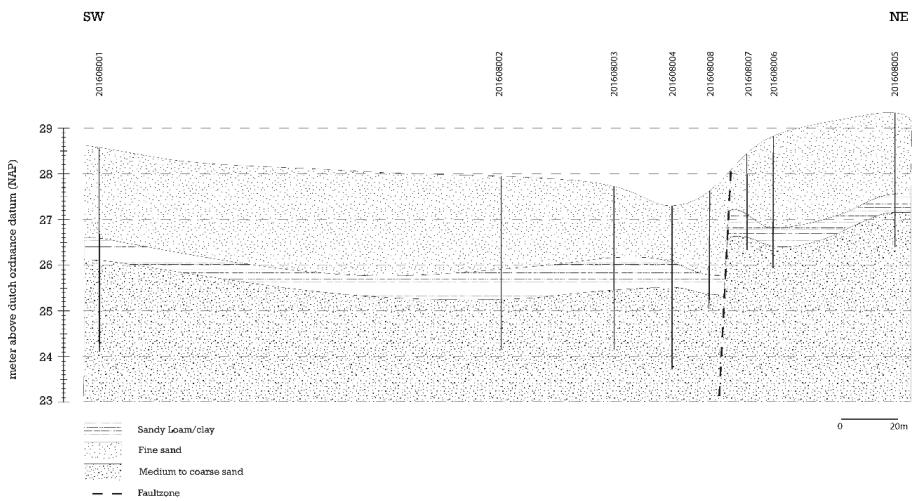




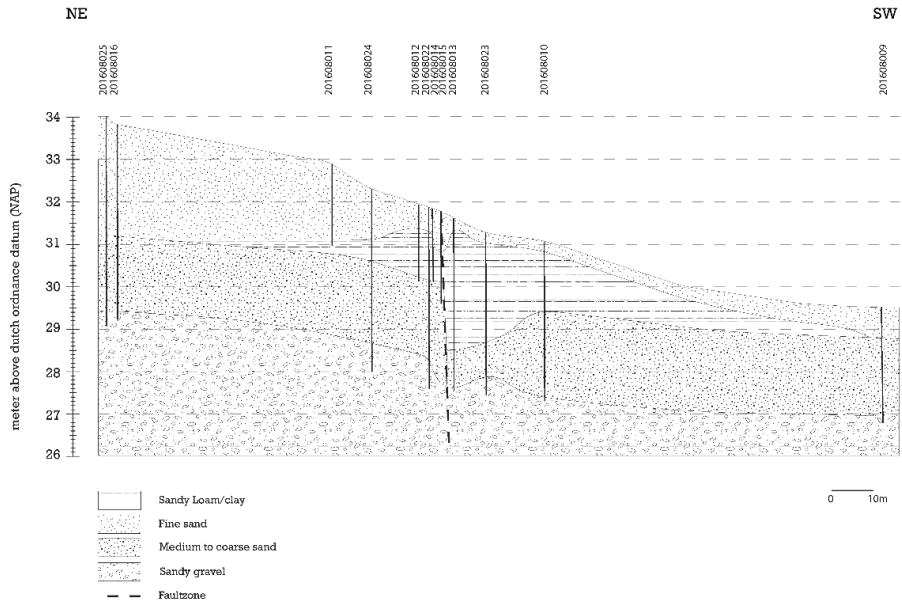




Assenray (PBFZ)



Herkenbosch (PBFZ)



Appendices to Chapter 5

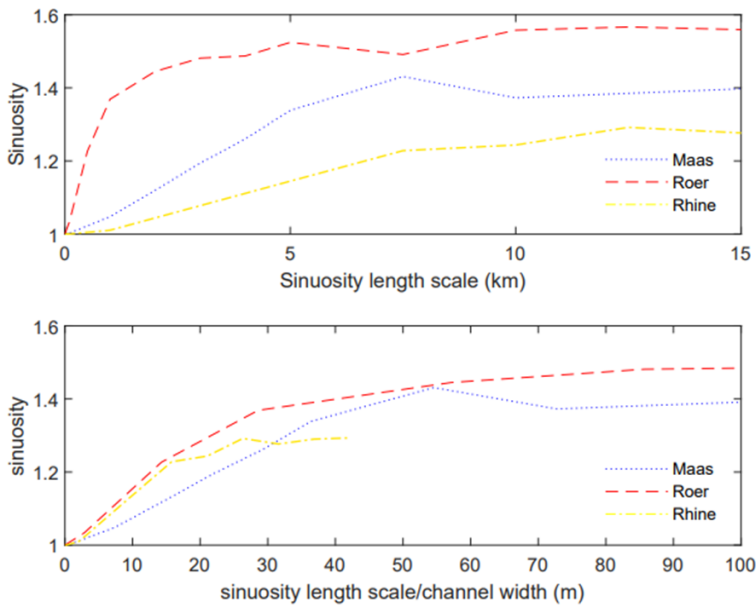
Appendix A

Calculation of backwater adaption length and Shields numbers

The backwater adaption length is approximated by $L = \frac{h_c}{S}$ where h_c = channel depth (m) and S = channel slope (-). The non-dimensional shear stress or Shields numbers for the gravel and sand reach of the rivers were calculated by $\theta = \frac{\tau}{(\rho_s - \rho)gD_{50}}$ where ρ_s is the density of sediment and ρ of water (kg m^{-3}). The shear stress is calculate as $\tau = \rho gRS$ with $R = \frac{W_a h_a}{W_a + 2h_a}$ where W_a = channel width and h_a = actual (measured) water depth (Kleinhans and Van den Berg, 2011).

Sinuosity length scale

Sinuosity versus length scale for the Meuse, Roer and Rhine rivers are shown in the figure below. Minimum length scales are 7.5, 3 and 12.5 kilometres for the Meuse, Roer and Rhine respectively. The coinciding profiles in the bottom panel show the relation between meander wavelength and channel width.



Appendix B

